The 2009 Cessna Aircraft Company/Raytheon Missile Systems Design/Build/Fly Competition Flyoff was held at TIMPA Field in Tucson, AZ on the weekend of April 17-19, 2009. This was the 13th year the competition was held. A total of 54 teams submitted written reports to be judged. 41 teams attended the flyoff, 39 of which completed the technical inspection. Approximately 600 students, faculty, and guests were present. Near ideal weather allowed for near non-stop flights to be conducted each day. Of the 133 official flight attempts, 49 resulted in a successful score divided among 32 teams. The quality of the teams, their readiness to compete, and the execution of the flights continues to improve each year.

The first two mission objectives for this year were to fly a high-drag payload, a simulated external fuel tank, both empty at high speed and full for endurance. The third mission was to fly an asymmetric load of wing stores, simulated missiles. The flight score was the sum of the three flight scores. In addition to the flight tasks, teams had to design their complete system for the minimum weight with a constrained package size, and were timed on how quickly they could prepare their aircraft for flight. As usual, the total score is the product of the flight score and written report score. More details can be found at the competition website: http://www.ae.uiuc.edu/aiaadbf

The top places were taken by teams from two universities: Oklahoma State University and The University of Southern California. Oklahoma State University Team Black scored first place with an excellent written report score, very low System Complexity Factor score, and successful scores for all three flight Missions. Oklahoma State University Team Orange finished in Second place, and The University of Southern California team Turbo Encabulator finished in Third. A new feature for the contest was the Design Engineering TC sponsored award for the Best Paper Score, which was won by the Wichita State University sUAVe entry with a score of 97.50. The complete standings are listed in the table below.

The fastest pre-mission assembly was 11.60 seconds by OSU Team Black. That surprised us. But then, the students always surprise us. The asymmetric loading mission was a challenge, as expected, with only three teams successfully completing the mission; OSU Team Black, USC team Turbo Encabulator and Georgia Tech Team Buzzed. Note that this year the difference between 2nd and 3rd place was a higher report score, not a higher flight score. This confirms the importance the contest places on a teams ability to document their design work as well as demonstrate successful flight performance.

Raytheon Missile Systems hosted another great DBF event. We owe our thanks for the success of the DBF competition to the efforts of many volunteers from Cessna Aircraft, Raytheon Missile Systems, the Naval Research Lab, and the AIAA sponsoring technical committees: Applied Aerodynamics, Aircraft Design, Flight Test, and Design Engineering. These volunteers collectively set the rules for the contest, publicize the event, gather entries, judge the written reports, and organize the flyoff. Thanks also go to the Corporate Sponsors: the Raytheon Missile Systems, Cessna Aircraft, and the AIAA Foundation for their financial support.

Finally, this event would not be nearly as successful without the hard work and enthusiasm from all the students and advisors. If it weren't for you, we wouldn't keep doing it.

Greg Page
For the DBF Governing Committee

WSU sUAVe

Design Report
AIAA/Cessna/RMS
Design/Build/Fly
2008-2009

Wichita State University
Department of Aerospace Engineering

March 2009

Table of Contents

Acronyms, Abbreviations, and Symbols

Δ	Change in Variable
Λ	Sweep Angle
β	Sideslip Angle
δ_e	Elevon Deflection Angle
δ_r	Rudder Deflection Angle
AC	Aerodynamic Center
AOA	Angle of Attack (also α)
AR	Aspect Ratio
b	Span
CA	Cyanoacrylate
CAD	Computer Aided Design
CBA	Computerized Battery Analyzer
C_{D0}	Parasite Drag Coefficient
CFD	Computational Fluid Dynamics
CG	Center of Gravity
C_L	Lift Coefficient
C_{Lmax}	Wing Maximum Lift Coefficient
c_{lmax}	Airfoil Maximum Lift Coefficient
C_{Ltrim}	Trimable Lift Coefficient
C_{M0}	Wing Zero-Lift Pitching Moment Coefficient
c_{m0}	Airfoil Zero-Lift Pitching Moment Coefficient
$c_{m\alpha}$	Slope of Airfoil Pitching Moment Curve
$C_{M\alpha}$	Slope of Wing Pitching Moment Curve
CP	Center of Pressure
DBF	Design/Build/Fly
FEM	Finite Element Method
FOM	Figure of Merit
FS	Flight Score
GO	Göttingen
L/D	Lift to Drag Ratio
LE	Leading Edge
MDO	Multi-Disciplinary Optimization
Mfg	Manufacturing
MLG	Main Landing Gear
NACA	National Advisory Committee on Aeronautics
NIAR	National Institute for Aviation Research
NiCad	Nickel Cadmium
NiMH	Nickel Metal Hydride
OML	Outer Mold Line
p	Roll Rate
Pa	Power Available
Pr	Power Required
q	Pitch Rate
r	Yaw Rate
RAC	Rated Aircraft Cost
Re	Reynolds Number
S	Planform Area
S&C	Stability and Control
SCF	System Complexity Factor
S_{LO}	Liftoff Distance
SM	Static Margin
sUAVe	Shocker Uninhabited Aerial Vehicle Engineering
t_{load}	Mission 3 All-Stores Loading Time
t_{ferry}	Mission 1 Ferry Flight Time
T/O	Takeoff
T/W	Thrust to Weight Ratio
V_{stall}	Stall Velocity
$V_{takeoff}$	Takeoff Velocity
W/S	Wing Loading
WSU	Wichita State University
WTT	Wind Tunnel Test

1.0 Executive Summary

This document details the design, testing, and manufacturing efforts of Wichita State University (WSU) Team sUAVe (Shocker Uninhabited Aerial Vehicle Engineering) in preparation for the 2008-2009 AIAA/Cessna/RMS Design/Build/Fly (DBF) competition. Team sUAVe's primary objective is to design a winning DBF aircraft by maximizing total score, which is a function of report score and flight score (FS). FS is determined by performance in three missions: Ferry Flight, Surveillance Flight, and Store Release Flight. The Ferry Flight and Surveillance Flight focus on payload capabilities, requiring the aircraft to carry an external four-liter simulated fuel tank. The Store Release Flight demands good handling qualities under asymmetric loading, requiring three wing-mounted store releases. Each mission score is a function of aircraft assembly time and total system weight. Design requirements constrain aircraft size (limited to two boxes with maximum 2x2x4 ft dimensions) and takeoff distance (100 ft maximum). A sensitivity study on FS reveals total system weight and assembly time as the most critical design parameters, each contributing 45.7% to FS.

Vehicle concepts are developed to meet mission requirements and achieve maximum FS. Five configurations are selected for further analysis: Conventional, Elliptical, Flying Wing, Inverted V-Tail, and Gull Wing. Figure of Merit (FOM) analyses are utilized to select aircraft configuration and components, which yield a flying wing configuration with a single tractor propeller, tricycle landing gear, winglets, and a hinging wing joint. Each component is selected to provide sufficient aircraft performance, while minimizing system weight and assembly time. The flying wing configuration with a single tractor propeller provides a lightweight, low drag design and has potential for quick assembly time. Tricycle landing gear provides superior ground handling capabilities, particularly during asymmetric loading. Winglets improve effective wing aspect ratio, further reducing drag. A hinged wing allows the vehicle to be stored in a single, compact piece.

A modular, multi-disciplinary optimization (MDO) architecture is developed and each core engineering discipline performs analysis on critical design parameters including: airfoil selection, wing span, sweep, and area, and propulsion system selection. A custom airfoil is designed to provide stability, while maintaining an adequate lift coefficient. The wing is sized to a 60 in span and a 756 in^2 area to meet the 100 ft takeoff distance, and a 30 deg wing sweep is selected to provide longitudinal stability. Propulsive analysis yields a NEU 1506/2.5Y motor with a 5.2:1 gear ratio. Mission 1's optimal propulsion system requires 12 Elite 1700 cells and an APC 14x10E propeller. Mission 2's optimal propulsion system requires 14 Elite 1700 cells and an APC 16x10E propeller. Mission 3's optimal propulsion system requires 12 Elite 2000 cells and an APC 14x10E propeller.

The predicted performance capabilities of Missions 1 / 2 / 3 are as follows: takeoff distances are 11 / 97 / 92 ft, thrust-to-weight ratios are 0.9 / 0.5 / 0.4, wing loadings are 0.7 / 2.4 / 1.8 psf, stall speeds are 15 / 27 / 24 mph, and cruise speeds are 47 / 41 / 48 mph. Predictions for Rated Aircraft Cost (RAC) and assembly time are 23.5 lbs and 12 seconds, respectively. These predicted performance and scoring parameters couple to result in a highly competitive mission-oriented vehicle.

2.0 Management Summary

Team hierarchy and schedule are developed to orchestrate an accelerated design timeline.

2.1 Team Organization

The organizational structure encourages an interdisciplinary approach to design and ensures cohesive team chemistry. This structure organizes five senior engineers into core disciplines and integrates manufacturing, testing, and CFD specialists. Undergraduate and graduate advisors also play a role in the team support structure (Figure 2.1).

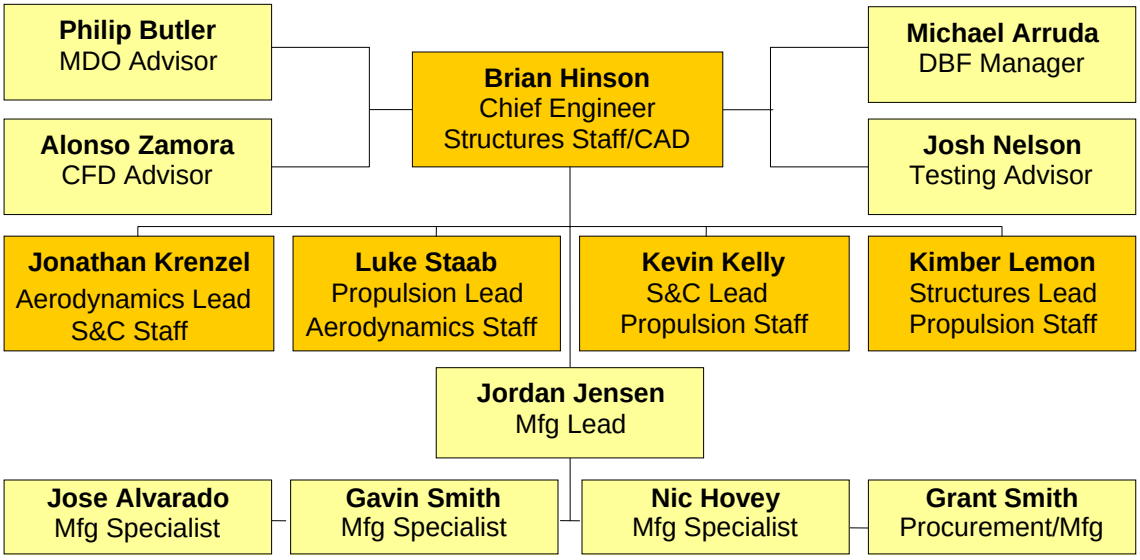

Figure 2.1 – Team Organizational Structure

Each core discipline is responsible for relevant aircraft parameters and developing analysis tools to support design. All core team members also hold cross-functional roles that help facilitate team communication and promote collaborative design decisions. The primary engineering groups and corresponding responsibilities are as follow:

- **Chief Engineer**: Responsible for organizing design optimization architecture. Tracks progress, assists all disciplines with design work, and promotes interdisciplinary communication.
- **Aerodynamics**: Responsible for selecting and designing wing, airfoil, and fairing geometry. Works with graduate CFD advisor to analyze wing and airfoil performance. Collaborates with S&C to conduct wind tunnel tests.
- **Propulsion**: Develops tools to analyze propulsion system performance. In charge of motor, gearbox, propeller, and battery selection. Collaborates with aerodynamics and S&C to predict aircraft performance.
- **S&C**: Calculates longitudinal and lateral/directional stability derivatives and predicts aircraft static and dynamic stability. Responsible for control surface sizing and placement. Works with aerodynamics and propulsion to predict aircraft performance. Directs wind tunnel testing.

- **Structures**: Responsible for designing primary structure and selecting materials. Calculates loads, stresses, and deformation. Develops CAD model and maintains mass properties database.

2.2 Design Schedule

An aggressive schedule, with key deadlines and design reviews, maintains a competitive focus. A Gantt chart tracks design, manufacturing, testing, and report progress (Figure 2.2).

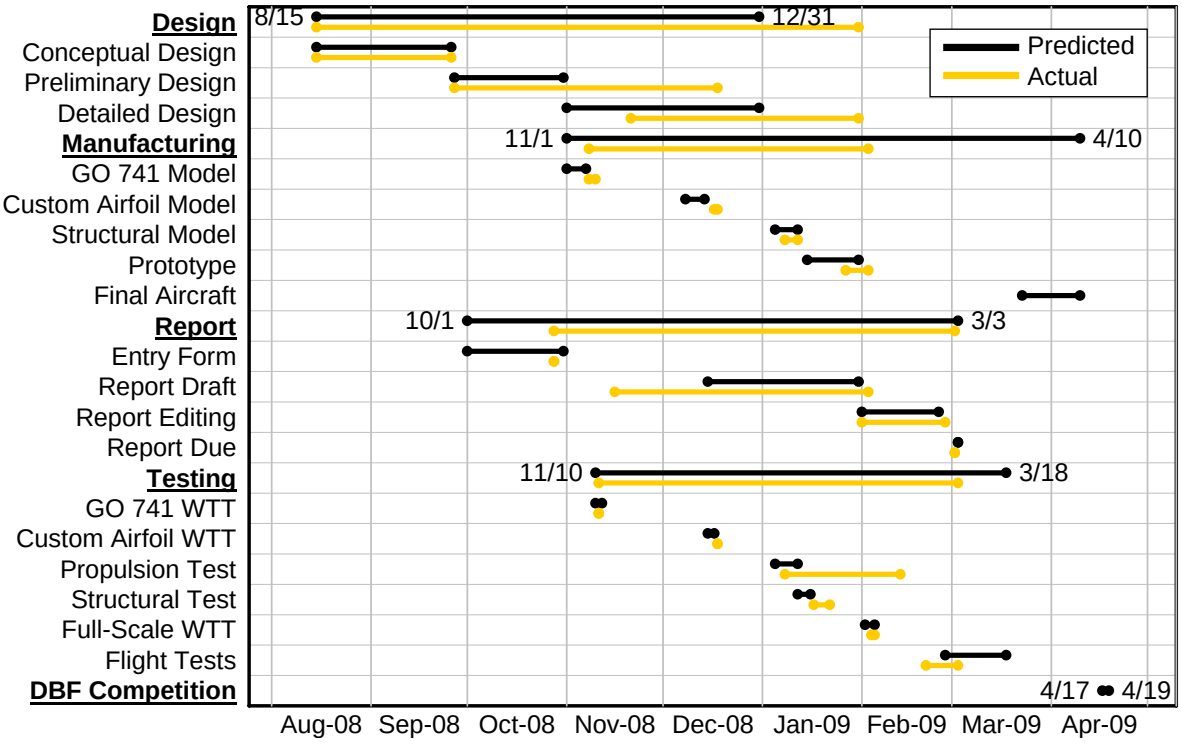

Figure 2.2 – Design Schedule

3.0 Conceptual Design

The 2008-2009 DBF contest rules[1] outline a ground mission and three flight missions. These mission constraints define competitive design requirements. FOM analyses determine the optimum vehicle configuration.

3.1 Mission Requirements

Total score is directly proportional to written report score and the sum of each mission's normalized flight score. Each normalized flight score is directly proportional to SCF as defined in §3.1. Contest-specified mission and vehicle requirements are as follows:

- Maximum battery weight of 4 lbs (only NiCad or NiMH batteries)
- 40 Amp (slow-blow fuse) current limit
- Maximum takeoff distance of 100 ft
- Maximum of two storage boxes with maximum exterior dimensions of 2x2x4 ft
- Any side of the box must withstand a 6 in drop onto pavement without damage to contents

- A 4 L centerline (15 in maximum faired length) tank serves as a simulated fuel tank store
- Four Estes Patriot rockets (ballasted to 1.5 lbs each) serve as wing-pylon mounted stores
- The inner rockets mount at least 24 in outboard of the aircraft centerline and the outer rockets mount at least 6 in outboard of the inner rockets
- All payloads must be mounted outside of the aircraft OMLs and be remotely releasable

Ground Mission

RAC is defined as the total system weight, including the storage boxes, flight vehicle with heaviest single battery pack, all assembly tools, flight equipment, and flight weight payloads[1].

Timed assembly begins when the storage boxes are first opened and is complete when all stores are mounted on the flight ready vehicle and all unused components are secured back in the storage boxes. Rules require propulsion battery and stores to be uninstalled prior to assembly. The vehicle is checked to verify that all control and propulsive systems are working. A wing tip lift test is conducted to verify the vehicles structural integrity with the aircraft configured for the maximum payload. SCF is determined as: **SCF = 1/(Assembly Time * RAC)** and is normalized to a maximum of 10.

Mission 1: Ferry Flight

The aircraft is configured with an empty centerline tank store. Flight time begins when the throttle first advances and ends with a flyover finish after the completion of two laps of the flight course shown in Figure 3.1. Aircraft must land on runway to receive a score. **Score = SCF/(Flight Time)**, normalized to a maximum of 50 points for all aircraft successfully completing mission.

Mission 2: Surveillance Flight

The aircraft takes off and flies four laps of the flight course while configured with a full (4-L water) centerline tank store. Aircraft completes a successful runway landing to receive a score. **Score = SCF**, normalized to a maximum of 75 points for all aircraft successfully completing mission.

Figure 3.1 – Course Diagram[21]

Mission 3: Store Release / Asymmetric Loads

After a timed loading of rocket stores the aircraft completes a set of three stores releases and four laps of the flight course. Loading time begins with stores secured in storage boxes and ends with four

rocket payloads mounted to aircraft and all unused stores and tools re-secured in the storage boxes. A shake test is performed to verify that no stores release prematurely. The aircraft takes off and flies a complete lap, lands and taxis to a 10 ft square area, releases a rocket store (in the order specified by flight judges) and comes to a complete stop on the runway. **Score = SCF/(Loading Time)**, normalized to a maximum of 100 points for all aircraft successfully completing mission.

3.2 Competition Scoring Analysis

Total Score is the product of Report Score, SCF, and Flight Score (Eq 3.1).

$$\text{Total\_Score} = \text{Report\_Score} * SCF * \left(\frac{50}{t_{ferry}} + 75 + \frac{100}{t_{load}} \right) \qquad \textbf{(Eq. 3.1)}$$

Maximizing report score is imperative to increasing total score. Initial flight queue order is based on report score ranking, which provides the opportunity to fly in calm weather. A survey of historical competition data[3] determines nominal values for this year's scoring parameters. Sensitivity studies, performed with the Kline-McClintock method[4], quantify each parameter's effect on total score. Ultimately, scoring analysis results in the determination of realistic and competitive design requirements and constraints.

Input Parameter	Nominal Value	Percent Effect on Flight Score
RAC	30 lbs	45.7%
Assembly Time	15 sec	45.7%
Ferry Flight Time	90 sec	0.3%
Loading Time	6 sec	8.3%

Table 3.1 – Flight Score Sensitivity Study Results

Percent change analysis is also performed to validate the results in Table 3.1. Each input parameter is varied independently to assess its overall impact on FS (Figure 3.2). Each trendline validates the respective percent effects determined via the Kline-McClintock method. RAC and assembly time are the most influential factors in flight score.

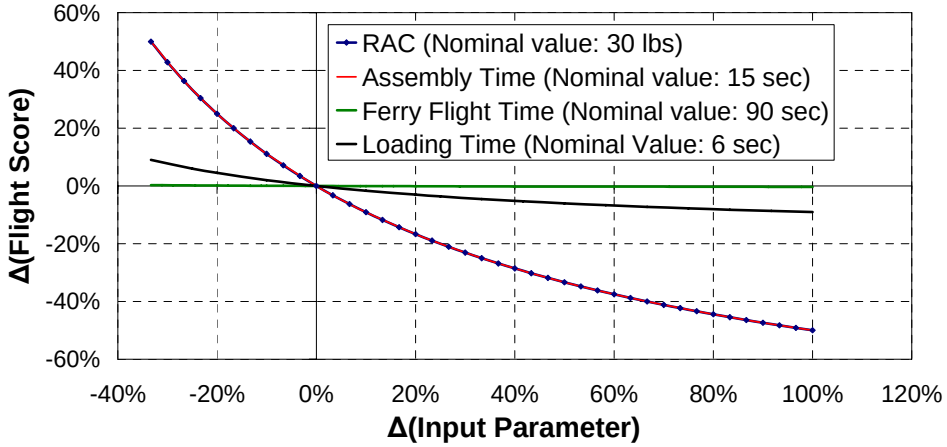

Figure 3.2 – Scoring Sensitivity Study (Percent Change Method)

3.3 Competitive Design Requirements

Competitive scoring analysis results determine a combination of requirements for a winning design:

- **RAC < 25 lbs**: Flight score improves by over 25% for RAC values at least 18% below the nominal value. Total score is most sensitive to decreasing RAC (Figure 3.2). Payload alone contributes approximately 15 lbs to RAC, leaving only 10 lbs for the aircraft, propulsion system, batteries, transmitter, assembly tools, and storage box. This goal is feasible with an unloaded flight ready aircraft weighing less than 4 lbs.
- **Assembly Time < 12 seconds**: Percent change in assembly time carries the same weight in total score as an equivalent percent change in RAC. By the same rationale, a competitive assembly time would be at least 18% below the nominal value (Figure 3.2).
- **Ferry Flight Time < 120 seconds**: Ferry flight time is negligible (Table 3.1). Ultimately, completion is Mission 1's only requirement. Thus, a high cruise speed is a secondary goal, though increasing cruise speed results in decreased wing area and weight.
- **Loading Time < 5 seconds**: FS significantly improves for loading times at least 15% less than the nominal value (Figure 3.2). Additionally, loading time is coupled with assembly time, which reinforces the significance of expeditious stores attachment.

3.4 Conceptual Design Selection Process

Success throughout the design process relies on careful conceptual design. As a result, the design schedule (Figure 2.2) allows significant time to determine the most viable concept. Objective criteria are established for an analytical design selection process. Evaluation of the competitive design requirements (§3.3) results in the following FOMs and their respective weightings:

- **System Weight (30%)**: Scoring sensitivity studies (Figure 3.2) demonstrate RAC's significance in competition scoring. Reducing the total system weight is pivotal to contest success. Historical data[3] are used to estimate aircraft weight for each conceptual configuration. Storage box weight is also a significant factor in RAC, thus it is considered during conceptual design.
- **Assembly Time (30%)**: Scoring sensitivity studies (Figure 3.2) demonstrate that assembly time is equally important to RAC for score determination. Reducing assembly time by several seconds is significantly easier than reducing RAC by several pounds, and is historically[3] a competitive edge for many teams.
- **Storage Options (10%)**: A concept with versatile storage options minimizes storage box size and weight, facilitating assembly.
- **Ground Handling (10%)**: An aircraft capable of consistent, precise, and efficient taxiing is necessary for Mission 3, which requires a set of three stores releases in specific locations[1].
- **Ease of Manufacturing (10%)**: Competition day rebuilds are common and demand an aircraft that can be re-assembled or rebuilt quickly.
- **Drag (10%)**: Drag reduction decreases battery capacity requirements and ultimately lowers total system weight.

A two-stage selection process (screening followed by scoring) utilizes an FOM analysis to pick a competitive conceptual configuration. Other vital design components are similarly selected.

3.5 Configuration Selection

Initial screening considers 22 team-developed concepts. Each concept is screened with a +/- rating for each FOM in §3.4. Scoring analysis is then performed on the most positively rated concepts. Subsequent down-selections and concept combinations result in five viable configuration concepts.

The conventional monoplane is chosen as the baseline configuration. The FOM analysis considers a five-point scale, where 1 = Poor, 2 = Below Baseline, 3 = Baseline, 4 = Above Baseline, 5 = Superior. Assigning point values to the concepts' FOMs determines the best of the following configurations:

- **Conventional** (baseline): A monoplane with a boom-mounted empennage and no fuselage. A conventional low-mounted horizontal stabilizer and a single vertical stabilizer comprise the tail. This concept is relatively simple to manufacture and assemble.
- **Elliptical**: A conventional concept with an elliptical wing planform. Increased wing efficiency reduces drag and lessens propulsion system requirements. However this concept is extremely difficult to manufacture.
- **Flying Wing**: A tail-less configuration with elevons used for longitudinal and lateral control. This concept is typically the lightest configuration for a given payload requirement[5]. Assembly time is potentially reduced, since the aircraft can be stored in a single, hinged piece.
- **Inverted V-Tail**: A conventional concept with twin-boom mounted inverted v-tail empennage. Despite upsizing requirements[6], tail area is reduced, resulting in decreased drag. However the twin-boom prohibits lightweight taildragger landing gear.
- **Gull Wing**: A flying wing with inboard anhedral and outboard dihedral. The centerline tank fits closely under the wing, resulting in shorter landing gear and thus improves ground handling stability. Conversely, weight increases due to gull joint structural requirements.

Figure 3.3 presents the scoring analysis results for the five concepts listed above.

Figure of Merit	Weight	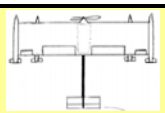 Conventional	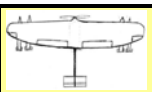 Elliptical	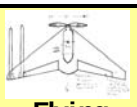 Flying Wing	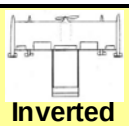 Inverted V-Tail	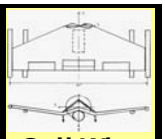 Gull Wing
System Weight	30	3	4	5	4	2
Assembly Time	30	3	3	3	3	3
Storage Options	10	3	3	4	3	4
Ground Handling	10	3	3	3	2	4
Ease of Mfg.	10	3	1	2	3	2
Drag	10	3	5	4	3	2
Total	100	300	330	**370**	320	270

Figure 3.3 – Concept Configuration FOM Analysis

The flying wing wins the initial FOM analysis due primarily to its weight and drag advantages. Sensitivity studies of the initial analysis are performed by diminishing extremum values (e.g. setting 5's to

4's and 1's to 2's), confirming the flying wing's superiority in all cases. The flying wing is, therefore, selected as the conceptual design configuration.

3.5.1 Propeller Location Selection

Once the flying wing configuration is chosen, motor/propeller number and placement are considered. An FOM analysis is performed to compare four configurations. A single motor and tractor propeller is chosen as the baseline configuration for the analysis. Point values are assigned to each configuration's FOMs to determine the most viable:

- **Single Tractor** (baseline): A conventional single motor/propeller configuration. This system benefits from being lightweight and is less prone to propeller strikes. However, this configuration produces a negative pitching moment (due to the negative vertical CG shift) during any payload mission, which makes rotation during takeoff more difficult.
- **Single Pusher**: A single motor/propeller configuration with an aft placement. This system also benefits from being lightweight. However, propeller ground clearance is an issue. The motor is pod mounted, which incurs extra structure and potentially offsets weight savings.
- **Dual Tractor**: A dual motor/propeller configuration with motors mounted on the wings. Advantages include smaller propellers to achieve the required takeoff thrust. Landing gear is shorter and lighter as a result, but the weight savings are minimal due to the dual motor configuration's inherent weight increase. Also, additional control considerations are required in the event of an engine failure.
- **Dual In-Line**: A combination of a tractor and a pusher propeller mounted along the centerline. Smaller propellers result in shorter, lighter landing gear, but dual motors offset these weight savings. However, motors are positionable to eliminate thrust/pitching moment coupling.

Figure 3.4 presents the scoring analysis results for the four concepts listed above.

Figure of Merit	Weight	 Single Tractor	 Single Pusher	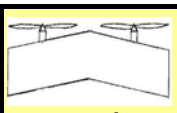 Dual Tractor	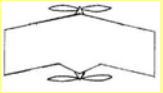 Dual In-Line
System Weight	50	3	2	2	2
Storage Options	10	3	3	4	2
Ease of Mfg	10	3	3	2	2
Pitching Moment Coupling	10	3	3	3	4
Drag	20	3	3	2	3
Total	100	**300**	250	230	240

Figure 3.4 – Propeller Location FOM Analysis

The single tractor, single motor configuration wins the FOM analysis. The single tractor benefits from being simple and light, requiring no extra structural weight for the longer landing gear necessary to avoid prop strike.

3.5.2 Landing Gear Selection

The Mission 3 ground handling requirements drive critical landing gear design parameters. Three concepts are selected as viable solutions.

- **Taildragger** (baseline): Taildragger gear is lightweight and has a small frontal area, due to its small tail wheel. In addition, the taildragger configuration permits high incidence angles, thus decreasing takeoff distance. However, taxiing instability can result in ground loops[6], which unnecessarily wastes battery capacity.
- **Tricycle**: Tricycle gear has prevalent nose gear in lieu of very small tail gear. Nose gear protrusion increases system weight and drag, but ground handling greatly improves through the employment of nosewheel steering.
- **Bicycle**: Two centerline gear are accompanied by a smaller outrigger gear, which balances the aircraft during taxiing. Weight and drag are comparable to tricycle gear, but wobbly ground handling can lead to difficult maneuvering during taxis and store releases.

Each gear style is analyzed for its effect on system weight, ground handling, and drag. A very large weighting is given to ground handling because it is the primary purpose of landing gear, while weight and drag are design consequences. Figure 3.5 presents FOM analysis for the three above gear styles:

Figure of Merit	Weight	 Taildragger	 Tricycle	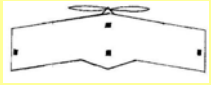 Bicycle
System Weight	40	3	2	1
Ground Handling	50	3	5	2
Drag	10	3	2	2
Total	100	300	**350**	160

Figure 3.5 – Landing Gear FOM Analysis

Despite the advantages of taildragger gear in weight and drag, tricycle gear wins the FOM analysis. Tricycle gear is selected for the conceptual design, due to its dependability in ground handling.

3.5.3 Vertical Stabilizer Selection

Mission 3's asymmetric loading requirements make crosswind a significant factor. Ideally, directional stability is achieved with minimal deflection of lightweight control surfaces. Additionally, control surfaces cannot interfere with payloads during deflection. These additional requirements merit the addition of two vertical stabilizer selection FOMs to the typical criterion:

- **Moment arm**: The distance from aircraft CG to stabilizer AC. Longer moment arms generate a larger moment with less control surface deflection, providing a significant advantage in Mission 3.
- **Interference**: An indicator of how much freedom the stabilizer leaves for payload locations.

The following five concepts are scored via FOM analysis:

- **Twin mid-span** (baseline): Two vertical stabilizers are mounted mid-span on each wing.

- **Centerline**: One large vertical stabilizer is mounted along the aircraft centerline. Moment arm is small, but propwash increases control surface dynamic pressure. No payloads are restricted.
- **Drooped**: Winglets oriented downward. Proverse yaw-roll coupling occurs[9], but interference exists with rocket payloads mounted near wingtips, requiring a slight increase in wingspan.
- **Endplates**: Winglets reflected about the wing chordline. Outboard rocket interference exists.
- **Winglets**: Similar to drooped vertical stabilizers or endplates. Payloads are not obstructed and (as with drooped verticals and endplates) induced drag is reduced via endplate effect.

Figure 3.6 presents the scoring analysis results for the five concepts listed above.

Figure of Merit	Weight	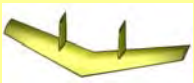 Twin Mid-Span	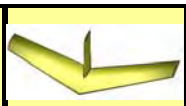 Centerline	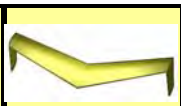 Drooped	 Endplates	 Winglets
System Weight	30	3	3	4	3	4
Moment Arm	25	3	2	4	4	4
Interference	20	3	4	2	2	3
Drag	15	3	3	4	4	4
Ease of Mfg	10	3	3	4	4	4
Total	100	300	295	360	330	**380**

Figure 3.6 – Vertical Stabilizer FOM Analysis

Upright winglets are chosen for their long moment arm, significant reduction of induced drag, and lack of interference with outboard rocket payloads. Additionally, manufacturing is simplified by modular design, with endplates attaching directly to the wingtips.

3.5.4 Wing Assembly Method Selection

Maximum storage box dimensions limit stored wingspan to four feet. However, Mission 3 payload spacing requires a five-foot minimum wingspan[1]. This dichotomy necessitates consideration of assembly methods during conceptual design. The following five concepts are scored via FOM analysis:

- **Single Slide-In** (baseline): One outboard wing is attached via alignment pins/clips.
- **Double Slide-In**: Both outboard wings attach to center section. Separated parts result in smaller storage box size, which reduces system weight.
- **Angled Pivot**: Outboard wing sections contact the inboard section on an angled butt joint. Connection occurs via rotation about a pin normal to this angled joint. Assembly time is decreased, but the mechanism's precise angles make it very difficult to manufacture.
- **Single Hinge**: One outboard wing section rotates about a hinge axis parallel to the wing centerline. The aircraft is stored as a single piece, thus reducing assembly time.
- **Double Hinge**: Both outboard wings rotate on hinge axes parallel to the wing centerline. System weight is reduced due to wing folding, while single part storage reduces assembly time.

Figure 3.7 presents the scoring analysis results for the five concepts listed above.

Figure of Merit	Weight	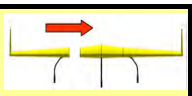 Single Slide-In	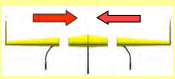 Double Slide-In	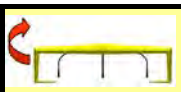 Angled Pivot	 Single Hinge	 Double Hinge
System Weight	40	3	4	2	3	4
Assembly Time	50	3	3	4	4	4
Ease of Mfg	10	3	3	1	2	2
Total	100	300	340	290	340	**380**

Figure 3.7 – Wing Assembly FOM Analysis

FOM analysis shows the double hinge as the best concept. This alternative permits the same storage box downsizing seen with separable parts, while maintaining the single part's quick assembly time.

3.6 Selected Conceptual Design

The selected conceptual design (Figure 3.8) is a flying wing with tricycle landing gear, winglets and a single tractor propeller. Wing hinges are chosen to accommodate the maximum box size. This design is selected for its potential to fulfill the competitive design requirements.

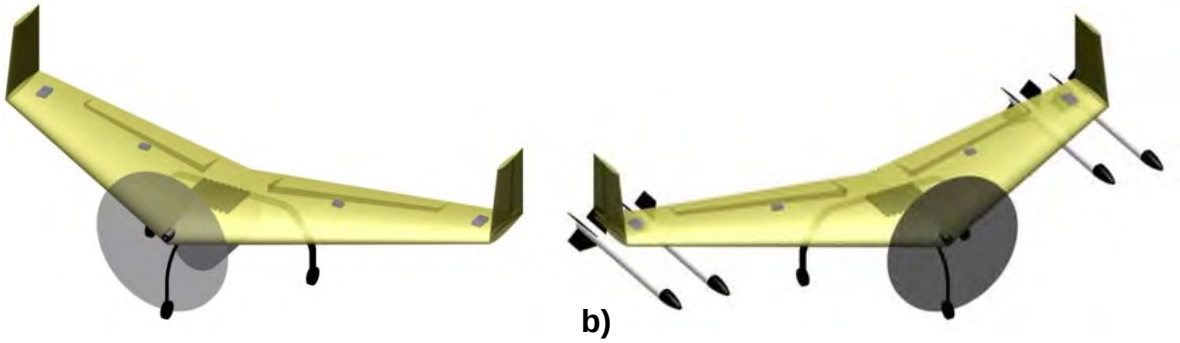

a) **b)**

Figure 3.8 – Conceptual Layout Model for a) Missions 1 & 2 and b) Mission 3

4.0 Preliminary Design

The preliminary design process begins with initial aircraft sizing, which is used to develop the aerodynamic, flight mechanic, propulsive, and structural characteristics of the aircraft. Trade studies are then conducted to evaluate competitive design alternatives. Finally, each core engineering discipline performs a synthesized optimization based on trade study results, and determines revised performance predictions.

4.1 Critical Design Parameters

Competitive design requirements (§3.4) drive the analyses of the selected design. Weight reduction leads to tight constraints on performance parameters. Each core engineering discipline assesses the conceptual design to determine the specific critical design parameters.

Aerodynamics Critical Parameters

- **Airfoil:** Airfoil selection is the most critical aerodynamic design parameter. A flying wing benefits from an airfoil with minimal negative pitching moment, which reduces control surface workload. A high lift airfoil reduces takeoff distance but increases cruise drag. Conversely, a low drag airfoil reduces battery capacity requirements, but also reduces lift.
- **Wing Area:** The takeoff distance requirement drives wing sizing. On one hand, increasing wing area reduces wing loading and helps to reduce takeoff distance. On the other hand, it also increases aircraft weight and drag, which both require more energy from the propulsion system.
- **Wing Span:** Wing span plays a crucial role in aerodynamic performance as it determines several parameters, such as wing aspect ratio. However, the trade-off for the aerodynamic benefit is increased structural weight. The optimal combination of wing span and wing area must be achieved to maximize aircraft performance.

S&C Critical Parameters

- **Static Margin:** Flying wings are inherently more sensitive to pitch disturbances than conventional tailed aircraft. Thus, selection of an appropriate static margin (SM) is crucial to preliminary design efforts. Ultimately, the SM provides a balance between minimizing pitch sensitivity and minimizing control surface deflections for trim. Appropriate SM values range from 5% to 15%, as determined from extensive flying wing flight test experience[5]. Additionally, the SM should not be so large as to require longitudinal control surface deflections beyond 20 degrees for trim. This constraint comes from a survey of historical data demonstrating control surface effectiveness as a function of deflection angle[10].
- **Wing Sweep:** Longitudinal trim and CG shift capabilities rely on proper selection of sweep direction and magnitude. According to Nickel[5], unswept flying wings are capable of longitudinal stability, but are extremely sensitive to pitch and inflexible to shifting CGs. Forward-swept flying wings are beneficial to takeoff distance, as they can trim out a nose-down pitching moment while increasing lift (control surfaces forward of CG), but have a high susceptibility to structural divergence[6]. Finally, aft-swept flying wings provide a balance between CG flexibility and structural integrity, but must decrease lift in order to trim out a nose-down pitching moment
- **Control Surface Location and Sizing:** Control surface deflections are limited to 20 degrees, based on the linearized method of Roskam[9], which predicts significant separation drag at larger angles. Control surfaces must hinge at the aft spar for structural redundancy. Span is limited by wing storage mechanisms that must exist to meet box dimension constraints. Control surface AC's must be located as far as possible from the CG (both longitudinally and laterally) in order to reduce control surface deflections for Mission 2 longitudinal trim and Mission 3 lateral trim.
- **Thrust/Pitch Coupling:** A high-mounted propeller has desirable ground clearance, but also increases negative pitching moment (due to vertical CG shift in payload missions), which

demands greater control surface deflections for longitudinal trim. Minimization of thrust/pitch coupling is beneficial, as demonstrated by design optimization (§4.6.2).

Propulsion Critical Parameters

- **Motor:** Total aircraft weight and power requirements influence motor selection. Contest rules[1] specify that only off-the-shelf, non-modified brushless or brushed electric motors are allowed. Brushless motors are preferred because they provide greater efficiency and are generally lighter than brushed motors[17]. In-runner or out-runner brushless motors are viable. In-runner motors are lighter, but result in increased part count, since a gearbox is required to satisfy system power requirements. Out-runner motors do not require a gear reduction, but are typically heavier[14].
- **Battery Cell Type, Capacity and Quantity:** The contest rules limit battery chemistry to either nickel cadmium (NiCad) or nickel metal hydride (NiMH) cells. NiMH cells are preferred to NiCad cells, due to their superior capacity-to-weight ratios[12]. RAC is determined with only the heaviest battery pack used for any individual mission[1], which merits propulsion optimization for the most critical case. The most demanding propulsion requirements are driven by the maximum 100 ft takeoff distance for all missions[1], which requires the largest quantity of battery cells. Mission 2 requires the heaviest payload and is the critical case for takeoff power required. Mission 3 is the critical case for battery capacity required.
- **Propeller:** Propeller selection has a direct effect on current draw and power available. Maximum diameter for the propeller is set at 16" for ground clearance, but the propeller is also sized for the 40 Amp current limit based on contest rules[1]. These requirements constrain propeller selection to those with moderate pitches (8-12 in) and moderate diameters (10-16 in). Initial propeller characteristics are determined using blade element/momentum theory[8]. Actual performance characteristics (thrust, torque, and power coefficients) are obtained from testing performed at WSU by Merchant and Miller[13].

Structural Critical Parameters

- **Spar Location:** A two-spar structural layout is advantageous for all missions. Such a layout permits balanced centerline store attachment and resists torsion due to rocket stores. The main spar is the aircraft's primary load path, and is located at 25% chord because of its proximity to the CP. The aft spar is a secondary load path, and is located to facilitate control surface attachment.
- **Spar Cross-section:** The spar's cross-sectional shape dictates its ability to withstand loads as a function of its section properties. Spar cross-sectional dimensions are limited by the airfoil thickness. Thus, various cross-sectional shapes must be considered to obtain the desired properties while minimizing structural weight.
- **Material Selection:** Lightweight materials are selected to fulfill the specific design requirements of each structural layout element. Availability and manufacturability of materials are imperative.
- **Wing Attach Location**: Structural layout, storage box configuration, and control surface span are constrained by wing attach location.

4.2 Mission Model

Each flight mission is modeled in four phases: T/O, climb, cruise, and turns (180 degree and 360 degree). Additionally, taxiing is considered for Mission 3.

- **Takeoff** - S_{LO} is calculated using a finite integration method based on the thrust curve and trimmed C_L values[6]. The model assumes a full-throttle setting, a 0.03 rolling friction coefficient and 0 mph wind speed. The AOA is assumed to remain constant at 2 degrees for C_{Dmin}. Rotation occurs when an adequate dynamic pressure is reached for T/O at 8 degrees AOA.
- **Climb** – A full throttle climb to 100 ft is assumed. Time-to-climb is calculated based on mission T/O weight and power available.
- **Cruise** – Level flight is modeled to find cruise speed for minimum thrust required. Mission 1 maintains a full-throttle position for cruise to minimize flight time. Mission 3 maintains full-throttle to maximize propulsion system efficiency. Cruise speed is optimized for a Reynolds number that minimizes drag and reduces battery capacity. Mission 2 implements throttle control to save energy and reduce current draw.
- **Turns** – Turn rates are calculated with a 2.5G load factor and the throttle settings used in cruise. Both the 180 degree and 360 degree turns are modeled using this turn rate.
- **Taxi** – Each Mission 3 taxi assumes a 10 Amp current draw for 15 seconds.

4.3 Optimization Tools and Methodology

A multidisciplinary design optimization (MDO) tool facilitates cross-disciplinary design. Each core engineering discipline programs and maintains modules and interfaces to control its design parameters (§4.1). Critical design variables are managed by a central database, to ensure concurrent design.

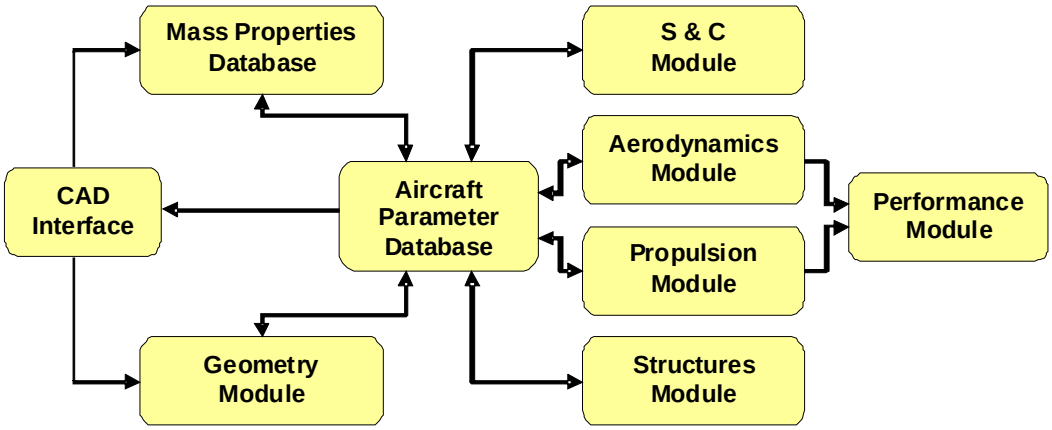

Figure 4.1 – Design and Optimization Architecture

Aircraft Parameter Database: Central design parameter control hub. All optimization modules link their critical parameters to this database, which results in multi-disciplinary optimization.

CAD Interface: Utilizes aircraft parameter database to construct loft and structure layout. Feeds structural mass properties and component locations to the mass properties database. Supplies geometry module with relevant component dimensions and locations.

Geometry Module: A visual representation of the design planform, as determined by unique inputs and linked values from other modules. Control surfaces, spars, landing gear, and components are graphed along with the reference planform to eliminate construction interference. Critical parameters include sweep, span, root chord lengths, and taper ratios for the reference wing and vertical stabilizers. Outputs include sizing values and percent chord sweep angles.

Mass Properties Database: Stores component weights and locations. Outputs include moments of inertia, component weight buildups, CG locations, and SM values for all three missions.

Aerodynamics: The wing's lift, drag, and pitching moment are calculated based upon the selected airfoil and outputs from the geometry module. All aerodynamic performance estimates are calculated using both U.S. Standard Atmosphere[24] and altitude-corrected air density for Tucson, Arizona, assuming no wind and the average April temperature[23] in Tucson plus 5°F. A full aircraft drag buildup is also calculated at flight velocities up to 100 ft/s. The parasite drag term is calculated based on total wetted area using methods outlined in Raymer[6] and Seddon[8]. The induced drag term is calculated based upon each mission's flight velocity and required design C_L. Both terms are combined and the maximum values are used to conservatively calculate the minimum required thrust in the propulsion module.

S&C: Control surface sizing and location, thrust line and angle, landing gear location, bank angles and turn radii, and S&C derivatives are determined and optimized. Longitudinal and lateral-directional trim deflections, as well as turning flight performance parameters are estimated using methods of Roskam[9,10]. Raymer's method[6] is used to locate the landing gear such that nosewheel traction and ease of takeoff rotation are optimized.

Propulsion: The propulsion module stores motor, propeller, gearbox, and battery parameters and determines combinations (motor/gearbox, propeller, number of battery cells) that meet mission requirements. The tool calculates thrust, voltage, current, brake power, and pitching moment due to thrust at flight velocities up to 100 ft/s. The module also calculates S_{LO} as described in §4.2. S_{LO} calculation is validated against performance module results. Figure 4.2 shows the propulsion module flow chart.

The propulsion module includes NiMH batteries[15] from 9 different vendors, 18 motors for both in-runner and out-runner variations[14], 14 propellers of varying diameters (10-16 in) and pitches (8-12 in)[13], and 5 gearboxes (1:1, 3.7:1, 4.2:1, 5.2:1, 6.7:1). The analysis begins with the critical power case, Mission 2. The program determines the most suitable propulsion system for Mission 2, which also sets the motor and gearbox for Missions 1 and 3 (contest rules state motors cannot be changed between missions)[1].

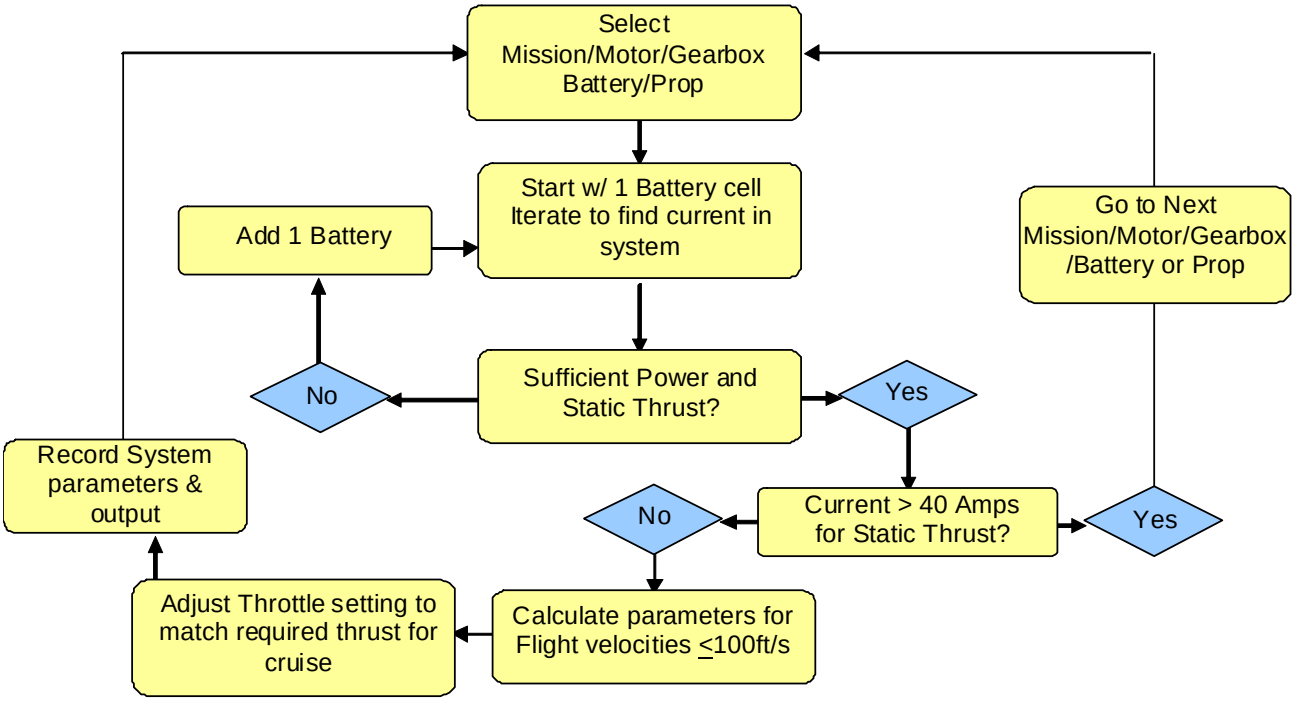

Figure 4.2 – Propulsion Module Flowchart

Structures: Landing gear loads and wing normal stress, shear stress, deflection, and twist are calculated for each mission using methods of Allen and Haisler[11]. This tool optimizes for variations in main and aft spar cross-sections and locations. Dynamic propulsive loads are calculated.

Performance: A tool that estimates takeoff distance based on the methods of Anderson[2] and Raymer[6]. Takeoff estimates determine propulsion system requirements.

4.4 Initial Sizing

Initial weight estimates are performed using Raymer's method[6], with empirical coefficients determined from DBF historical data[3]. Only data for top five teams are considered for coefficient determination, where trends recur in wing loading and aspect ratio. After an initial weight estimate is made, the wing is sized using the takeoff performance equations provided in Anderson[2]. Anderson's method, while simplified, provides an ideal starting point for initial sizing based upon takeoff distance as only a few variables are required.

In addition to parametric weight estimation, historical data[3] provides initial thrust, C_{Lmax}, and C_{Do} estimates. Anderson's assumptions for $V_{takeoff} = 1.2*V_{stall}$ and ground effects are used to calculate lift and drag. Rolling resistance is assumed to be 150% of Anderson's paved surface recommendation[2] to provide conservative results. These variables are then used to obtain the minimum required wing area. Sensitivity studies are performed to determine which variables have the greatest effect on takeoff performance and require the most attention during preliminary design.

Larger spans inherently result in increased weight, due to structural requirements imposed by increased main spar bending moment. Therefore, minimizing span is critical to reducing weight.

However, rocket payload requirements (§3.1) result in a minimum wingspan of 60 inches. Takeoff analyses estimate parametric takeoff weight and distance, where wing span is constant at 60 inches and wing areas vary from 550 in^2 to 825 in^2. Takeoff weight increases linearly with wing area (Figure 4.3a). Therefore, RAC's high percentage in total score (§3.2) necessitates as small a wing as can meet takeoff distance requirements. A conservative 85 ft takeoff distance constraint is set by the design team for initial wing sizing to ensure the aircraft meets contest requirements while still minimizing RAC. Takeoff distances closer to 100 ft are only permitted after the implementation of more sophisticated takeoff analysis tools (§4.2). The 85 ft takeoff requirement results in a wing area of approximately 750 in^2 (Figure 4.3b).

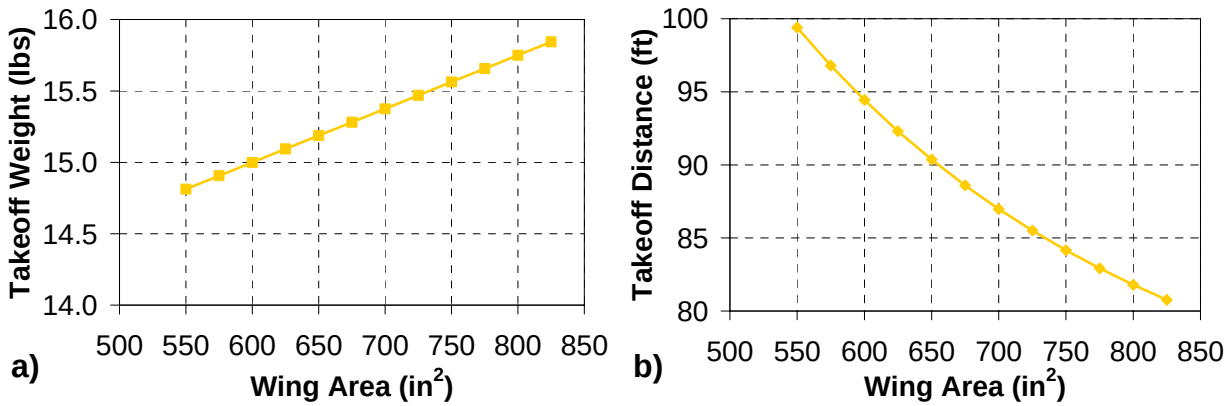

Figure 4.3 – a) Takeoff Weight and b) Takeoff Distance Estimates for Varied Wing Areas

The combination of wing sweep, root chord length, and taper ratio (Table 4.1) is determined based on wing area requirements, maximum storage box dimensions, S&C critical requirements, and aerodynamic performance needs. Wing sweep is constrained by storage box size. However, maximized wing sweep is desired for increased control surface moment arms. Wing span, the largest linear dimension of the aircraft, requires the maximum box length (48 in), which leaves the 24 in dimension for the longitudinal distance from root apex to tip trailing edge. Root chord is set by wing size requirements and maximum box dimensions, while tip chord, and thus taper ratio, is set by vertical stabilizer sizing requirements. Final results of sizing studies are presented in Table 4.1.

Parameter	Value
Area	756 in^2
Leading Edge Sweep Angle	30 deg
Geometric Aspect Ratio	4.76
Effective Aspect Ratio	5.67
Root Chord	18 in
Span	60 in
Taper Ratio	0.4

Table 4.1 – Preliminary Wing Sizing Parameters

4.5 Aerodynamics

After initial sizing, analysis is performed to select the aerodynamic parameters outlined in §4.1.

4.5.1 Airfoil Selection

An airfoil is selected to fulfill the unique requirements of a flying wing (Table 4.2).

Parameter	Requirement	Rationale
c_{m0}	~ 0	Reduce control surface workload for longitudinal trim
$c_{m\alpha}$	~ 0	Decrease control force requirements Increase control surface effectiveness
$c_l (\alpha=8°)$	> 1.1	Takeoff rotation achievable without high lift devices Reduce takeoff thrust

Table 4.2 – Airfoil Selection Requirements and Rationale

A survey of 115 airfoils identifies viable design options, including symmetric, reflexed, and standard airfoils by Gottingen, Hepperle, Eppler, and NACA[7, 28]. After the initial survey, 10 airfoils are selected for further review. These include both symmetric and reflexed airfoils by Gottingen, Hepperle, and NACA. From these, the GO 741 is selected based on the data in Miley[7] (Figure 4.4).

GO 741 wing testing (§7.1) shows payload-induced AC shifts up to 7.5% greater than linearized lifting line theory predictions. Centerline tank interference increased lower surface stagnation, which negated the wing center section "lift valley" common to flying wings[5]. Finally, GO 741 lift performance was 30% lower than predicted (Figure 4.5).

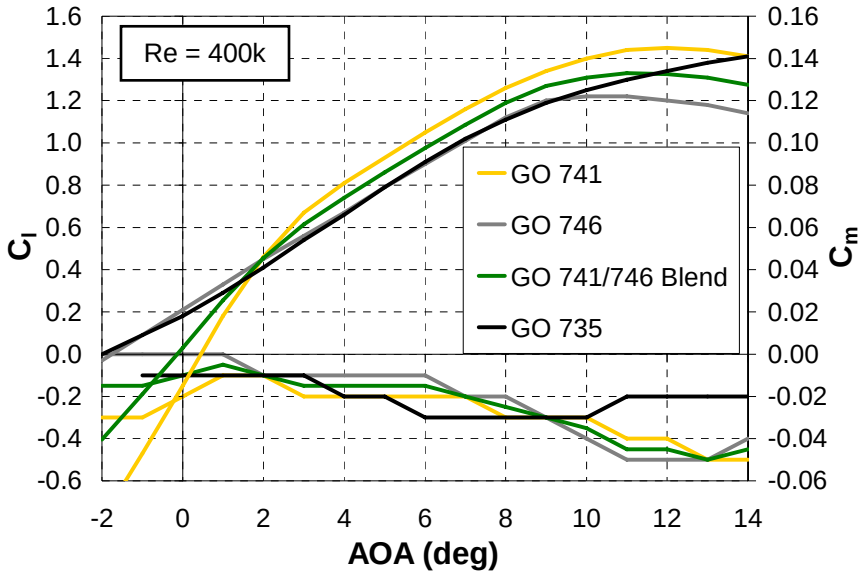

Figure 4.4 – Lift and Moment Polars for Final Four Airfoils

Insufficient performance demonstrated by the half-scale WTT merits a 2-D CFD analysis[25] to better understand the GO 741's performance. The CFD analysis yields results which differ from the published data[7] (Figure 4.6) and, consequently, fail to meet airfoil requirements (Table 4.2). However, predicted 3-D performance correlates closely with wind tunnel results (Figure 4.5). An expanded airfoil survey is

conducted to determine if another airfoil is viable; however, the GO 741 is once again deemed the most appropriate airfoil.

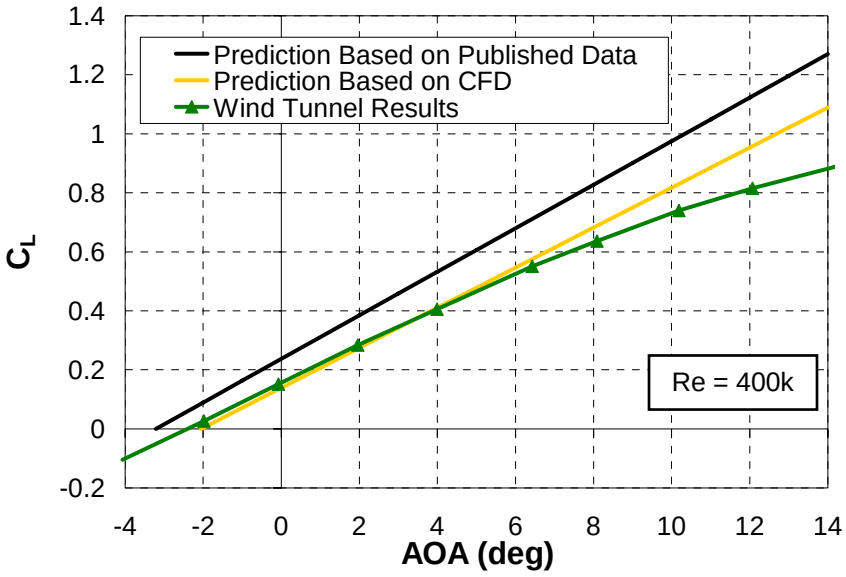

Figure 4.5 – Comparison of 3-D Performance Predictions based on GO 741 Airfoil and CFD Data

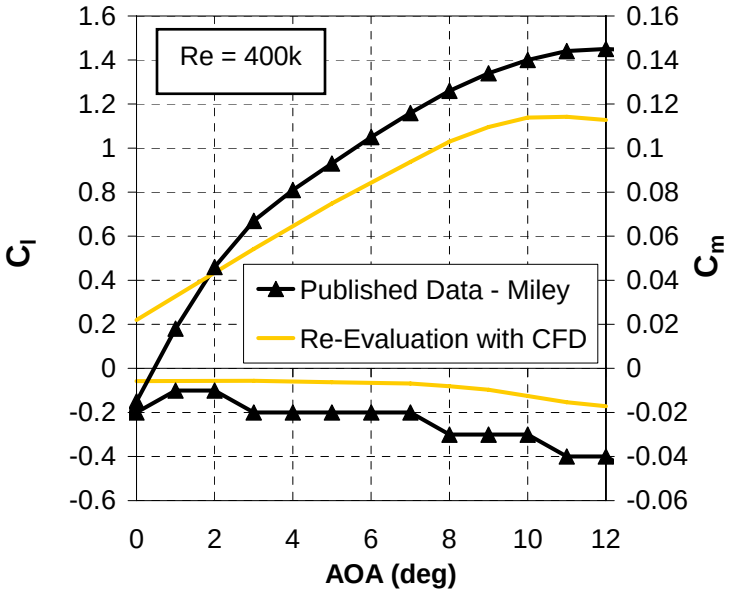

Figure 4.6 – Comparison of GO 741 Published Data to CFD Results

GO 741 performance yields a takeoff distance estimate of 97ft, which exceeds original constraints. A trade study is performed, comparing increases in wing area, wing span, and thrust (Table 4.3).

	Root Chord Increase	Wing Span Increase	Static Thrust Increase
ΔS_{LO} (ft)	5.0	-8.3	-7.0
ΔWeight (lbs)	0.10	0.19	0.051

Table 4.3 – Results of Wing Sizing/Thrust Increase Trade Study

Increasing wing area via a root chord increase alone proves to be ineffective, lengthening the takeoff distance by 5 ft and adding 0.10 lbs to the total aircraft weight. Both the static thrust increase and the wing span increase are viable options. The wing span increase results in an 8.3 ft decrease in takeoff distance, but an additional 0.19 lbs in total system weight. Increasing the static thrust decreases takeoff distance by 7.0 ft, but adds only 0.051 lbs to the aircraft weight. Although the study yields acceptable results, a more optimal solution is desired. Therefore, an airfoil trade study is conducted.

DBF aircraft normally operate in a narrow aerodynamic range (small difference between cruise and takeoff velocities), facilitating the design of an airfoil to meet design requirements throughout the flight regime. A fixed design point is specified using a takeoff Reynolds number of 300,000 and a design cruise Mach number of 0.05. A NACA 8-H-12 airfoil is selected as the starting airfoil due to its positive pitching moment and constant pitch stiffness[28] and is modified using XFOIL[27] to meet the design requirements. Camber, thickness, leading-edge radius, camberline, maximum thickness location, and maximum camber location are optimized to maximize lift and positive pitching moment (Figure 4.7).

Figure 4.7 – GO 741 and Custom Airfoil Cross Section Comparison

CFD analysis[26] is utilized to examine the final custom airfoil design at the same conditions as the GO 741. XFOIL[27] and 2-D CFD[25,26] results are reviewed and CFD comparisons are presented in Figure 4.8. CFD results are verified using half-scale WTTs (§7.1) and the custom airfoil is subsequently selected.

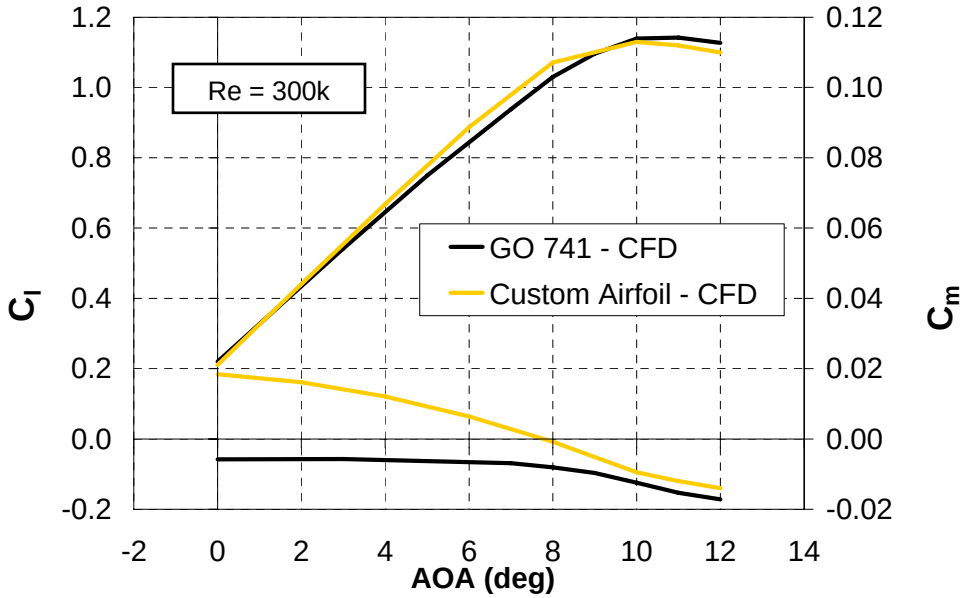

Figure 4.8 – Lift and Moment Polars for GO 741 and Custom Airfoil

4.5.2 Aerodynamic Performance Predictions

Preliminary aerodynamic performance predictions are based on airfoil data and parasite drag buildup (Figure 4.9 and Figure 4.10).

Parasite Drag Buildup		
Component	**C_{Do}**	**% of total**
Wing	0.0175	44%
Vertical Stabilizer	0.0034	8%
Centerline Tank	0.0090	23%
Landing Gear/Wheels	0.0100	25%
Total	**0.0399**	100%

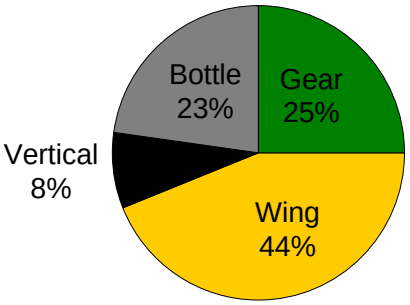

Figure 4.9 – Parasite Drag Buildup

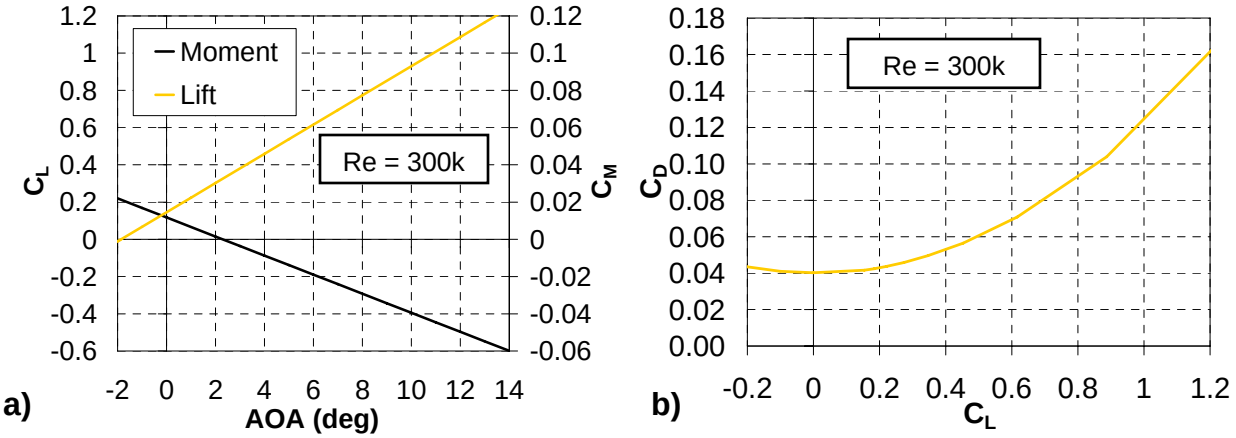

Figure 4.10 – Predicted Mission 2 a) Lift and Moment (about CG) Polars and b) Drag Polar

4.6 Stability and Control

Airfoil performance characteristics drive the selection and sizing of control surfaces to meet static S&C requirements (§4.1).

4.6.1 Control Surface Sizing and Placement

Initially, longitudinal control surface selection is based on lessons learned from past WSU flying wing design efforts[22], which utilize wingtip elevons and a center section control surface dubbed a “platypus” (Figure 4.11). This control surface combination is designed to negate losses in lift during a flying wing takeoff rotation. All control surfaces are modeled as plain flaps using the method of Roskam[10]. The platypus is sized with a 30% chord and span from wing root to wing attachment location. Elevons are sized for the critical longitudinal trim case (Mission 2 takeoff), which yields a 30% chord, spanning from 50% wing semi-span to wingtip. Sizing for Mission 2 longitudinal trim inherently satisfies the critical lateral trim case (Mission 3 with two rockets on one wing), which proves to be less demanding.

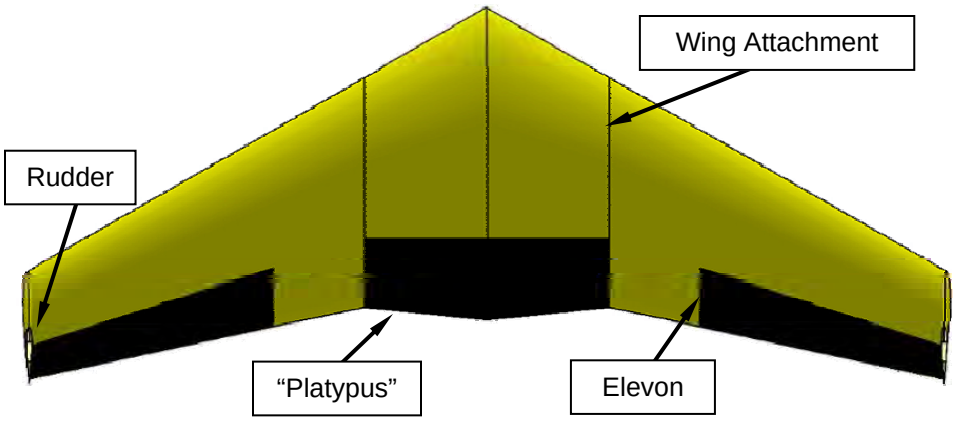

Figure 4.11 – Initial Control Surface Selection

Wind tunnel testing is performed on a half scale model with deflectable split flaps (§7.1) to validate control surface effectiveness predictions. Figure 4.12 demonstrates the range of resulting lift coefficients after control surfaces are deflected for longitudinal trim.

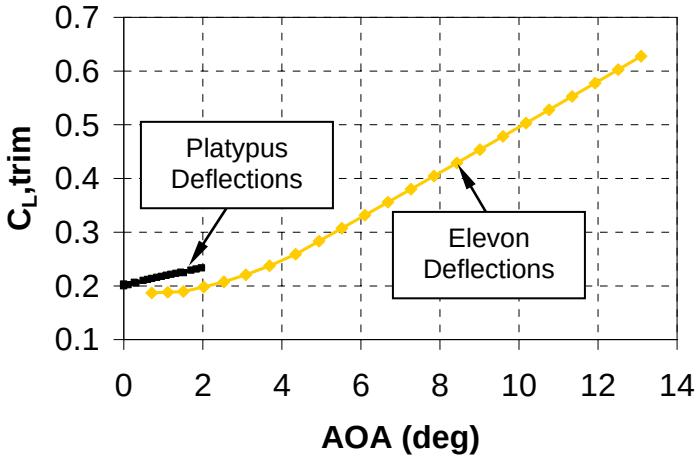

Figure 4.12 – Comparison of Control Surface Effectiveness

The platypus' ineffectiveness in longitudinal trim is primarily attributed to its short moment arm and the centerline store's flow disturbance. Thus, elevons are chosen as the sole longitudinal trim device, while elevon/rudder mixing is chosen for lateral/directional trim. A fixed platypus is retained, increasing wing area without incurring additional weight in the spar or storage box.

The custom designed airfoil results in reduced negative pitching moment for given lift coefficient values. This yields reduced control surface deflections for longitudinal trim, doubling of maximum trimmed lift coefficient, and increased range of trimmable AOAs (Figure 4.13).

Vertical stabilizers are sized based on methods of Raymer[6], where the largest recommended area is beneficial to increasing crosswind stability, though dutch roll is more prominent[9]. Fifty-percent chord rudders are sized for increased control authority in crosswind, based on past WSU DBF experience[17,21].

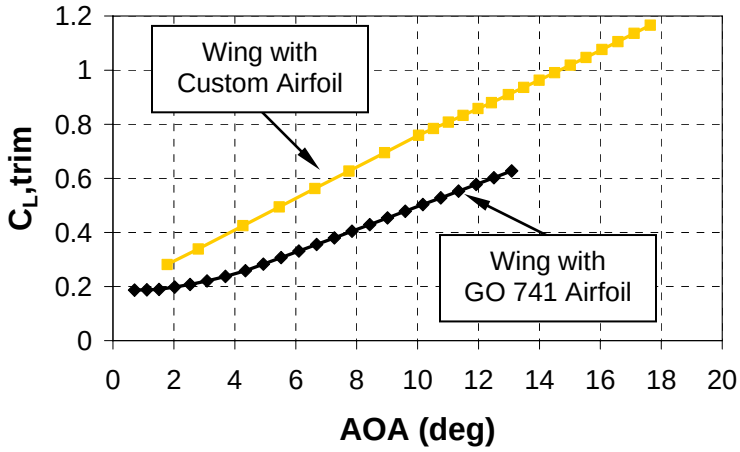

Figure 4.13 – Performance Comparison for Custom Airfoil and GO 741

4.6.2 Thrust/Pitch Coupling

Conceptual design places the motor at the wing apex (§3.5.1). However, the fully-loaded centerline tank (Mission 2) moves the total aircraft CG approximately 2.5 inches below the thrust line. Analysis of this configuration results in a significant nose-down pitching moment at takeoff. Significant increases in tail volume for longitudinal trim are not applicable to the flying wing, so pitching moment reduction solutions are assessed.

Analysis of a lowered motor shows reduced negative pitching moment in Mission 2, but further limits propeller diameters. Analysis of thrust line angles inclined to remove Mission 2 thrust/pitch coupling demonstrates a proverse effect on longitudinal trim for Missions 1 and 3. Figure 4.14 demonstrates that motor inclination provides a larger range of trimmable AOAs as compared to a lowered motor. Performance and longitudinal trim improvements lead to the selection of motor inclination as the most viable solution.

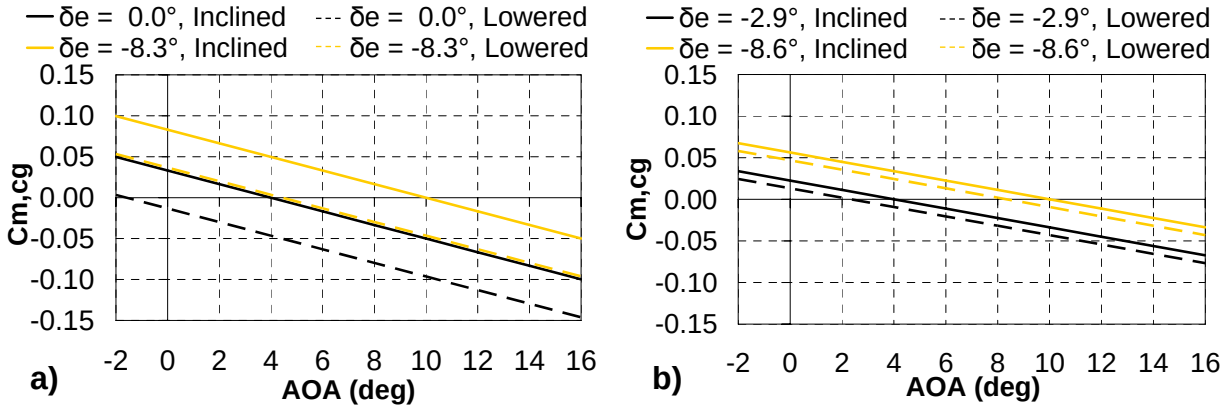

Figure 4.14 – Effects of Thrust/Pitch Coupling Solutions on Trim for a) Mission 1 and b) Mission 3

4.6.3 Stability and Control Performance Predictions

SM values for each flight mission are listed in Table 4.4, where AC locations for bottle and rocket payloads are determined based on half-scale WTT results (§7.1). CG locations for each mission are calculated by the Mass Properties module.

	Mission 1	Mission 2	Mission 3			
Payload	**Empty Tank**	**Full Tank**	**4 Rockets**	**3 Rockets**	**2 Rockets**	**1 Rocket**
AC Location (in)	11.7	11.7	11.7	11.7	11.7	11.7
CG Location (in)	10.8	10.8	10.8	10.8	10.8	10.8
Static Margin	6.7%	6.4%	6.4%	6.4%	6.4%	6.4%

Table 4.4 – Static Margin Values

The S&C module utilizes methods of Roskam[10] and Raymer[6] to estimate trim deflection requirements for each mission's takeoff and cruise segments. Longitudinal trim deflections are well within the 20 degree constraints, as demonstrated in Figure 4.15. Mission 3 payload releases shift the CG upward, which increases pitching moment due to thrust and ultimately reduces trim deflections (Table 4.5).

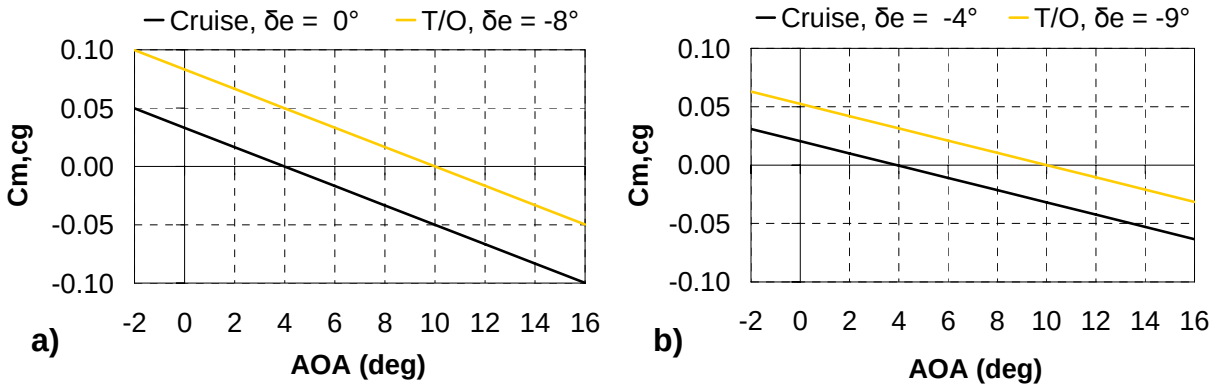

Figure 4.15 – Longitudinal Plots for a) Mission 1 and b) Mission 2

Mission 3 Longitudinal Trim		
Payload	**Cruise Elevon Deflection**	**Takeoff Elevon Deflection**
4 Rockets	-2.9°	-8.6°
3 Rockets	-2.2°	-7.8°
2 Rockets	-1.2°	-6.8°
1 Rocket	0.4°	-5.1°

Table 4.5 – Longitudinal Trim Deflections for All Portions of Mission 3

S&C derivatives (Table 4.6) are estimated using methods of Roskam[10]. Static derivatives are validated by a full scale WTT (§7.4). According to methods of Roskam[10], an 85th percentile[23] (13 knot) crosswind is trimmable for the worst case T/O asymmetric loading (2 rockets on 1 wing), with 20 degrees of differential elevon deflection, and 38 degrees of rudder deflection. Dynamic mode approximations[9] demonstrate high frequency dutch roll and short period modes due to the aircraft's low moments of inertia. Additionally, the spiral mode is unstable. However, handling qualities are acceptable, as judged by the pilot during flight testing (§7.6).

Stability and Control Derivatives for Mission 3 T/O (Critical Lateral/Directional Trim Case)												
$C_{L\alpha}$	3.4883	$C_{M\alpha}$	-0.2549	Cy_{β}	-0.3038	$Cy_{\delta a}$	0	$Cy_{\delta r}$	0.5889	Cy_{p}	-0.0456	Cy_{r}	0.1081
$C_{L,\delta e}$	1.1855	$C_{M,\delta e}$	-0.3460	$C_{l\beta}$	-0.1126	$C_{l\delta a}$	0.2585	$C_{l\delta r}$	0.0349	C_{lp}	-0.3661	C_{lr}	0.1419
C_{Lq}	4.9601	C_{Mq}	-1.0572	Cn_{β}	0.0559	$Cn_{\delta a}$	-0.0057	$Cn_{\delta r}$	-0.1083	Cn_{p}	0.0399	Cn_{r}	0.0071

Table 4.6 – Estimated Stability Derivatives (1/rad) for Mission 3 Takeoff (AOA = 10 deg)

4.7 Propulsion

Preliminary propulsion system design focuses on optimization of battery, motor, gearbox, and propeller combinations using the method specified in §4.2.

4.7.1 Battery Trade Study

Lessons learned from previous WSU DBF teams[17] prompt an evaluation of battery discharge rates. Although the manufacturer's advertised nominal voltage on NiMH cells is 1.2 V[15], the discharge rate has a significant effect on cell voltage[17]. Figure 4.12 shows the available power of three different cells (Elite 1500, Elite 1700, Elite 2000) discharged at 20 Amp and 40 Amp. Power curves are constructed using the initial propulsion configuration efficiencies (APC 14x10 E propeller[13] and a NEU 1506/2.5Y motor[14]).

The results of battery testing (§7.2.1) show that the Elite 1500 cells cannot handle the Mission 2 takeoff current of 40 amps at a usable voltage and are not suitable. Thus, Mission 2 requires Elite 1700 or Elite 2000 cells. While the lighter Elite 1500's are capable of the discharge rates required for Missions 1 and 3, choosing these cells provides no additional benefit. The total flight score only factors in the heaviest battery pack[1] and Mission 2 requires the greatest number of cells due to the takeoff power required. The propulsion module determines that 12 Elite 1700 cells are required for Mission 1, 14 Elite 1700 cells for Mission 2, and 12 Elite 2000 cells for Mission 3.

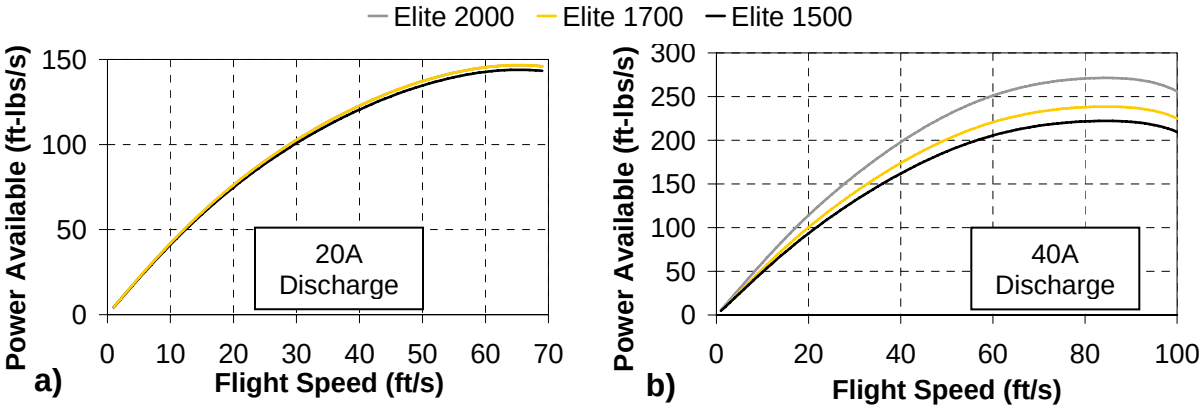

Figure 4.16 – Power Curves for a) Mission 3, 12 cells at 20A and b) Mission 2, 14 cells at 40A

4.7.2 Propeller Optimization

Initially an APC 14 X 10 E propeller is chosen as the optimal solution. Larger diameter propeller data is not available in the desired pitches. The testing method of Merchant and Miller[13] is used to expand WSU's propeller database. APC 15 X 10 E and APC 16 X 10 E propellers are characterized in the WSU 3x4 ft wind tunnel (§7.2.2). Also, the effects of payload blockage on thrust available are assessed for

Mission 2. Results (Figure 4.17) show a negligible improvement in propeller performance with the bottle placed in the slipstream. Thus, the bottle effects are not accounted for in propeller selection analysis. The propulsion system configuration is shown in Table 4.7.

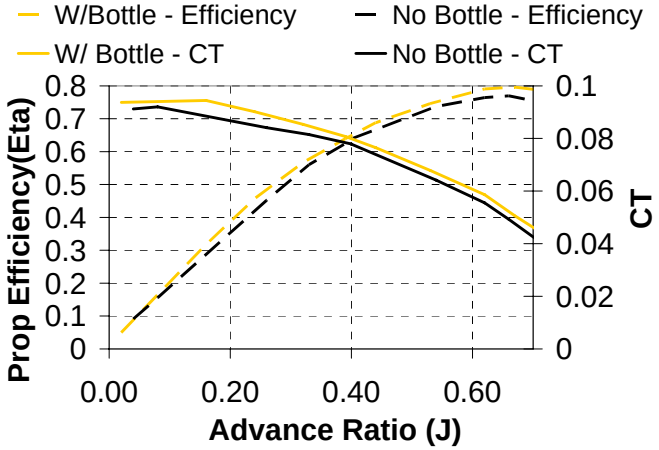

Figure 4.17 – Results of Blockage Testing

Propulsion Configuration			
	Mission 1	**Mission 2**	**Mission 3**
Motor	NEU 1506/2.5Y		
Gearbox	G5.2		
Propeller	APC 14 x 10 E	APC 16 x 10 E	APC 14 x 10 E
Battery	Elite 1700	Elite 1700	Elite 2000
# Cells	12	14	12
Total Weight (lbs)	1.33	1.50	1.45

Table 4.7 – Propulsion System Configuration

4.7.3 Propulsion Performance Predictions

Predicted power and thrust curves are presented in Figure 4.18a and Figure 4.18b, respectively.

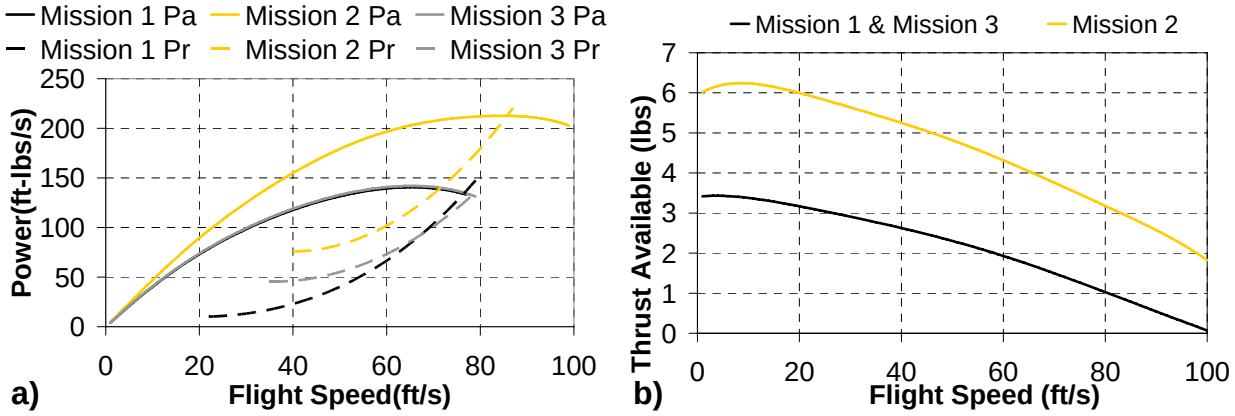

Figure 4.18 – a) Power Curves and b) Thrust Curves for each Mission

4.8 Structures

Preliminary structural layout is designed to withstand expected loads and maintain the aircraft OML. Structural weight is minimized using the optimization of design parameters specified in §4.1.

4.8.1 Layout Studies

Layout studies yield a two spar configuration, with the main spar located at 25% chord and the aft spar located at 70% chord for elevon attachment redundancy. A box carrythrough structure transmits wing, motor, and landing loads to main bulkheads. Critical loads (§4.8.3) and load paths are identified, and major structural components are correspondingly placed (Figure 4.19).

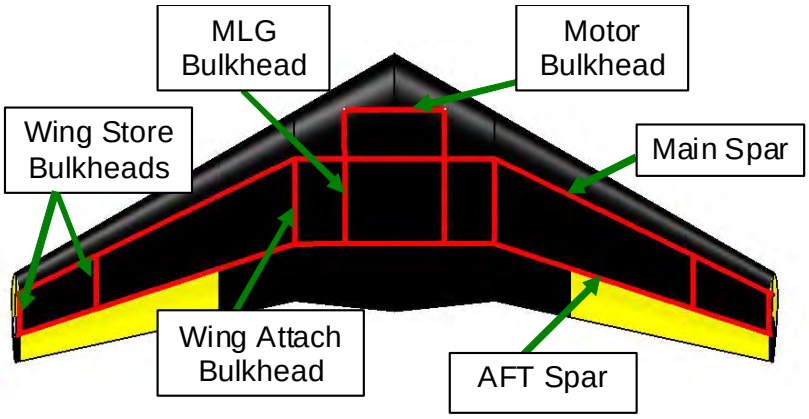

Figure 4.19 – Structural Layout & Load Paths

4.8.2 Material Selection

A semi-monocoque structure is chosen for ease of manufacturing and repair. Wing spars are designed with balsa shear webs and spruce caps. Bulkheads are fabricated from spruce plywood to handle higher shear loads.

The ground mission wing tip test is identified as the critical load case for wing shear and bending moment, and Mission 3 is found to be the critical case for wing torsion. Basic inertia and area requirements for each component are calculated for critical loads assuming a simple, homogeneous beam[11]. A c-channel cross section is selected for each spar, and is sized to meet section property requirements. More refined analysis incorporates modulus-weighted section properties and wing taper to optimize structural geometry[11]. Each component is resized using Von-Mises yield criterion and a safety factor[11] of 1.2. Final sizing yields the following geometry and materials:

- Main Spar: ⅛ in balsa shear web and ¼ x ¼ in spruce caps
- Aft Spar: ⅛ in balsa shear web and ⅛ x ⅛ in spruce caps
- Bulkheads: ⅛ in 3-ply spruce plywood
- Ribs: ⅛ in balsa
- Skin: MonoKote™ covering

4.8.3 Critical Load Analysis

The wing is modeled as a stressed-skin multi-cell beam and analyzed using the methods of Allen and Haisler[11]. Comprehensive stress and deformation calculations for each mission verify safety factor constraints. Figure 4.20 shows the ground mission CG check, with a maximum normal stress of 2,200 psi.

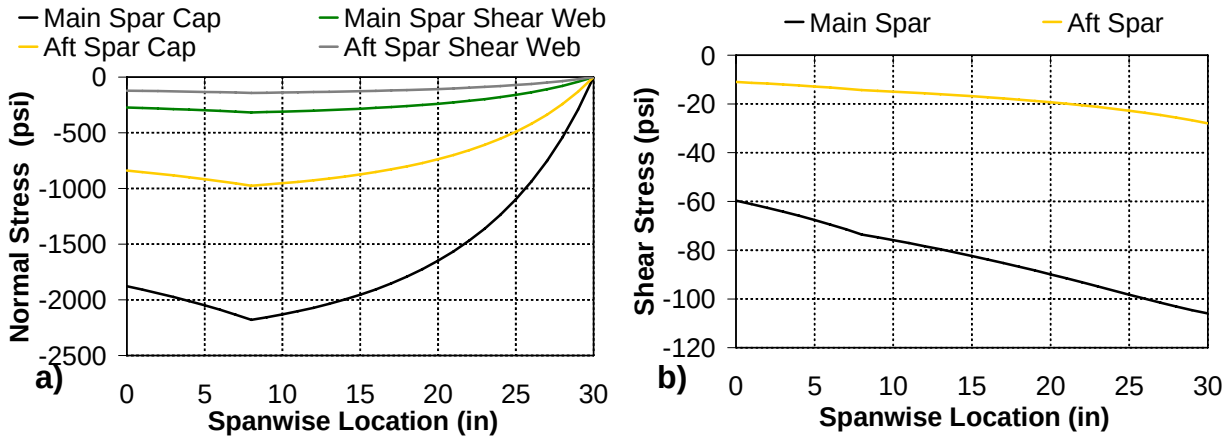

Figure 4.20 – Critical loadings in Ground Mission a) Normal Stress and b) Shear Stress

Basic structure is designed using a CATIA[29] model, from which preliminary weight estimates are calculated. The preliminary aircraft structural weight is 1.2 lbs, which aligns with competitive design constraints (§3.4) for an empty weight less than 4 lbs.

The aircraft's modular, hinging design creates a stress concentration at the wing attach bulkhead. A simplified FEM model is developed to predict behavior at the joint, and the Abaqus solver plugin for CATIA[29] is used to compute principal stress (Figure 4.21). Results show a 150% increase over predicted stress at the wing joint. The wing hinge joint is designed to withstand this load concentration (§5.5.1).

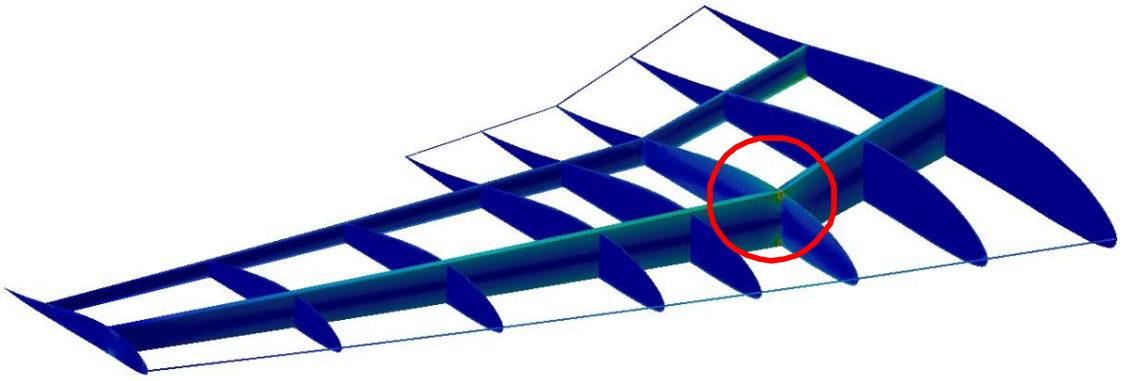

Figure 4.21 – FEM Analysis of Principal Stress in Wing Joint

4.8.4 Landing Gear

Raymer's[6] method determines landing gear placement for a tip-back angle of 15 degrees, allowing sufficient ground handling stability near stall AOAs. Lateral gear spacing is similarly determined to provide

a 15 degree side-tip angle during Mission 3 worst case asymmetric loading. The MLG is split to increase lateral spacing with minimal weight penalty. A breakaway plate attaches each MLG strut to the MLG bulkhead (Figure 4.22). Hard landings will break the gear away from the flight vehicle, but will leave the main wing spar intact. The MLG structure is designed for the critical case where it resolves 84% of 4G landing loads (Mission 2). Commercial off-the-shelf landing gear is selected to reduce manufacturing workload. The carbon fiber main landing gear is fabricated by Graph Tech RC. The main gear is constructed of carbon fiber composite and the steerable nose gear is ⅛ in steel wire.

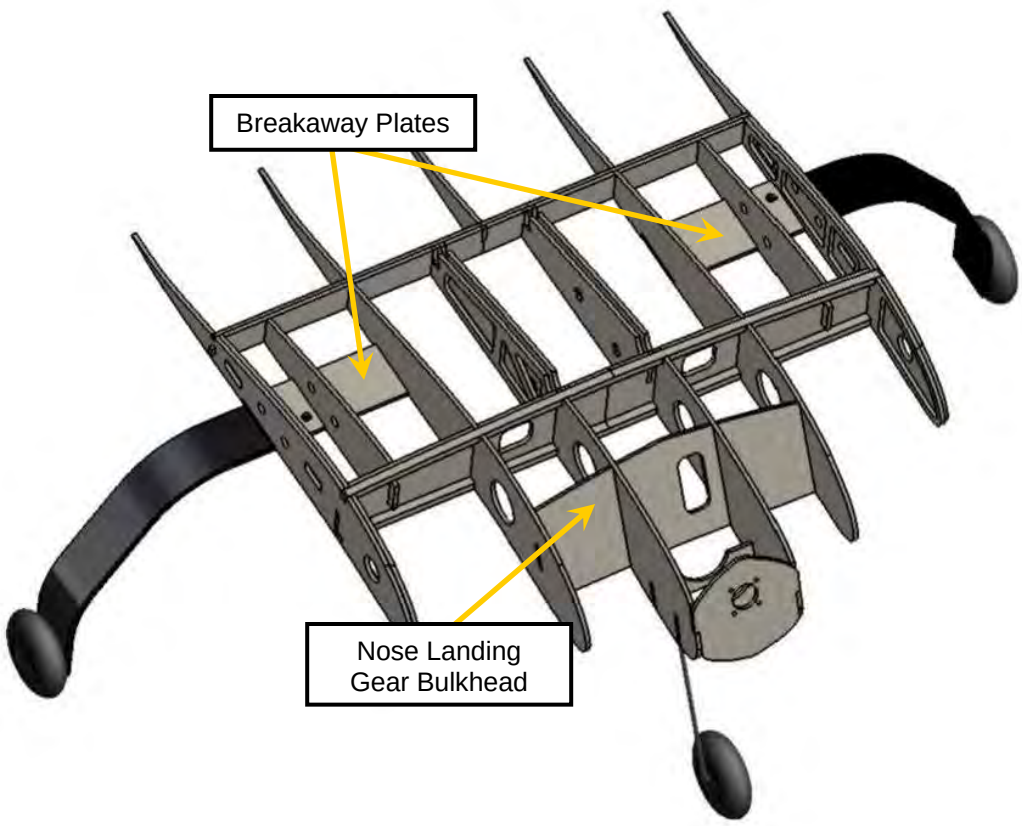

Figure 4.22 – Landing Gear Layout

4.8.5 Motor Loads

Mission 2 takeoff requires the greatest thrust of any mission segment and is thus identified as the critical case for the motor mount bulkhead. The maximum loads are 10 lbs forward, 0.8 lbs laterally, 2.5 lbs vertically, and a 7.6 in-lbs torque. The motor mount bulkhead material is 3-ply plywood, and attaches to the innermost ribs via a notched joint (Figure 4.23). The motor mount is angled to facilitate the thrust angle. The motor shaft protrudes through the motor mount and the motor attaches with four machine screws. Two balsa supports with round cutouts cradle the motor from below. This layout effectively distributes loads throughout the center section.

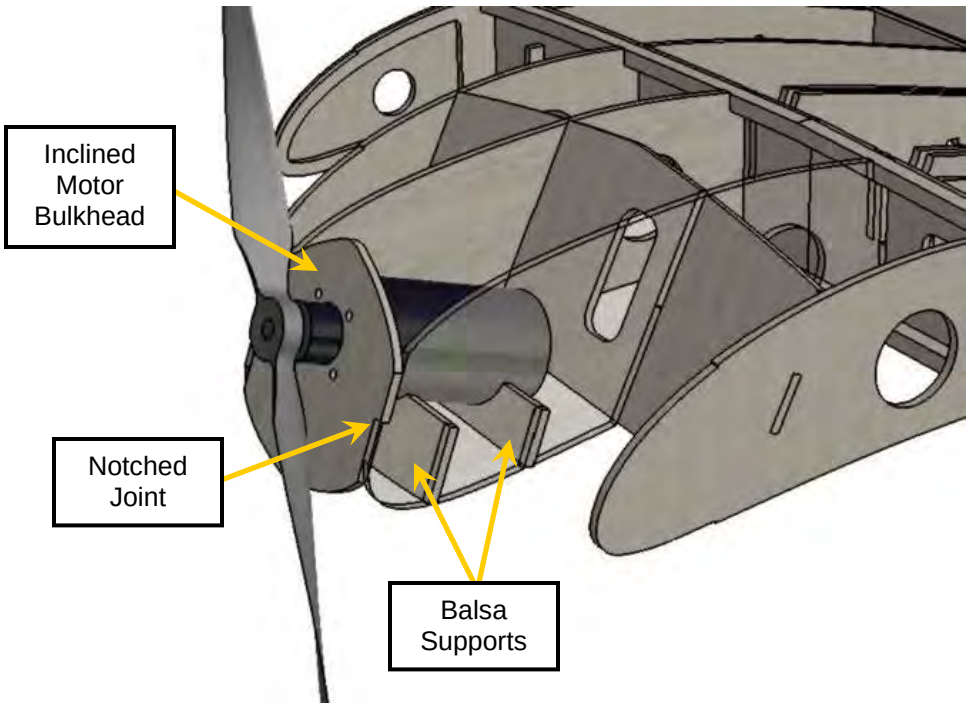

Figure 4.23 – Motor Mount Solution

4.9 Preliminary Mission Performance Predictions

Performance estimations are shown in Table 4.8 for each of the three mission profiles. The critical case for the majority of parameters is Mission 2 with a takeoff weight of 12.55 lbs. These performance predictions are validated through flight testing.

Performance Parameter	Mission 1 (Empty Bottle)	Mission 2 (Full Bottle)	Mission 3 (4 Rockets)
CLMax	1.39		
Oswald Efficiency Factor	0.82		
CD0	0.0517	0.0517	0.0495
(L/D)Max	8.3	8.3	9.9
Takeoff Weight (lbs)	3.98	12.55	9.50
W/S (lb/ft2)	0.76	2.39	1.81
T/W	0.86	0.48	0.36
Takeoff Distance (ft)	11.2	96.7	91.7
Cruise Speed (ft/s)	69.0	60.0	71.0
Stall Speed (ft/s)	22.4	39.8	34.6
Total Flight Time (sec)	91	252	329
Capacity Required (mAh)	504	1486	1834

Table 4.8 – Preliminary Mission Performance Predictions

5.0 Detail Design

After the preliminary design is frozen (with sizing parameters as listed in Table 5.1), work begins on system level integration and optimization. Electrical components are selected, and solutions are developed for propulsion system cooling, wing assembly, storage accomodations, and payload releases. Weight and CG build-up calculations are improved based on manufacturing experience (§6.3), and RAC is assessed to ensure competitive design requirements (§3.3) are met. Flight performance (§5.7) and mission performance parameters (§5.8) are revised to reflect all detail design improvements.

Wing	Value	Vertical Stabilizer	Value	Elevon	Value
Reference Area	756 in^2	**Reference Area**	33 in^2	**Reference Area**	80 in^2
LE Sweep Angle	30 deg	**LE Sweep Angle**	30 deg	**% of Wing Chord**	30%
Geometric AR	4.76	**AR**	2.19	**% of Wing Span**	27%
Effective AR	5.67	**Root Chord**	7.2 in	**Inboard Location**	14 in
Root Chord	18 in	**Span**	6 in	**Outboard Location**	30.25 in
Span	60.5 in	**Taper Ratio**	0.52	**Rudder**	**Value**
Taper Ratio	0.4	**Cant Angle**	0 deg	**Reference Area**	16 in^2
Airfoil	Custom	**Airfoil**	Flat Plate	**% Chord**	50%

Table 5.1 – Final Aircraft Dimensional Parameters

5.1 Electrical Component Selection

Lightweight electrical systems are downselected to reduce RAC (Table 5.5). The payload attachment solution (§5.5.3) eliminates two servos; a total of eight servos remain for both flight control and payload release mechanisms. A nine channel receiver is chosen for its lightweight and compact form factor. Electrical components and servo locations are shown in the Drawing Package (§5.9).

Component	Mission 1	Mission 2	Mission 3
Battery Pack	12 Elite 1700	14 Elite 1700	12 Elite 2000
Propeller	APC 14x10E	APC 16x10E	APC 14x10E
Component	**All Missions**		
Motor / Gearbox	Neu 1506 / 2.5Y (5.2:1)		
Speed Controller	CC Phoenix 45HV ESC		
Receiver	Hitec Fusion9		
Elevon Servos	Qty 2: HS-82MG Micro		
Rudder Servos	Qty 2: HS-65MG Micro		
Steering Servo	HS-65MG Micro		
Payload Servos	Qty 3: HS-65MG Micro		

Table 5.2 – Electrical System Components

5.2 Aircraft Component Weight and CG Buildup

Accurate weights and CG locations are presented for each mission (Table 5.3). Consistent flight handling characteristics result from minimal change in SM between missions (Table 4.4). However, only batteries and payloads are relocated between missions. Particular attention is paid to Mission 3, where constant longitudinal CG location is desired between store releases. All possible Mission 3 CG locations are determined (Table 5.4) to locate landing gear (§4.8.4) and for flight testing planning (§7.6).

Empty	Weight (lbs)	CG Location (in)		
		x	y	z
Airframe	1.11	12.20	0	0.65
Motor/Gearbox	0.52	2.79	0	0.47
Propeller	0.10	0.00	0	0.47
Servos	0.50	15.22	0	0.17
Main Landing Gear	0.30	12.66	0	-3.56
Nose Landing Gear	0.10	-1.38	0	-3.75
Radio Receiver	0.05	7.00	0	0.25
Total	**2.67**	**9.94**	**0**	**-0.13**

Mission 1	Weight (lbs)	CG Location (in)		
		x	y	z
Batteries	0.76	13.00	0	0.00
Empty Bottle	0.60	11.10	0	-3.50
Total	**3.98**	**10.87**	**0**	**-0.44**

Mission 2	Weight (lbs)	CG Location (in)		
		x	y	z
Batteries	0.94	10.80	0	0.00
Full Bottle	8.98	11.75	0	-3.50
Total	**12.61**	**10.85**	**0**	**-2.47**

Table 5.3 – Component Weight and CG Buildup

Mission 3 - Potential Rocket Payload Configurations				Weight (lbs)	Center of Gravity (in)		
Outboard Left	Inboard Left	Inboard Right	Outboard Right		x	y	z
X	X	X	X	9.34	10.80	0	-1.62
X	X	X		7.84	10.79	-5.74	-1.41
X	X		X	7.84	10.79	-4.59	-1.41
X	X			6.34	10.77	-12.77	-1.11
	X	X		6.34	10.77	0	-1.11
X			X	6.34	10.77	0	-1.11
X		X		6.34	10.77	-1.42	-1.11
	X			4.84	10.75	-7.43	-0.62
X				4.84	10.75	-9.29	-0.62

Table 5.4 – Weight and CG Buildup for All Possible Mission 3 Payload Configurations

5.3 Centerline Tank Aerodynamics

The centerline tank is a major contributor to parasite drag (Figure 4.9). A fairing is designed to reduce drag caused by both the bottle itself and interference between the aircraft and bottle. Drag reducing shapes from Hoerner[19] are used to improve the adverse pressure gradient and reduce flow separation. An attachment fairing is also created to decrease interference drag by blending the centerline tank to the wing lower surface. The attachment fairing also uses shapes from Hoerner[19]. The faired, filleted centerline store is pictured in §5.5.3 and §7.4, with performance results in §8.0.

5.4 System Cooling Solution

Lessons learned from past WSU DBF teams demonstrate the need for battery cooling and comprehensive propeller data[17,21]. Particularly, battery cell nominal voltage and capacity specifications fall short of manufacturers' claims during periods of high discharge rates. Extreme battery temperatures encountered during high rate discharge testing (§7.2.1), specifically for Mission 2 modeling, result in insufficient battery pack performance. Therefore, battery cooling is a vital aspect of propulsion detail design. The flying wing design constrains the battery packs to an enclosed area. Air ventilation routes are designed into the structure as a solution to ensure acceptable battery cooling. Figure 5.1 illustrates the path of air through the internal compartments of the aircraft. Openings are positioned to provide a positive pressure on the lower surface and a negative pressure on the upper surface, facilitating flow through the motor and battery compartments.

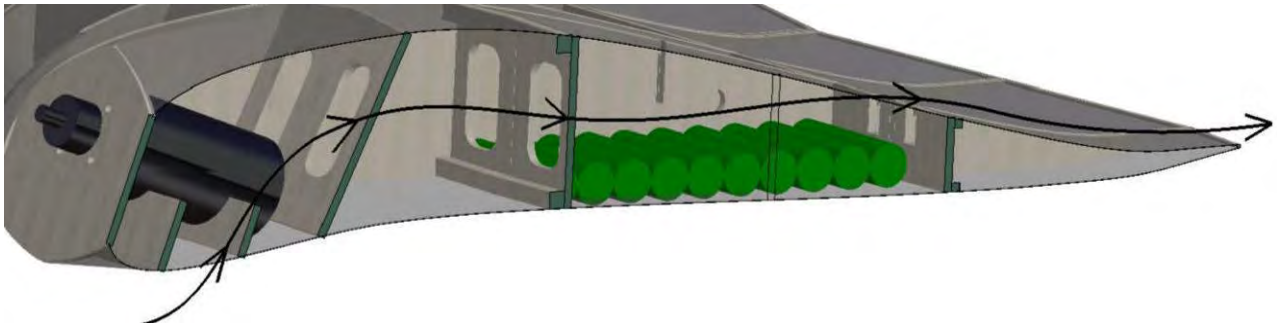

Figure 5.1 – System Cooling Design

5.5 Structures

Weight reduction is the primary objective of structural design, thus lightening holes are cut where structurally plausible. Span-wise stress distribution aides weight optimization, pinpointing potential low stress areas where material can be trimmed.

5.5.1 Wing Assembly Solution

Scoring sensitivity studies (§3.2) and box sizing constraints (§3.4) call for a creative wing assembly method that minimizes both assembly time and weight. Conceptual design selects a hinged wing as the wing assembly method. It is apparent after airfoil selection that the drooped leading edge significantly hinders the wing joint's hinging ability. Upon further analysis, an interlocking joint (Figure 5.2) is developed to transfer the loads from each wing's outboard portion to the aircraft's center carrythrough section, while minimizing weight and assembly time. The outboard wing dowel extensions slide into a friction-fit slot in the wing attach bulkhead. Two horizontally oriented quick release buckles are utilized to reduce assembly time (Figure 5.2). The wing joint efficiently transfers outboard transverse and axial loads to the center wing section. Adequate assembly at competition is ensured by the buckles' audible click.

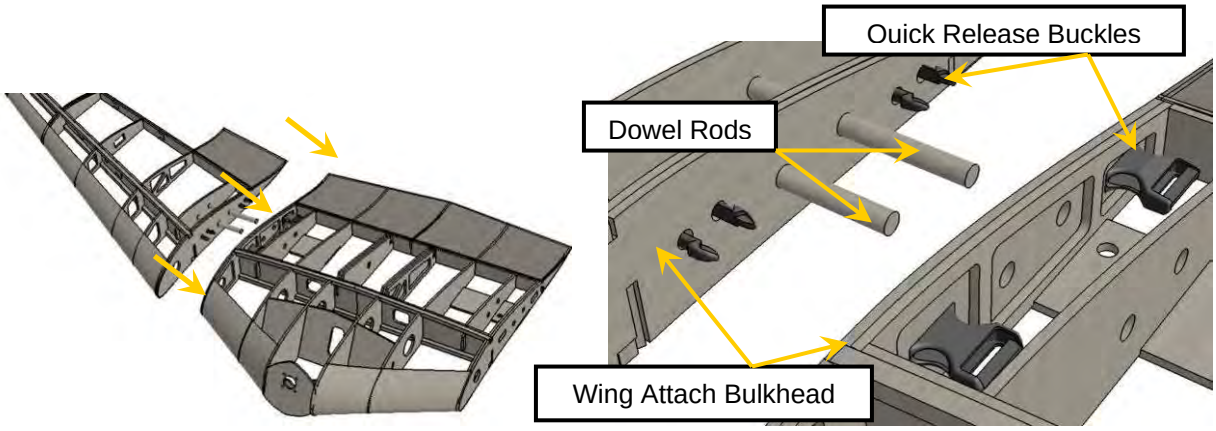

Figure 5.2 – Wing Assembly Mechanism

A wing tip lift test is conducted (§7.3); failure occurs at 13.3 lbs. Upon failure the outboard rib cracked, the overlapping spars displaced, bending their pins and the shear web separated from the spar. The wing tip lift test shows stress concentrations around cutouts, which result in crack propagation and premature

failure. High stress areas are re-evaluated and balsa padups are added around cutouts to increase strength. The wing tip test is re-conducted and the modified structure yields at a 22.1 lb load.

5.5.2 Storage Box Solution

The box design is essential to accomplishing two primary competitive design requirements, minimizing RAC and assembly time. All box structural members and hardware must be lightweight. Additionally, efficient aircraft component layout enables minimal assembly time. The box must sustain the loads that result when the box is dropped on any side. The box structure consists of a truss of ¼ x ¼ inch birch rods. The number and positioning of truss elements were determined using the stiffness method outlined in Haisler[11].

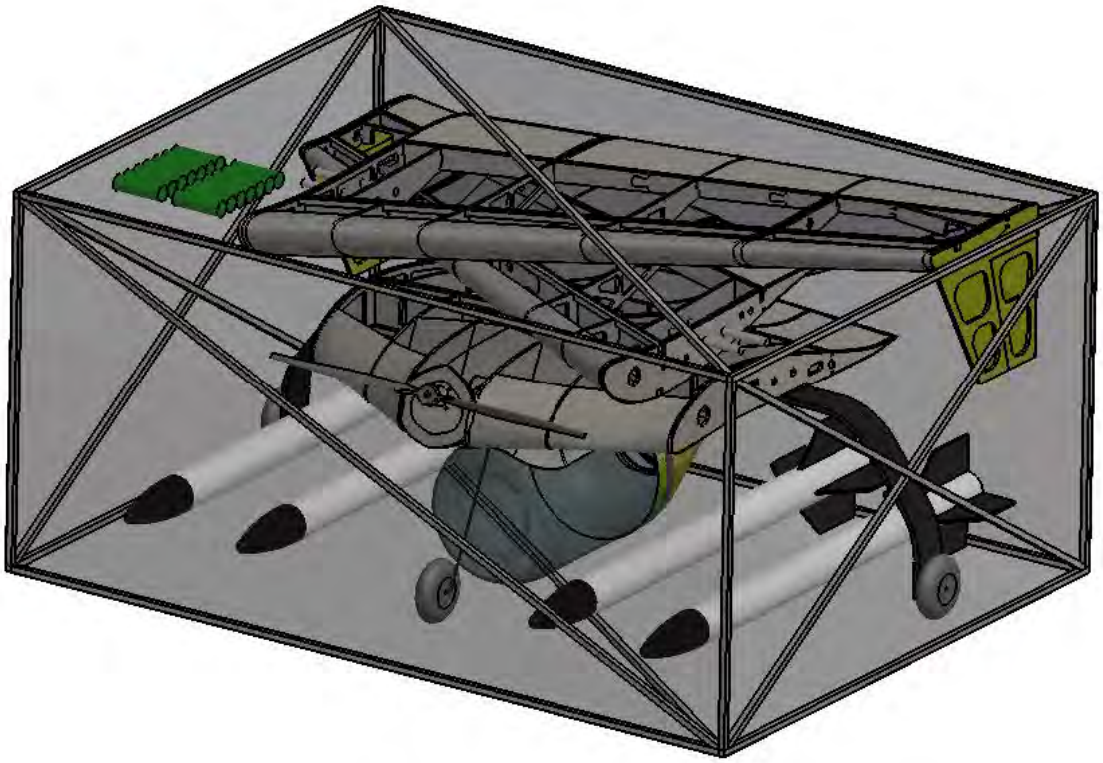

Figure 5.3 – Fully-Loaded Storage Box Solution

MonoKote™ covers the four side panels to increase rigidity and eliminate porosity. Balsa/fiberglass sheeting covers the lid and the base of the box. The material properties of balsa/fiberglass sheeting are obtained from WSU DBF material database[17]. The lid of the box hinges about a dowel rod and latches with a buckle. All components are secured with Velcro attachment to either the lid or base of the box, eliminating movement upon rotation and drop.

5.5.3 Payload Attachment Solution

The payload attachment allows fast and secure attachment of all stores while providing an audible clicking sound when properly attached. The payload attachment solution consists of two ribs spaced ⅛ in apart with the center of the gap located at 24 and 30 in outboard, normal to the aircraft centerline. The

outboard rib for the inner rocket store and the inboard rib for the outer rocket store each contain cutouts for two DU-BRO™ Hatch Latches. These hatch latches are mounted to allow the spring-loaded latch to extend into the gap between each rib. Each rocket pylon has two holes cut to allow the hatch latch to secure the pylon when it is inserted between the ribs (Figure 5.4). A single servo is placed between both rocket stores. This servo is then attached via 20 AWG wire to each hatch latch. Rotation in one direction releases one rocket and rotation in the other direction releases the other rocket. The centerline tank is attached in a similar manner using four hatch latches. When the centerline tank servo is actuated, all of the hatch latches are opened, releasing the bottle (Figure 5.5).

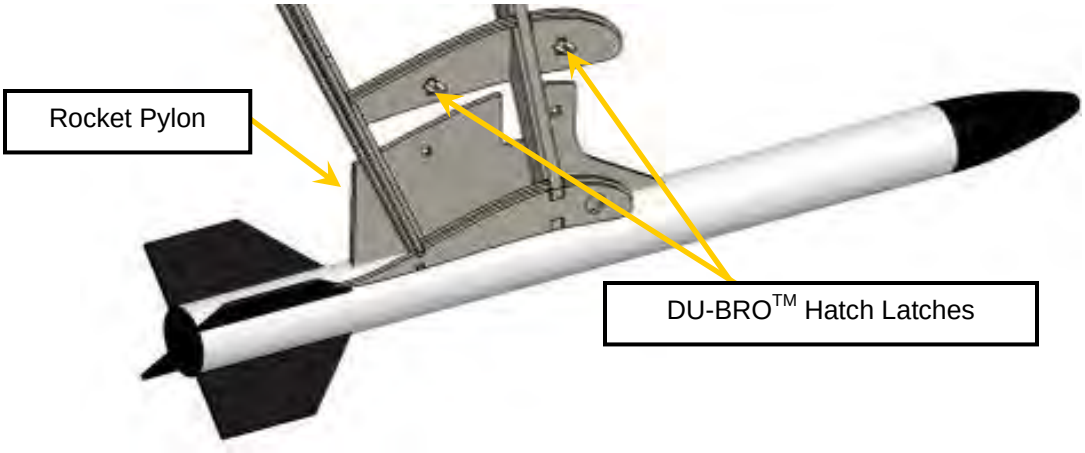

Figure 5.4 – Rocket Store Attachment Solution

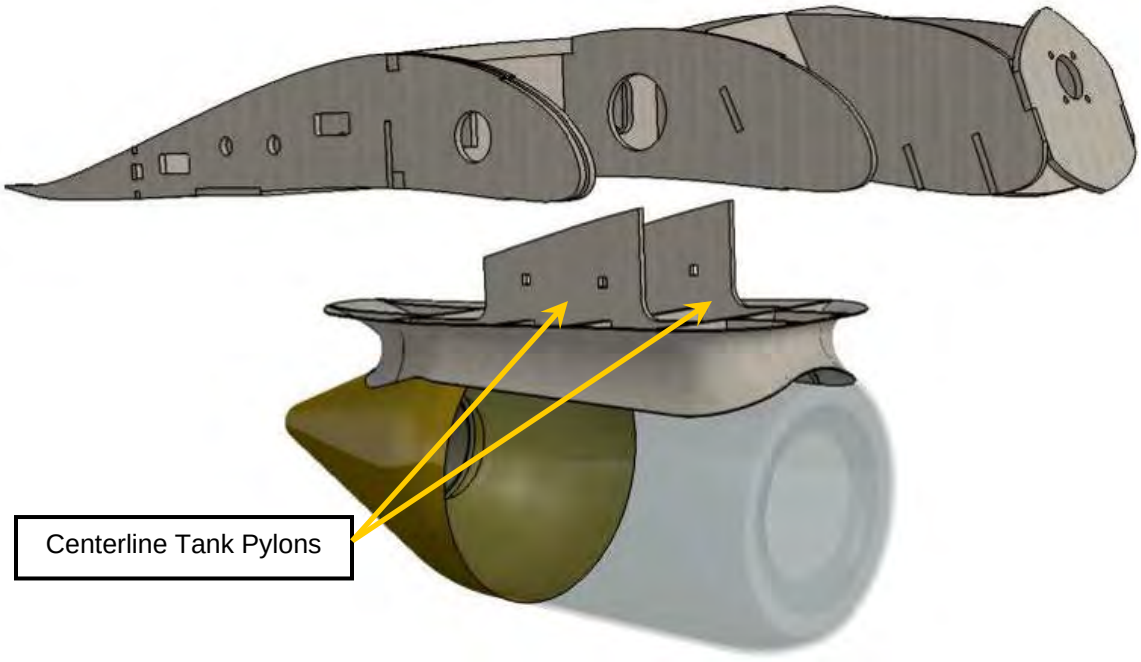

Figure 5.5 – Centerline Tank Store Attachment Solution

5.6 RAC Summary

Competitive scoring analysis identifies RAC as contributing 45.7% of the overall flight score (§3.2) and competitive design requirements (§3.3) demand an RAC of under 25 lbs The mandatory payload weight, dictated by the contest rules[1] is 14.98 lbs, therefore the remainder of the RAC, including the storage box, airframe, and systems cannot weigh more than 10 pounds. Table 5.5 details the RAC breakdown.

RAC Component Buildup					
Sub-Group	**Component**	**Weight(lbs)**	**Sub-Group**	**Component**	**Weight(lbs)**
Box	Truss Elements	0.60	**Systems**	Heaviest Batteries	0.88
	Sheeting	0.95		Receiver	0.05
	MonoKote	0.17		Propellers	0.15
	Buckle	0.02		Motor	0.52
	Attachments	0.50		Servos	0.50
	Subtotal	**2.24**		Transmitter	1.76
Airframe	Ribs / Bulkheads	0.53		Speed Controller	0.12
	Spar Caps	0.14		Fuse	0.10
	Shear Webs	0.03		Wires	0.40
	MonoKote	0.15		**Subtotal**	**4.48**
	Sheeting	0.17	**Payloads**	Full Bottle	8.98
	Main Gear	0.31		Fairings	0.25
	Nose Gear	0.25		Rockets	6.00
	Subtotal	**1.58**		**Subtotal**	**15.23**
Total RAC: 23.53 lbs					

Table 5.5 – RAC Summary for Final Design and Storage Box Solution

5.7 Flight Performance Summary

Table 5.6 details flight and mission performance parameters. Applicable final predictions are compared to actual test results in §8.0.

Performance Parameter	Mission 1 (Empty Bottle)	Mission 2 (Full Bottle)	Mission 3 (4 Rockets)
C_{LMax}	1.39		
Oswald Efficiency Factor	0.82		
C_{D0}	0.0517	0.0517	0.0495
$(L/D)_{Max}$	8.31	8.31	9.93
T/W	0.86	0.48	0.36
Takeoff Weight (lbs)	3.98	12.55	9.50
Cruise Speed (ft/s)	69	60	71
Max Speed (ft/s)	67	88	69
Stall Speed (ft/s)	22	40	35
Max Turn Rate (deg/s)	61	70	60
Max Rate of Climb (ft/min)	1435	720	492

Table 5.6 –Flight Performance Parameters

5.8 Mission Performance Summary

Table 5.7 presents the battery capacity, current draw, and time budgets for each of the three missions.

Mission 1				Mission 2			
	Current (Amps)	Time (sec)	Capacity (mAh)		Current (Amps)	Time (sec)	Capacity (mAh)
Takeoff	18.5	0.5	2.7	Takeoff	34.3	2.7	26.1
Climb	18.5	4.2	21.5	Climb	34.3	8.3	79.3
Cruise (2000 ft/lap) (x2)	17.5	29.0	281.8	Cruise (2000 ft/lap) (x4)	19.7	33.3	727.8
180 deg Turn (x4)	17.5	2.9	57.1	180 deg Turn (x8)	19.7	2.6	111.6
360 deg Turn (x2)	17.5	5.9	57.1	360 deg Turn (x4)	19.7	5.1	111.6
Descent	17.5	4.2	20.3	Descent	19.7	8.3	45.5
Total (20% Margin)	-	**108.4**	**528.7**	**Total (20% Margin)**	-	**232.3**	**1322.1**
Available Energy	-	-	**1600.0**	**Available Energy**	-	-	**1600.0**
Excess	-	-	**1071.3**	**Excess**	-	-	**277.9**

Mission 3							
LAP 1	**Current (Amps)**	**Time (sec)**	**Capacity (mAh)**	**LAP 2**	**Current (Amps)**	**Time (sec)**	**Capacity (mAh)**
Takeoff	18.5	3.2	16.5	Takeoff	18.5	2.2	11.2
Climb	18.5	12.2	62.7	Climb	18.5	13.8	70.7
Cruise (2000 ft/lap)	17.1	28.2	133.6	Cruise (2000 ft/lap)	16.9	27.8	130.1
180 deg Turn (x2)	17.1	3.0	28.7	180 deg Turn (x2)	16.9	3.1	28.7
360 deg Turn	17.1	6.0	28.7	360 deg Turn	16.9	6.1	28.7
Taxi Payload Drop	10.0	15.0	41.7	Taxi Payload Drop	10.0	15.0	41.7
Descent	17.1	12.2	57.9	Descent	16.9	13.8	64.4
LAP 3	**Current (Amps)**	**Time (sec)**	**Capacity (mAh)**	**LAP 4**	**Current (Amps)**	**Time (sec)**	**Capacity (mAh)**
Takeoff	18.5	1.4	7.0	Takeoff	18.5	0.7	3.7
Climb	18.5	12.3	63.0	Climb	18.5	12.7	65.4
Cruise (2000 ft/lap)	16.4	27.0	123.1	Cruise (2000 ft/lap)	16.2	26.7	119.8
180 deg Turn (x2)	16.4	3.2	28.7	180 deg Turn (x2)	16.2	3.2	28.7
360 deg Turn	16.4	6.3	28.7	360 deg Turn	16.2	6.4	28.7
Taxi Payload Drop	10.0	15.0	41.7	Descent	16.2	12.7	57.1
Descent	16.4	12.3	55.9				
				Total (20% Margin)	-	**361.5**	**1676.08**
				Available Energy	-	-	**1850.00**
				Excess	-	-	**173.92**

Table 5.7 – Mission Performance Predictions

5.9 Drawing Package

The drawing package includes: 3-view (dimensioned), structural arrangement, systems layout, and payload accommodation drawings.

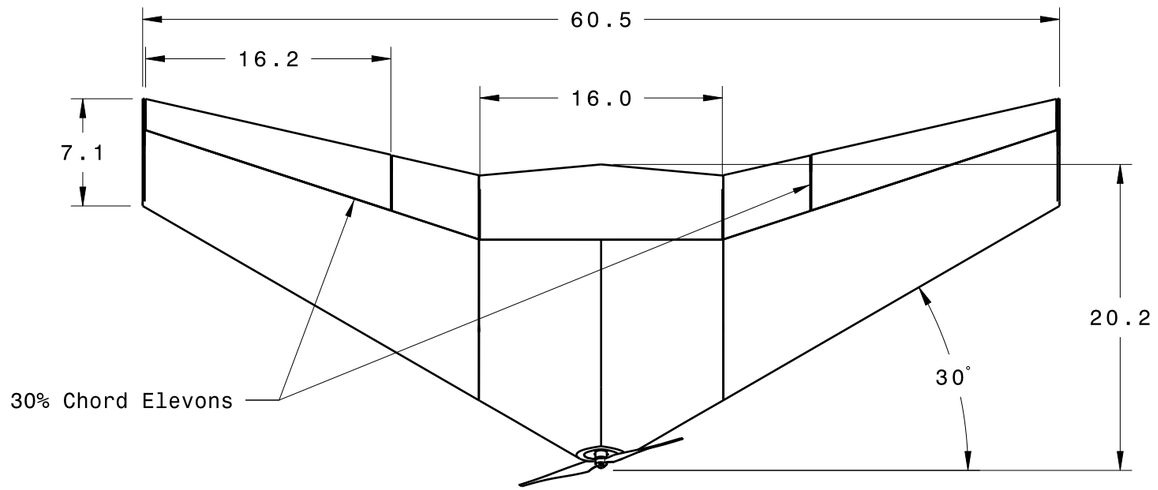

Top View

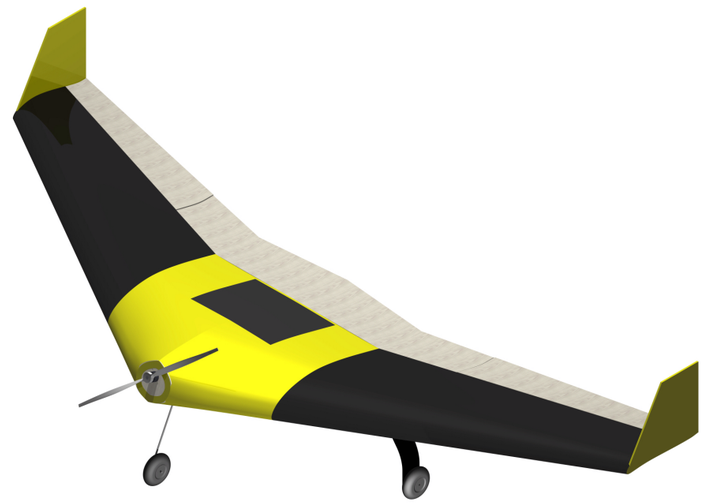

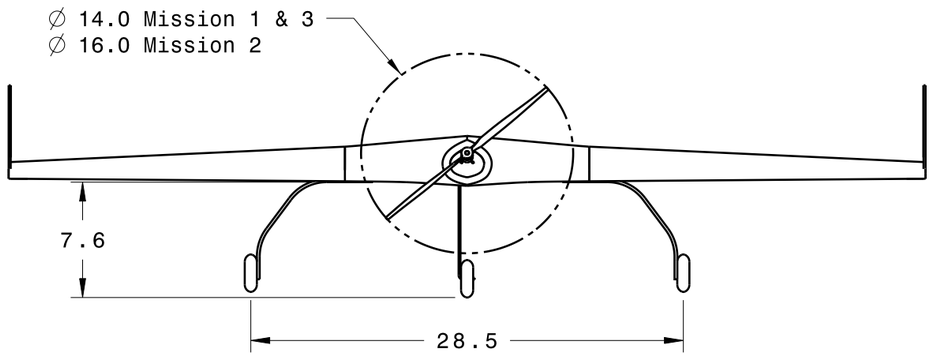

Front View

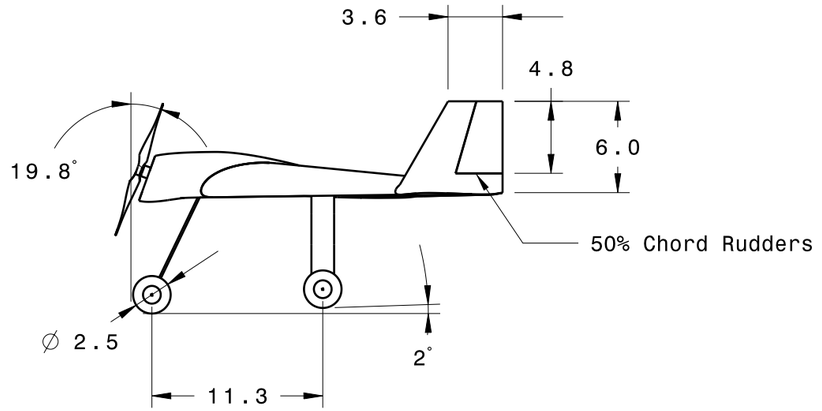

Right View

DRAWN BY B. HINSON	DATE 2/25/2009	Wichita State University Team sUAVe	
CHECKED BY K. KELLY	DATE 2/26/2009		
APPROVED sUAVe	DATE 2/26/2009	TITLE Aircraft Three-View	
UNLESS OTHERWISE SPECIFIED DIMENSIONS ARE IN INCHES TOLERANCES ON DECIMALS .XX = ±.03 .XXX = ±.010 ANGLES ±30'		SIZE B	DWG NO 2009-001 REV C
		SCALE 1:10	REPORT PAGE 42 OF 58 SHEET 1 OF 4

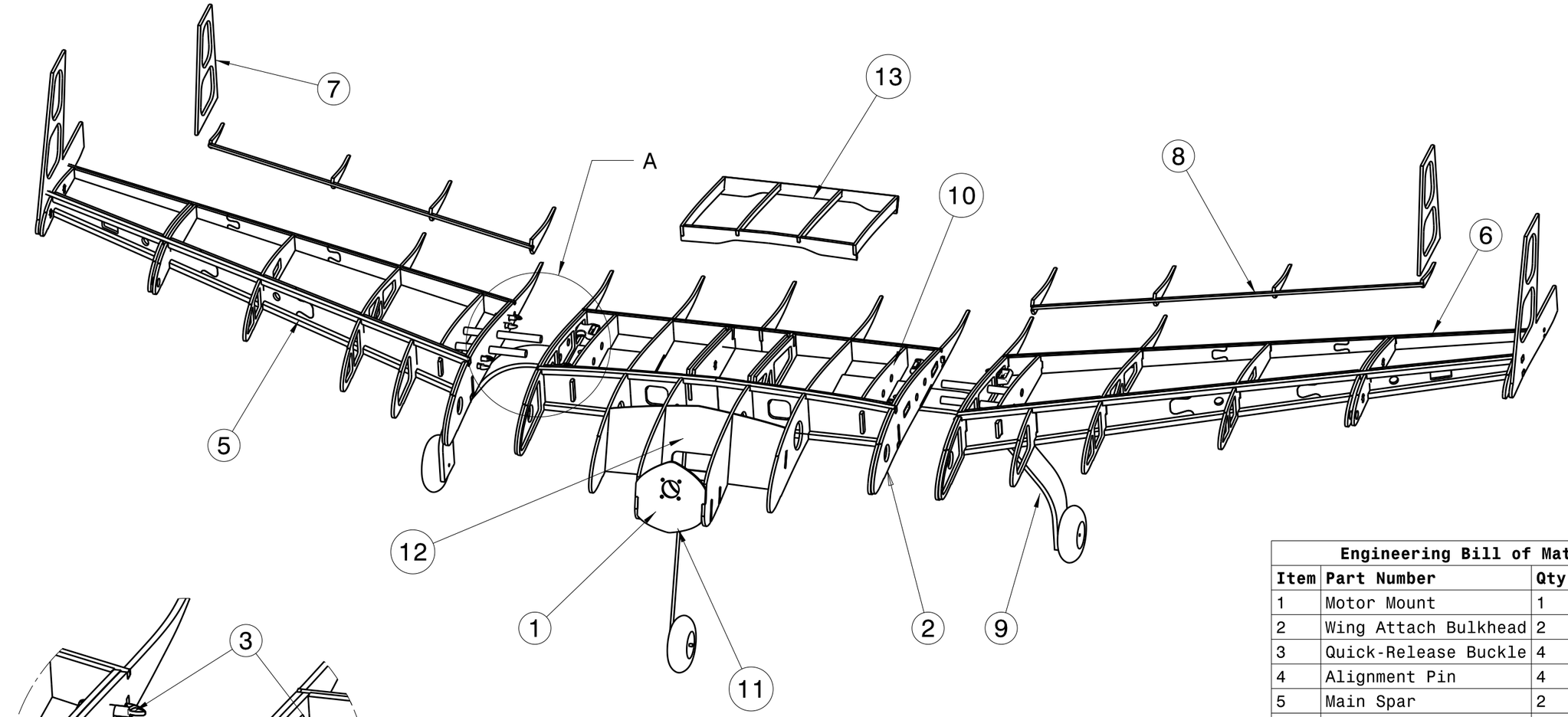

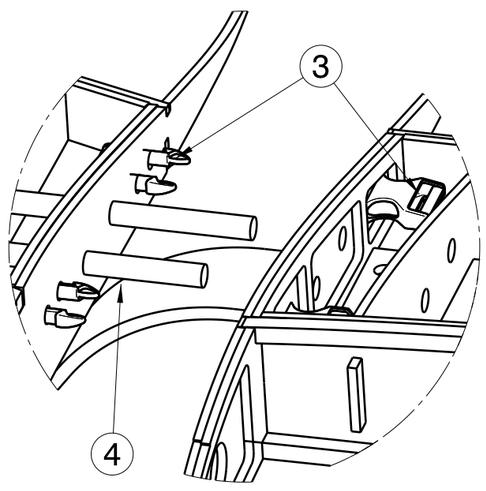

Detail A
Scale: 1:2

Engineering Bill of Materials			
Item	**Part Number**	**Qty**	**Material**
1	Motor Mount	1	3-Ply
2	Wing Attach Bulkhead	2	Balsa/3-Ply
3	Quick-Release Buckle	4	Plastic
4	Alignment Pin	4	Dowel Rod
5	Main Spar	2	Balsa/Birch
6	AFT Spar	2	Balsa/Birch
7	Rudder Assy	2	Balsa/3-Ply
8	Elevon Assy	2	Balsa
9	Main Landing Gear	2	Carbon Fiber
10	MLG Bulkhead	2	3-Ply
11	Nose Landing Gear	1	Steel Wire
12	Nose Gear Bulkhead	1	3-Ply
13	Hatch Assy	1	Balsa

DRAWN BY: B. HINSON	DATE: 2/25/2009	Wichita State University Team sUAVe	
CHECKED BY: K. LEMON	DATE: 2/26/2009		
APPROVED: sUAVe	DATE: 2/26/2009		
UNLESS OTHERWISE SPECIFIED DIMENSIONS ARE IN INCHES TOLERANCES ON DECIMALS .XX = ±.03 .XXX = ±.010 ANGLES ±30'		TITLE: Structural Arrangement	
		SIZE: B	DWG NO: 2009-002
		REV: C	
		SCALE: 1:5	REPORT PAGE 43 OF 58
		SHEET: 2 OF 4	

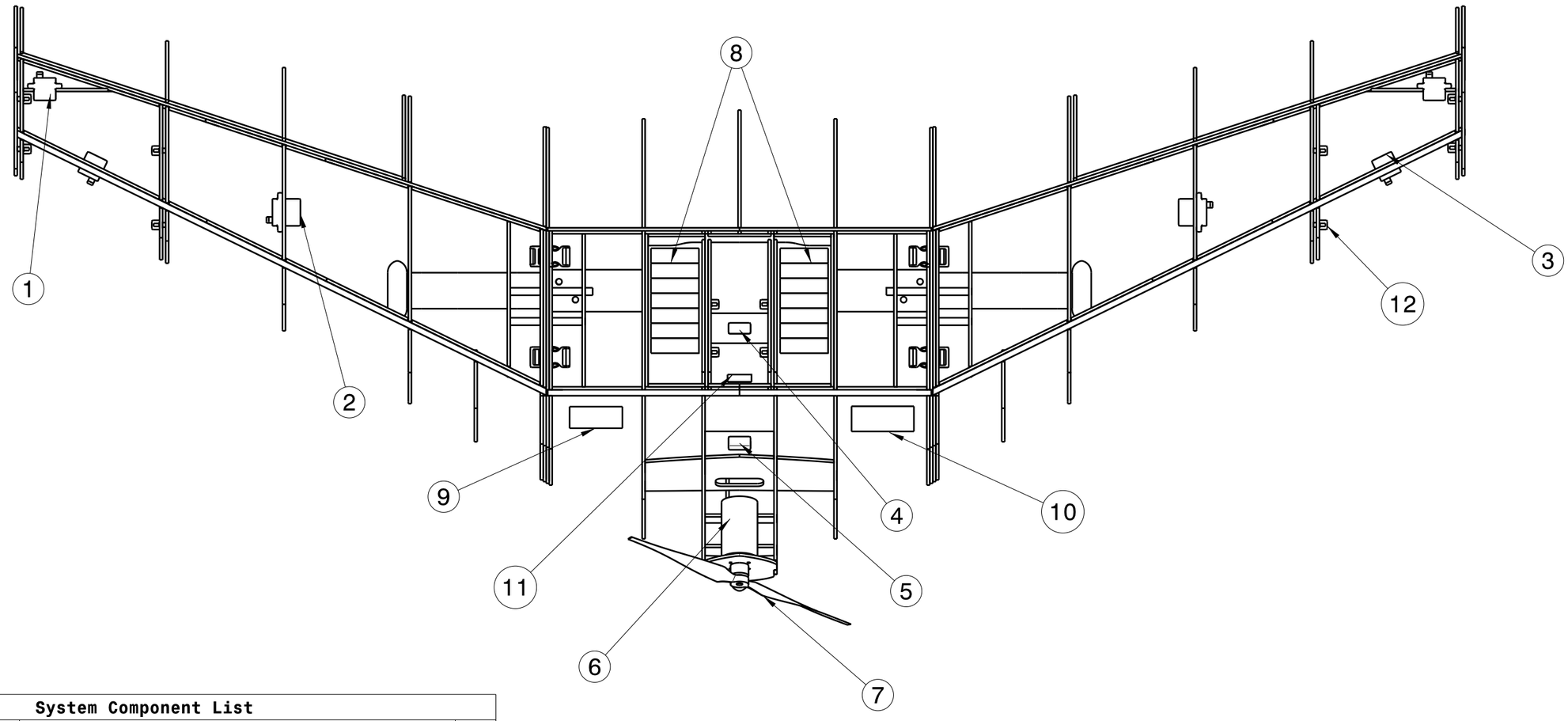

System Component List			
Item	**Part Number**	**Source**	**Qty**
1	Rudder Servo	Hitech HS-65MG	2
2	Elevon Servo	Hitech HS-82MG	2
3	Rocket Servo	Hitech HS-65MG	2
4	Fuel Tank Servo	Hitech HS-65MG	1
5	Steering Servo	Hitech HS-65MG	1
6	Motor/Gearbox	Neu 1506/2.5Y (5.2:1 Gear Ratio)	1
7	Propeller	APC 14x10E/APC 16x10E/APC 14x10E	1
8	Battery Pack	12 Elite 1700/14 Elite 1700/12 Elite 2000	1
9	Receiver	Hitech Fusion9	1
10	Speed Controller	CC Phoenix 45HV ESC	1
11	Fuse	Maxi Slow-Blow 40 Amp Fuse	1
12	Payload Latch	DU-BRO Hatch Latch	12

DRAWN BY B. HINSON	DATE 2/25/2009	Wichita State University Team sUAVe	
CHECKED BY L. STAAB	DATE 2/26/2009		
APPROVED sUAVe	DATE 2/26/2009	TITLE Systems Layout	
UNLESS OTHERWISE SPECIFIED DIMENSIONS ARE IN INCHES TOLERANCES ON DECIMALS .XX = ±.03 .XXX = ±.010 ANGLES ±30'		SIZE B	DWG NO 2009-003 REV C
		SCALE 1:5	REPORT PAGE 44 OF 58 SHEET 3 OF 4

Fuel Tank Store Release Mechanism

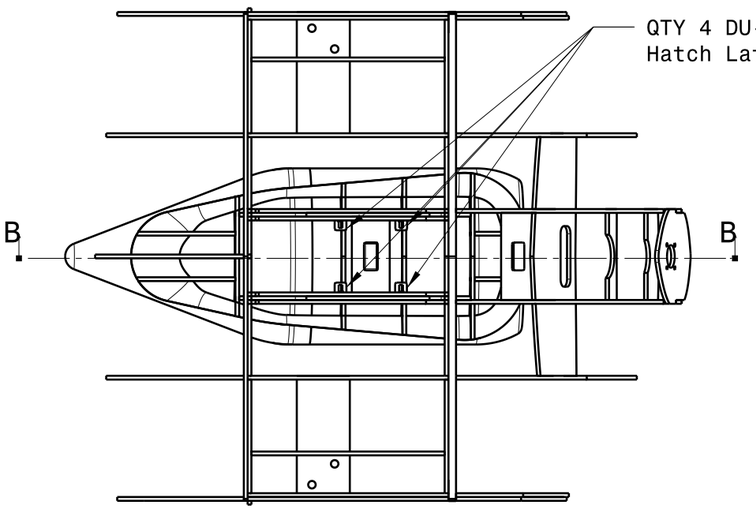

Top View

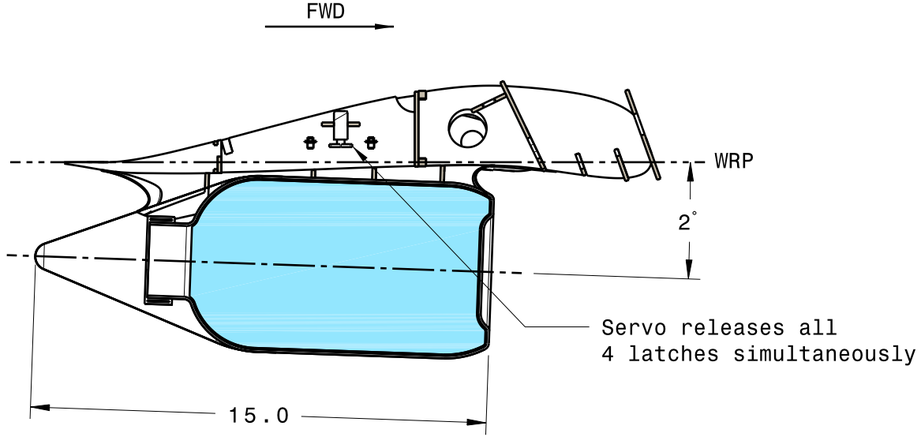

Section view B-B

Rocket Store Release Mechanism

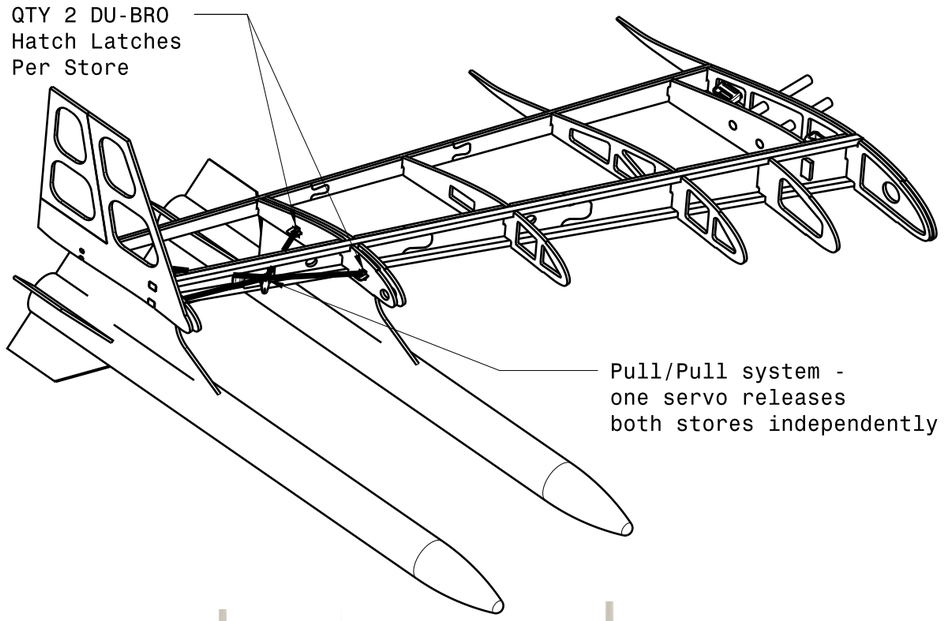

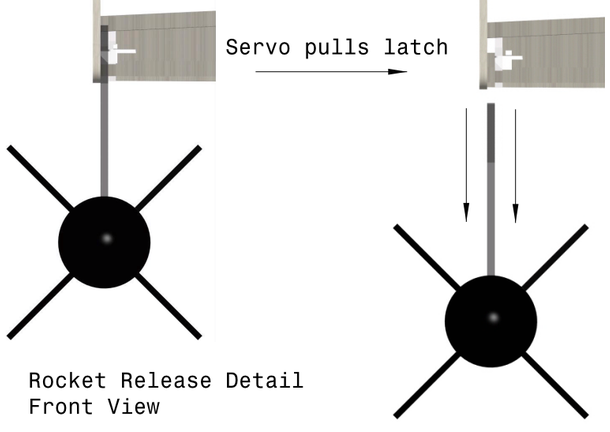

Rocket Release Detail
Front View

DRAWN BY	B. HINSON	DATE	2/25/2009
CHECKED BY	J. KRENZEL	DATE	2/26/2009
APPROVED	sUAVe	DATE	2/26/2009

UNLESS OTHERWISE SPECIFIED
DIMENSIONS ARE IN INCHES
TOLERANCES ON

DECIMALS
.XX = ±.03
.XXX = ±.010

ANGLES
±30'

Wichita State University
Team sUAVe

TITLE

Payload Accommodation

SIZE	DWG NO	REV
B	2009-004	B

SCALE 1:5 REPORT PAGE 45 OF 58 SHEET 4 OF 4

6.0 Manufacturing Plan and Processes

Practice refines the manufacturing approach throughout the course of the design process. The manufacturing team includes the five senior engineers as well as underclassmen, who hold regular meetings to practice and refine building skills.

6.1 Manufacturing Figures of Merit

Flying wings allow for a simple manufacturing method, where a single process allows fabrication of the entire aircraft. Manufacturing process selection hinges upon team experience and financial constraints. Each potential method is evaluated using the following FOMs:

- **Weight**: Weight reduction is the primary objective of material and process selection. A manufacturing process that yields a lighter weight vehicle directly improves flight score.
- **Ease of Manufacturing**: Build time must be less than six hours in the event of a rebuild at competition. Difficult or time-consuming processes hinder manufacturing efforts, requiring the team to be well-versed in the chosen method.
- **Reparability**: Although strength and weight inherently drive material selection, field repairs must be quick and simple without compromising structural integrity and weight.
- **Cost**: Financial constraints limit material selection.

FOM analysis evaluates the following manufacturing processes:

- **Balsa Build-Up**: Wood frame components are precision laser cut in-house directly from CAD drawings. MonoKote™ stressed skin gives the wing its aerodynamic shape. This method allows for quick construction and easy integration of tooling. Duplicate parts are cut, facilitating relatively simple field repair.
- **Foam Core Composite**: A hot wire cutter fabricates a foam wing. Fiberglass and epoxy cover the foam core. Special attention must be paid to ensure a smooth surface finish, which results in a rigid structure. Foam core wings have excess strength, and thus excess weight. Field repairs, however, consist of simple patches around damaged areas.
- **Molded Composite**: A foam male mold is constructed in a similar fashion to the foam core composite method. Female molds for the upper and lower wing surface are built around a male mold using thick fiberglass cloth. A release agent allows the molds to separate, from which multiple identical wings can be fabricated. This method yields a strong monocoque structure that can be repaired with patches in the field[17].

Figure of Merit	Weight	Balsa Build-Up	Foam Core Composite	Molded Composite
Weight	40	3	1	2
Ease of Manufacturing	25	3	2	3
Reparability	20	3	4	4
Cost	15	3	2	2
Total	100	**300**	200	265

Figure 6.1 – Manufacturing Process FOM

Balsa build-up is chosen as the most viable manufacturing process, primarily for its low weight and simplicity. High weight and time-consuming foam core or molded composites are ruled out to maintain a lightweight, simple design.

6.2 Manufacturing Schedule

A manufacturing schedule is developed to support testing and refine the build process. A Gantt chart (Figure 6.2) tracks prototype and final aircraft build progress.

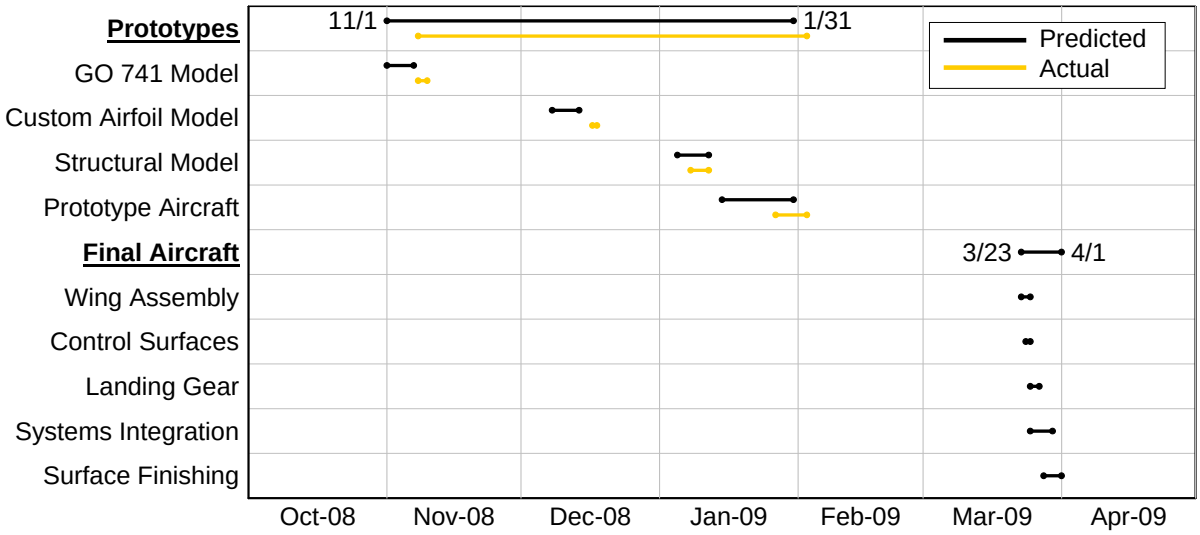

Figure 6.2 – Manufacturing Schedule

6.3 Prototypes

Four prototypes are constructed prior to the initial flight ready model. A half-scale, foam prototype is fabricated using a handheld hot wire, which traces airfoil-shaped endplates. Initial efforts demonstrate that hot wire cutting is not effective for reflexed airfoils or complex planforms.

Figure 6.3 – Underclassmen Build the GO 741 Planform and Custom Airfoil Planform

The second and third prototypes are half-scale models of the GO 741 planform and the custom airfoil planform, respectively. A comprehensive CAD model is used to facilitate precision and repeatability throughout the development of the manufacturing technique. A laser cutter fabricates structural elements

from the CAD model. Both models are constructed similarly with spruce structural elements, MonoKote™ skin, and foam fillers to maintain the LE geometry. This method is effective at producing a smooth aerodynamic shape, but still heavy. The foam LE is covered in packing tape, while the remainder of the model is covered in MonoKote™. The second and third models demonstrate that the balsa build-up method produces a prototype that is more precise and lighter than a foam model.

The first full-scale prototype is constructed as an exact replica of the aircraft for structural testing (§7.3). This prototype has a greater LE radius, which allows experimentation with LE sheeting that was not possible on the half-scale prototype. Additionally, the full-scale airfoil allows the interlocking spar joint to be constructed. Wing joint fabrication demonstrates that the wing attachment bulkhead must be constructed from plywood rather than balsa.

6.4 Aircraft Manufacturing

The first flight prototype is built for full-scale wind tunnel testing, ground testing, and flight testing (§7.6). Assessment of construction methods during the build determines potential weight reductions.

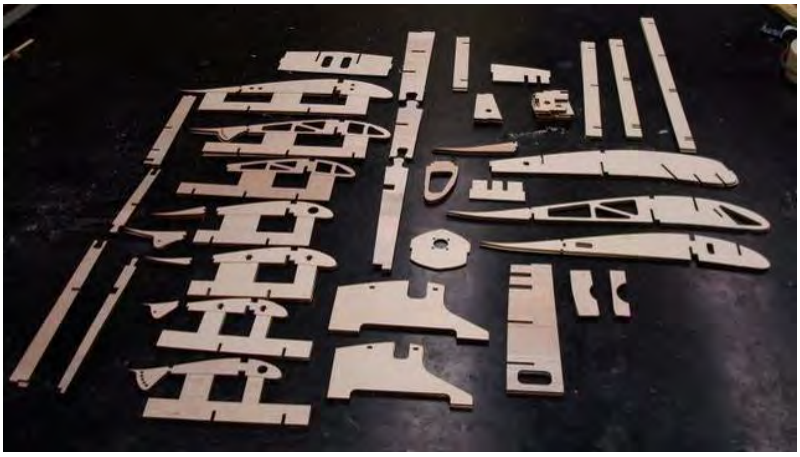

Figure 6.4 – CAD developed, Laser Cut Structural Elements and Tooling

6.4.1 Tooling

Flying wings inherently facilitate a simple build process requiring only single-tier assembly integration. However, planform complexity introduces obstacles atypical to DBF aircraft. Early build experiences reveal that classic “ruler and square” layout methods are imprecise and lengthy processes. The half-scale prototypes require build times in excess of eight hours, with insufficient final product quality. A rapid, precise, and repeatable manufacturing method is sought.

Breakaway tooling[18] is a viable, simple solution. This method incorporates tooling into each rib and bulkhead along the wing. Alignment members ensure accurate wing geometry and improve joint construction quality. Perforation along ribs allows tooling to be cleanly removed after construction is complete. Figure 6.5 demonstrates a finalized wing structure aligned by tooling.

Figure 6.5 – Manufacturing Tooling Design

6.4.2 Airframe

The balsa build-up method is used to fabricate complementary wings and the center section. A plywood wing attachment bulkhead, two plywood wing store bulkheads, and two balsa ribs maintain the airfoil geometry on the outboard wings. The motor bulkhead, MLG bulkhead, and wing attachment bulkhead are all laser cut from three-ply-plywood on the center section. Main and aft spar construction follows the composition details in §5.9. The leading edge and upper trailing edge are sheeted with 1/32 in balsa. CA is used to bond elements. MonoKote™ covers the wing.

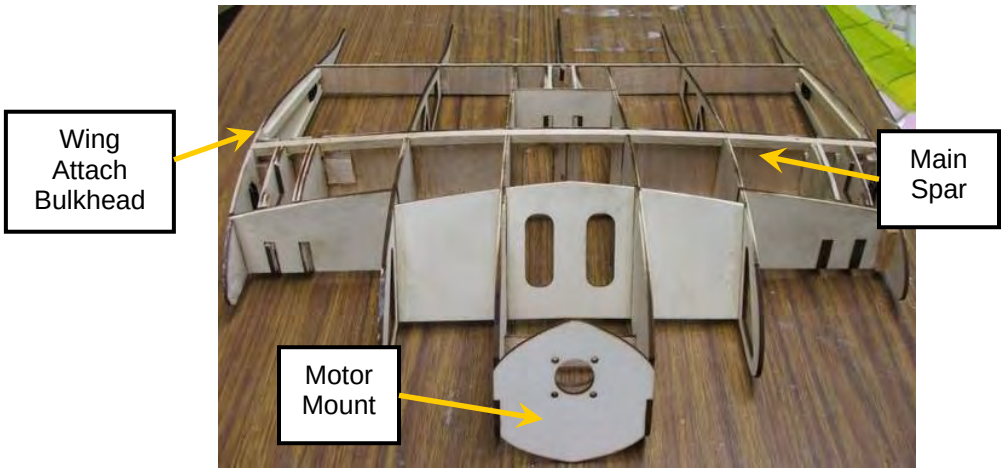

Figure 6.6 – Center Section

6.4.3 Wing Joint

The wing joint consists of two major components, the dowel extensions and the quick release clips (Figure 5.2). The wing joint is fabricated as outlined in §5.9. The two dowel extensions slide into the center section, where they fit into friction-fit holes.

6.4.4 Control Surfaces

Elevons are fabricated using ribs which are then sheeted with 1/32 in balsa. Sheeting is utilized to ensure the elevon structural rigidity and to retain airfoil reflex. Elevons are attached to the aft spar using two CA hinges. Rudders are fabricated using a flat plate, which is laser cut from 1/8 in plywood. MonoKote™ is applied to maintain aerodynamic shape.

6.4.5 Storage Box

The box is fabricated from ¼ x ¼ in birch sticks, balsa/fiberglass sheeting, Velcro™ attachments, and CA. This technique was selected primarily because of birch's appropriate strength to weight ratio, which enables a lightweight and sufficiently strong design. Additionally, the manufacturing team has gained confidence working with these materials throughout the manufacturing process.

7.0 Testing Plan

Conceptual testing focuses on planform performance to reveal potential design complications early in the design process. Preliminary design testing focuses on validation of custom airfoil design and AC location predictions. Detail design testing begins as component level with propulsion testing and progresses into an all-up approach in ground and flight testing. Complex analysis methods are validated before construction begins.

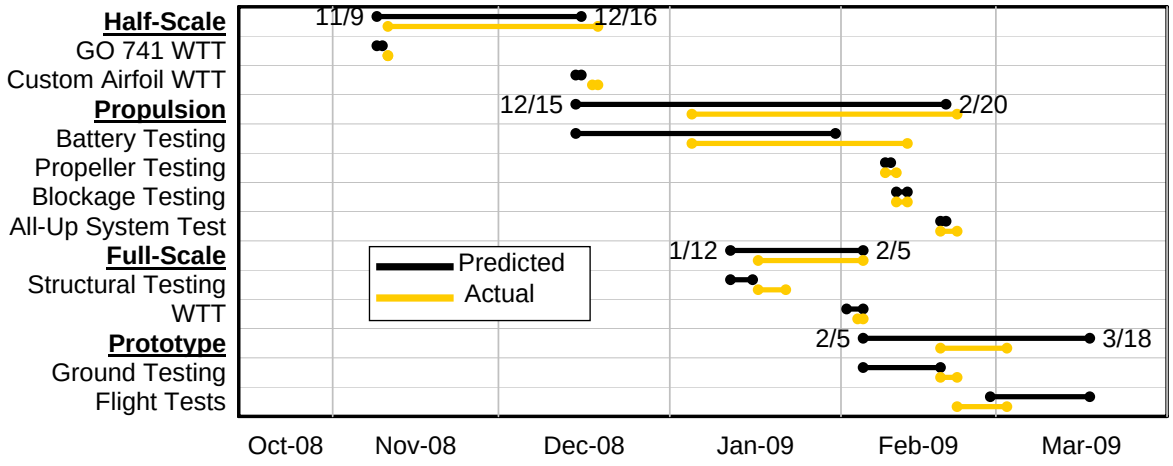

Figure 7.1 – Testing Schedule

7.1 Half-Scale Wind Tunnel Testing

Two half-scale wind tunnel tests are conducted in WSU's 3x4ft Low Speed Wind Tunnel.

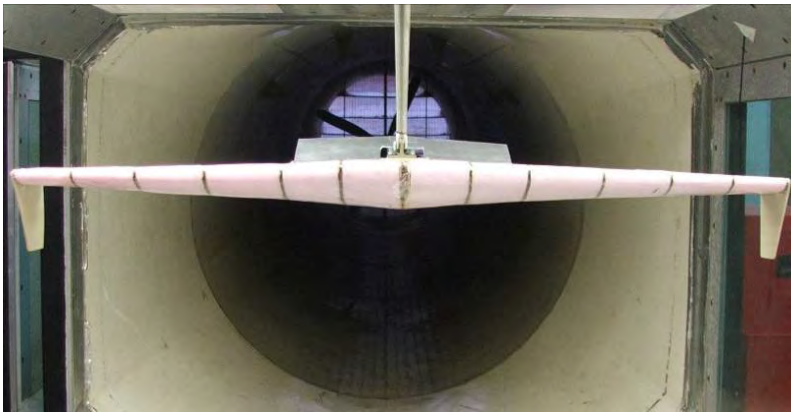

Figure 7.2 – Half-Scale Model Mounted in WSU's 3x4ft Wind Tunnel

These tests are conducted to validate aerodynamic and stability calculations for both the GO 741 and the custom airfoil. The test plan matrix is shown in Table 7.1:

Run #	q (psf)	α	δe	Comments	Output
1	15	-4,20;2	Off	Takeoff conditions	L, D, and M Polars at T/O
2	15	-4,20;2	Off	Repeat Run 1	Drag Counts Repeatability at $C_{D,min}$
3	15	-4,20;2	Off	Tripped at 25%c	Simulate Higher Re #
4	15	-4,20;2	Off	Repeat Run 3	Drag Counts Repeatability at $C_{D,min}$
5	15	-4,20;2	-20	Full elevon deflection	Validate elevon analysis estimates
6	15	-4,20;2	-10	Medium elevon deflection	Validate elevon analysis estimates

Table 7.1– Half-Scale Wind Tunnel Test Matrix

7.2 Propulsion System Testing

Propulsion system and component testing is vital to analyze the chosen configuration (§4.7.2). Individual component test data are used as inputs into the propulsion module, while full system testing is used to validate and provide confidence in full configuration modeling.

7.2.1 Battery Testing

Battery testing is performed using a West Mountain Radio Computerized Battery Analyzer (CBA) available through the Aerospace Engineering department at WSU. The CBA monitors the voltage output by a battery pack while it applies a specified load. Mission profiles are simulated and the battery performance is recorded as scatter plots of capacity used throughout each testing portion. The testing process of WSU's 2008 DBF team AeroShock is followed to ensure accurate results[17] (§4.7.1). Figure 7.3 shows a typical battery test setup. New and used packs of Elite 1500's, 1700's, and 2000's are tested.

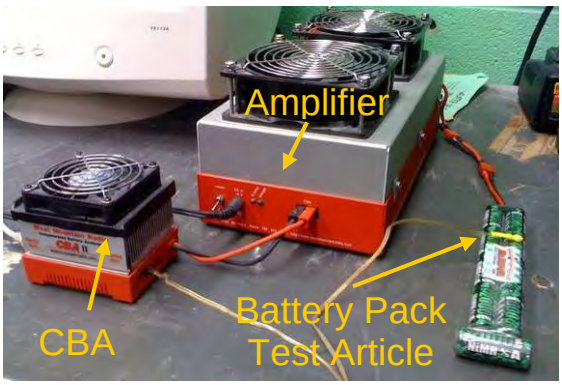

Figure 7.3– Battery Test Setup

7.2.2 Propeller and Blockage Testing

The effects of bottle blockage on thrust available are determined through propeller testing. Figure 7.4b shows an APC 15x10 E propeller in WSU's 3x4 ft wind tunnel mounted on a sting load cell for standard propeller characterization. The results of these tests (Figure 4.17, §4.7.2) are added to WSU's propeller database[13]. Figure 7.4a illustrates the blockage testing performed on the same APC 15x10 E propeller. Blockage testing results are presented in Figure 4.17.

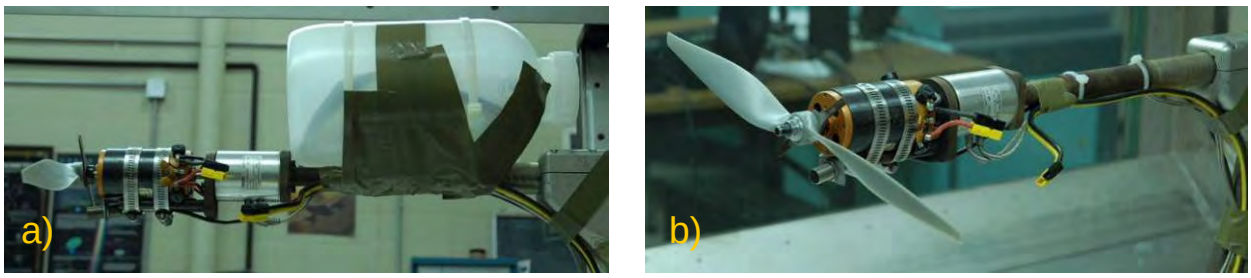

Figure 7.4 – Propeller Test Setup in WSU's 3x4 ft Wind Tunnel a) with Blockage and b) Clean

7.2.3 All-up Propulsion System Testing

The selected propulsion system (Table 4.7, §4.7) is tested in the 3x4 ft Low Speed Wind Tunnel. The motor is mounted on the same sting and three component balance as is used in the propeller and blockage testing (§7.2.2). Figure 7.5 shows the testing setup. The results are compared to predictions in §8.0. Table 7.2 shows the propulsion system testing matrix.

Run	Type	Battery Configuration
1	q-sweep (0,0.1,0.5,1.5,4,6,10psf)	Power Supply to Characterize Resistances w/ APC 14x10 E Prop
2	q-sweep (0,0.1,0.5,1.5,4,6,10psf)	12 Elite 1700 Cells w/ APC 14x10 E Prop (Mission 1)
3	q-sweep (0,0.1,0.5,1.5,4,6,10psf)	12 Elite 2000 Cells w/ APC 14x10 E Prop (Mission 3)
4	q-sweep (0,0.1,0.5,1.5,4,6,10psf)	14 Elite 1700 Cells w/ APC 16x10 E Prop (Mission 2)

Table 7.2 – Propulsion System Test Matrix

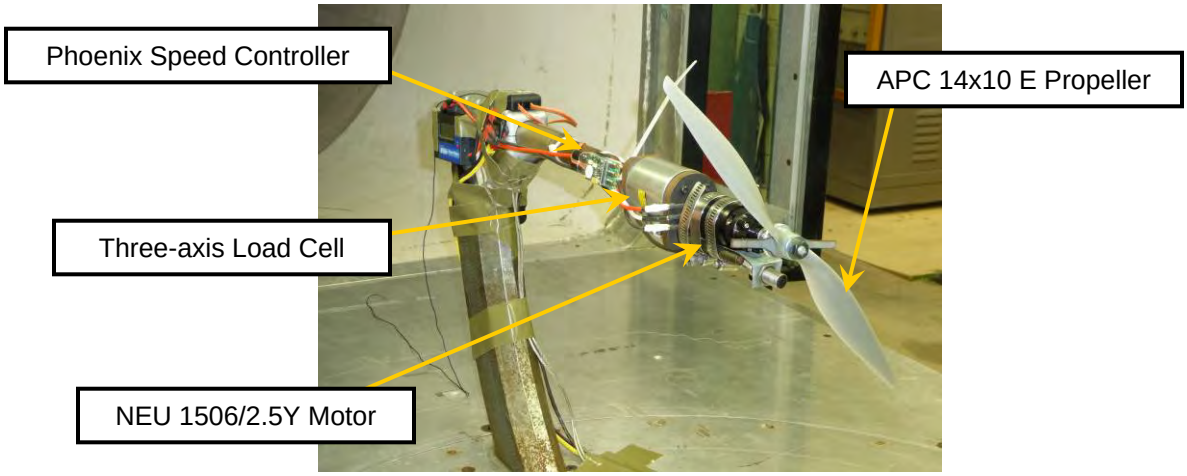

Figure 7.5– Motor, Propeller, ESC in Test Section

7.3 Structural Testing

The Ground Mission wingtip lift test is the critical case for both normal stress and shear stress. Two structural tests are performed on each wing joint design. Full scale models of the aircraft structure (without MonoKote™) are built. The centerline store is attached to the aircraft to simulate Ground Mission. Three pounds of water are added to the bottle and a wing tip lift test is conducted. Since the aircraft CG is not on the wing tip, a third lift point (at the aircraft apex) is used to balance the loads. Water is added to

the centerline store in one pound increments and lift tests are conducted until the centerline store is filled. A second centerline store is attached below the original store (Figure 7.6). Water is added in the same manner until failure occurs. Results are presented in §5.5.1.

Figure 7.6– Ground Mission Wingtip Test

Mission 3 payloads create significant torsion because the rockets are ballasted well in front of their pylon attachment point to maintain a constant CG. A test is conducted to validate the predicted wing twist. Two ballasted rockets are snapped into the release mechanisms at 24 in and 30 in on a full scale model of the wing. This test ensures that the wing twist is negligible and that the pylons can withstand the moment at the release mechanism.

7.4 Full Scale Wind Tunnel Testing

The first full-scale prototype is constructed using the balsa and MonoKote™ build-up outlined in §6.4. Electrical components are not installed, but all S&C features are modeled, including pin-positioned adjustable elevons and rudders. Wing sections are attached with clips. A spinner is attached to the wing apex to simulate critical aspects of the propulsion system geometry. The model is installed in the WSU NIAR 7x10 ft Walter H. Beech Memorial Wind Tunnel with full accommodations for mission payload configurations. Mission 2 drag reduction experiments are performed on clay fillets (Figure 7.7) and rockets are mounted for Mission 3 simulation (Figure 7.8). The testing matrix is shown in Table 7.3.

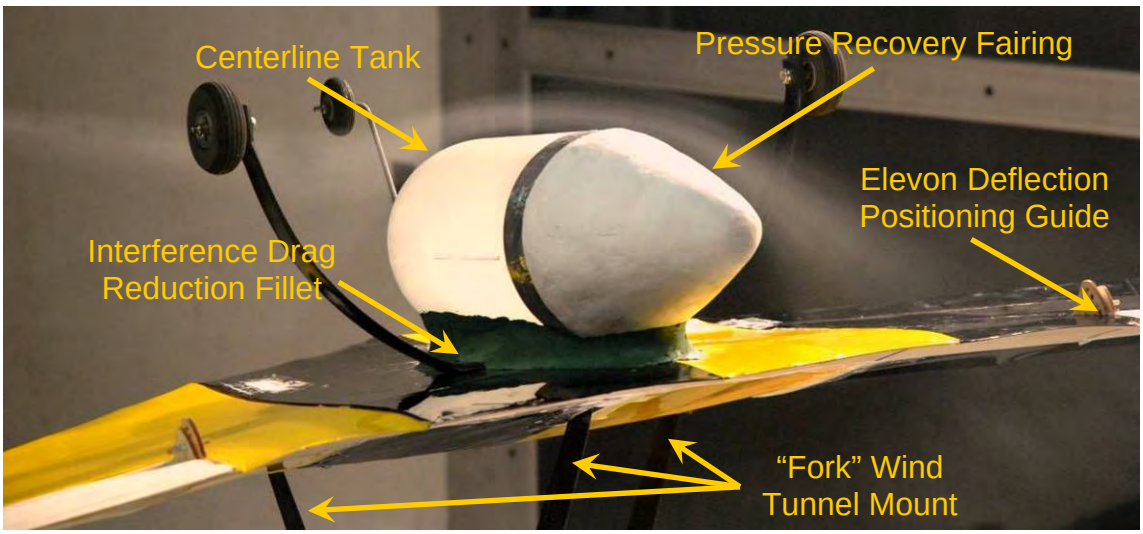

Figure 7.7 – Smoke Flow Visualization on Faired Centerline Tank in WSU’s 7x10ft Wind Tunnel

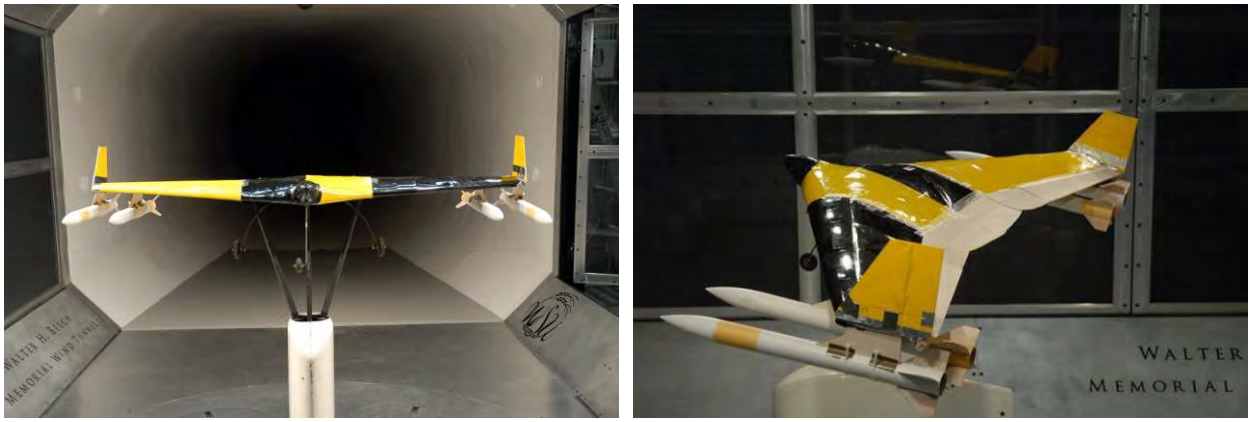

Figure 7.8 – Rocket Payloads Installed in 7x10ft Wind Tunnel

Run	Re / ft	α (°)	Ψ (°)	δe (°), P/S	δr (°)	Output
1	300K	-4,20;2	0	0	0	Lift, Drag, and Moment Polars
2	400K	-4,20;3	0	0	0	"
3	300K	-4,20;4	0	0	0	Effect of 4 rockets on clean polars
4	300K	-4,20;5	20	0	0	Side force due to high crosswind
5	300K	10	-20,20;4	0	0	Sideslip derivatives at takeoff
6	400K	0	0	0	0	Polars for 4 rockets at cruise
7	300K	-4,20;2	0	0	0	RM due to worse case asymmetric
8	300K	-4,20;2	20	0	0	Side force due to high crosswind
9	300K	10	-20,20;4	0	0	Sideslip derivatives at takeoff
10	400K	-4,20;2	0	0	0	Polars for 2 rockets at cruise
11	300K	-4,20;2	0	-20 / -20	0	Elevon effectiveness in blockage
12	300K	0,10;2	0	+20 / -20	0	"
13	300K	-4,20;2	0	+20 / +20	0	"
14	300K	-4,20;2	0	-10 / -10	0	"
15	300K	0,10;2	0	+10 / -10	0	"
16	300K	-4,20;2	0	+10 / +10	0	"
17	300K	-4,20;2	0	0	15	Rudder effectiveness
18	300K	0,10;2	0	0	30	"
Model inversion occurs to accommodate centerline store						
19	300K	-4,20;2	0	0	0	Interference effects of mount
20	400K	-4,20;2	0	0	0	"
21	300K	-4,20;2	0	0	0	Polars for unfaired bottle
22	300K	-4,20;2	0	0	0	Polars for faired bottle
23	300K	-4,20;2	20	0	0	SF and RM on faired bottle in X-wind
24	300K	10	-20,20;4	0	0	T/O sideslip derivatives w/ faired bottle
25	300K	-4,20;2	0	-20 / -20	0	Elevon effectiveness with shifted AC
26	300K	-4,20;2	0	-10 / -10	0	"
27	300K	-4,20;2	0	+10 / +10	0	"
28	300K	-4,20;2	0	0	0	Beneficial moment due to VGs?
29	300K	-4,20;2	0	0	0	Flow separation reduction methods?

Table 7.3 – Full Scale Wind Tunnel Test Matrix

Upright and inverted run comparisons demonstrate the wind tunnel mounting system's negligible aerodynamic interference effects. Lift, drag, and moment polars are obtained for all mission payload

configurations and compared to predictions (Figure 8.2). S&C derivatives are determined for all missions and compared to predictions (Table 8.1). Drag reduction techniques are assessed at the end of testing.

7.5 Ground Testing

Proper operation of electrical subsystems and the propulsion system is verified upon completion of prototype aircraft. The competition ground mission is simulated, with the aircraft and all equipment in the storage box. Structural integrity is inspected after a 6 in box drop[1]. Timed assembly of the equipment, stores, and aircraft is performed to improve assembly time.

7.6 Flight Testing

Extensive flight testing is performed to validate performance estimates, assess dynamic modes, and ensure proper completion of all mission profiles. The pre-flight checklist (Table 7.4) and flight test plan (Table 7.5) are designed for DBF competition simulation. Multiple flight tests are scheduled to familiarize the pilot with all the aircraft's handling and performance aspects. Pilot feedback is utilized to improve the design's electrical reliability, reduce weight in non-critical areas, and improve flight handling qualities.

Figure 7.9 – Maiden Flight February 22, 2009

Item	Description	Initial
Electrical System	Verify all wires are connected, check fuse	
Propulsion System	Batteries charged? Battery, motor, & prop. secured?	
CG Location	All systems, payload, and batteries are positioned for correct CG	
Payload Release	Verify release systems work properly for all stores	
Hatch	Closed and secured?	
Radio	Battery charged? Range check with antenna down at 200 ft	
Flight Controls	Correct channel settings, trim, limits, and unrestricted movement	
Structural Integrity	Verify functionality of flight controls during wing tip test	
Pilot Briefing	Describe flight profile and discuss predicted handling qualities	
Ground Run	Perform full-throttle run-up for five seconds	
Wind Characterization	Determine and record wind speed and direction	
Runway Safety Check	Verify that no foreign objects or hazards are obstructing the runway	

Table 7.4 – Pre-Flight Checklist

Flight #	Mission / Pilot Comments	Output
1	Empty aircraft, complete two 180 degree turns and land. **Pilot feedback:** smooth, fast takeoff with minimal control input required. Longitudinal trim for cruise is inherent. Roll response is crisp. Single damped longitudinal oscillation at takeoff. Handling qualities are satisfactory. Fun to fly.	S_{LO} (used to validate performance code). Dynamic mode behavior. Handling qualities.
2	**Fly Mission 1 course profile** (empty centerline tank)	S_{LO} < 100 ft? Acceptable handling?
3	**Fly Mission 2 course profile** (full centerline tank)	S_{LO} < 100 ft? Endurance / Handling
4	**Fly Mission 3 course profile for the following payloads:**	S_{LO} < 100 ft? Acceptable handling? Control authority for asymmetric loading in T/O crosswinds.
a	Lap 1: 4 rockets, taxi to 10'x10' box and release 1 rocket	
b	Lap 2: 3 rockets (2 left and 1 outboard right), taxi/release	
c	Lap 3: 2 rockets (both on left wing), taxi/release	
d	Lap 4: 1 rocket (inboard left wing), taxi/release	
5	**Fly Mission 3 course profile for alternate payload release**	Handling consistency and authority for all rocket payload combinations.
6	**Fly Mission 3 course profile for alternate payload release**	Handling consistency and authority for all rocket payload combinations.

Table 7.5 - Flight Testing Matrix

8.0 Performance Results

The propulsion system testing results (§7.2.3) are presented in Figure 8.1a. The predictions from the propulsion module are 10-15% higher than the experimental data. This discrepancy is attributed to the difference in propeller blade Reynolds numbers seen during full system testing as compared to those in WSU's propeller database[13]. Experimental uncertainties include wiring and equipment connection, which also contribute to the difference. New propeller coefficients are found and input into the module. The results (Figure 8.1b) lie within 2-6% of the empirical results, which validate the propulsion module code. Currently, further battery research is being conducted to investigate inconsistencies in Mission 2 results.

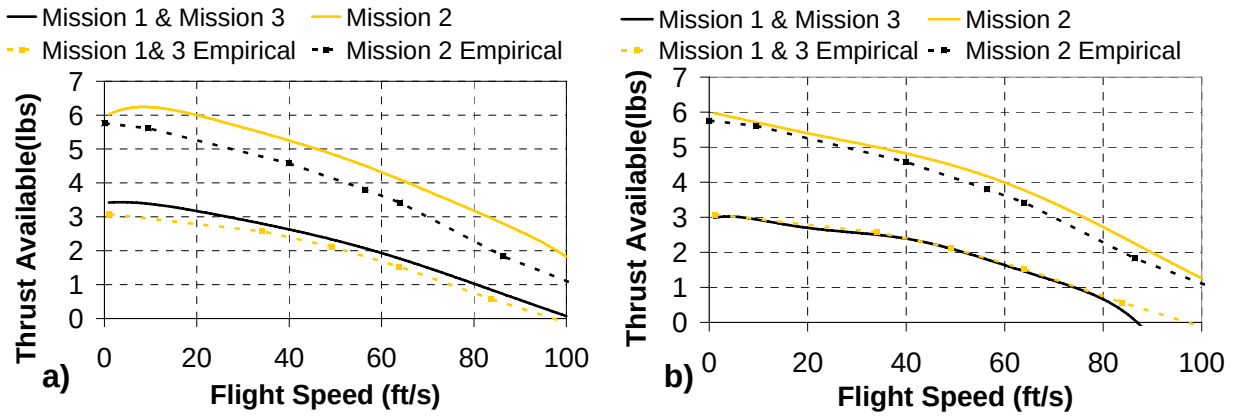

Figure 8.1 – Propulsion Predictions and Experimental Results

Half-scale (§7.1) and full-scale (§7.4) WTT results are compared in Figure 8.2. Half-scale model manufacturing imperfections (due to the foam and packing tape leading edge, Figure 7.2) induce flow separation, which decreases C_{Lmax} by 30%, generates a negative C_{Mo}, and increases C_{Do} by 32%.

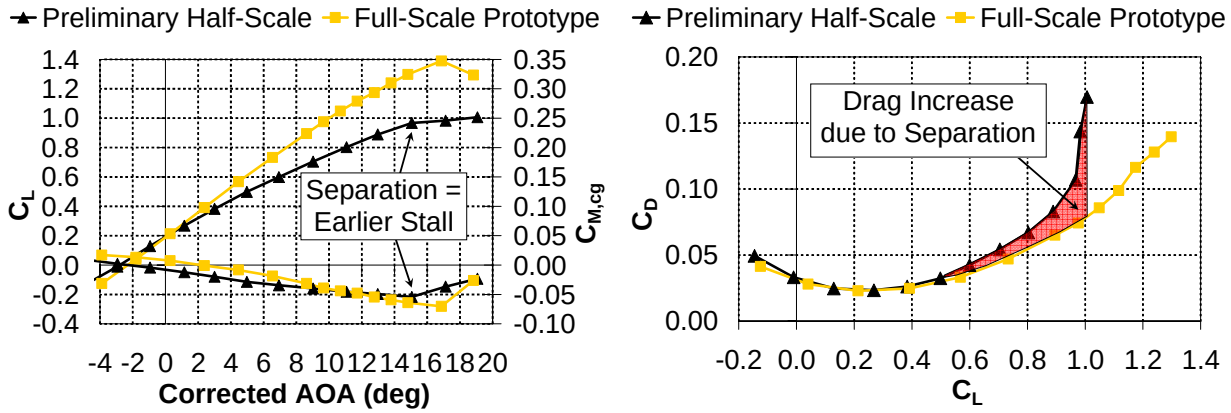

Figure 8.2 - Lift, Moment, and Drag Polar Comparison for Half-Scale and Full-Scale WTTs

Full-scale WTT results are compared to predictions in Table 8.1. Differences in C_{Lo}, C_{Lmax}, C_{Do}, and C_{Mo} are attributed to separated flow as discussed above. Additionally, differences from predictions are highlighted for Cn_{β}, $Cy_{\delta r}$, and $Cn_{\delta r}$. The 105% increase in Cn_{β} is attributed to the large vertical surface area behind the CG, as well as payload vertical surfaces exposed in sideslip, which were not modeled for predicted values. The rudder ineffectiveness seen in WTT data for $Cn_{\delta r}$ is attributed to turbulent spanwise flow, as seen with smoke flow visualization. Flight testing with a boundary layer fence is scheduled.

Parameter	Predicted Value	WTT Result	Percent Difference
C_{Do}	0.0399	0.0273	-32%
C_{Lo}	0.1311	0.1662	27%
$C_{L\alpha}$	4.0788	4.6018	13%
C_{Lmax}	1.0541	1.3653	30%
C_{Mo}	-0.0083	0.0075	**190%**
$C_{M\alpha}$	-0.2549	-0.2620	3%
Cy_{β}	-0.3038	-0.4165	37%
Cl_{β}	-0.1126	-0.1074	-5%
Cn_{β}	0.0559	0.1147	**105%**
$C_{L,\delta e}$	1.1855	0.9456	-20%
$C_{M,\delta e}$	-0.3460	-0.3351	-3%
$C_{l,\delta a}$	0.2585	0.2997	16%
$C_{n,\delta a}$	-0.0057	-0.0059	4%
$C_{Y,\delta r}$	0.5889	0.1941	**-67%**
$C_{l,\delta r}$	0.0349	0.0311	-11%
$C_{n,\delta r}$	-0.1083	-0.0350	**-68%**

Table 8.1 – Summary of Demonstrated Aircraft Performance Parameters

9.0 References

[1] "AIAA Design/Build/Fly Competition -2008/09 Rules", 26 Aug. 2008, <http://www.aiaadbf.org/>.

[2] Anderson, J. D. Introduction to Flight. 5th ed. Boston: McGraw, 2005.

[3] Metheny, M. "The Podium." TerraBreak.org: An independent Design/Build/Fly support site. 24 April 2008. TerraBreak. 24 Sep 2008 <http://www.terrabreak.org/podium/>.

[4] Miller, L. S. "AE 512 Experimental Uncertainties".

[5] Nickel, K. Tailless Aircraft in Theory and Practice. 2nd ed. London: AIAA Education Series, 1994.

[6] Raymer, D.P. Aircraft Design: A Conceptual Approach. 4th ed. Reston, VA: AIAA, 2006.

[7] Miley, S.J. A Catalog of Low Reynolds Number Airfoil Data for Wind Turbine Applications. U.S. Dept. of Energy, 1982.

[8] Seddon, J. Basic Helicopter Aerodynamics. 2nd Ed. Reston, VA: AIAA, 2001.

[9] Roskam, J. Airplane Flight Dynamics and Automatic Flight Controls: Part 1. 5. Lawrence, KS: Design Analysis Research Corporation, 2007.

[10] Roskam, J. Airplane Design Part VI: Preliminary Calculation of Aerodynamic Thrust and Power Characteristics. 2. Lawrence, KS: Design Analysis Research Corporation, 2000.

[11] Allen, D. & Haisler, W. Intro. to Aerospace Structural Analysis. College Station, TX: Wiley, 1985.

[12] Zamora, A., et. al. DBF Propulsion Manual. Wichita State University. 2007.

[13] Merchant, M., and Miller, L.S., "Propeller Performance Measurement for Low Reynolds Number UAV Applications", AIAA paper 2006-1127, 2006.

[14] "Motors - 1500 Series." NeuMotors. 2 Dec 2008 <http://www.neumotors.com/>.

[15] "Loose Cells - NiMH." CheapBatteryPacks. 2 Dec 2008 <http://www.cheapbatterypacks.com/ >.

[16] "Product Listing -Thin-Electric." APC Propellers. 2 Dec 2008 <https://www.apcprop.com/ >.

[17] Anyasi, J., et. al. WSU Aeroshock, Design/Build/Fly Design Report, Wichita State University, Mar. 2008.

[18] Butler, P., et. al. WSU DCM-006, Design/Build/Fly Design Report, Wichita State University, Mar. 2005.

[19] Hoerner, S.F. Fluid Dynamic Drag. 1st ed. Bakersfield, CA: Hoerner, 1965.

[20] Hoerner, S.F. Fluid Dynamic Lift. 2nd ed. Bakersfield, CA: Hoerner, 1992.

[21] Larsen, T., et. al. Wu-Haul, Design/Build/Fly Design Report, Wichita State University, Mar. 2008.

[22] Bahopia, N., et. al. SOS, Design/Build/Fly Design Report, Wichita State University, Mar. 2004.

[23] "NWS Tucson." NOAA. <http://www.wrh.noaa.gov/twc/aviation/windrose_TUS.php>.

[24] NOAA, NASA, USAF. U.S. Standard Atmosphere 1976, GPO, Washington DC; 1976.

[25] Zamora, A. Personal/Email interview (GO 741 CFD Analysis). 20 Nov. 2008.

[26] Zamora, A. Personal/Email interview (Custom Airfoil CFD Analysis). 8 Dec. 2008.

[27] Drela, M., XFOIL. Vers. 6.94. Computer software. MIT, 2001. Windows P4, 532 KB, Download.

[28] Stivers, L & Rice, F., Aerodynamic Characteristics of Four NACA Airfoil Sections Designed for Helicopter Rotor Blades. NACA-RB-L5K02. Langley, Langley Field, VA: 1946.

[29] CATIA, Software Package, Vers. 5.18, Dassault Systemes, Vélizy-Villacoublay, France, 2008.

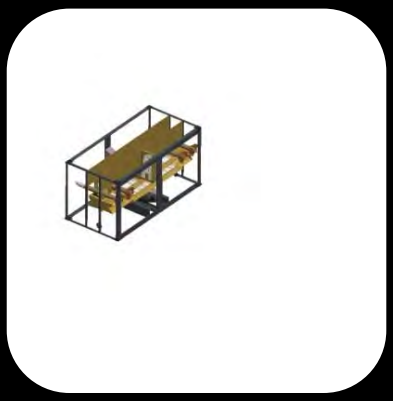

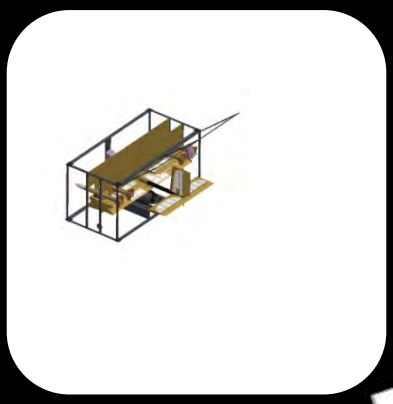

FASTBACK


Oklahoma State University
Team Black
AIAA Design/Build/Fly 2008/2009

TABLE OF CONTENTS

1.0 EXECUTIVE SUMMARY

This report details the design, testing, and manufacturing processes used by Oklahoma State University Team Black to prepare for the 2008/09 AIAA/Cessna/RMS student Design/Build/Fly competition. The primary objective of the design is to maximize the competition score based on the equation provided for the competition. A comprehensive management plan was developed and implemented to foster innovative design solutions and to allocate team resources effectively.

1.1 Design Development & Alternatives

Design development begins with an analysis of the scoring function that is comprised of a report and flight score (FS). The FS is based on a pre-mission aircraft assembly time and three sequential flight missions: a ferry flight, surveillance flight, and payload release/asymmetric loads. Factored into the FS is a system complexity factor (SCF), which is a function of assembly time and rated aircraft cost (RAC). The RAC is defined for the first time in the history of the competition as total system weight and includes aircraft, payloads, storage box, ground control system, and all assembly tools rather than just aircraft weight. During the pre-mission, the box and its stored contents must also pass a flip test and a 6 in drop test. The most important design constraints include a 100ft take-off distance; a maximum of two storage boxes no greater than 2 ft x 2 ft x 4 ft each; the capability to deploy a 4 liter center payload and four 1.5 lb wing-mounted payloads remotely and independently; a 24 in minimum span wise spacing between wing payloads and the centerline and a 6 in minimum span wise spacing between wing payloads. The SCF weighting in the flight score places an emphasis on non-flight performance factors in the competition this year. Score analysis confirms this and shows that assembly time is the most critical score variable to optimize the competition score.

Several solution concepts are presented to minimize assembly time and balance the other design requirements of low RAC, low flight time for mission 1, and low loading time of wing payloads for mission 3. Design constraints limit the wingspan from 5 ft to 8 ft, which is greater than the maximum box dimension and is thus factored into the solution concepts. They are (i) an aircraft with detachable wings in a single box; (ii) an aircraft with folding wing tips and an extendable tail boom in a single box; (iii) an aircraft with detachable wings in one box with payloads stored in a second box. A down select analysis using Figures of Merit (FOM) selected an aircraft with folding wings and an extendable tail boom for the best assembly time. Wing hinges align outer and inner wing segments for rapid assembly, clip-in release mechanisms allow for simultaneous installation of all five payloads, and an extendable tail boom is included to meet geometrical constraints. A rigid rectangular box is used to store system components and allow for accurate alignment of payloads with the release mechanisms for rapid installation. The selected aircraft configuration has a conventional tail for short take-off, and the empennage and control surfaces are sized to accommodate a short coupled aircraft with asymmetrical loads. A tricycle undercarriage is selected for stable ground handling characteristics, and additional outrigger landing gear are mounted on

the wings to prevent a tip over while taxiing with asymmetrical wing loads. A single-stack battery configuration is chosen for its high power to weight ratio, and a self-installing battery box is used to minimize battery installation time. A Multidisciplinary Optimization Code (MDO) program is used to optimize the competition score by analyzing different combinations of the critical design variables, including wing area, span and airfoil, motor and gearbox, propeller, and battery selection and quantity.

1.2 Optimized Design Summary

The optimized system design integrates a folding wing aircraft with automatically loading payloads and battery box for the best possible assembly time. Combined with a light weight airframe and storage box for low RAC, an optimum SCF is obtained. SCF is the most important parameter for score optimization.

The wings are sized to a 6.93 ft wingspan with a total wing area of 6.00 ft^2 and a MH 114 airfoil to meet takeoff distance requirements for mission 2. A NACA 0009 airfoil is selected for the horizontal and vertical tails and sized to provide the required stability, and all control surfaces are sized to provide sufficient control power for asymmetrical loading combinations in mission 3. Propulsion optimization suggests that a Neu 1905/1.5Y motor geared to 5.2:1 provides optimal performance for all three missions, and the combination of 24 Elite 1500 cells with an 18x10 propeller yields the highest score. A Spectrum DX7 radio system is selected to minimize control system weight and incorporates an arm/disarm switch for safety. An open frame carbon fiber box provides the required strength for pre-mission tests, rigidity for the accurate self-installation of payloads during pre-mission assembly, and a low weight of 7 lb. The extended fuselage length is 37.11 in and the stored fuselage length is 23.16 in.

1.3 System Performance and Capabilities

The following total mission performance is predicted: Pre-mission Assembly - 6 seconds; Ferry Flight - total flight time 74 seconds; Surveillance Flight - 20% power remaining at mission completion with five mph winds, with 25 mph or above 0% power remaining; Payload Release/Asymmetric Loads: loading time 8-10 seconds. The system passes the box flip test, 6 in drop test, shake test, as well as the wing tip test to simulate a 2.5G wing load. Using the predicted 30.56 lb RAC, the estimated competition score is 199 out of a theoretical maximum of 225.

2.0 MANAGEMENT SUMMARY

2.1 Design Team Organization

The 2009 Team Black consists of 26 mechanical and aerospace engineering students ranging from sophomores to seniors at Oklahoma State University. The team organizational chart is shown in **Fig. 2.1**.

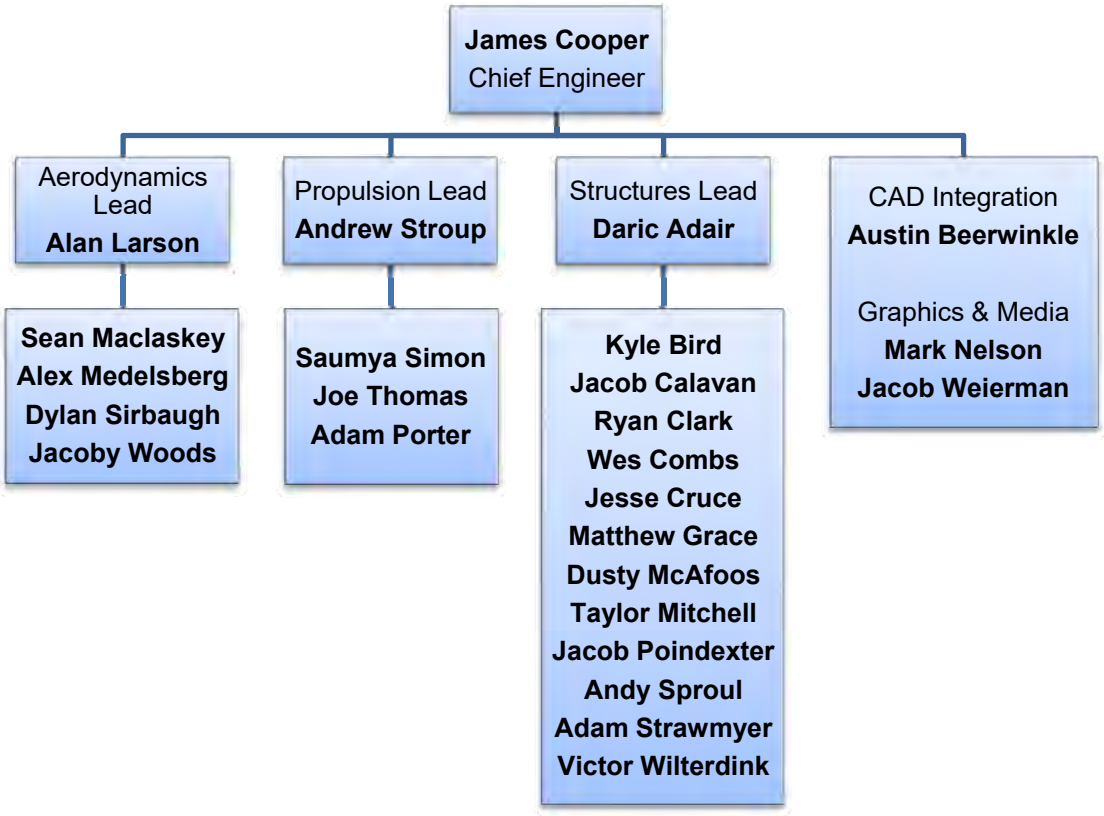

Figure 2.1: Team Organization Chart

The team is headed by a chief engineer and four technical lead engineers who are collectively responsible for the management and coordination of four technical groups: aerodynamics, propulsion, structures, and CAD integration. The objective of the aerodynamics group is to optimize the aircraft configuration for maximum mission performance, ensure stability and control, and predict flight testing performance. The propulsion group is responsible for the optimization of the propulsion system, the analysis of power requirements for each mission, and the selection and testing of propulsion system components. The structures group is responsible for the detailed design and construction of the integrated aircraft system. This includes the aircraft, box, and payload deployment mechanisms. The CAD integration lead is responsible for compiling system component designs into the master CAD drawing for manufacturing and publication.

2.2 Milestone Chart

This design project is conducted over a single sixteen-week semester at OSU. With this short time frame, the implementation of a structured design schedule throughout the semester is vital to develop a highly competitive design and meet all milestones and competition deadlines. The Gantt chart below, **Fig. 2.2**, outlines the sequence of critical tasks for successful project completion.

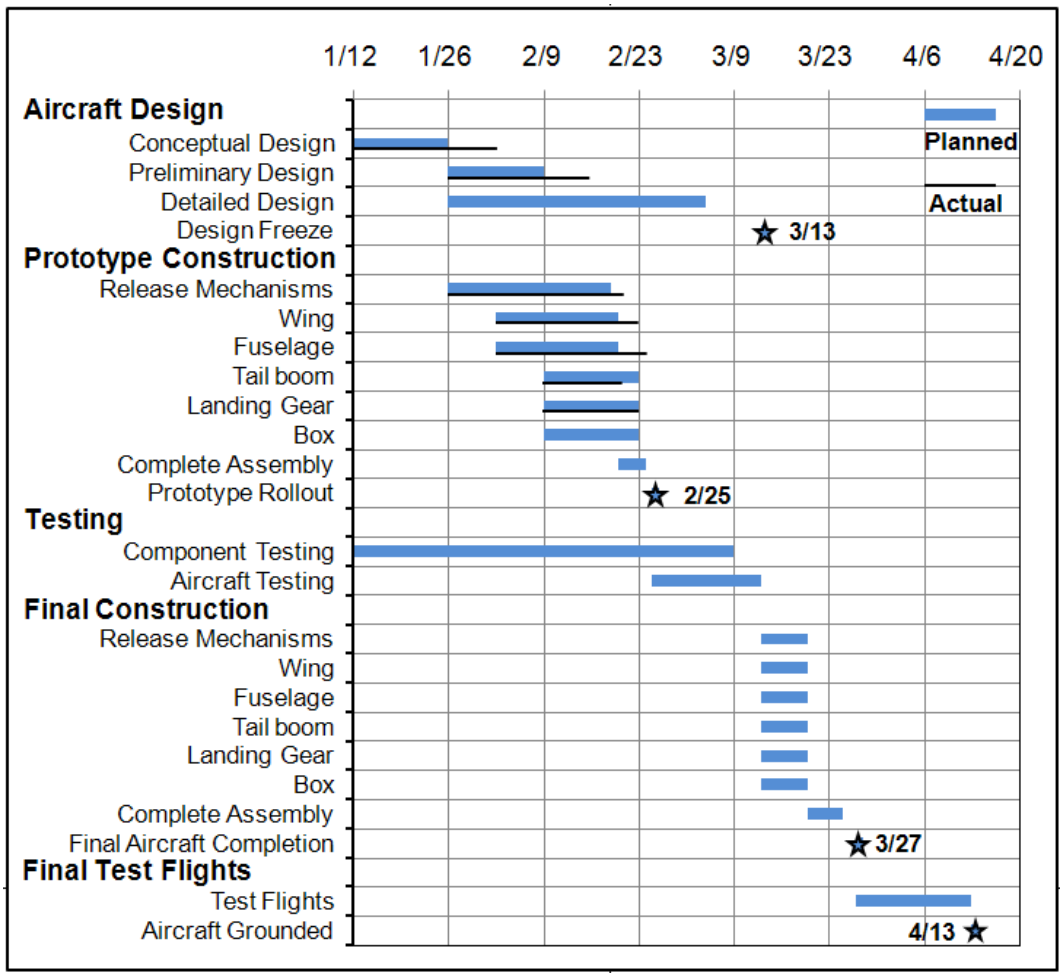

Figure 2.2: Milestone Chart

3.0 CONCEPTUAL DESIGN

Conceptual design begins by determining mission requirements and design constraints. The design variables and goals are determined to perform Figure of Merit (FOM) analysis and integrated box and aircraft configurations are presented and evaluated.

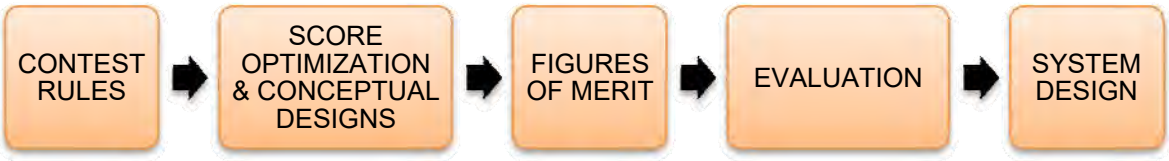

Figure 3.1: Conceptual Design Methodology

3.1 Mission Requirements

The competition score is the product of the written report score (100 points) and the total flight score, where the latter is the sum of normalized scores for mission 1 (ferry flight), mission 2 (surveillance flight), and mission 3 (payload release/asymmetric loads). Each mission includes a weighting factor which gives each sequential mission a greater mission score importance. Furthermore, missions must be completed in order, and no score is awarded for partial missions. This ensures that all competitive design solutions will be optimized for all missions. General specifications and mission specifications are listed below.

- Maximum of two storage boxes with outside dimensions no greater than 2 ft x 2 ft x 4 ft. Aircraft and all support equipment, assembly tools, and payloads must fit to these boxes.
- Maximum take-off distance of 100 ft.
- Aircraft must support multiple payload combinations and be able to release payloads remotely and individually.
- 4 x wing payloads: Estes Patriot rockets #2056 ballasted to 1.5 lb each, 2 per wing. At least 6 in spanwise separation between payload centerlines; innermost wing payload location at least 24 in outboard from aircraft centerline.
- 1 x 4 liter centerline payload: 4 liter Nalgene bottle #2121-0010. Nose and tail fairings may be added to the centerline payload, with total length not exceeding 15 in.
- Maximum battery limit 4 lb; 40 amp current limit.

3.1.1 Pre-Mission: Assembly

A timed assembly of the aircraft is required with all five payloads. Timed assembly begins with all components and payloads initially uninstalled and secured in the boxes and ends with a flight ready aircraft and re-secured boxes with tools inside. The pre-mission score is the **System Complexity Factor:**

SCF = 1 / (Assembly Time x RAC), where the **Rated Aircraft Cost (RAC)** is the combined weight of the aircraft, boxes, payloads, and assembly tools. The structural integrity of the boxes is also tested: boxes are rotated and placed face down on all sides and then dropped from a height of 6 inches on one side. The boxes and their contents must not be damaged and all control and propulsion systems in the assembled aircraft are also checked to ensure that are functioning. Failure of any system to operate will result in no score. The SCF is normalized to a maximum of 10.

3.1.2 Mission 1: Ferry Flight

Mission 1 requires the airplane to fly two laps with the centerline tank empty. The score is given by **M1 = SCF / Flight Time** and flight time begins when the throttle is advanced for takeoff and ends when the aircraft passes over the finish line at the end of the required laps. The aircraft must also complete a successful landing on the runway for the mission to be scored. The Mission 1 score is normalized to a maximum of 50.

3.1.3 Mission 2: Surveillance Flight

Mission 2 requires the aircraft to complete four laps with a four liter centerline tank attached and full with water. The score is given by **M2 = SCF**. The aircraft must complete the mission and successfully land on the runway for the mission to be scored. The Mission 2 score is normalized to a maximum of 75.

3.1.4 Mission 3: Payload Release/Asymmetric Loads

Mission 3 requires the aircraft to fly flour laps with four 1.5 lb rockets mounted on wing pylons (two per wing). The aircraft must land after each lap and release one payload as specified by the flight line officials within a designated 10 ft^2 area. The aircraft must come to a complete stop at the marked take-off position before each subsequent take-off. The score is given by **M3 = SCF / Loading Time**. Loading time starts with an assembled aircraft and all payloads in secured boxes and ends with a flight ready aircraft with all wing payloads installed and boxes re-secured with assembly tools and center payload inside. After the timed loading, the aircraft must pass a shake test to assure all payloads are secure before take-off. The Mission 3 score is normalized to a maximum of 100.

3.1.5 Score Sensitivity Analysis

A score sensitivity study is conducted to evaluate the effects of mission scoring parameters on the competition score. The normalized competition score equation is shown below where M1best, M2best and M3best are the best competition scores for missions 1, 2, and 3 respectively.

$$Competition\ Score = Written\ Report * SCF\left(\frac{50}{Flight\ Time * M1best} + \frac{75}{M2best} + \frac{100}{Loading\ Time * M3best}\right)$$

Best score estimates must be made for each score parameter due to score normalization. In **Table 3.1**, score parameter estimates are listed based on DBF aircrafts from 2004, 2005, and 2006 which had comparable payload and take-off distance requirements.

Parameter		Best Case
RAC	Aircraft Weight	5 lb
	Box Weight	5 lb
	Total Store Weight	15 lb
	Transmitter Weight	1.75 lb
Assembly Time		8 sec
Mission 1 Flight Time		60 sec
Mission 3 Loading Time		5 sec

Table 3.1: Score Sensitivity Assumptions

Data from these competitions indicate that the required wingspan is greater than the 4 ft maximum box dimension and the mission 1 lap time is approximately 60 seconds based on average maximum speeds. Estimates for assembly time and load time were based on the assumption that folding or detachable wings would be required and timed simulations were conducted using a mock-up cardboard aircraft and box. The box weight estimate was based on a single open frame box of maximum allowable dimensions using carbon fiber and honeycomb composite. A transmitter weight of 1.75 lb is based on commercially available radio control equipment that meets the mission and safety requirements for control systems. These best score assumptions are incorporated into the score sensitivity analysis shown in **Fig. 3.2** with a best RAC estimate of 26.75 lb. The RAC curve is modified to better represent the impact of system weight changes on score by excluding the payload weight constants.

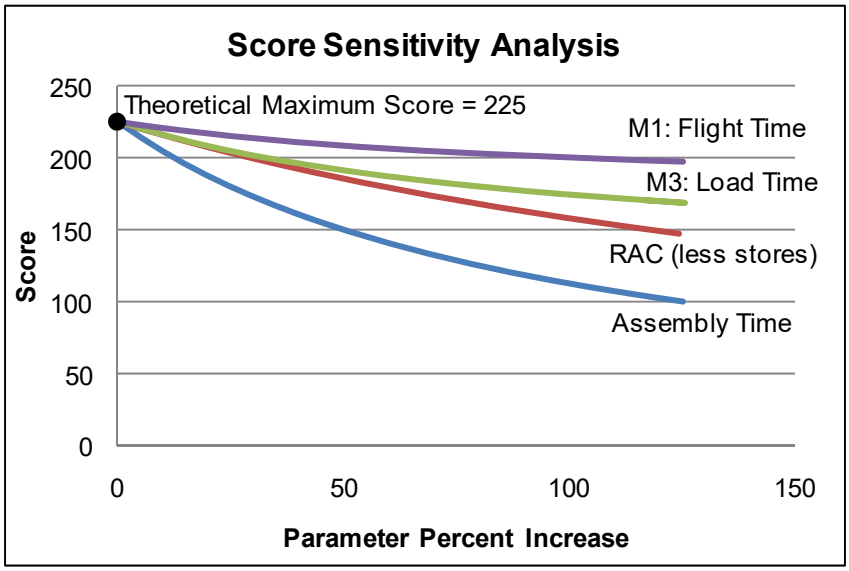

Figure 3.2: Comparative Score Sensitivity Analysis

Inspection of **Fig. 3.2** indicates that competition score is most sensitive to assembly time, followed in order of decreasing importance by RAC, load time, and flight time. Therefore assembly time and RAC are the most important factors for mission score optimization. Design objectives must focus total system integration not just flight performance optimization, which has been the historical emphasis of the AIAA DBF competition.

A large degree of uncertainty associated with assembly time and RAC is also important to score optimization. For example, theoretical assembly times for different system concepts can vary significantly, although mechanical reliability and human error may also have a large impact on assembly time in practice. For similar reasons, RAC also has a large degree of uncertainty. Given the importance of assembly time and RAC, special attention should be given to system reliability as well.

3.2 Design Requirements Definition

After conducting a score analysis and evaluation of past DBF aircraft, the team concluded that the design solution must have the following design objectives and requirements:

- Pre-mission: Assembly - Create a design solution to minimize assembly time.
- **Mission 1: Ferry Flight** - Minimize center payload drag to reduce ferry flight time.
- **Mission 2: Surveillance Flight** – Optimize propulsion system performance, wing size, and airfoil to minimize overall aircraft weight.
- **Mission 3: Payload Release/Asymmetric Loads** – Design landing gear to ensure stable ground handling characteristics with asymmetric loads, size control surfaces to ensure adequate flight handling characteristics with asymmetric loads, and develop a fast-loading payload method.
- **Manufacturing** – Produce a light weight aircraft (< 6 lb) and box solution (< 10 lb) to minimize RAC. Aircraft and box designs must have high strength-to-weight ratios.
- **Payload releases** – create reliable, light-weight release mechanisms to secure and deploy center payload and wing payloads.

3.3 Solution Concepts and Configurations

The following solution concepts for combined box, aircraft, and payload configurations are capable of meeting the stated design objectives requirements, which is shown in **Fig. 3.3**.

- **One Box, Detachable Wings** – The fuselage is longitudinally oriented in the box with detachable wings supported by the side walls. Payloads are mounted for quick clip-in assembly. Potential damage to aircraft by payloads during pre-mission testing is a potential problem, and increasing structural support to avoid this can significantly increase RAC. The potential for unwanted payload installation during pre-mission is also a concern.
- **One Box, Folding Wings, Extendable Tail Boom** – The fuselage is laterally oriented in the box with folding wings. Payloads are mounted for quick slot-in assembly as the aircraft is pulled out from the box and the tail boom extends to full length. Similar to the previous configuration, the potential for aircraft damage, increased RAC, and premature or failed

installation of payloads is possible and an extendable tail boom also increases system complexity. However, the strength of this configuration has the potential for a very fast assembly time.

- **Two Boxes, Aircraft and Payload Stored Separately** – Similar to the first concept, the fuselage is orientated longitudinally in the box with detachable wings supported by the side walls. Payloads are stored in a second box. Potential damage to aircraft by payloads during pre-mission testing is minimized, and the structural requirements for that aircraft box are decreased. RAC is potentially lower than the first two concepts, even with second box. A Triangular box is shown as an alternative, which can reduce surface area.

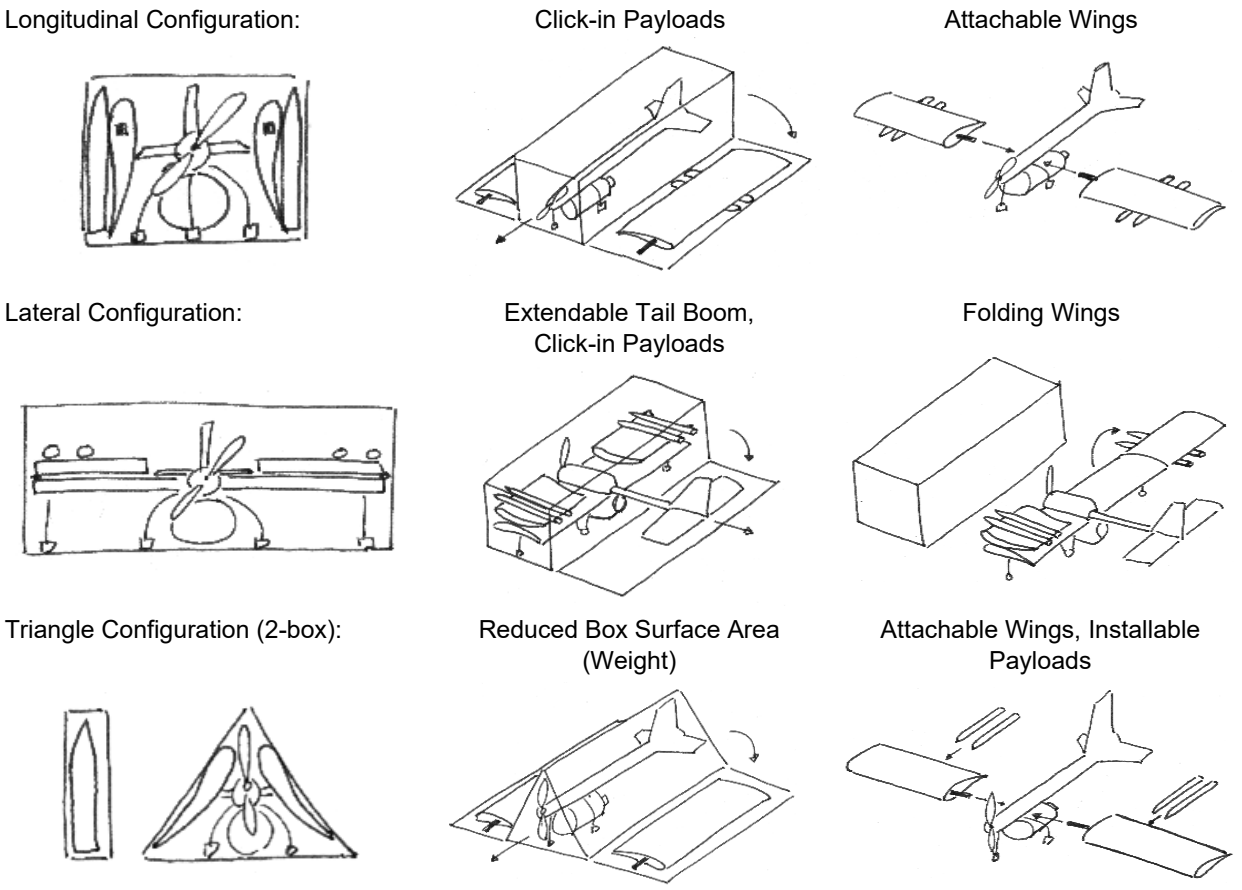

Figure 3.3: Conceptual Design Alternatives

3.4 Concept Weighting, Selection Process, and Results

3.4.1 System Configuration

Based on the solution concepts and configurations developed, a down-select process for the entire system was performed to identify the best alternative.

Figures of Merit

The following FOMs were assigned weighting factors and used to evaluate system alternatives. A scale of -1 to 1 was used to comparatively evaluate alternatives. A total score was then calculated to identify the best alternative as shown below.

- **Assembly Time** – This parameter establishes how fast the system can be assembled during pre-mission. The sensitivity analysis indicates that assembly time is the most important factor in the overall aircraft score.
- **Rated Aircraft Cost (RAC)** – Behind assembly time, RAC is the next most important Figure of Merit and is used as a fundamental parameter for every component and configuration.
- **Manufacturability** – This is a measure of how complex the configuration is to construct. With multiple options for aircraft design and box configuration, a simple and reliable design is critical.
- **Durability and Reparability** – The durability of the system is critical for mission completion, including all pre-mission tests. Additionally, reparability is also of importance.

Weighted Decision Matrix

The proposed solution concepts are evaluated based on the developed Figures of Merit, shown in the **Table 3.2**.

System Weighted Decision Matrix		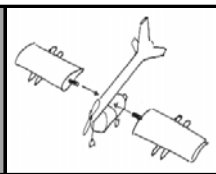	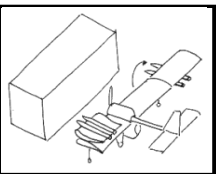	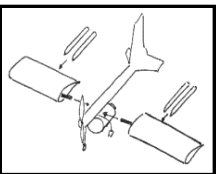
Figures of Merit	**Weight**	**Detachable**	**Folding**	**Two Box**
Assembly Time	0.5	-1	1	-1
RAC	0.3	0	-1	0
Manufacturability	0.1	1	-1	0
Durability and Reparability	0.1	0	0	0
Total	**1.0**	**-0.4**	**0.1**	**-0.5**

Table 3.2: General System Decision Matrix

Configuration

From the Weighted Decision Matrix results, the folding wing configuration was determined to be the most effective system design for this year's competition. Although the design had the heaviest weight model and required difficult construction methods, the reduction in assembly time resulted in the best score.

3.4.2 Landing Gear

For an aircraft supporting such a wide variety of payload configurations, the design selection of the landing gear played a larger role in the conceptual design process than in previous contests.

Figures of Merit

The following list identifies two FOMs for under-carriage selection.

- **Ground Handling** – Ground handling is a measure of how well the aircraft taxis with different payload configurations. Since there is a possibility for asymmetric payloads, the aircraft needs to have good ground handling.
- **Take-off Distance –** The landing gear affects the take-off angle, limiting the take-off distance. The take-off angle is limited if the landing gear is placed too far forward, but if the landing gear is placed too far aft; it is difficult to create a big enough moment to take-off.
- **Lateral C.G. Change** – The ability to handle lateral C.G. movement for asymmetric loads.

Alternatives

When developing alternatives for landing gear configurations, research was conducted on previous plane designs. Since outboard payloads would be carried for the competition, it was determined that outriggers could be necessary in addition to the main gear configuration. These would help keep the aircraft balanced on ground missions and on take-off and landing. Three main landing gear types were considered, which are listed below.

- **Tail Dragger –** The tail dragger uses two main gears with one gear on the tail. This configuration is light weight, but has poor ground handling.
- **Bicycle –** The bicycle configuration uses two main gears on the aircraft centerline. Due to the centerline payload this configuration becomes difficult to design around.
- **Tricycle –** The tricycle configuration uses two rear wheels for support and a front nose gear for steering.

Weighted Decision Matrix

In order to create a balanced comparison between landing gear options, a Weighted Decision Matrix was developed, identifying the advantages and disadvantages for each concept. To emphasize the critical parameters, each option was scored based upon the Figures of Merit, as shown in **Table 3.3**.

Landing Gear Weighted Decision Matrix		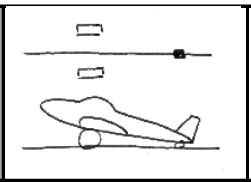	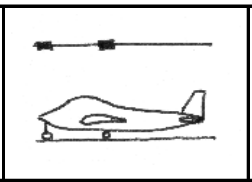	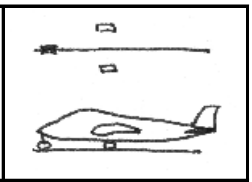
Figures of Merit	**Weight**	**Tail Dragger**	**Bicycle**	**Tricycle**
Ground Handling	0.4	-1	0	1
Take-off Distance	0.3	1	-1	1
Lateral C.G. Change	0.3	1	-1	0
Total	**1.0**	**0.2**	**-0.6**	**0.7**

Table 3.3: Landing Gear Weighted Decision Matrix

Configuration

The tricycle configuration has good ground handling characteristics and is suitable for short take-offs. The configuration is able to rotate about its aft wheels and its C.G. placement is not susceptible to instability like the tail dragger.

After the selection of the gear configuration was conducted, initial sizing for the tricycle landing gear consisted of a static calculation to determine the instability of the aircraft caused by asymmetric loads. In **Fig 3.4**, calculations were completed to the distance X to prevent the plane from rotating about point A.

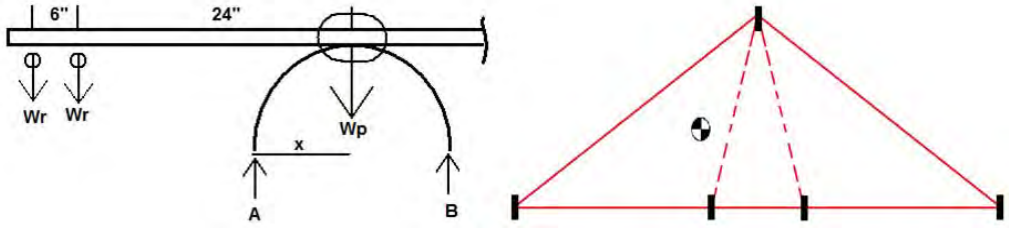

Figure 3.4: Landing Gear Sizing

Working with an assumed concentrated plane weight [W_p] of 4 lbs, the distance 'X' would need to be at least 11.5 in. It was determined that the use of a bow gear with a span of 23 in was unnecessarily heavy, which led to the use of wing-mounted outriggers. The addition of outriggers would keep the center of gravity of the airplane within the outline of the wheel base, as shown in the figure above. Without the outriggers, the C.G. falls outside of the area covered by only the tricycle gear and easily allows the aircraft to tip during taxiing, especially with wind conditions and the asymmetrical payload possibilities. The outriggers are lightweight, increases stability by maintaining the center of gravity inside the wheel area, but increase overall drag.

3.4.3 Tail

Many tail configurations were considered due to how the aircraft is packaged in the box. The tail needs to provide good stability characteristics while meeting geometric constraints of the box.

Figures of Merit

Tail FOMs are based on the assumption that all configurations yield the same assembly time.

- **RAC –** Low weight is important to increase competition score.
- **Stability –** This is a measure of relative stability and control benefits of a tail configuration.
- **Drag –** Low drag is beneficial because it reduces power requirements and, therefore, battery weight.

Alternatives

The tail alternatives were narrowed to three configurations based on how well they integrated with the overall system concept. Three alternatives are presented that can be incorporated with an extendable tail boom. The alternatives for the tail are listed below.

- **Conventional –** The conventional tail provides the lowest weight while providing good stability and control.
- **U-Tail –** The U-tail was considered due to lack of vertical space in the box. Since the U-tail has two vertical stabilizers, it allows for more vertical tail volume without using additional height.
- **V-Tail –** The V-tail has two angled stabilizers to provide both pitch and yaw stability.

Weighted Decision Matrix

A Weighted Decision Matrix was developed using the FOMs for the down-select process.

Tail Weighted Decision Matrix		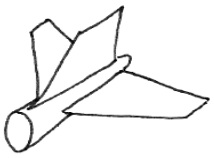	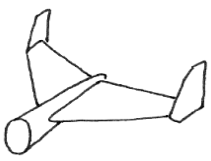	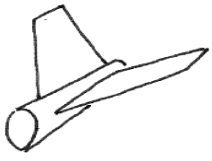
Figures of Merit	**Weight**	**Conventional**	**U-Tail**	**V-Tail**
RAC	0.5	0	-1	-1
Stability	0.3	0	0	0
Drag	0.2	0	1	-1
Total	**1.0**	**0**	**-0.3**	**-0.7**

Table 3.4: Tail Weighted Decision Matrix

Configuration

The conventional tail was determined to be the best configuration. The team chose the conventional design for increased aerodynamic control and reduced structural complexity.

3.4.4 Payload Releases

Different payload release concepts were developed, which were both lightweight and reliable. Lightweight and reliable release mechanisms are a critical design requirement for all missions.

Figures of Merit

The payload release FOMs were developed to consider a wide range of factors required to successfully complete all missions.

- **Loading Speed** – Loading speed is a measure of how fast the payloads can be installed on the aircraft.
- **Manufacturability –** A measure of how complex the mechanism is to construct. Since there are five payload release mechanisms on the aircraft, it is essential that they not difficult to mass produce.
- **RAC –** Low weight is important to increase competition score.
- **Reliability –** This is a measure of how many times the mechanism can be operated without failure.

Alternatives

Different payload release alternatives were developed by reverse engineering current devices. The alternatives that fulfill the mission requirements are listed below.

- **Electromagnet –** The magnetic configuration uses electromagnets to hold and release the payloads. This configuration is the only one that does not require servos, but instead uses relays.
- **Claw Device –** The claw device uses a clamp wrapped around the whole body of the payload.
- **Spring Loaded Pin –** This system uses a spring loaded pin to hold the payloads into place.
- **Archery Release –** The locking mechanism of an archery release can be used as a payload release, which is capable of supporting heavy loads and requires low input force to release.

Weighted Decision Matrix

The Weighted Decision Matrix below compares the payload releases based on the FOMs, which can be shown in **Table 3.5**.

Payload Release Weighted Decision Matrix		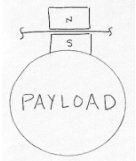	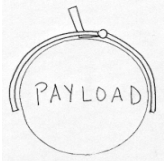	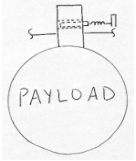	
Figures of Merit	**Weight**	**Magnetic**	**Claw Device**	**Spring Loaded**	**Archery Release**
Loading Speed	0.4	0	1	0	1
Manufacturability	0.1	1	0	1	0
RAC	0.3	0	1	-1	1
Reliability	0.2	1	-1	0	1
Total	**1.0**	**0.3**	**0.5**	**-0.2**	**0.9**

Table 3.5: Payload Release Weighted Decision Matrix

Configuration

The archery release mechanism was selected for both payload types due to the light weight design and the ease of integration into the overall system configuration. By using the same mechanism for both payload types, time will be saved in the design, manufacturing, and testing phases of the project.

3.5 Final Conceptual System Selection

After completing an integrated conceptual design process, Team Black determined the overall configuration of the aerospace system to consist of the following:

- A system that performs simultaneous payload installation and tail boom extension
- A conventional fuselage design for minimal drag and weight
- Folding wings for assembly speed and increased wing area
- Extendable boom and conventional tail for short take off distance
- Outriggers for optimal ground control with asymmetric payloads
- A rectangular box design, with one opening door

Team Black selected this configuration for streamline integration of system components and rapid assembly. **Fig. 3.5** shows the complete design solution in the assembled configuration.

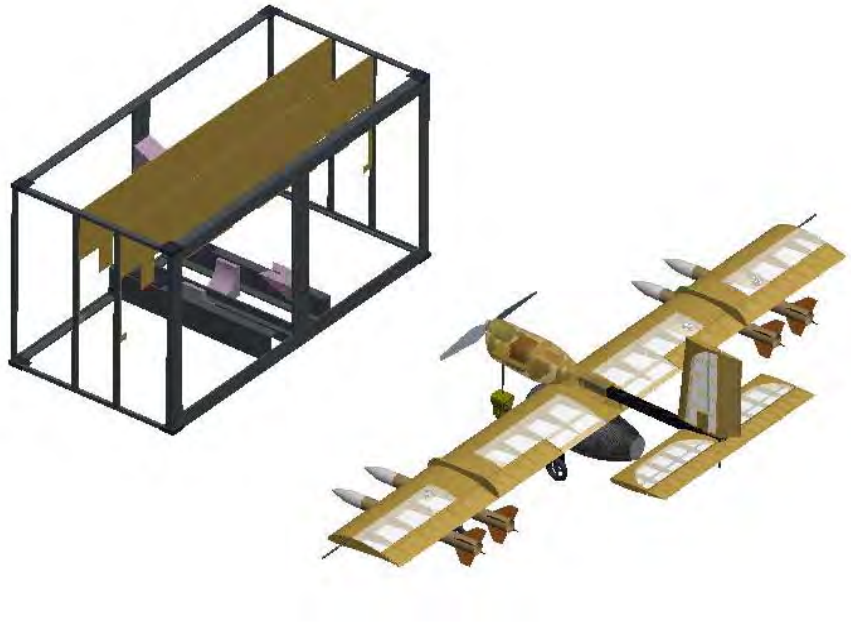

Figure 3.5: Conceptual Design

4.0 PRELIMINARY DESIGN

The design configuration selected from the conceptual design phase was separated into three groups to analyze and develop: aerodynamics, propulsion, and structures. In each design group, critical parameters were formed and assist in the design process. A mission model was developed and used for optimization together with a propulsion performance model. These programs optimized the main design parameters and the remaining parameters were subsequently sized and optimized.

4.1 Design and Analysis Methodology

To refine the conceptual design, a list of critical design parameters was developed. Each one is discussed, identifying the method by which trade studies were performed.

4.1.1 Wing Area

The selection of wing area is important to meet the specified take-off distance less than 100 ft. A larger wing area provides a short take-off distance and larger payload capacity, but cruise velocity is also reduced. Since the score sensitivity analysis indicates that cruise speed is not as important as other score parameters, a larger wing is preferred for short take-off capability.

4.1.2 Wingspan

Large wingspans are preferred for greater efficiency, but the wingspan is limited to 7 feet for storage in the box to avoid interference with the fuselage.

4.1.3 Airfoil

Airfoil selection is important because it affects take-off distance, cruise velocity, and stall characteristics. A large maximum lift coefficient is desirable to reduce take-off distance, but a high lift airfoil also increases drag and decreases cruise velocity. Wing thickness is also a consideration for sufficient strength to support the wing payloads and to provide space for servos and release mechanisms mounted on the wing.

4.1.4 Battery Type and Quantity

Selecting the battery type and quantity requires balancing weight and performance. Each battery type investigated was rated for a given capacity and weight. By dividing the capacity of a single cell by its weight, a single term can be used to characterize the battery, known as energy density. In general, a higher energy density is desirable, but a trade study of how weight affects score is warranted to note any maximum conditions.

4.1.5 Motor and Gear Box

When selecting a propulsion system, the selection of a motor and gear box is a critical process. A high efficiency motor is desired, but must meet other sizing requirements, such as maximum power. Additionally, trade-offs between the no-load current and internal resistance must be considered, affecting the motor's capability to adequately convert the electric power to torque and RPM. The gear box allows the motor to reduce the motor RPM output, allowing for more torque to be generated.

4.1.6 Propeller Pitch and Diameter

Propeller performance is an important component of the propulsion system, determining the capabilities of the aircraft take-off and cruise velocity. A significant trade study was conducted to determine optimal propellers for various conditions such as different contest mission and wind. In general, a low pitch is desired for a quick take-off, but limits the maximum cruise velocity. Likewise, increasing the pitch increases the maximum velocity the aircraft can travel, but greatly increases the take-off distance required due to blade's airfoil characteristics. Additionally, the diameter is important, being one of the largest contributors to current draw by the motor. Adequate sizing is critical for optimal propulsion design.

4.2 Mission Modeling and Optimization Analysis

To perform the necessary trade studies of each critical design parameter, mission modeling was conducted to perform an optimization analysis. This section outlines the developed model used, its capabilities and uncertainties.

4.2.1 Mission Profile Optimization Program

A Multidisciplinary Optimization (MDO) code was developed to analyze the mission profile and determine the optimum aircraft configuration. The program consists of mathematical models for aerodynamic characteristics, propulsive efficiency, and the weight of the proposed aircraft; and the program allows for quick comparison of different aircraft configurations. The MDO includes a weight, drag, and propulsion model.

The mission profile was analyzed and performance characteristics were calculated for each mission phase: take-off, climb, turns, and cruise, which can be noted in the figure below. Power required and time taken was found for each of these flight phases as well as maximum G-loading during the turns. These individual components were then combined into a full flight profile so different configurations could be compared.

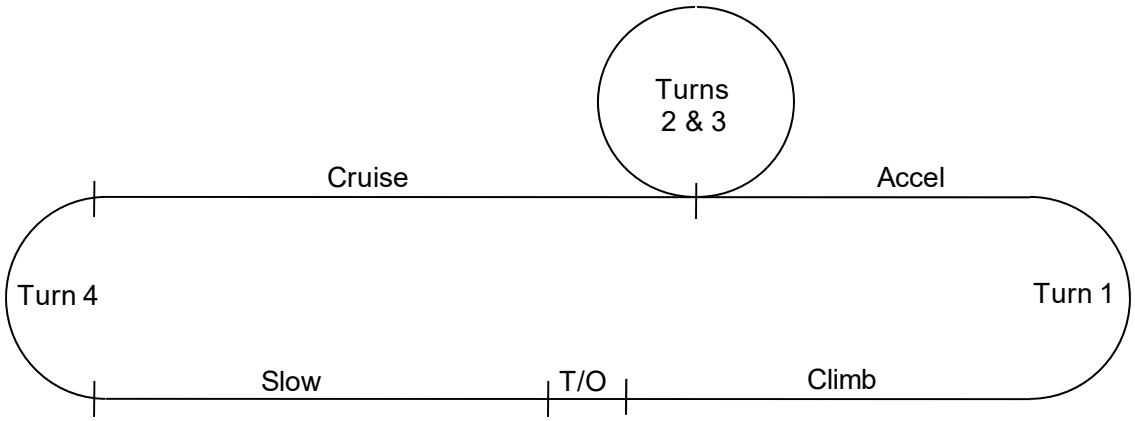

Figure 4.1: Mission Profile Breakdown

Each configuration was compared by energy consumed, time taken, and resulting system weight. A total score was then developed for each configuration based on the competition score function. Several assumptions were made to achieve comparable yet realistic scores.

It was assumed that if the aircraft was able to complete Mission 2, it would be able to complete Mission 3 based on relative energy consumption and the same number of laps. Because of this assumption, there was no modeling done for the third mission. The effect of pre-mission assembly time and mission three loading time were not considered in the score. Wing sweep and wing taper were not considered in the configurations due structural difficulties and the resulting increased weight.

The weight model was based upon historical data for DBF aircraft that carried similar payloads; both center store and wing stores. Included in the weight model was battery weight, which was calculated conservatively to provide a margin of safety. The drag model was based on a complete drag workup of the aircraft using drag build-up methods found in Raymer (1999). A factor of safety was then applied to the drag build-up to provide a conservative estimate of drag. The propulsive efficiency model was

constructed based on historical data of a single motor configuration, and conservative efficiency estimates were included to allow for individual component efficiency variations.

These models were inserted into the program and combined with average atmospheric parameters based on historical data for the competition site. Wind speed was entered as 5 mph, and the cruise altitude was entered as 50 feet, determined as a safe flight altitude for model aircraft. The program then optimized the configurations and returned optimum wing span, wing area, cruise velocity, and battery weight using these models and aerodynamic parameters for flight score.

4.2.2 Propulsion System Analysis Program

Alongside the Aerodynamic MDO code, a propulsion program was utilized to identify the optimal motor and propeller configuration to meet the requirements calculated by the Aerodynamics group. An iterative process was performed between the Aerodynamics and Propulsion team to converge to the best aircraft configuration possible.

The propulsion program required the user to enter in motor and propeller performance data, which was used, along with the MDO code assumptions and calculations, to determine an array of performance data such as take-off capabilities, cruise conditions, energy consumption, wind considerations, and endurance capabilities. The program focused on two main conditions: take-off requirements and cruise conditions.

The take-off requirements listed various parameters, such as current draw, thrust, velocity, power required, and take-off distance. This condition also allowed for wind user input determining aircraft capabilities of conditional environments. The cruise conditions calculated cruise velocity and current draw at a specified throttle, overall efficiency and power consumption. Along with initial calculations, further investigation of mission completion time and aerodynamic parameters were calculated for reference purposes with the MDO code and test flight data. The output parameters from the propulsion program were used to conduct various trade studies of the aircraft.

4.2.3 Mission Model Flow Chart

In **Fig. 4.2**, a flow chart was developed to explain the key procedural steps performed for the developed MDO code and propulsion program.

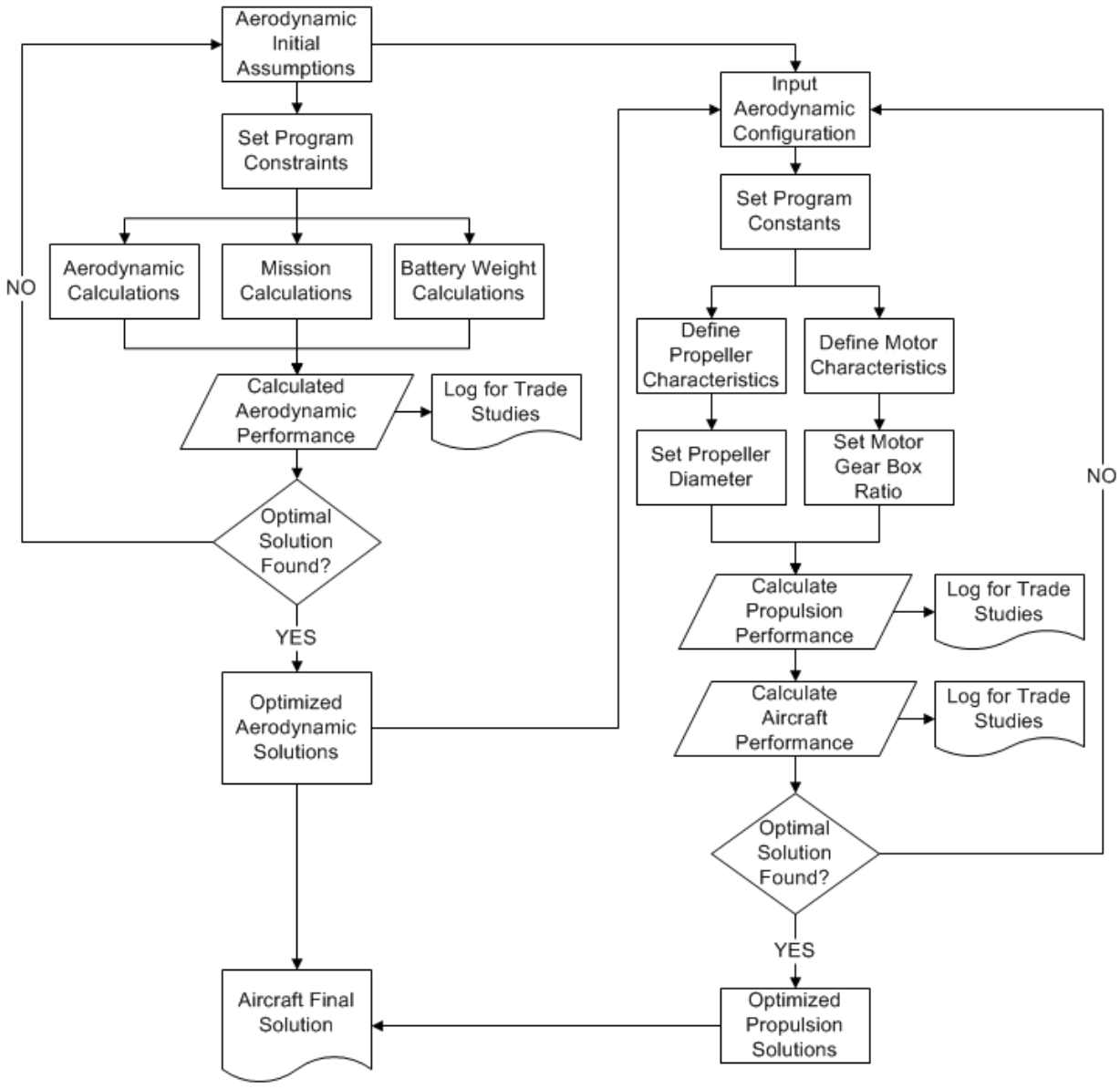

Figure 4.2: Multidisciplinary Optimization Code Flow Chart

4.3 Design and Sizing Trade-offs

4.3.1 Mission Profile Program Results

The MDO code returned several configurations that optimized score. **Fig. 4.3** shows these optimum configurations and illustrates the relationships between score and the aerodynamic parameters of wingspan, wing area, and battery weight, respectively. This comparison was made using three separate airfoils: the MH114, the E423, and the SD 7034, which are all discussed in more detail in the following subsection. These graphs were used to determine airfoil selection and then the trends were used to determine the optimum wing area, wing span, and battery weight.

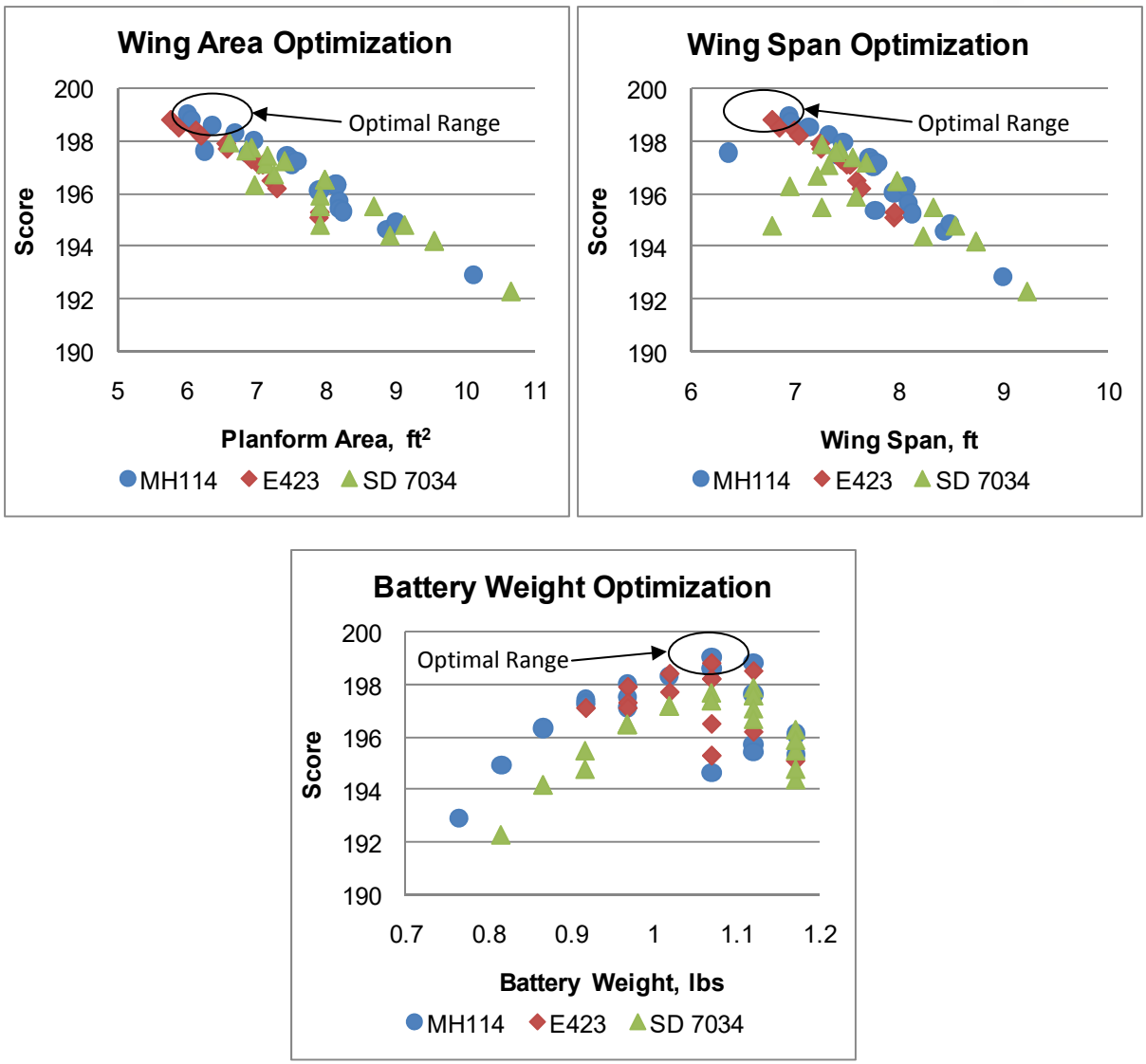

Figure 4.3: a) Wing Area, b) Wing Span, c) Battery Weight Optimization

Wing Airfoil

Using a database of airfoils used by previous OSU teams, three low Reynolds number airfoils were down selected and their drag polars were inserted into the mission optimization program. A high-lift airfoil, the Eppler 423, a low drag airfoil, the Selig Donovan (SD) 7034, and a more balanced airfoil, the Martin Heppeler (MH) 114 were considered. The MDO results indicate that the SD 7034 does not generate scores as high as the other two airfoils as show in the figures above. The MH114 and the E423 have comparable scores for similar wing spans and wing areas. The MH114 was selected because it has a slightly higher peak score and relatively flat bottom for easier wing construction.

Wing Area

The effect of wing area on flight score is highlighted in **Fig. 4.3a**. The MDO code tended to minimize wing area to increase score, with the wing area constrained by the maximum take-off distance. This limit can be seen from the absence of optimum configurations below a certain wing area. The optimum wing area was chosen to be the maximum value obtained from the MDO code. The wing area chosen was 6 square feet.

Wing Span

Once the wing area was selected to optimize score, the wingspan was then selected. The maximum wingspan imposed by selected box configuration was 7 feet. This constraint allows the folded wing to lie flat inside the box without interfering with the fuselage. The selected MH114 airfoil has an optimum wingspan of 6.93 ft as shown in **Fig. 4.3b**.

Battery Weight and Cruise Velocity

The MDO code was used to perform trades between power, speed, and weight of batteries to determine the optimal number of cells to use. Batteries were selected from a database of previously tested cells at Oklahoma State University, including the Elite 1500, 2000, 3300, and 4000 cells as well as the GP 2000 cell. The MDO code calculated the number of battery cells required based on an initial battery type selection to provide just enough energy to complete the Mission 2, since this mission requires the most endurance. The battery found to optimize under these conditions and achieve the highest score possible was 24 cells of the Elite 1500 (1000 mAh, 25 amp max, 0.051 lb, 19608 mAh/lb each). Total battery weight is 1.23 lb and power required is 630 Watts.

This battery power, along with the power requirements for each portion of the flight profile, was used to calculate the optimum cruise velocity for both Mission 1 and 2. The cruise velocities for both missions were very close to each other, a range of 50 to 60 ft per second. These values were then used to calculate the required power from the general propulsion system used by the MDO code, which served as a reference point for design requirements for the Propulsion Team.

4.3.2 Propulsion Program Results

When conducting trade studies for the primary components of the propulsion system, several major manufacturers were identified to serve as references for sizing and performance values. Data from previously tested components were initially used for both motors and propellers, allowing for general calculations. A filter was applied on various critical system parameters and the solutions in **Table 4.1** were further investigated further.

Motor		Performance Parameters				
Description	W (g)	Prop	P (W)	T/O (ft)	Eff	Laps
Kontronik 600-13	270	18x10	678	85.0	51.0	7.2
Medusa MR-036-050-1600V2-3F	230	18x10	643	85.2	52.6	7.6
Neu 1415/2Y	297	18x10	734	83.1	50.4	7.1
Neu 1905/1.5Y	181.4	18x10	714	83.1	49.3	7.1
Neu 1907/1Y	235.3	18x10	702	88.9	51.4	7.4
Neu 1512/2Y	280	18x10	713	81.7	50.7	7.2
Neu 1512/3D	280	18x10	717	82.4	49.1	7.1

Table 4.1: Motor and Propeller Selection

Motor and Gear Box

The motor selection process used performance characteristics of readily available motors. Each motor was paired with an 18x10 propeller. A careful examination of the aircraft performance parameters was conducted to determine the optimal motor and gear box, balancing all values. Also, great consideration was given to the weight of the motors, one of the key design parameters. Each motor examined was required to be capable of providing more than 630 Watts, based on the MDO code requirements. From the table above, the Neu 1905/1.5Y that was selected had average performance parameters compared to other motors examined, but had a significantly lighter weight.

Propeller Pitch and Diameter

The selection of the propeller required a careful balance between pitch and diameter. Noting the dimensional constraints of the aircraft, the propeller was sized to provide adequate take-off distance for all missions and sufficient velocity while in flight. Using in-house propeller test data, performance characteristics were used to size the propeller. A maximum diameter of 18 inches was set based on the aircraft ground clearance. Using the maximum diameter, the pitch was varied until take-off distance was below 90 ft and was still capable of completing all missions. The final selection had a diameter of 18 inches and a pitch of 10 degrees, which was used to check performance parameters with all potential motor and gear box solutions.

4.4 Analysis Methods and Sizing

4.4.1 Aerodynamic Sizing

Fuselage and Tail Boom

The aircraft length in the box is constrained to two feet by an external box dimension, significantly restricting the overall length of the fuselage and tail boom. The distance from the propeller to back of the tail is approximately 23 inches in the stored configuration, with a maximum extended fuselage length of approximately 40 inches. This results in a short coupled aircraft requiring the fuselage and tail to be maximized, subject to geometrical constraints. The sized fuselage length is 18 inches and the tail boom is 16 inches.

Tail Size

The horizontal tail must provide enough moment to rotate for takeoff and provide longitudinal stability. Initial horizontal tail sizing was performed using tail volumes from previous DBF aircraft that flew similar missions. By using a horizontal tail volume of 0.51, the tail area was initially sized to 1.75 square feet with a conventional symmetric airfoil. This tail size with a conventional elevator provided the needed moment to rotate for takeoff, but an initial stability analysis yielded a high static margin, reducing the area to 1.5 sq. ft. Since the tail boom slides into the fuselage, the chord of the horizontal tail was limited to 8 inches; therefore, the tail was sized to a 28 inch span by an 8 inch chord.

The vertical tail was also sized using previously designed tail volumes. By assuming a vertical tail volume of 0.02, the vertical tail area was initially sized to approximately 0.6 square feet. The vertical tail root chord was sized to 9 inches to stay close to the chord of the horizontal tail, while the tip chord was 8 inches for aesthetic reasons. This required the overall span of the vertical tail to be 11 inches, which is the maximum height to fit within the box.

4.4.2 Structural Analysis

Based on the sizing calculations performed by the aerodynamic and propulsions teams, the structures team developed solutions to meet the specified requirements. Utilizing the selected conceptual design and benchmarking previous successful DBF aircraft, trade studies were conducted to select structural configurations. In general, many of the trade studies performed for the structural components were conducted based on initial prototypes that were constructed and evaluated, which are discussed in later sections.

Wing and Empennage

Once aerodynamic sizing for the wing and tail areas had been determined, internal structural investigation was conducted. The wing structures needed to be strong enough to withstand the forces of flight from carrying the center payload and wing stores. Since a large load will be applied on the wing surface, adequate spar strength was required. While the tail does not have the same direct loads, a strong spar was required to support the large horizontal tail span. Experimental construction methods were employed for exact sizing and material selection. After construction and prototype testing had been completed, the designs were evaluated and changes made to strengthen insufficient parts or reduce weight in oversized sections.

Landing gear

The landing gear design is particularly important to accommodate the range of payload weight distributions for the three missions. A tricycle configuration with additional outriggers was selected in the conceptual design phase to provide the ground handling characteristics required for asymmetrical loads.

For the main landing gear, carbon fiber composites were selected for high strength-to-weight ratio; and the bow shape of the main gear allows for impact absorption on landing. Carbon fiber composites were also selected for the outriggers. While not a primary support mechanism, the outriggers must also be strong enough to withstand a hard landing, as it is anticipated that the plane will not land level every flight. Actual design for the landing gear was selected based on testing and refinement of an initial prototype.

The nose gear is important for precise ground maneuvering. The nose gear supports approximately 10-15% of the aircraft's total weight to provide adequate traction for steering. Although supporting a smaller weight, the nose gear is made of carbon fiber and Kevlar in a contoured layup to absorb impact forces during landing.

Box

The aircraft configuration, self-loading payloads, and the box dimension constraints were the primary determinants of box sizing. The box was designed around the aircraft configuration to minimize assembly time and the following solution was selected: a rear opening door for removal of the aircraft by the tail, with payloads that lock in place automatically as the tail boom is extended. To minimize payload loading time in Mission 3, various concepts were considered, including additional door concepts or auxiliary speed loaders. The selected solution requires only a repositioning of box to place the door on the top surface, allowing for easy access to the wing payloads for quick removal. The final external box dimensions are 2 ft x 2 ft x 4 ft.

The drop test requirement also constrains material selection and bracing support orientation. The payload release system also requires the box to be sufficiently rigid to keep all payloads aligned during installation. The box solution includes a carbon composite beam for strong, lightweight construction, and prototype testing and timed mock assembly trials were used to develop the detailed components of the design. Structural testing was used to determine the final carbon composite layup required to prevent system damage in the drop test.

Release mechanisms

Due to its simplicity, strength, and reliability, all payloads releases are modeled on a bow release mechanism. The basic mechanism was modified included to accommodate the centerline and wing payloads. In an effort to save weight, Delrin was selected as the base material for the plates and mounting brackets. It was also noted that non-weight bearing parts could be constructed from built up pieces of aircraft grade plywood.

Since the centerline payload release was designed to fit inside the wing and fuselage, drag was not a primary concern. However, the wing store releases were designed to be mounted under the wing, requiring modifications to mount them horizontally to reduce frontal area. While two design orientations

were necessary, the two release design met the required functionality constraints with minimal complexity and weight.

4.5 Lift, Drag & Stability Characteristics

After an initial aircraft design was determined, aerodynamic performance analysis was conducted for the conceptual aircraft design to find the optimum size characteristics for the contest. A detailed drag model was created for the entire aircraft, giving an accurate thrust requirement range for the propulsion team. Aircraft stability derivatives and characteristics were also approximated using a stability analysis code developed for the contest. With these values optimized, the final aircraft layout was determined, and final dimensions were selected for the chosen design.

4.5.1 Aerodynamic Qualities

The selected airfoil for the main wing is a MH114 airfoil. This airfoil provides an optimum range of lift over drag values, allowing the aircraft to be flown efficiently at a number of cruise attitudes. The MH114 airfoil is a high lift airfoil, which is required for an aircraft with the design constraints provided in the contest. For aerodynamic modeling, the lift is optimized by varying wing span and area. The system of equations used in the optimization program sets the required lift for certain performance situations, and optimizes the wing dimensions to fit the best design. To provide the lift required and minimal drag, the wing is designed for an incidence of -2°. This is based on the high lift airfoil design, an optimum lift to drag ratio, and larger range to advert stall. The calculated lift to drag ratio was plotted against angle of attack, which is shown in **Fig. 4.4**.

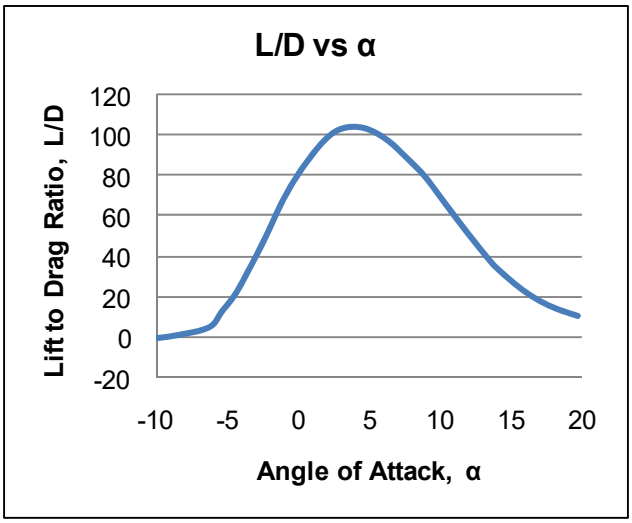

Figure 4.4: Lift to Drag Ratio vs. Angle of Attack

The NACA 0009 airfoil was selected for both horizontal and vertical tail due to the symmetric profile and ease of construction. This airfoil is thin, lightweight, and commonly used for most tails. The tail was designed to be mounted at an incidence of -4°.

With the wing, tail and fuselage sized, a more accurate drag model of the aircraft was created. This model was used to finalize the propulsion system as well as accurately profile the missions. Using methods describe by Raymer, the complete drag profile was compiled using basic equations for skin friction, form factor, and wetted area. **Fig. 4.5** lists the drag buildup of the aircraft components

Total Aircraft Drag	
Aircraft (No Payloads) C_{D0}	0.03482
Center Payload	0.00675
Wing Stores	0.00355
Mission Configurations	
Mission 1 C_{D0}	0.04158
Mission 2 C_{D0}	0.04158
Mission 3 C_{D0} (4 Stores)	0.03838
Mission 3 C_{D0} (1 Stores)	0.03571

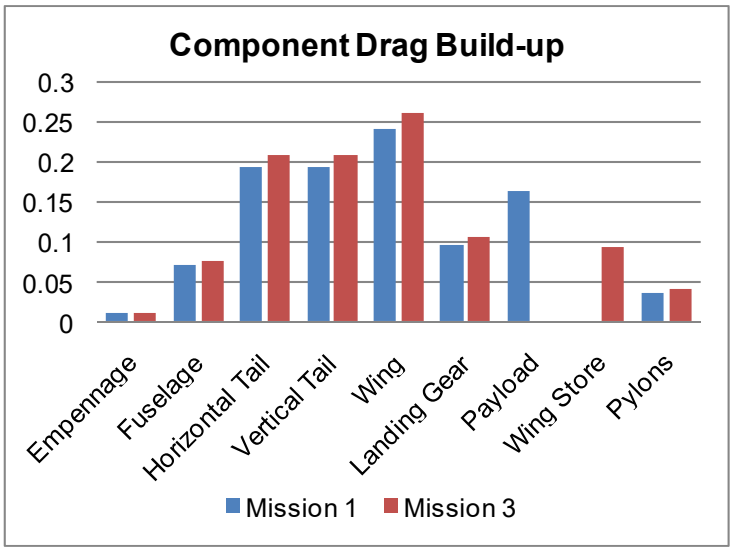

Figure 4.5: Component Drag Buildup and Mission Parasite Drag

Once the parasite drag profiles were tabulated, a plot normalizing the drag coefficient for the entire aircraft was created. Since the drag profiles vary greatly from mission to mission in this contest, a comprehensive drag analysis gave members of the propulsion team a more concrete value to base thrust calculations, assuring that the thrust required for each mission and associated aircraft drag value could be attained. The drag polar for the various mission configurations is shown in the **Fig 4.6**.

The changes in drag coefficient can be viewed for the different missions, giving the propulsion team an accurate drag profile for initial propulsion sizing. The analysis is shown to be within 10% of early drag estimates used in conceptual aircraft approximation.

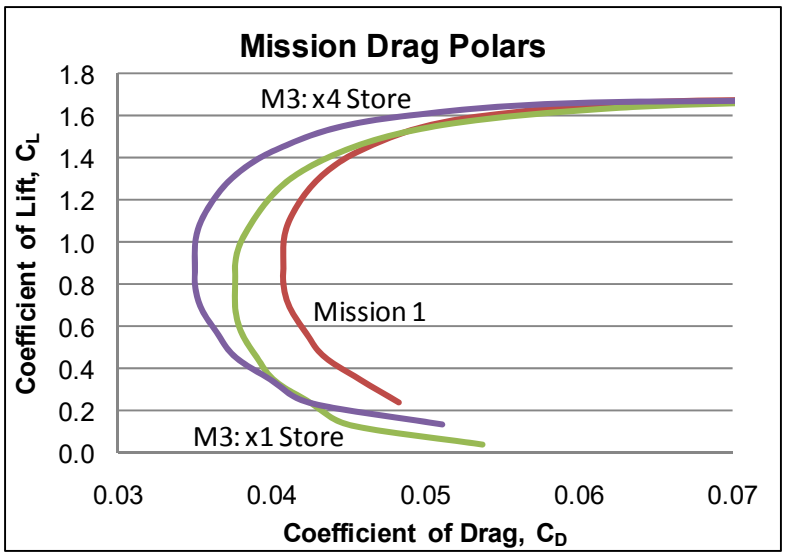

Figure 4.6: Mission Drag Polars for Total Aircraft Configuration

4.5.2 Stability Characteristics

Initial stability and control analysis was performed to ensure a statically stable aircraft and an acceptable static margin. By creating a simple C_m diagram for each component and the aircraft, the static stability of the aircraft was established. **Fig. 4.7** shows the static stability of the aircraft and the contributions of each major component to the aircraft moment.

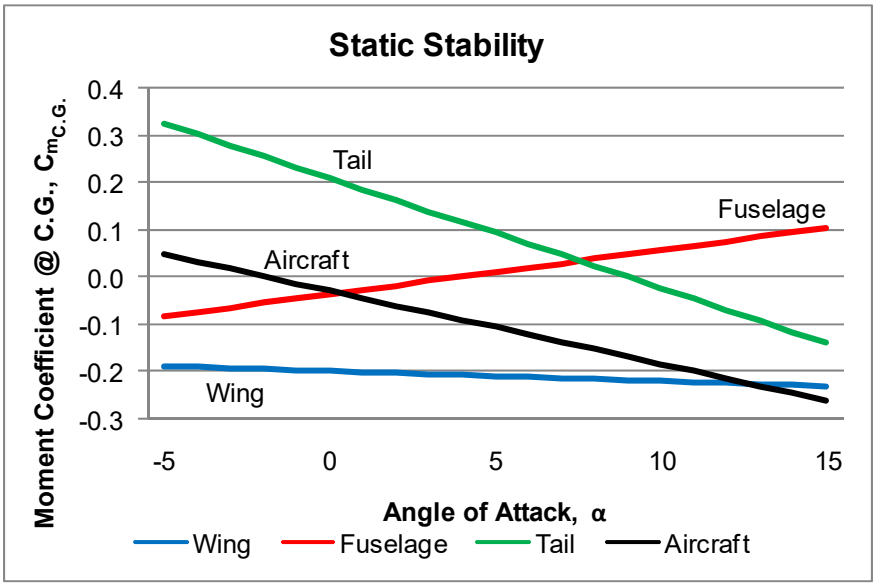

Figure 4.7: Static Stability Chart

Using this data, the neutral point and static margin of the aircraft were determined. For this aircraft the neutral point is at 0.548 of the chord length, giving the aircraft a static margin of approximately 32%. Compared to conventional aircraft, 32% static margin is a high value, but when benchmarked against previous DBF aircraft designs, 32% is a more typical static margin.

Once the static stability had been established, an analysis on dynamic stability was also performed. Stability coefficients were calculated for both longitudinal and lateral motion as well as data for all five modes of the aircraft. The stability coefficients were used to create over 25 stability derivatives to predict the aircraft modes. **Fig. 4.8** below shows the real response (η), the frequency/ imaginary response (ω), the damping ratio (ζ), and the time to half of each aircraft mode for Mission 2 at cruise.

Aircraft Mode Eigenvalues				
Mode	**η**	**ω**	**ζ**	**$t_{1/2}$**
Short P	-7.81	13.51	0.578	0.09
Phugoid	-0.02	0.81	0.022	39.83
Roll	-22.03	0.00	-	0.03
Dutch Roll	-0.81	5.29	0.153	0.86
Spiral	0.13	0.00	-	5.19

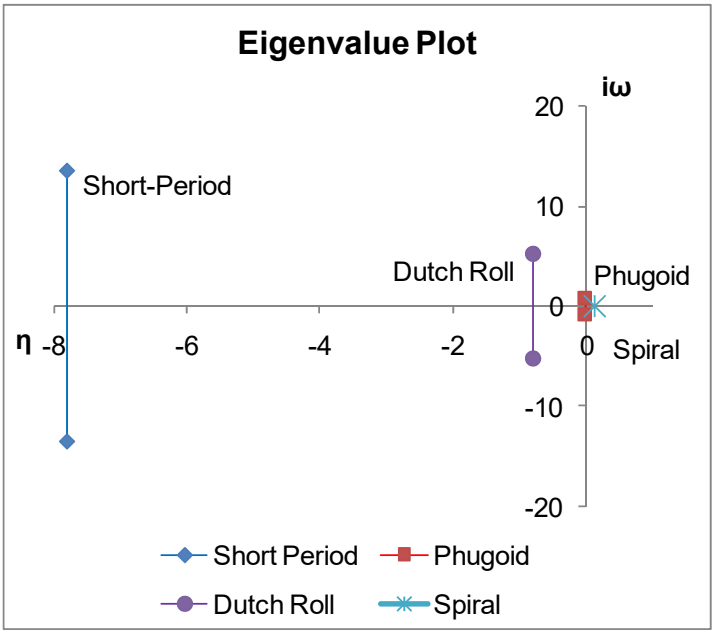

Figure 4.8: Aircraft Mode Eigenvalues and Plot

From this data the only unstable mode of the aircraft is the spiral mode, which is a typical flight dynamic quality. Since the spiral mode has a very low doubling time, this instability should be easy for the pilot to overcome. All other modes of the aircraft are stable and within reasonable ranges for this type of aircraft.

4.5.3 Control Surface Sizing

The control surfaces were sized using previous aircrafts as a benchmark, with general sizing for a number of aircrafts being considered. The ailerons were designed around the asymmetric payload scenario. After using a standard elevator sizing of 30% of the horizontal tail area and a ±20° maximum deflection, a moment calculation was performed using X-Foil for the lift of a deflected control surface to ensure the tail could provide the required moment to take-off. The rudder was sized to an area of 35% of the vertical tail area with ±20° maximum deflection based on benchmarking. The ailerons were sized

using X-Foil to provide enough roll control during turning and take-off for the worst case payload configuration. Both inboard and outboard ailerons were sized to a total area of 18.5% wing area with +20°/ -5° maximum deflections. These deflections were chosen because the wing is highly cambered; therefore, high negative deflections tend to stall the wing, especially at higher angles of attack.

In addition to sizing, a torque analysis was performed in X-Foil to determine servo size. Since all control surfaces required similar torque, the same high-torque micro servos were used for each control surface to allow for interchangeability.

4.6 Aircraft Mission Performance

Beyond calculating aircraft parameters, such as physical dimensions and propulsive performance, predictions on mission performance was calculated between the Aerodynamic and Propulsion Team's optimization programs. These values were used as a reference for system design and were compared to actual test flight data.

4.6.1 Pre-Mission: Assembly

Assembly time predictions were estimated based upon best case scenarios during the conceptual design phase. No optimization model could be generated to provide quantitative predictions of the assembly time. A general estimation of assembly time was determined from assembly of practice parts in a simulated environment, which closely represented the competition setup. Under these constraints, the estimated assembly time was recorded to be approximately 7 seconds.

4.6.2 Mission 1: Ferry Flight

Mission completion time was determined to be the focus of score optimization for this mission. Although the aerodynamic and propulsion optimization programs focused heavily on Mission 2 performance, special case analysis was conducted within the propulsion program to determine estimated values. By generating a mission profile, energy consumption could be estimated, allowing for a calculation of summed flight time segments. The ferry flight mission was predicted to be capable of completing the mission within 75 seconds. **Table 4.2** gives an example of the flight profile.

Mission 1 Profile (5mph Wind)				
Mission Phase		**V (ft/s)**	**Distance (ft)**	**Time (s)**
Lap 1	Takeoff	0 - 44.3	16.0	1.0
	Climb	56.2	168.7	3.0
	Cruise	70.0	331.3	4.7
	First Turn	56.2	84.4	1.5
	360° Turn	56.2	168.7	3.0
	Cruise	70.0	1000.0	14.3
	180° Turn	56.2	84.4	1.5
Lap 2	Cruise	70.0	1000.0	14.3
	180° Turn	56.2	84.4	1.5
	360° Turn	56.2	168.7	3.0
	Cruise	70.0	1000.0	14.3
	180° Turn	56.2	84.4	1.5
	Cruise	70.0	500.0	7.1
	Additional Time for Acceleration/Decelration			4.0
Total				**74.7**

Table 4.2: Mission 1 Profile Performance

4.6.3 Mission 2: Surveillance Flight

Completing the mission was noted to be the only factor for a successful Surveillance Flight mission. The aerodynamics group generated a base model, which optimized around mission completion. The propulsion group further calculated aircraft performance using an energy consumption model for the entire flight mission. **Table 4.3** gives a profile of the mission with the energy used during each phase.

Mission 2 Energy Consumption					
Mission Phase		**Vel (ft/s)**	**Time (s)**	**I (Amp)**	**Energy (mAh)**
Lap 1	Takeoff	0 - 44.3	4.56	26.31	33.33
	Climb	47.4	10.10	26.31	73.81
	First Turn	54.2	8.40	10.61	24.76
	Cruise (1500 ft)	54.2	8.40	26.31	61.39
	360 Turn	54.2	9.60	26.31	70.16
	180 Turn	54.2	4.80	26.31	35.08
Laps 2 - 4	Cruise (2000 ft)	54.2	28.97	10.61	85.38
	180 Turn (x2)	54.2	9.60	26.31	70.16
	360 Turn	54.2	9.60	26.31	70.16
Total					**975.63**

Table 4.3: Mission 2 Profile Performance

This table shows that the total energy used is about 976 mAh. For the chosen batteries, total energy is typically 1200 mAh, so this mission will use about 81% of the total battery energy.

4.6.4 Mission 3: Payload Release/Asymmetric Loads

The two main factors required for success in Mission 3 were flight lap completion and payload delivery/release reliability. Similar to the assembly time trials, mock payload install missions were conducted, and with a number of practice sessions, an install time of 8 seconds was predicted. From the aerodynamic and propulsion optimization programs, mission completion was determined successful since optimization centered on Mission 2, which required higher endurance and gross weight. Successful payload delivery/release required reliable payload releases and sufficient ground stability for "worst-case" asymmetric loads. The release mechanisms chosen were selected for this purpose and will be tested for concept validation.

5.0 DETAIL DESIGN

5.1 Dimensional Parameters

Table 5.1 provides primary dimensions and performance parameters for the system.

Fuselage		**Box**	
Collapsed Length (in)	23.75	Length (ft)	4
Extended Length (in)	36.75	Width (ft)	2
Width (in)	4	Height (ft)	2
Height (in)	5	Weight (lb)	6
Horizontal Stabilizer		**Vertical Stabilizer**	
Airfoil	NACA 0009	Airfoil	NACA 0009
Span (in)	28	Span (in)	11
Chord (in)	8	Root Chord (in)	9
Tail Volume	0.46	Tip Chord (in)	8
Incidence Angle (deg)	-4	Tail Volume (in2)	0.029
Elevator Area (in^2)	56	Rudder Area (in^2)	22
Aircraft Weight and Balance		**Wing**	
Airframe (lb)	3.95	Airfoil	Martin Hepperle 114
Propulsion systems (lb)	2.06	Span (in)	83.2
Control Systems (lb)	0.48	Chord (in)	10.4
Payload Systems (lb)	1.06	Area (in^2)	865
Maximum Payload (lb)	8.8	Aspect Ratio	8.0
Max Empty Weight (lb)	7.55	Incidence Angle (deg)	-2
Max Gross Weight (lb)	16.44	Aileron Area (in^2)	164
CG location (in)	11.77	Max Thickness (in)	1.36

Table 5.1: System Dimensional Parameters

5.2 Structural Characteristics and Capabilities

The aircraft and box were designed to create a system that has the fastest assembly time possible. The aircraft is equipped with a hinged wing and an extendible boom tail so that most of the aircraft assembly is done by simply pulling the aircraft from the box. Since the payloads must all lock in place during this one motion, it was vital to ensure precision between the aircraft release mechanisms and the box, while still maintaining the rigidity to withstand the six inch drop test.

The aircraft allows for quick assembly through a hinged wing and an extendable tail while still maintaining features that provide the structural integrity required for this competition. The wing uses a Kevlar hinge to quickly unfold the wing and a carbon fiber sliding spar to lock the wing in place. Since using a hinged wing allows for a strong joining section with the fuselage, the aircraft is easily capable of completing the required wing-tip test. The landing gear is also capable of withstanding large impact forces from heavy landings. From prototype tests on the main landing gear, it is determined to be capable of a straight drop with a full center payload of more than six inches, which simulates a hard landing.

Since the box must be capable of holding the aircraft for the six inch drop test as well as play a key role in the assembly of the aircraft, it is designed to be both precise and sturdy, while still minimizing weight. The box is designed to rapidly open and close so that the aircraft and payloads fit closely against the box to protect it during the drop test, while also maintaining the alignment needed for simultaneous payload installation. Precise alignment is essential for quick assembly time of the aircraft.

5.3 System Design, Component Selection, Integration, and Architecture

5.3.1 Fuselage and Tail Boom

With quick assembly in mind, the fuselage has been designed around the tail boom, with all of the interior parts organized around the sliding tail boom. Taking advantage of this extending boom, some areas have been designed to fall into place after the boom slides out; reducing assembly time and avoiding conflicts with contest rules.

In a coordinated effort between all teams, the fuselage was designed around aerodynamics, propulsion, and electronics, with obvious considerations for structural integrity. The most difficult part of this component design was the challenges that pertain to designing such a complex form, which organizes all components to maintain a stable C.G. location. Mounting batteries with large forward and aft tolerances provide minor C.G. adjustments. One requirement for the fuselage configuration is the use of an off-center mounted nose-gear strut. This is for structural reasons, with the tail boom slide reducing mounting options for the gear. Locating the nose-gear strut just starboard of the aircraft centerline allows the strut to be attached to more area of the front bulkhead for added rigidity. **Fig. 5.1** shows the fuselage and tail boom integration.

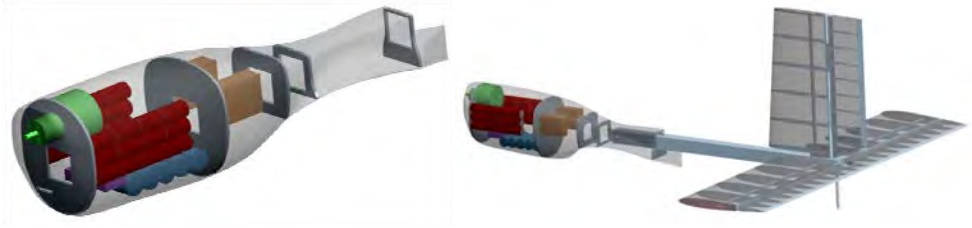

Figure 5.1: Fuselage and Tail Boom Configuration

The tail boom allowed the aircraft to fit into the dimensional constraints of the box. Additionally, the manufacturing process provided structural support for the conventional tail configuration when fully extended. Consideration was given to methods for securing the tail boom once extended as well as handling moment and torsion loads. A locking mechanism was created so that once the boom was fully extended a spring loaded pin and notch would slide out locking the boom in place. This prevents the boom from sliding back into the fuselage during flight and provides multiple stress points to prevent fracture of either locking mechanism.

5.3.2 Folding Wing

A folding wing was incorporated into the design to allow for quick assembly out of the box. The system uses a hinge to ensure the wing is easily and precisely aligned during assembly, but also uses a sliding spar to give it the required structural support during flight. This method is the fastest way to assemble the wing because there is no error in the system since the entire assembly is self aligning, therefore greatly reducing assembly time.

Incorporating a folding wing design to the system provided unique challenges to the team. The added complexity that was created by this design was more than compensated for by the major decrease in assembly time. Designing a strong, yet lightweight method for hinging the wing at an optimum distance was the key function in the auto-loading concept.

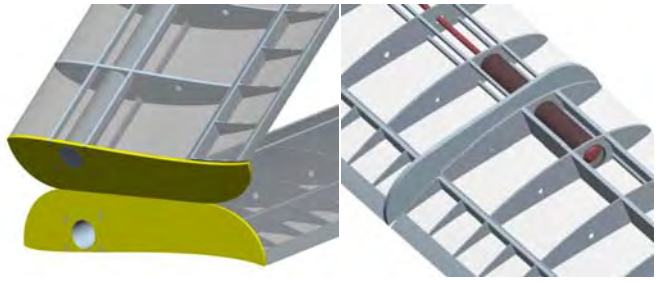

Figure 5.2: Folding Wing Configuration

The main details of this component are the hinged wing and locking spar concept. These components provide for a much larger wingspan and area, allowing for weight to be carried more efficiently and creating more available lift. Using lightweight materials were important in order for this concept to remain an advantageous design, overcoming system complexity and the added weight from these components.

5.3.3 Landing Gear

A tricycle with outrigger combination was selected because of its ground handling stability for asymmetric loads. This landing gear configuration includes the nose gear, bow gear, and two outriggers. The nose gear consists of a carbon fiber shaft which protrudes through from bottom to the top of the fuselage for structural support and is offset to clear the tail boom.

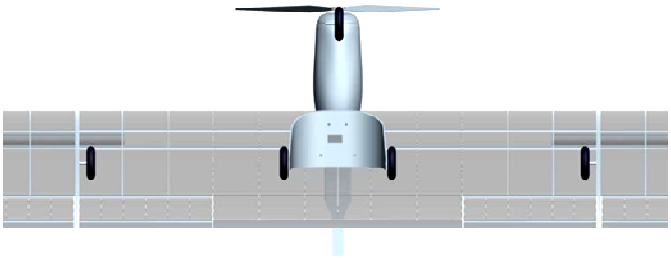

Figure 5.3: Landing Gear Configuration

The main characteristic of the landing gear configuration is the outrigger design. The tricycle gear type is conventional in its design, but the added use of outriggers brings a greater need for sizing optimization and ground stability calculations for asymmetrical payload configurations. Placing the outriggers on the inboard section of the wing reduced complexity and stress on the wing hinge, and also reducing the amount of load that would be carried by the sliding wing spar locks.

5.3.4 Payload Release

Both types of payloads carried by the aircraft are attached and released using automatic loading clip-in releases. This release mechanism was adapted from an archery style bow release. After careful study of the bow release, both types of payload releases were reverse engineered to meet the needs of the aircraft.

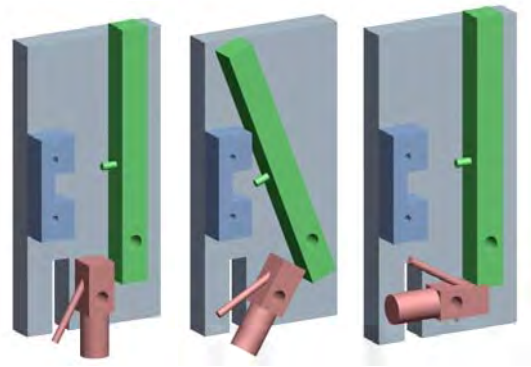

Figure 5.4: Payload Release Configuration

The centerline payload release was closely modeled after a bow release, with the release using the same basic layout of components, specifically the placement of the hinge pins. The wing payload release also follows the same basic idea as the centerline payload release, with the only major difference being the fact that the gate and latch operate in perpendicular planes instead of the same plane. This allows the release to have a smaller frontal area so it can be placed under the wing, causing less drag while still securely holding the rockets in place.

5.3.5 Box

The box was designed around the aircraft to provide a precise fit for payload placement and to ensure little movement during the six inch drop test. Since the entire aircraft is designed around a quick assembly time, it is essential that each payload is precisely aligned with the aircraft to create a quick reliable assembly. Also, to ensure the aircraft survive the six inch drop test, heavy components must be isolated to ensure no matter which direction the box is dropped, the aircraft remains intact.

The size and shape of the box was determined by the overall configuration of the plane aircraft. The folding wing configuration requires the length of the box to be 4 feet to maximize the wingspan before the fold in the wing. With the telescoping tail boom, the width dimension was maximized to 2 feet to allow for the maximum moment arm for the tail. The box height dimension filled the maximum dimension of 2 feet to allow for optimum tail volume.

Figure 5.5: Box Configuration

It was critical to isolate the water payload and plane from each other to the structure of the box to minimize the chance that the payload would crush the plane when demonstrating the drop test. The payloads and plane are isolated separately within the box in order that their masses are be independent of one another, minimizing damage in the event of a failure. Secure placement of landing gear, wing tips, and rocket payloads were also necessary for the system to withstand structural tests on contest day.

5.4 Weight and Balance

Each mission requires a different payload configuration, which ultimately affects the C.G. location of the aircraft. Since the aircraft was designed to have as little longitudinal C.G shift as possible, the C.G. location remains the same for the first two missions. **Table 5.2** lists the weight and balance for an empty aircraft, as well as for different payload configurations.

Empty Weight and Balance				
Component		Weight (oz)	Arm (in)	Moment (oz-in)
Structure	Fuselage	4.48	9.4	42.24
	Wing	28.54	14.9	424.62
	Horizontal Tail	3.81	32.9	125.26
	Vertical Tail	1.83	32.9	60.31
	Boom	1.98	24.6	48.65
Propulsion	Batteries	20.32	7.3	148.11
	Motor and Gearbox	14.11	2.9	40.78
	Propeller	2.47	1.4	3.43
Avionics	AV Battery	3.95	7.4	29.20
	Reciever	2.40	10.9	26.09
Payload	Port Rocket Release	1.41	13.9	19.67
	Far Port Rocket Release	1.41	13.9	19.67
	Starboard Rocket Release	1.41	13.9	19.67
	Far Starboard Rocket Release	1.41	13.9	19.67
	Center Store Release	1.13	13.9	15.73
Landing Gear	Front Gear	1.22	3.0	3.60
	Port Outrigger	1.48	13.0	19.19
	Starboard Outrigger	1.48	13.0	19.19
	Bow Gear	6.35	15.7	99.68
Total		**101.18**	**11.7**	**1184.75**

Mission Weight and Balance				
Component		Weight (oz)	Arm (in)	Moment (oz-in)
Mission 1	Center Store	9.66	11.7	113.17
Total		**110.84**	**11.7**	**1297.92**
Mission 2	Center Store	142.53	11.7	1668.90
Total		**146.09**	**11.7**	**2853.65**
Mission 3	Port Rocket	24.02	11.7	281.28
	Far Port Rocket	24.02	11.7	281.28
	Starboard Rocket	24.02	11.7	281.28
	Far Starboard Rocket	24.02	11.7	281.28
Total		**197.26**	**11.7**	**2309.85**

Table 5.2: Mission Weight and Balance

In Mission 3 the longitudinal C.G. location once again remains the same; but when individual rocket payloads are released, the lateral C.G. shifts. Since this C.G. shift greatly affects roll control and ground control, the aircraft was designed to handle the worst case scenario where there are two payloads on one wing with none on the other causing a 7.69 inch C.G. shift. **Fig. 5.6** illustrates the change in weight and C.G. location for each possible Mission 3 payload configuration.

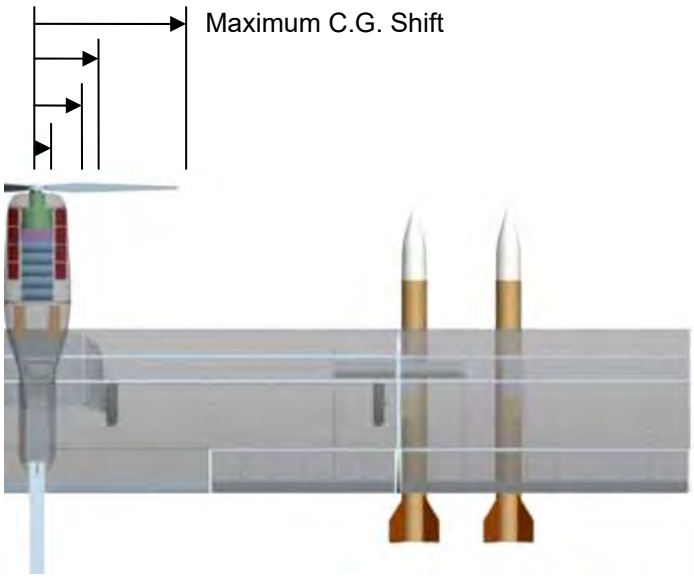

Mission 3 Weight and Balance		
Payload Configuration (R = Rocket Attached)	Weight (lb)	C.G. Shift (in)
R / R / R / R	13.05	0.00
R / R / R / -	12.05	-3.73
R / R / - / R	12.05	-2.99
R / - / R / R	12.05	2.99
- / R / R / R	12.05	3.73
- / - / R / R	10.55	7.69
- / R / - / R	10.55	0.85
- / R / R / -	10.55	0.00
R / - / - / R	10.55	0.00
R / - / R / -	10.55	-0.85
R / R / - / -	10.55	-7.69
R / - / - / -	9.05	-4.97
- / R / - / -	9.05	-3.98
- / - / R / -	9.05	3.98
- / - / - / R	9.05	4.97

Figure 5.6: Mission 3 Weight and Balance

5.5 Flight Performance Parameters

Using the final aircraft design, flight performance parameters were calculated to help in mission performance modeling. The general aerodynamic and flight performance qualities for the aircraft are shown in **Table 5.3**.

Flight Performance				
Aircraft Parameters		**Mission Parameters**	**Mission 1**	**Mission 2**
C_{L0}	0.62	Max Climb Rate (ft/s)	9.27	5.72
C_{Lmax}	1.14	Stall Speed (ft/s)	25.54	37.69
e	0.81	Cruise Speed (ft/s)	70	54.19
C_{D0}	0.035	Take-off Distance (ft)	10	86
		Maximum Speed (ft/s)	77.4	78.7
		Max G-Load	7.1	1.5
		Turn Rate (deg/s)	120	38.3

Table 5.3: Flight Performance Parameters

5.6 Rated Aircraft Cost

The scoring sensitivity analysis identified the second most important variable was RAC. Using our current system design, weights for every component were found. **Fig. 5.7** shows the RAC values for these components.

Component	Weight (oz)	Percent
Fuselage	8.98	1.84%
Wing	24.57	5.02%
Empennage	13.97	2.86%
Prop. System	11.58	2.37%
Releases	7.23	1.48%
Batteries	19.17	3.92%
Propeller	2.20	0.45%
Landing Gear	15.97	3.27%
Avionics Batt.	5.23	1.07%
Reciever	2.40	0.49%
Box	112.10	22.93%
RC Controller	28.57	5.84%
Tank Payload	140.92	28.82%
Rocket Stores	96.08	19.65%
Total	488.97	100.00%

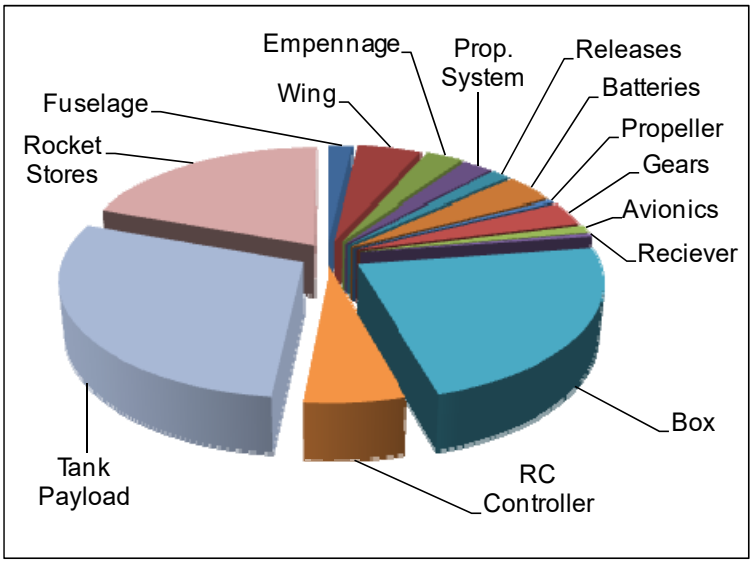

Figure 5.7: RAC Breakdown and Pie Chart

This RAC analysis shows the majority of RAC comes from the payloads, which cannot be reduced. The next largest component in RAC comes from the box. In order to minimize this weight value for the system, therefore increasing the overall score, further research into box manufacturing processes as well as other methods to minimize weight are planned.

5.7 Mission Performance

Once the design was finalized, mission performance was reevaluated to give more accurate goals and expectations for mission performance.

5.7.1 Pre-Mission: Assembly

Based on preliminary testing and prototyping, a final assembly time of six seconds was estimated; a decrease of one second from our initial prediction. Although the decrease in assembly time only decreased by one second, the percent change is 14.3% and greatly impacts the overall score.

5.7.2 Mission 1: Ferry Flight

Using the final design, Mission 1 was profiled with different wind conditions and propellers to gage a minimum flight time. Since the aircraft weight is so low in this mission, takeoff is not a problem with any wind condition. Battery energy was also not an issue since the flight can be made at maximum velocity, even in turns with over 20% energy remaining in all wind conditions. A total flight time of 74 seconds was estimated on Mission 1. This was based on flying at maximum cruise velocity throughout the mission and slowing down only to minimize the turn radii.

5.7.3 Mission 2: Surveillance Flight

In Mission 2 the main performance concern is endurance. A mission profile for this mission was created to minimize battery energy used in the mission. A mission profile for this mission was created from the initial aircraft optimization. For this mission, the aircraft is to fly at cruise velocity the entire flight including turns. Based on this profile, for a mission with five mph wind conditions, the aircraft has 20% battery power remaining. Energy consumption reaches 0% for missions of 25 mph or more.

5.7.4 Mission 3: Payload Release/Asymmetric Loads

Since Mission 3 has a lighter aircraft weight and the same number of laps as Mission 2, battery energy is not a concern. Therefore, Mission 3 performance is based entirely on payload loading time. Since the aircraft is designed to maximize the pre-mission assembly time, there is a slight loss in Mission 3 loading time due to the way the payloads fit into the box and how they load into the aircraft. Based on initial box layouts and testing, the Mission 3 loading time is predicted to be between 8 and 10 seconds.

5.8 Drawing Package

<INSERT DRAWING PACKAGE BETWEEN PAGES 43-48>

6.0 MANUFACTURING PLAN & PROCESSES

6.1 Investigation & Selection of Major Components & Assemblies

Many manufacturing processes were researched to determine the most reliable light weight process for each major assembly. The different processes used to manufacture each major component are listed in the following section.

6.1.1 Fuselage

The fuselage had three major methods considered for its construction. While weight was still the dominating factor for this piece of the aircraft, maintenance was also highly considered. The increase was warranted due to its integration role for all components of the aircraft. The following methods were chosen as fuselage construction alternatives.

- **Balsa Build Up** – This is done by creating a fuselage frame work and then building the fuselage skin around the framing.
- **Lost Foam Core** – Very similar to the foam core method, except the internal foam is removed for component mounting.
- **Mold Method** – A foam model of the fuselage is created by hand, which is then used to create a gypsum mold. This mold can then be used to create a strong fiberglass-balsa composite fuselage.

Each alternative was compared to a list of FOMs in a weighted decision matrix, which referenced the initial design parameters defined in the conceptual design, noted below in **Table 6.1**. The best construction method was determined to be the mold method due to weight savings, construction capability, and ease of maintenance.

Figures of Merit	Weight	Balsa Build Up	Lost Foam Core	Mold Method
Weight	0.40	1	-1	1
Construction Speed	0.10	0	1	-1
Construction Skill	0.20	-1	0	0
Maintenance	0.30	-1	0	0
TOTAL	**1.00**	**-0.1**	**-0.3**	**0.3**

Table 6.1: Fuselage Manufacturing Weighted Decision Matrix

6.1.2 Folding Wing and Tail

Three main methods were considered for construction of the wing and tail surfaces.

- **Composite/Balsa Build Up** – this method consisted of laying down carbon fiber spars and gluing balsa ribs to them before mounting internal components and covering the wing with Microlite.

- **Foam Core** – The airfoil section would be cut in the shape of the wing and then covered with either balsa or a composite material.
- **Molded Wing** – This method would require the construction of a plug mold, where parts could then be laid up and constructed.

A Weighted Decision Matrix was developed to clearly define the best method, shown in **Table 6.2**

Figures of Merit	Weight	Composite/ Balsa Build Up	Foam Core	Mold Method
Weight	0.40	1	-1	1
Speed of Construction	0.10	0	1	-1
Skill for Construction	0.25	1	0	-1
Maintenance	0.25	0	0	0
TOTAL	**1.00**	**0.65**	**-0.3**	**0.05**

Table 6.2: Folding Wing and Tail Manufacturing Weighted Decision Matrix

The Composite/Balsa Build Up method was chosen as the best construction method based primarily on weight and construction skill.

6.1.3 Tail Boom

The manufacturing of the square tail boom presented a unique challenge to maintain shape and tight tolerances. A Computer Numerical Control (CNC) machine was used for construction of two molds for the boom and sleeve. After layup and curing, the pieces were cut to the specified size. Each boom consisted of three sides of carbon fiber and a fourth side of fiber glassed balsa for structural support, which also served as a wiring enclosure for the tail control surfaces.

6.1.4 Landing Gear

The landing gear consisted of three different pieces: bow gear, nose wheel, and outriggers. Benchmarking previous designs, a composite layup construction method was used. The molds for the bow gear and nose wheel were made of high density foam which provided a smooth surface for composite layup. The final construction layup of the bow gear consisted of a balsa core, carbon fiber composite layup. The nose gear was also a composite layup, but with a Kevlar fabric core, which provided durability and a higher spring constant.

The two major methods for outrigger construction were piano wire bent to shape and a balsa core composites layup. While both proved easy to manufacture, the weight of the piano wire and its inability to support required loading conditions eliminated this construction technique.

6.1.5 Payload Release

Both types of aircraft payload releases were modeled after an archery release and machined out of Delrin for its wear characteristics and ease to machine. The placement of the pins and moving pieces

were critical to the releases' smooth operation, requiring the part to be machined on a HAAS 3-axis CNC mill. This provided tight tolerances and helped uniformity among the machined parts.

6.1.6 Box

A composite layup method was selected for the box construction method. Individual panels of the box were constructed and epoxied together to form the outer shell. The panels were made of a balsa core, carbon fiber layup with extra reinforcement. Tension cross braces were installed for additional structural support. Internal mounting points were added to secure the plane, centerline tank, and four rockets; consisting of a combination of high density foam and carbon fiber bracing.

6.2 Milestone Chart

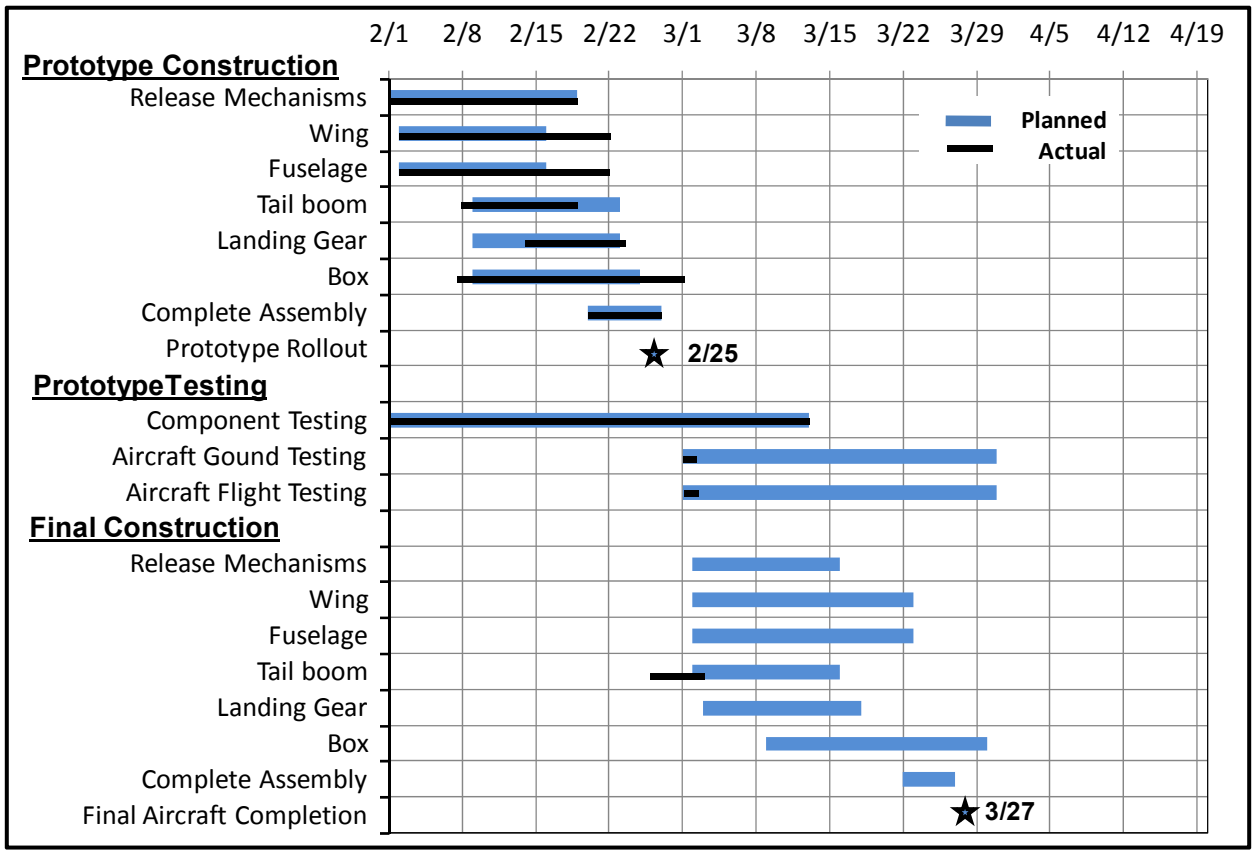

Figure 6.1: Milestone Chart

7.0 TESTING PLAN

Testing of the system and subassemblies were performed to ensure functionality and reliability for competition readiness. This included both strength and operations testing to verify the design of the systems.

7.1 Objectives

Test objectives were developed for each critical component of the system design; which was put into a test plan, determining performance characteristics. This plan allowed for a refinement of the system and construction methods to obtain the optimal design.

7.1.1 Component

Folding Wing

To demonstrate the wing spar's ability to withstand the loads of maneuvering at maximum gross weight, a test for maximum load was conducted. The wing was subjected to a three point bending test to determine the bending moments and stress applied to the carbon fiber spars.

Tail Boom

The main source of failure to the empennage section is torque from elevator and rudder induced forces. To determine such failure, a destructive test was conducted by securing one end of the boom and applying a measured torque from the free end.

Landing gear

The primary component tested for the landing gear was the bow gear, as it was designed to handle the initial forces during a hard landing, while supporting the bottle. This was simulated by securing the gear to a cantilevered beam with varying weights and dropping the bow gear from a series of heights.

Payload Release

Testing was conducted on the release mechanism for the centerline tank to check the material performance and repeatability of operation. Dynamic loads were investigated, which represented the forces experienced during a hard landing with a full centerline payload. To simulate the dynamic condition, the centerline release was mounted in a wing test section, weights secured in the release, and weights dropped from a measured vertical distance. The primary objective was to inspect how the Delrin housing with aluminum pins would interact and make design or material changes as needed. A secondary test was conducted to test the carbon beams used to hold the release mechanism in the airplane. This test was conducted with the same configuration of a three-point bending test, with weights dynamically applied.

7.1.2 Propulsion

To validate the data used to size the aircraft and propulsion system as well as determine if the chosen system was optimum for the aircraft, individual tests were conducted on the battery, motor, and propeller. The approach and objectives of these tests are outlined in the following section.

Battery

Battery testing was conducted to ensure battery capacity was accurately predicted for aircraft optimization. The batteries were initially cycled through charging and discharging to ensure they were at their optimum state. Once the batteries had been cycled a sufficient number of times, they were fully charged and discharged using a Computerized Battery Analyzer (CBA). The CBA tested the batteries at a fixed current output while measuring the voltage to gage the actual capacity of the battery or battery pack. This data was then used to create battery packs from the best batteries available and ensure the required battery capacity to complete each mission.

Propeller

For initial data collection, a selection of propellers was tested using the Oklahoma State University wind tunnel while the motor and power supply was held constant. These tests would output valuable data such as the torque, thrust, RPM, and power output at varying speeds. Using this data, efficiency plots of each propeller were created to help decide the optimum propeller for each mission.

Motor

Once the best propellers were selected, the motor was tested using the same setup in the wind tunnel as the propellers. In these tests, the motor is tested with each of the selected propellers to ensure the motor efficiency and gearbox match the estimated calculations. These tests also determine any additional problems with the motor from unexpected issues such as heat.

Propulsion System

Once all the individual components had been tested, the complete system was tested in the wind tunnel. This showed the overall efficiency of the system in different conditions. This test also demonstrated the actual battery life using the selected system as well as motor and battery temperatures to determine whether additional cooling is required.

7.1.3 Assembly

To evaluate the assembly for the overall system, a testing plan was developed to boost contest score by reducing time required to assemble the aircraft from the in-box configuration. Team tryouts were held to form a designated ground team for assembly. A number of practice sessions and tests were then conducted to develop the best process for assembly. Drop testing was used to analyze structural integrity of the aircraft and box to meet contest requirements. The results from the tests were used to maximize score, improve methods for assembly, and aid in survivability of the system in the various structural assessments of the contest.

7.1.4 Flight Test

In order to evaluate the overall design, actual flight testing was performed upon initial prototype completion. This process gave the team a better picture of aircraft performance in various flight conditions, and actual data to compare with theoretical values. Initial flight tests were simple maneuvers with an unloaded aircraft. Once the pilot became more familiar with the aircraft and the initial flight test data was analyzed, the complexity of the flight pattern increased until the actual missions were simulated. To coordinate these flight tests and maximize the information gathered from each flight, a test plan detailing the procedures and maneuvers was created, including data to be compiled during testing.

7.2 Master Test Schedule

A schedule for each test section was developed in Gantt chart form to identify a critical path line in system testing and construction, which is shown in the table below.

Test	Objective	Dates
Wing	Ensure wing strength is sufficient for flight dynamics	2/13, 2/23
Landing Gear	Verify gear and withstand forces of hard landing/drop test	2/19 - 2/23
Releases	Check strength and relability	2/9 - 2/22
Tail Boom	Check torsional and axial strength for tail forces	2/16 - 2/27
Box	Check drop test & alighenment of self loading payloads	2/14 - 4/11
Prop	Find prop that meets efficiency standards for all missions	2/3 - 3/15
Motor/Battery	Optimize system for mission profile	2/3 - 3/15
Ground Crew	Practice loading and decrease time to load	3/2 - 4/15
Flight	Check flight parameters of the aircraft	3/2 - 4/11

Table 7.1: Master Test Schedule

7.3 Pre-Flight Check List

Based upon competition mission requirements and continual propulsion testing, a pre-flight check list was developed to ensure flight readiness and prevent accidents. The pre-flight check list can be noted in the table below.

Pre-Flight Checklist	
Structural Integrity	
Visual inspection on each part for damage	
☐ Boom	☐ Vertical Stabilizer
☐ Wing	☐ Control Surfaces
☐ Fuselage	☐ Hatch Lid
☐ Wing Hinges	☐ Landing Gear
☐ Horizontal Stabilizer	☐ Bolts
Avionics	
Ensure all wires are firmly attached and components perform as needed	
☐ Servo Wiring	☐ Store Releases
☐ Avionic Power Test	☐ Battery Charge
☐ Range Test	☐ Battery Temperature
☐ Servo Test	☐ Failsafe
☐ Zero All Servos	
Propulsion	
Make sure motor performs as desired	
☐ Motor Wiring	☐ Motor Test
Final Checks	
Alert all in the area that the test will begin	
☐ Ground Crew	☐ Pilot and Spotter
☐ Final Visual Inspection	

Table 7.2: Pre-Flight Check List

8.0 PERFORMANCE RESULTS

After testing, the results were analyzed and component designs were corrected if inadequate. The performance details of critical components and changes to the design as a result of testing are explained in the section below.

8.1 Subsystems

8.1.1 Component

Wing

The center wing tested had a 46 inch span with a loading location at the center, utilizing a foam plate to distribute the load over an area roughly equal to the area of the fuselage-wing contact, shown in **Fig. 8.1**.

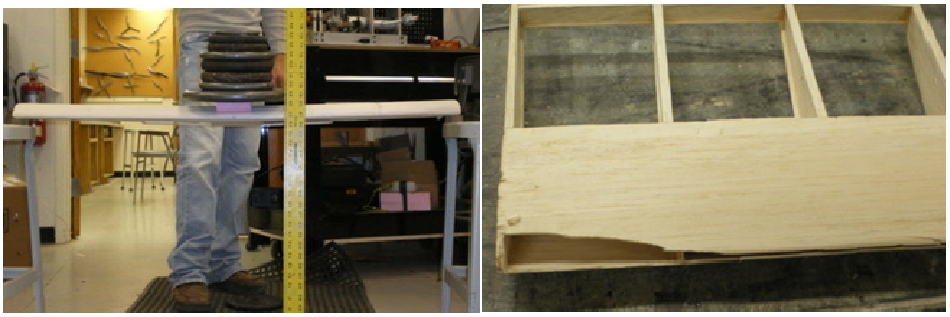

Figure 8.1: Wing Performance Test

The test was designed to validate the wing capability to support a 2.5G loading in Mission Two with an assumed total weight of 16 lbs. This span held a 90 lb load before failure of the balsa skin on the port side support; with no noticeable damage to the carbon spars. This translated to an approximate 2,070 lb-in bending moment at the center of the test wing. Comparing this value to the assumed full plane weight of 16 lb and a 2.5G wing loading, a bending moment of 1664 lb-in would be applied. Therefore the wing design had a margin of safety of 1.24, providing enough structural support to complete all competition missions.

Tail Boom

The torque on the tail boom from the rudder was the major factor tested in the design and fabrication of the boom. The boom performed quite well, with failure occurring at the balsa wood cap/shear web. Clamping the first 4 inches of the beam on the test table, 16 inch of the beam was left to test the torque, which closely resembles the exposed length of the boom when on the aircraft, noted in **Fig. 8.2**.

Figure 8.2: Tail Boom Performance Test

With a 10 inch moment arm, the beam failed with a 5 lb load, resulting in a 50 lb-inch load. This moment is much greater than the team calculated the tail to exert on the boom and fuselage. This overdesign provides a large margin of safety but also an avenue for the team to possibly use less material and lighten the total aircraft in later iterations.

Landing Gear

Multiple tests were conducted on the landing gears. The first landing gear was found to be highly over designed as it did not fail until a 30 inch drop with a 17 lb load, as shown in the **Fig. 8.3**.

Figure 8.3: Landing Gear Performance Test

The carbon fiber layup was greatly reduced on the second design, which yielded more suitable results. While the second failed on a 9 in drop with a 10 lb load, occurring on a post-impact sideways bounce. A simple modification to the design was introduced by angling the sides of the landing gear inward, preventing this type of failure in future gears as well as provides spring force to cushion a hard impact landing.

Payload Release

The Delrin centerline tank releases were tested dynamically by attaching a 10 lb weight to the support pin and dropping the weight from a measured height. Problems emerged after a few tests, where the two plates separated allowing a release of the weights. This required a reselection of materials, using aluminum plates for the centerline tank, while retaining the Delrin for the rocket releases. The new design allowed for acceptable tolerances to handle realistic loads during flight missions.

8.1.2 Propulsion

Battery

Initially, batteries were cycled following a defined test regime and then discharged via the CBA hardware, recording the voltage versus capacity, listed in the figure below. Once all batteries were tested, battery combinations were arranged to provide the highest capacity for numerous battery packs.

The final battery tests were performed by discharging the battery packs at 21.6 volts and 3 amps. Although the system is not capable of testing the entire battery pack at the current that will be used in the actual aircraft, the test results can be reduced by 5-10% to get a more realistic result. The data for the first five battery packs constructed are shown in **Fig 8.4**.

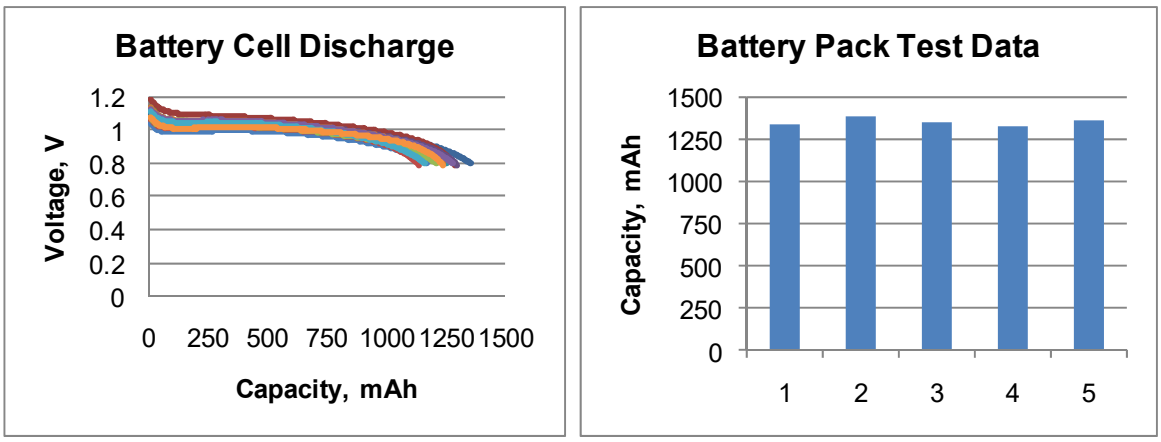

Figure 8.4: Battery Performance Results

The figure shows that all five battery packs peaked around 1300 mAh. Even at a 10% reduction to account for higher current draws during flight, these packs are still much better than the 1000 mAh predicted, allowing for better performance or longer endurance capabilities. Investigation on how the change in battery capacity affects the performance of the aircraft will be investigated based upon these findings.

Motor

The selected motor was tested in the wind tunnel with different propellers and at different speeds. With the first motor tested, the efficiency measured was only 85%, compared to the projected efficiency of 91%. The motor also had an overheating issue. After a number of runs, it would become extremely hot and shut down. This shows that the motor needs a sufficient amount of cooling to function efficiently. A smaller, lighter motor is expected to be tested once it arrives that may have an efficiency closer to what was predicted.

Propeller

A number of propellers were tested to determine the optimal design for each mission. Mission 1 requires a fast completion time, while Mission 2 is an endurance mission. **Fig. 8.5** plots the performance characteristics of some of the major propellers tested.

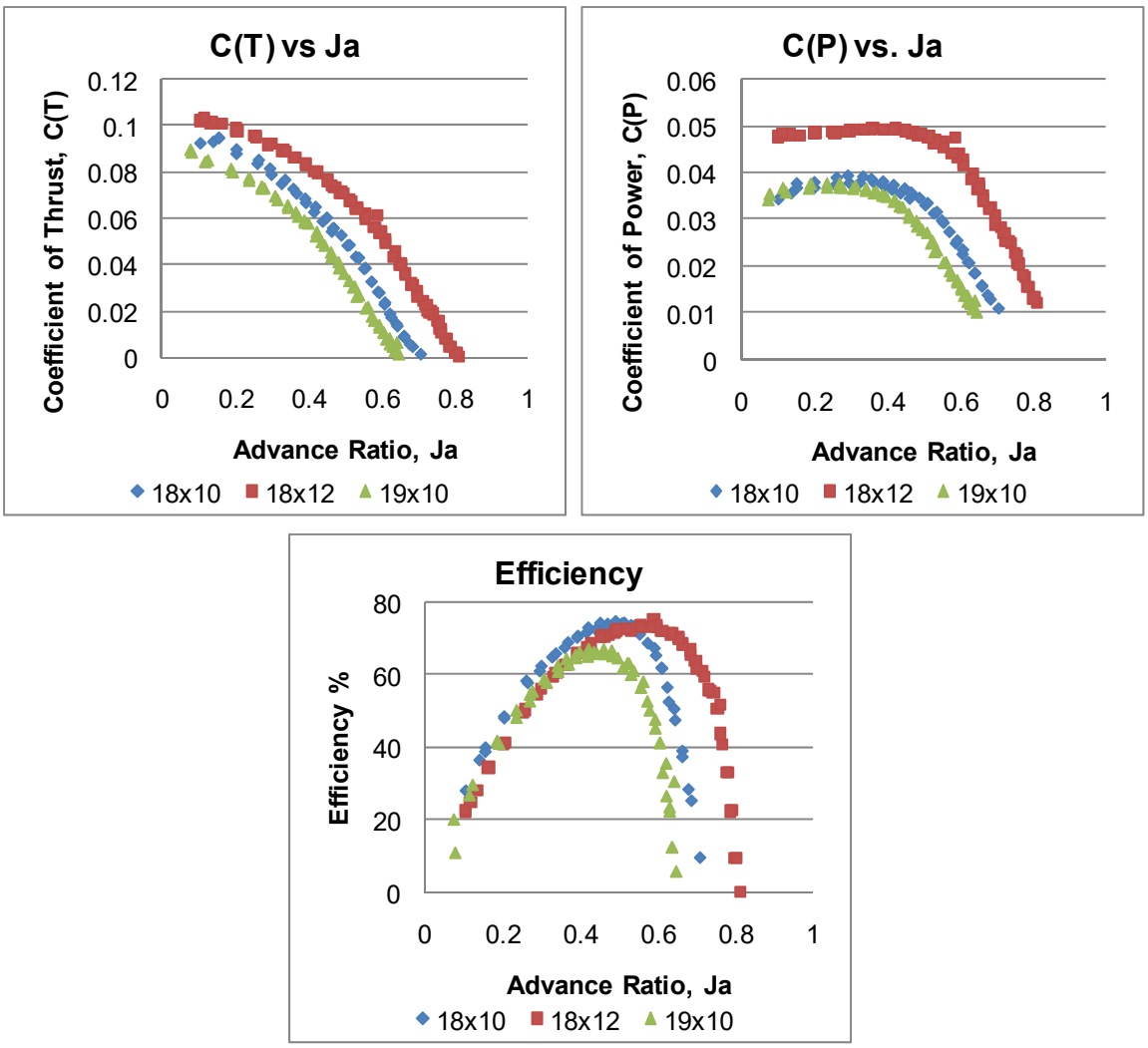

Figure 8.5: Propeller Performance Results

In Mission 1, takeoff distance and battery consumption are not an issue; a higher pitch propeller will yield a higher score because it allows for more thrust and therefore a greater maximum velocity. Similarly, for Mission 2, efficiency is more important than top speed. Based on optimized cruise velocity, the best propeller will be most efficient at that advance ratio, Ja.

Propulsion System

The entire system was tested in the wind tunnel, similar to the propeller and motor tests. The system was tested at 13 Amps for 3.8 minutes to simulate Mission 2. The battery pack used a total of 1033 mAh, about 77% of the total capacity. This test was conducted without any direct cooling and both the batteries and motor had significant heat buildup. The batteries reached temperatures of over 150°F. This test also confirmed the both batteries and motor require significant cooling.

8.2 System

The aircraft had to be consistent in both assembly and flight. Therefore extensive testing was done to ensure a reliable and quick assembly. Flight testing was also performed to practice flying the missions in the optimized mission plan as well as ensure the aircraft was capable of completing each mission.

8.2.1 Pre-Mission

Structural Tests

Part of the pre-mission requires the aircraft to survive a six inch box drop as well as a wing tip test to simulate a 2.5G load. The drop test was successfully conducted on each side of the box a number of times to ensure the system will pass at the competition no matter which side is chosen. The aircraft also passed the wing tip test by holding the aircraft on the wing tips with the center payload attached.

Assembly

Initially a prototype box was tested to ensure the payloads load into the aircraft smoothly and reliably. A final box was designed that consistently loaded the payloads quickly and allowed for easy access for aircraft and component placement. Once a final box design was created, timed tests were performed to minimize assembly time for the competition. These tests were conducted as if assembly began with the team standing next to the box.

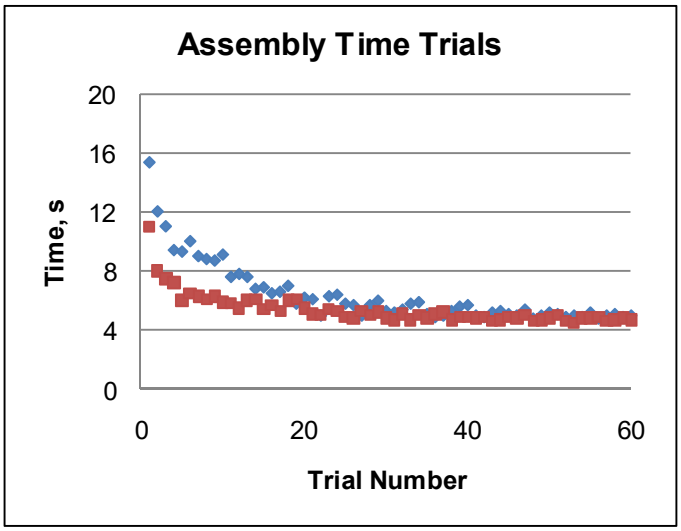

Figure 8.6: Assembly Time Trials

The time trials for the assembly team were about five seconds. The prediction during the design phase was seven seconds, which greatly improved the projected assembly time. This improved overall score.

8.2.2 Flight Testing

Flight testing started with basic maneuvers with empty weight and slowly progressed to heavier weights and entire mission simulations. All three missions were flown at various moderate wind speeds to ensure versatility in wind condition.

Mission 1 was the first complete mission flown due to its light weight and little variation in C.G throughout the mission. This mission proved that when flown at various speeds and bank angles the main concern was structural integrity rather than propulsion system. Takeoff distance was no problem in any of the tested wind conditions where each of the takeoff distances were less than 50 ft. After a few flight tests, times for mission completion ranged from 80 to 90 seconds which is a significant increase from the predicted 75 second time. Even though the flight time is lower, this will not decrease the score very much since Mission 1 flight time has the least effect on overall score.

Mission 2 was the last mission to be fully completed due to the propulsion system constraints. Therefore, extensive testing had to be done in advance to ensure enough battery capacity to complete the mission. Initial flight testing was done for wind speeds of between five and fifteen miles per hour. For these tests, battery capacity at the end of the mission ranged from between 9-17 %. Initial predictions for these wind conditions ranged from 12-20%, which shows a slight decrease in battery capacity remaining. Also, takeoff distance was very close to the 100 ft limit at low wind conditions, so further testing will be done to ensure a shorter takeoff distance.

Mission 3 was tested by changing different rocket configurations until the pilot was familiar with the effects of the asymmetric payloads. For this mission the main concern was the roll stability immediately after takeoff with asymmetric payloads. After enough tests the pilot was able to control the aircraft in all phases of the flight well enough to complete the mission.

OKLAHOMA STATE UNIVERSITY TEAM BLACK

FASTBACK | 02/27/2009 | SHEET 1

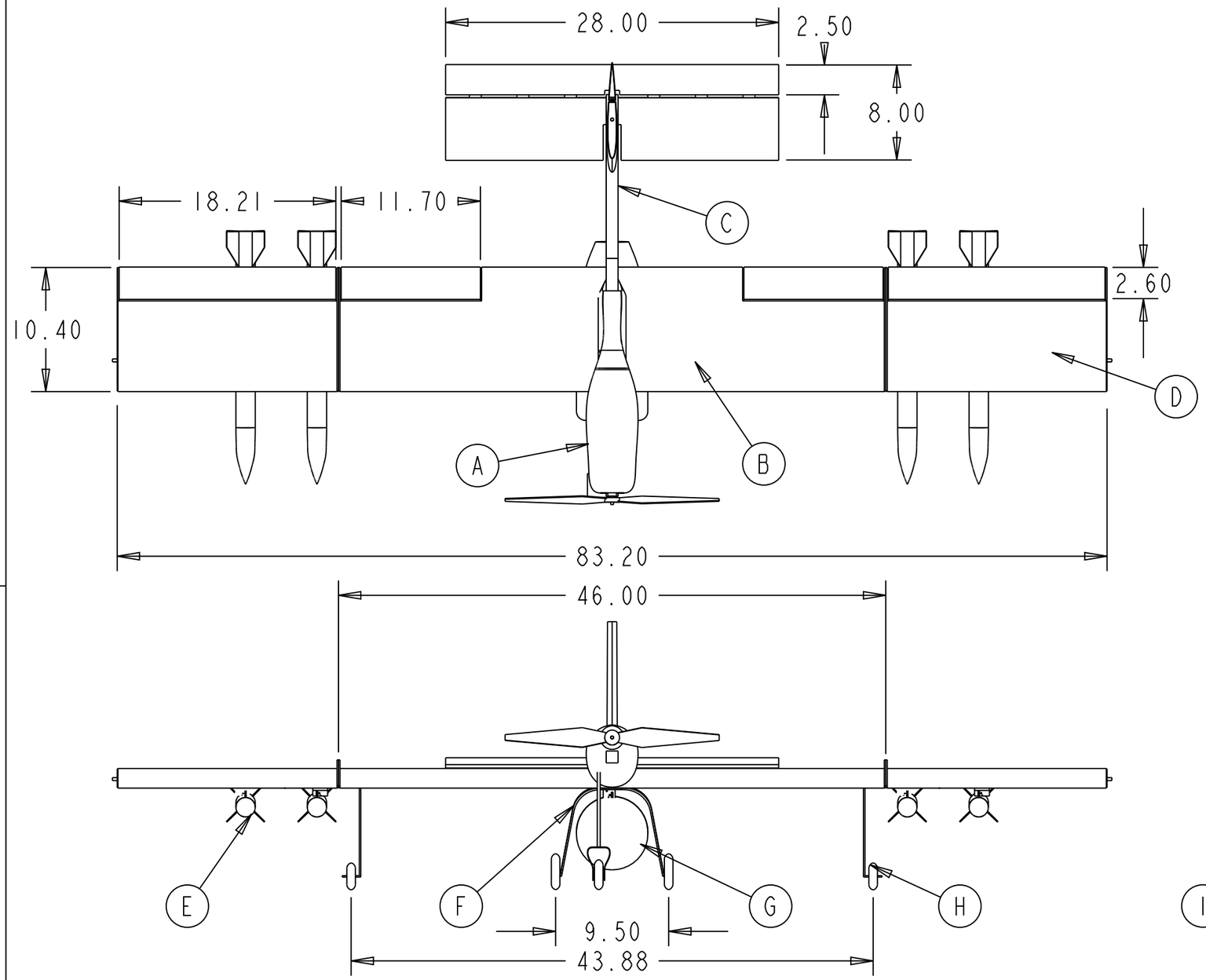

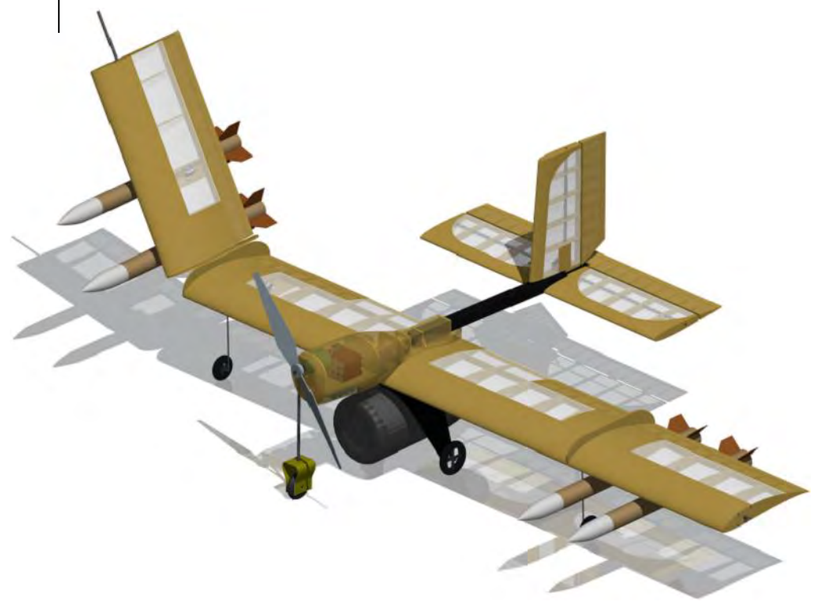

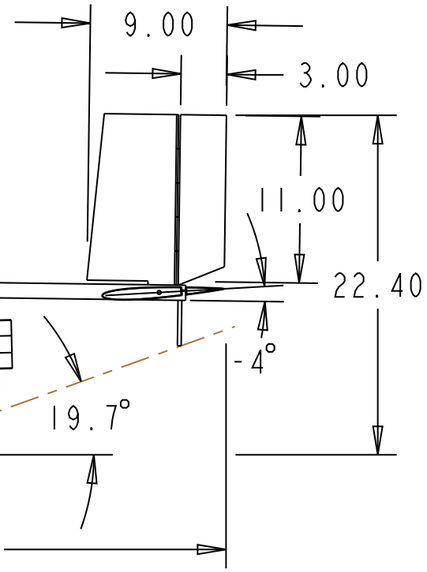

PRIMARY COMPONENTS					
A	FUSELAGE	D	FOLDING WING ASSM (2)	G	CENTER STORE PAYLOAD
B	MAIN WING ASSM	E	WING STORE PAYLOAD (4)	H	OUTRIGGER GEAR (2)
C	TAIL / SHAFT ASSM	F	MAIN LANDING GEAR	I	NOSE LANDING GEAR

NOTE: ALL DIMENSIONS ARE GIVEN IN INCHES

OKLAHOMA STATE UNIVERSITY TEAM BLACK
CESSNA-RAYTHEON-AIAA DESIGN/BUILD/FLY 2009

DOCUMENT TITLE

AIRCRAFT 3-VIEW

DRAWN BY: A. BEERWINKLE

CHIEF ENGINEER: J. COOPER

SIZE	APPROVAL DATE	REPORT TITLE	REV #
B	02/27/2009	DRAWING PACKAGE	A

SCALE 1/10

	NAME	MATERIAL	QTY
1	FUSELAGE SKIN	COMPOSITE REINF. BALSA	1
2	BULKHEAD	GLASS LAMINATE PLY	6
3	BOOM SLEEVE	4-PLY CARBON FIBER	1
4	TAIL BOOM	4-PLY CARBON FIBER	1
5	VERTICAL STAB	BALSA	1
6	RUDDER	BALSA	1

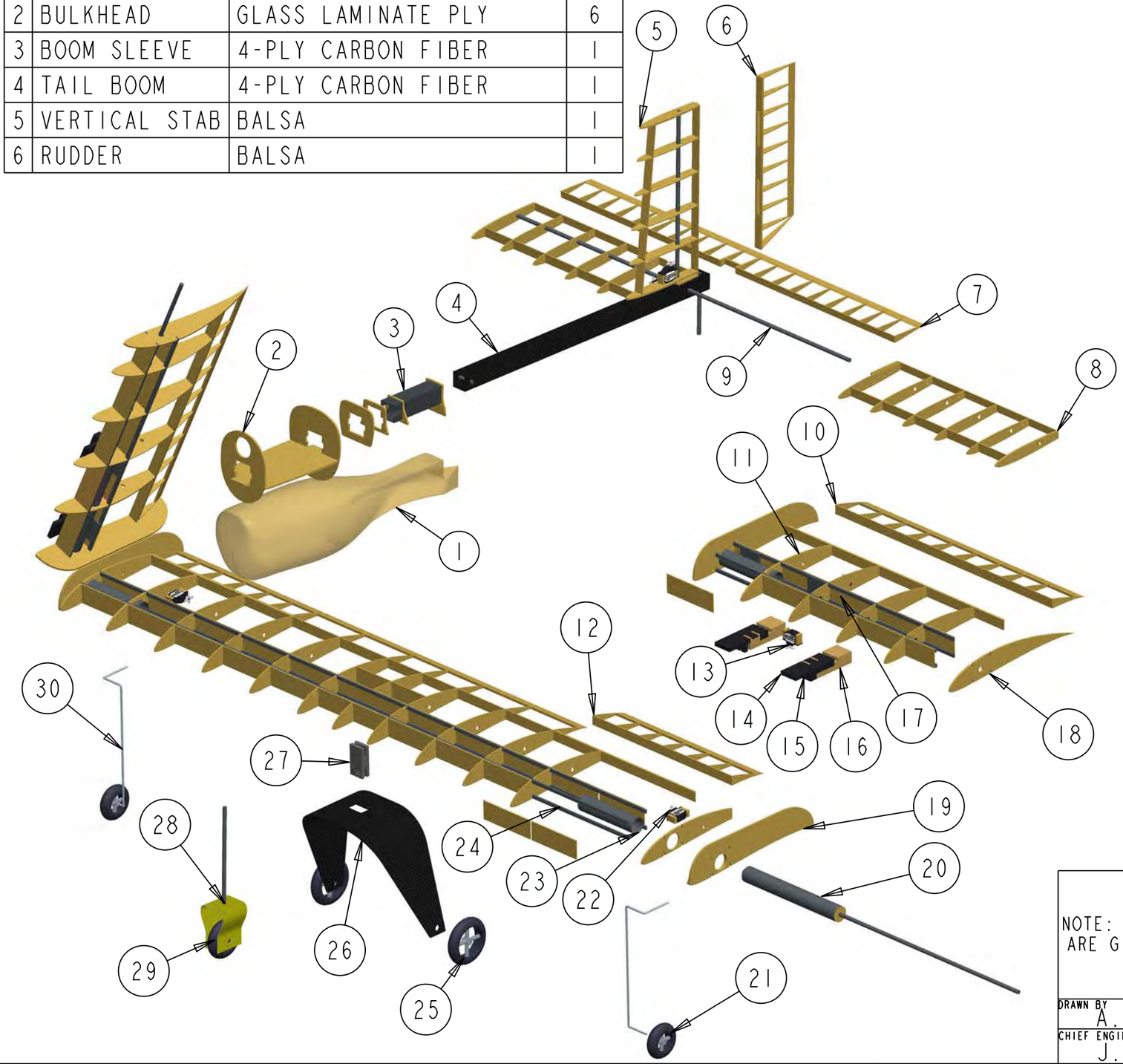

7	ELEVATOR	BALSA	1
8	HORIZ STABILIZER	BALSA	2
9	TAIL SPAR	CARBON TUBE	2
10	18.2" OUTER AILERON	BALSA	2
11	INNER RIB	BALSA	21
12	11.7" INNER AILERON	BALSA	2
13	RELEASE SERVO	FUTABA 3156	3
14	UPPER RELEASE PLATE	DELRIN	4
15	RELEASE GATE	STEEL	5
16	LOWER RELEASE PLATE	BALSA PLY	4
17	MAIN SHEAR WEB	BALSA	44
18	OUTER RIB	BALSA PLY	2
19	WING HINGE RIB	BALSA PLY	4
20	PUSH ROD SPAR	CARBON TUBE	2
21	OUTRIGGER WHEEL	2.25" DIA.	2
22	AILERON SERVO	FUTABA 3156	4
23	PUSH ROD TUBE	CARBON TUBE	4
24	WING SPAR	UNIWEB CARBON	12
25	MAIN GEAR WHEEL	3" DIAMETER	2
26	MAIN LANDING GEAR	KEVLAR/CARBON	1
27	CENTER RELEASE	ALUMINUM	1
28	NOSE LANDING GEAR	KEVLAR/CARBON	1
29	NOSE GEAR WHEEL	2.5" DIAMETER	1
30	OUTRIGGER SHAFT	CARBON	2

NOTE: ALL DIMENSIONS ARE GIVEN IN INCHES

OKLAHOMA STATE UNIVERSITY TEAM BLACK
CESSNA-RAYTHEON-AIAA DESIGN/BUILD/FLY 2009

DOCUMENT TITLE
STRUCTURAL ARRANGEMENT

DRAWN BY	SIZE	APPROVAL DATE	REPORT TITLE	REV #
A. BEERWINKLE	B	02/27/2009	DRAWING PACKAGE	A
CHIEF ENGINEER J. COOPER	SCALE 0.150			PAGE 2 OF 5

OKLAHOMA STATE UNIVERSITY TEAM BLACK

FASTBACK | 02/28/2009 | SHEET 3

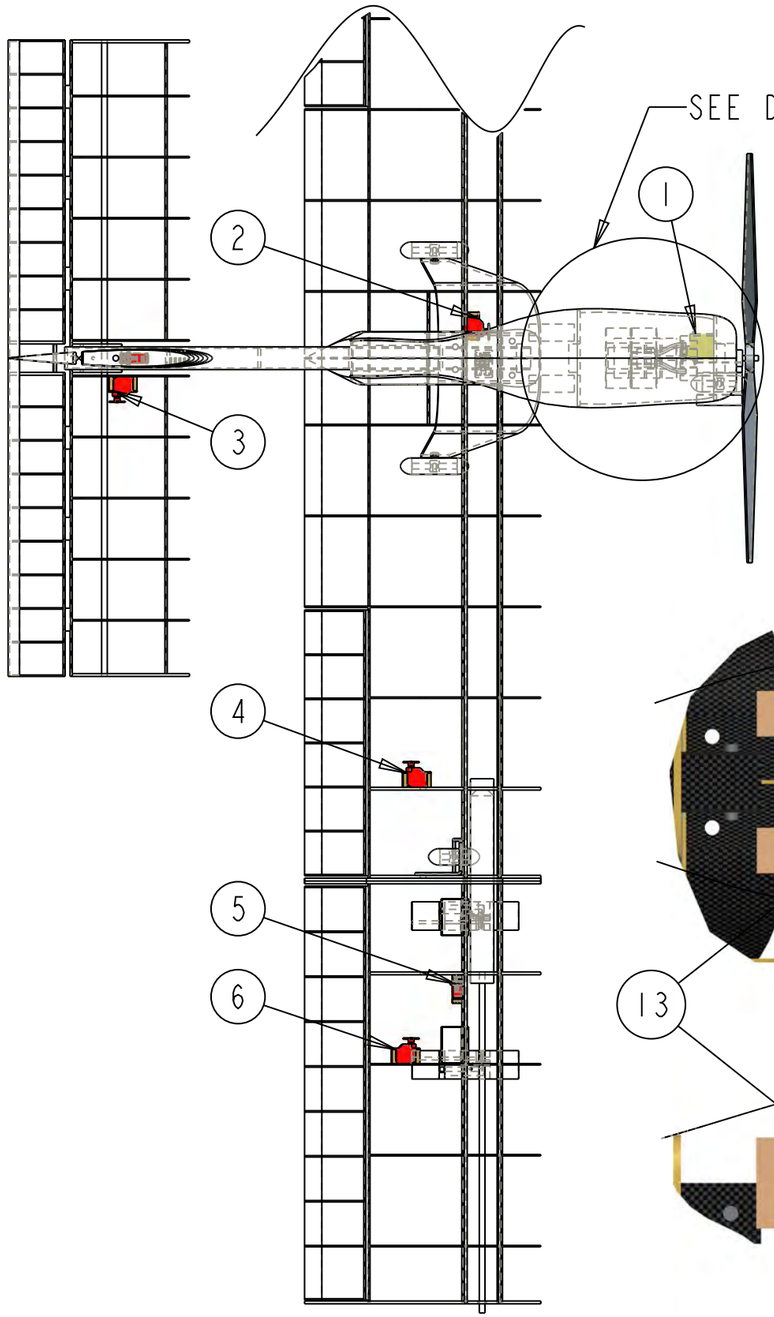

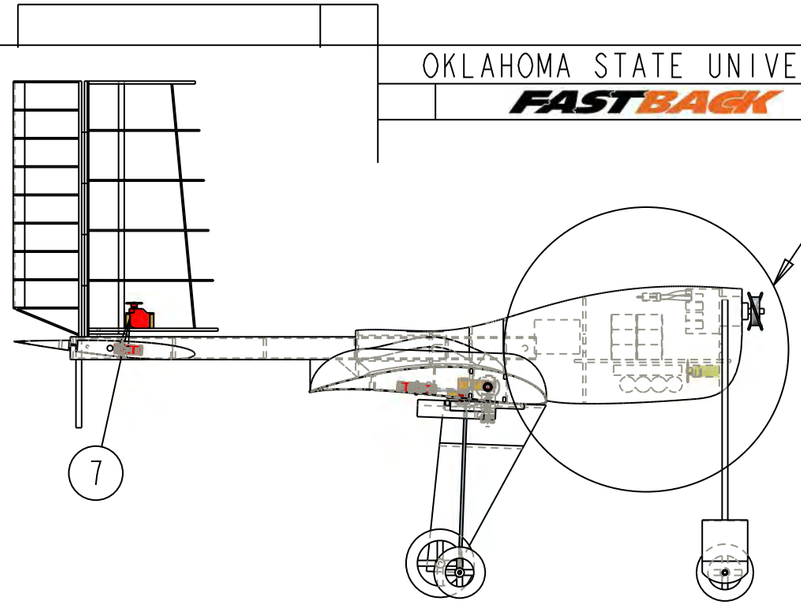

DETAIL A
SCALE 0.400

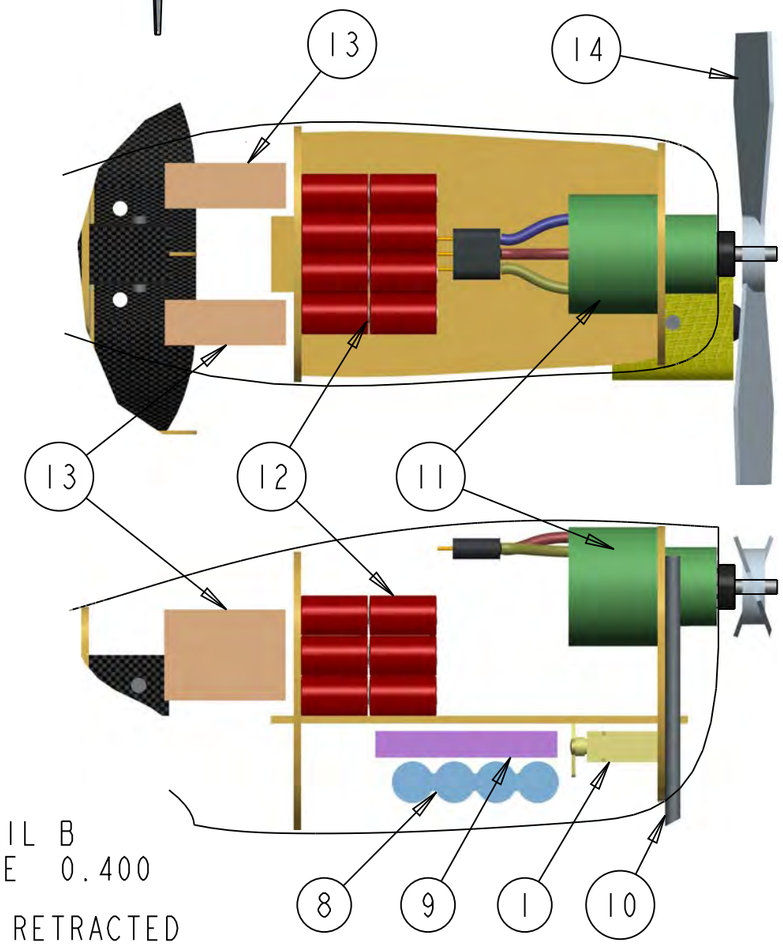

DETAIL B
SCALE 0.400

NOTE: TAIL BOOM SHOWN PARTIALLY RETRACTED

	ITEM	MANUF.	MODEL	QTY
1	NOSE GEAR SERVO	FUTABA	S3102	1
2	CENTER RELEASE SERVO	FUTABA	S3156	1
3	ELEVATOR SERVO	FUTABA	S3156	1
4	INBOARD AIL. SERVO	FUTABA	S3156	2
5	WING RELEASE SERVO	FUTABA	S3156	2
6	OUTBOARD AIL. SERVO	FUTABA	S3156	2
7	RUDDER SERVO	FUTABA	S3156	1
8	RECEIVER BATT.	SPECTRUM	1100 mAh	1
9	E.S.C.	KONTRONIK	55-10-32	1
10	NOSE LANDING GEAR	-	-	1
11	MOTOR	NEU	1905/1.5Y	1
12	2/3A BATTERY	ELITE	1500	24
13	RECEIVER	SPECTRUM	AR9000	2
14	PROPELLER	APC	18X10	1

NOTE: ALL DIMENSIONS ARE GIVEN IN INCHES

OKLAHOMA STATE UNIVERSITY TEAM BLACK
CESSNA-RAYTHEON-AIAA DESIGN/BUILD/FLY 2009

DOCUMENT TITLE
SYSTEMS LAYOUT

DRAWN BY: A. BEERWINKLE
CHIEF ENGINEER: J. COOPER

SIZE: B | APPROVAL DATE: 02/27/2009 | REPORT TITLE: DRAWING PACKAGE | REV #: A

SCALE: 0.150

PAYLOAD RELEASE DETAIL DESIGN

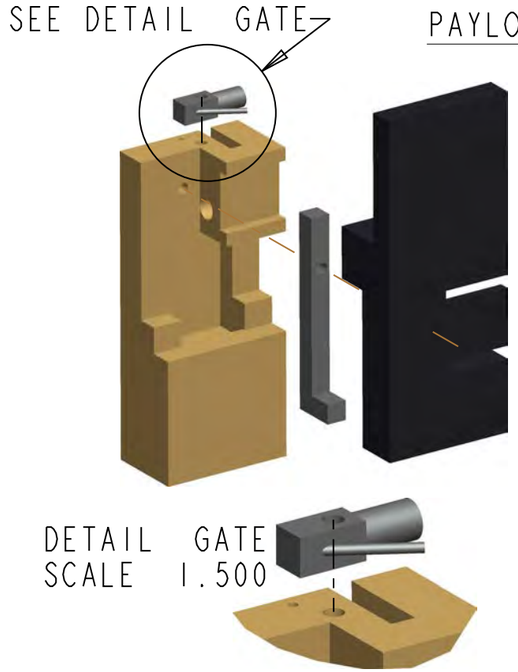

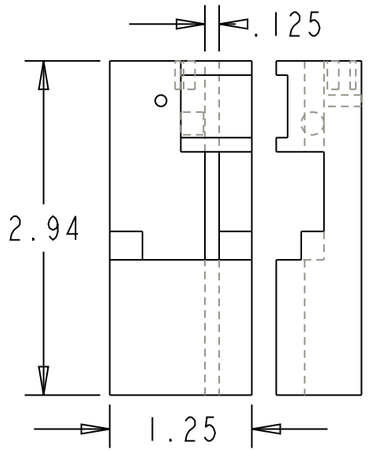

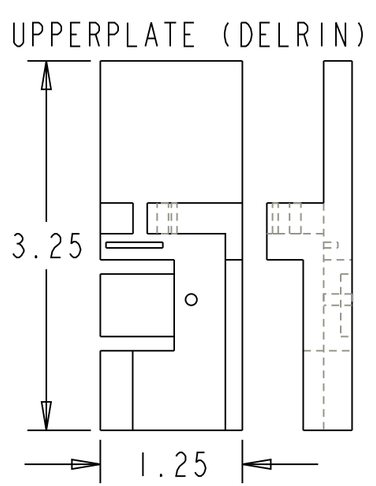

SCALE 0.750

WING STORE ACCOMODATION

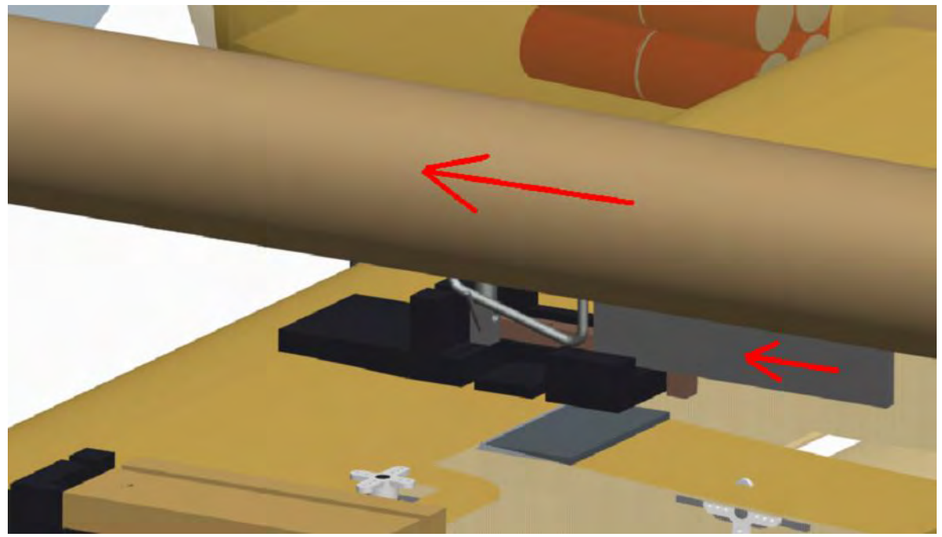

OVERALL LAYOUT / VERIFICATION OF REQUIRED DIMENSIONS

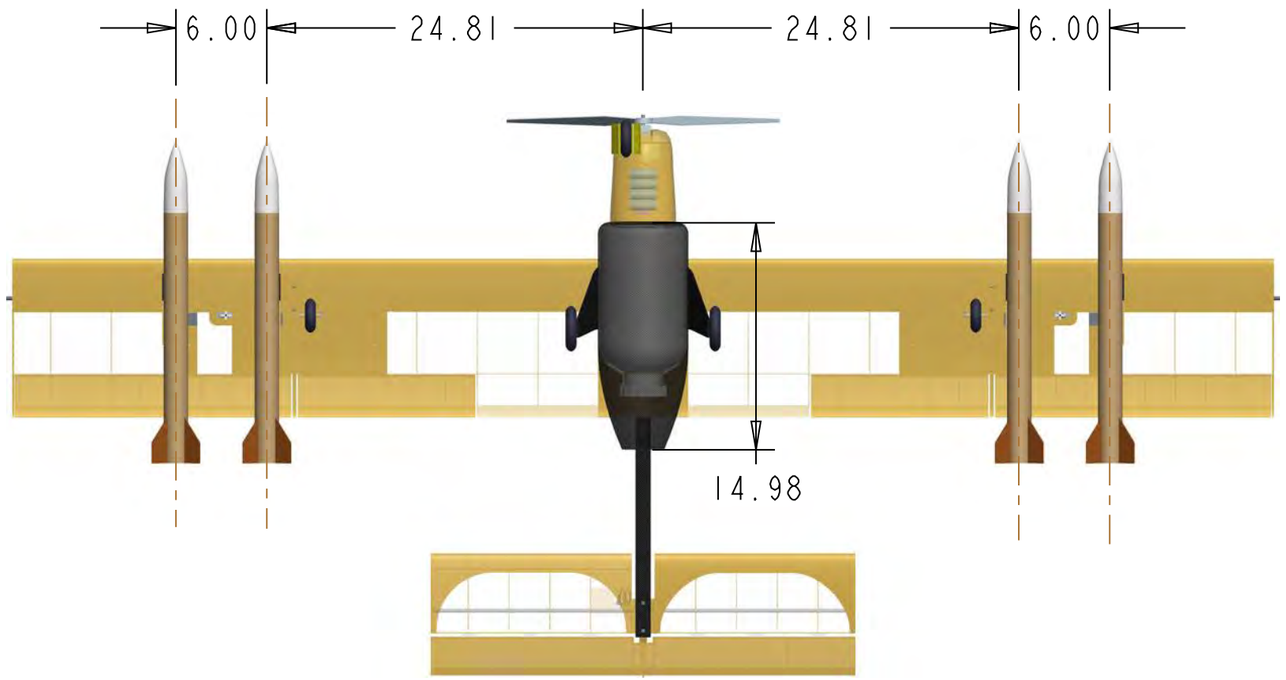

CENTERSTORE ACCOMODATION

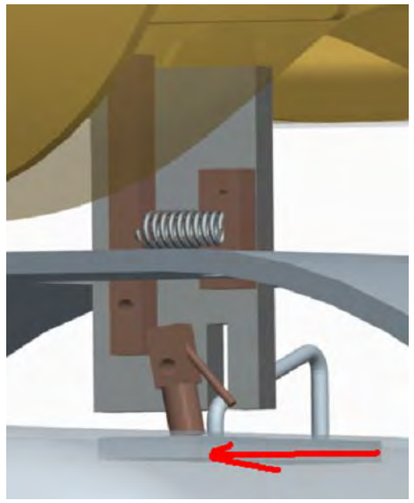

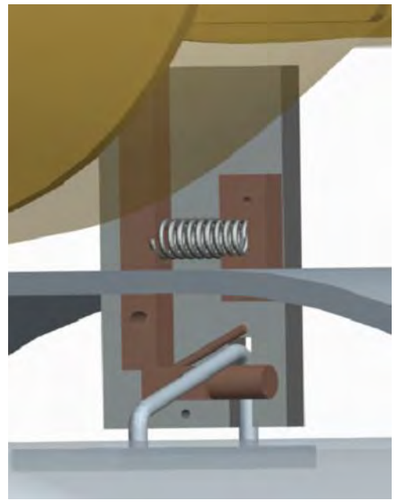

NOTE: ALL DIMENSIONS ARE GIVEN IN INCHES

OKLAHOMA STATE UNIVERSITY TEAM BLACK
CESSNA-RAYTHEON-AIAA DESIGN/BUILD/FLY 2009

DOCUMENT TITLE
PAYLOAD ACCOMODATION

DRAWN BY	SIZE	APPROVAL DATE	REPORT TITLE	REV #
A. BEERWINKLE	B	02/27/2009	DRAWING PACKAGE	A
CHIEF ENGINEER J. COOPER	SCALE 0.150			PAGE 4 OF 5

BOX FRONT/SIDE VIEW

KEVLAR FIBER HINGE

BALSA SUPPORT WALL

CARBON FRAME

FOAM AIRCRAFT SUPPORTS

SCALE 0.080

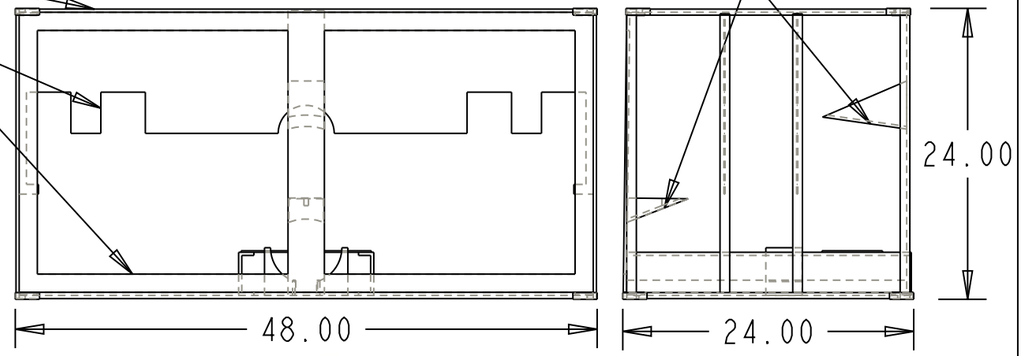

ASSEMBLY PROGRESSION

SCALE 0.070

SCALE 0.100

STOWED AIRCRAFT

NOTE: ALL DIMENSIONS ARE GIVEN IN INCHES

OKLAHOMA STATE UNIVERSITY TEAM BLACK
CESSNA-RAYTHEON-AIAA DESIGN/BUILD/FLY 2009

DOCUMENT TITLE
STOWED ARRANGEMENT

DRAWN BY	SIZE	APPROVAL DATE	REPORT TITLE	REV #
A. BEERWINKLE	B	02/27/2009	DRAWING PACKAGE	A
CHIEF ENGINEER J. COOPER	SCALE 0.060			PAGE 5 OF 5

Oklahoma State University

Orange Team

Design Report

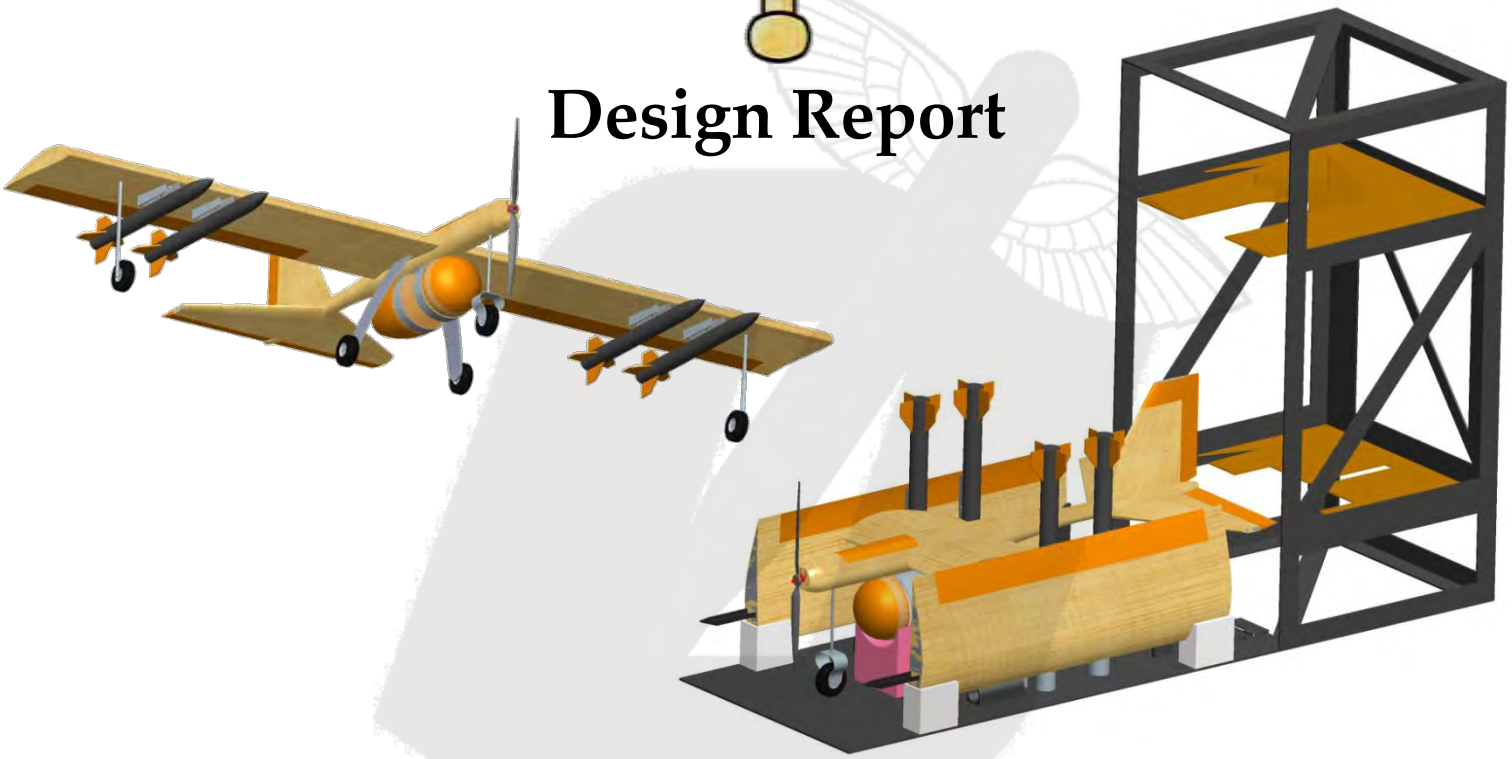

2008/2009 AIAA Foundation

Cessna/Raytheon Missile Systems

Design Build Fly Competition

Table of Contents

1.0 EXECUTIVE SUMMARY

The 2009 Design/Build/Fly contest presents a multitude of interesting challenges ranging from highly asymmetric flight loading to ultra-fast aircraft assembly. The OSU Orange Team's design process focused upon contest requirements generating unique solutions for this year's contest. The team, composed of 17 members, solved these challenges to present a detailed solution of the system which best meets the mission requirements and optimizes the overall score.

1.1 SUMMARY OF DESIGN PROCESS AND OUTCOME

The design approach started with studying the mission requirements then translating these requirements into the best design methodology to achieve the highest score. To start this process, the conceptual design phase was conducted to explore the range of possible design solutions. By comparing these concepts according to the translated design requirements, the designs could be chosen intelligently. The overall system configuration consists of a mid-mounted mono-wing airplane attached to a sleek fuselage, conventional tail, all within a rectangular reverse-opening lid box. The design, while very traditional in appearance, contains several unique and innovative qualities which allow it to perform for maximum score. The box fulfills the mission in two major ways: it is light weight yet sturdy, and has a stowed configuration that allows for an extremely low assembly time. A five wheel style landing gear configuration was chosen to deal with the necessity to perform taxiing maneuvers with asymmetric loads.

Having selected a design, the team was divided into specialized groups to execute the preliminary design phase. The aerodynamics, propulsion, and structures teams were formed to analyze the selected configuration. This phase optimized independent sub-systems and the final integrated system design.

The final stage of the design process was to carry out a detailed design. The groups formed from the previous stage were held throughout the remainder of the process to allow the overall design to progress as one while encouraging specialization and focus on details. In this stage, the exact parameters of the design were resolved and the CAD models built to facilitate construction.

1.2 MISSION REQUIREMENTS AND DESIGN SOLUTIONS

As stated, the design began with a diligent study of the rules and mission requirements. Many of the mission requirements promoted specific solutions and aspects of the design. For instance, the pre-mission score in itself drives much of the overall score of the competition; surpassed only by the contribution of the design report. The pre-mission score directly affects the score for the three missions through a standard term called the System Complexity Factor (SCF). This is determined by two parameters: the Rated Aircraft Cost (RAC) or weight of all components used at the contest, including the box, and the time to assemble the flight-ready aircraft out of the box (Assembly Time). The SCF is equal to the inverse of the product of these two parameters. This means that the most important design criteria are to reduce speed of assembly and total system weight. Not only does the aircraft have to be light

weight, but the box does as well. Additionally, a 6 inch drop test of the system requires that the box also remain sturdy. The box design has a high strength skeletal structure with minimal skin to reduce weight and ensure rigidity. Additionally, only one box was used in the design, placing a sizing constraint on the aircraft which was kept light through similar structure.

To minimize assembly time, the box must open quickly and the aircraft come together with as few movements a possible. In addition, the rules require the batteries and payloads to be uninstalled while in the box. The payloads required by the contest consist of one four liter water bottle and four model rockets; each of which, must be individually remotely releasable. For this, specialized systems were devised to ensure reliability, stability, and speed of loading for the pre-mission and mission 3.

For Missions 1, 2, and 3, the aircraft must takeoff within 100 feet. The first mission requires the aircraft to make two laps around a pre-defined course while being timed. The centerline payload (4 liter tank) will be attached, but not filled. The score comes from the SCF divided by flight time. Mission 2 requires the aircraft to fly four laps with a full centerline tank where score is equal to SCF, if completed. Mission 3 requires a timed loading of the wing store payloads from the box to the aircraft. The score will be SCF divided by loading time, but cannot be achieved without performing a complete mission. This consists of flying four laps and remotely dropping a payload after each lap, resulting in asymmetric loading conditions while on the ground and in the air.

These challenges were prominently addressed through design solutions that include rectangular and triangular boxes in addition to traditional aircraft configuration concepts. Primary discussion focuses on the interaction of the box and aircraft together to reduce the assembly time for the entire system.

1.3 System Performance and Capabilities

To perform best during the pre-mission assembly test, the system can be assembled in a total of two moves made in parallel by each of the three member crew, allowing for exceptionally low assembly times. The total system achieves this capability through several solutions as follows: the box opens on one hinge revealing the entire aircraft with no residual blocks and can be gravity closed. The wing store payloads are loaded by one action of lifting the wing and the centerline is loaded by the action of pulling the aircraft forward from the box. To facilitate this as well as the release of the payloads, a spring-hook mechanism was installed at each location. Additionally, the wings have removable sections that are re-attached by a tapered insert which fits into the central fuselage-wing section. Performance estimates for assembly time and loading time are currently 7 and 5 seconds, respectively. Additional considerations made for mission 3 include the use of outriggers on the wings to keep the plane balanced while taxiing and large ailerons to allow for control during asymmetric loading. Tested aircraft performance parameters include a maximum velocity of 76 fps for mission 1 and a max rate of climb at 6 fps for mission 2.

2.0 MANAGEMENT SUMMARY

Through the conceptual design phase, the team acted in unison developing key concepts for the overall design. Later, defined roles allowed the team to optimize the aircraft and box solution.

2.1 DESIGN TEAM ORGANIZATION

The Orange team was divided into three distinct groups: Structures, Aerodynamics, and Propulsion. Due to the box also scoring in the RAC, the Structures team was given more emphasis in personnel distribution as shown in Figure 1. The Chief Engineer for the team guided the development of the design and managed all aspects of the project. Each group had a designated lead who managed their groups' day-to-day tasks. Lastly, there was a designated CAD lead that managed all the drawings for the project and was responsible for attention-to-detail during the construction process.

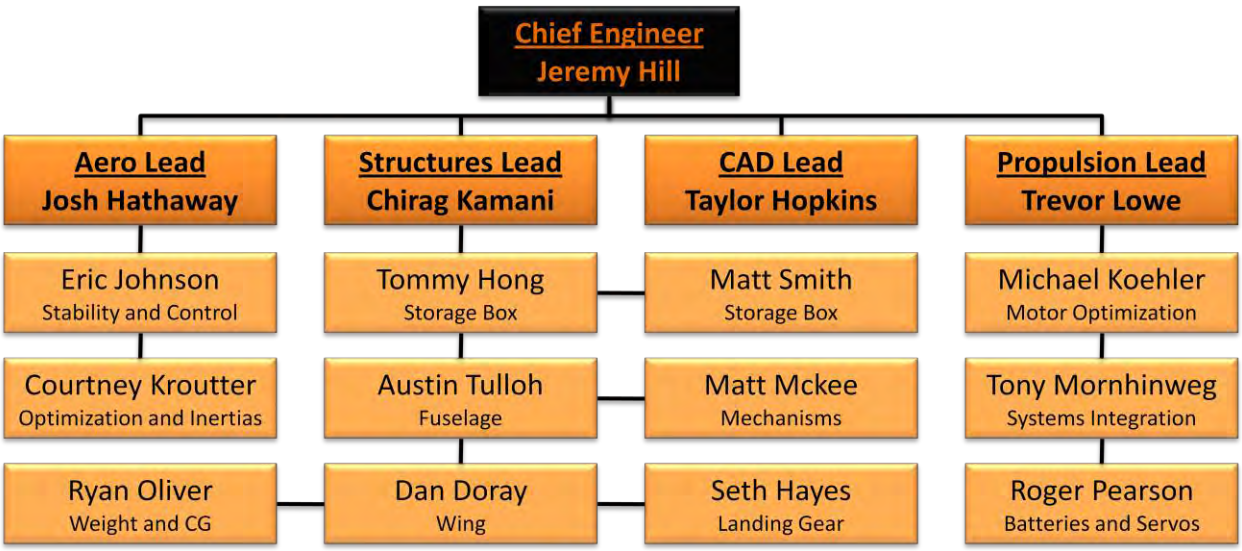

Figure 1: Team Organization

2.2 DESIGN PROCESS SCHEDULE

In order to keep the project on schedule, a Gantt chart in Figure 2 mapped out milestones for design, construction, and testing. Beginning with an accelerated two-week conceptual phase, the project continued into the preliminary design phase simultaneously with component testing where the conceptual design was taken to the next level. Next, the detailed dimensions were added in the detailed design phase in preparation for construction. Finally, the construction phase led directly into test flights and full system testing.

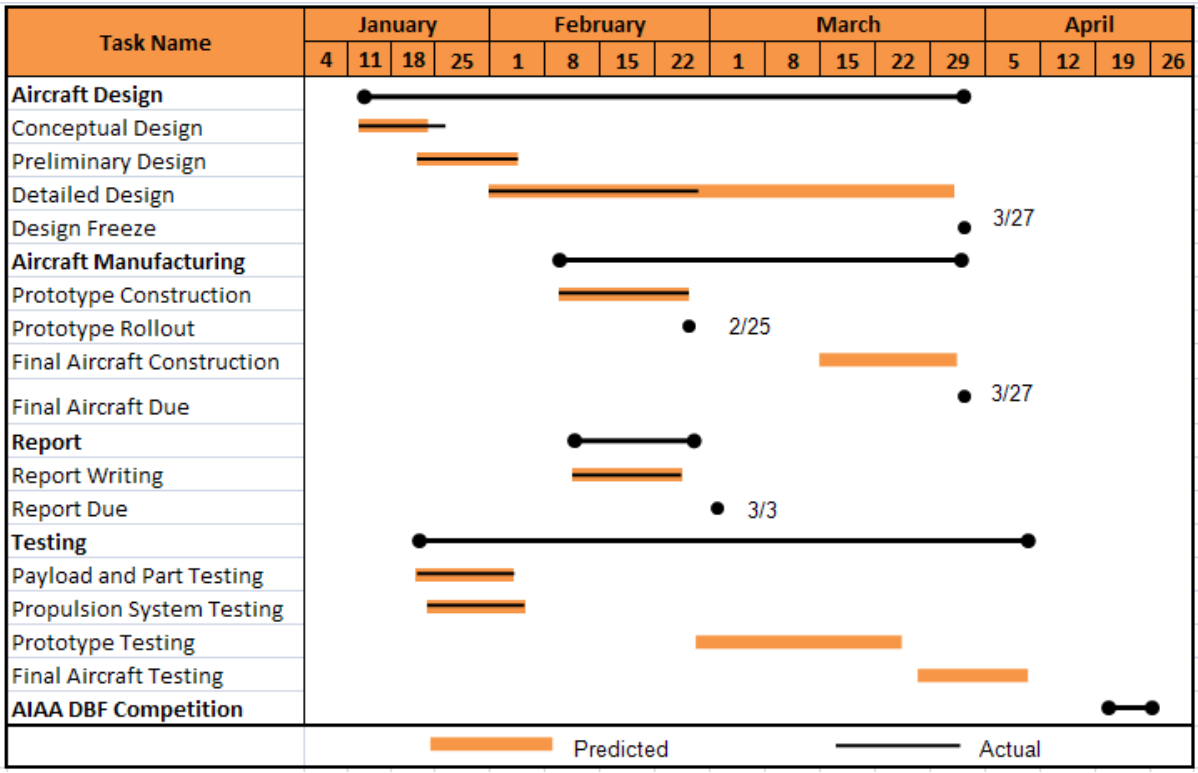

Figure 2: Project Gantt Chart

3.0 CONCEPTUAL DESIGN

The conceptual design phase began the process of analyzing the rules of the contest. Using a sensitivity analysis, figures of merit (FOMs) were established and translated into design requirements for the system solution. Solutions were then generated and compared in order to select the best scoring aircraft and box system configuration.

3.1 CONTEST MISSION REQUIREMENTS

The 2009 AIAA Design Build Fly competition consists of one pre-mission and three missions. The three flight mission scores will be normalized to 50, 75, and 100 points each. The total score is a function of the report score multiplied by the total flight score. Aside from the report score, the pre-mission defines the most critical scoring function within the total score through the System Complexity Factor (SCF). The pre-mission begins with the box being turned on all sides and then dropped from 6” above the ground. All contents must remain secured and undamaged. A structural wing tip test will simulate a 2.5g load on the aircraft by lifting each end of the aircraft’s main wing with a 4 liter bottle filled with water installed. After these tests, the design will be evaluated based on weight and assembly time. The pre-mission assembly time begins with all the system components unassembled in the box, and ends with the flight-ready aircraft and the box re-secured. The total system weight will be used in the Rated Aircraft Cost (RAC).

RAC = Weight of no more than two boxes, fully packaged. The complete system includes: air vehicle, batteries, transmitter, tools (if needed), and all wing stores at flight weight. The rules define the SCF in the following equation. SCF = 1 / (RAC*Assembly Time). The following missions determine the Flight Score.

- **Mission 1:** This mission is the only one that depends on Flight Time. The aircraft will fly 2 laps with an empty centerline payload. The time begins when the aircraft takes off and ends when it crosses the starting line. The scoring function for Mission 1 = SCF / (Flight Time).
- **Mission 2:** This is similar to Mission 1, but with the Centerline payload full of water. In addition, the aircraft is now required to fly a total of 4 laps. This mission uses the SCF as the only scoring function. Mission completion is, therefore, the only aircraft performance concern for Mission 2.
- **Mission 3:** Mission 3 depends heavily upon wing store (rocket) payload Loading Time as well as the SCF. The Loading Time for Mission 3 begins with the aircraft fully assembled and the wing stores still in the box. The ground crew must take the wing stores out of the box and install them on the wing as fast as possible. The time ends with the aircraft flight-ready and box re-secured. After the timed loading, the aircraft must fly 4 successful laps. After each lap, the aircraft must land and remotely deploy 1 one of the wing store payloads in a 10 ft squared area. The aircraft will then take off again and fly another lap. Because payloads are each ballasted at 1.5 pounds and spaced at least 24” and 30” from the centerline, the aircraft must both taxi and fly with significant asymmetric loads. The scoring function for the Mission 3 = SCF / (Loading Time). Similar to Mission 2, the main objective during flight is mission completion.

3.2 Translated Design Requirements

The requirements for mission completion and scoring are then translated into figures of merit to optimize the overall score. For mission completion, standard tests that must be overcome include: testing of the structural integrity of the box via the drop test, wings with the wing tip test, and landing gear for Mission 2 landings with the large centerline payload. In addition, aerodynamic and propulsion challenges include taking off within 100 feet and overcoming asymmetric loadings for Mission 3. The second requirement for the system is to optimize for the maximum Flight Score. As described in the previous section, the SCF influences every mission score and warrants the most attention before designing the system. The Flight Time for Mission 1 and Loading Time from Mission 3 were also analyzed alongside the SCF parameters of Assembly time and RAC in determining the change in total Flight Score. These parameters are then prioritized for selecting the best box and aircraft system according to the rules.
A sensitivity analysis for Total Flight score was based upon initial estimates for values of Assembly, Flight, and Loading Times as well as RAC weight. These estimates include: Assembly Time (AT) = 10 seconds, Weight (RAC) = 28 pounds, Flight Time from Mission 1 (FT) = 180 seconds, Loading Time from Mission 3 (LT) = 5 seconds. Not shown in Table 1 is that the Flight Score is composed of the normalized mission scores by multiplying percentages 22.2%, 33.3%, and 44.4% to Missions 1, 2, and 3, scores

respectively. The change in Total Flight Score was calculated to get a Percentage Change in Flight Score for each measurable parameter.

Scoring Parameter (below)	Baseline	AT + 10%	RAC + 10%	FT + 10%	LT + 10%
Assembly Time = **AT (s)**	10	11	-	-	-
Weight = **RAC (lb)**	28	-	30.8	-	-
Mission 1 - Flight Time = **FT (s)**	180	-	-	198	-
Mission 3 - Loading Time = **LT (s)**	5	-	-	-	5.5
Updated SCF	0.0036	0.0032	0.0032	-	-
Total Flight Score	0.0015	0.00137	0.00137	0.00151	0.00148
Percent Change in Flight Score	0%	- 9.1%	- 9.1%	- 0.03%	- 1.9%

Table 1: Flight Score Sensitivity Analysis

Looking closely at the changing variables, the weight for the RAC must change 2.8 pounds in order to equate to 1 second's worth of Assembly Time. This heavily weights the FOM parameter for reducing the assembly time first and RAC weight second.

Thus, study of the rules show that assembly time will be the critical scoring factor for the 2009 AIAA DBF competition accomplished with the following design philosophy: design a plane and box system that wins on the ground via reduced Assembly Time and RAC weight while being able to complete all pre-mission and mission requirements.

3.3 Box and Release Mechanism Solution Concepts

Study of the contest requirements revealed that the storage box would be a key component in the aircraft system and a driving factor for the aircraft design. For this year's contest, the teams are limited to no more than 2 X 2 X 4 feet. Within each box, aircraft configurations are limited and inevitably connected to the design of the box to minimize the assembly time. Therefore, each system solution started with a box design.

3.3.1 Storage Box Opening Methods

Since opening methods drive the overall box design, this was considered first. The list of opening methods included: regular opening top-lid, reverse opening bottom-lid, 5-sides folding open, a double-hinged 2-sided folding open for the rectangular box and a triangular box with 4-sides folding open.

In order to refine the rectangular and triangular box designs, multiple opening methods for the boxes were analyzed in order to determine the configuration that would optimize assembly time while retaining simplicity and reliability for repeated tests. Five final box designs were considered for the storage of the aircraft and ranked based upon the weighted figures of merit of speed to assemble, weight, complexity, and reliability, as seen in Figure 3: Box Opening Method (left to right): Figure 3.

- **Hinged Door:** A traditional configuration, having a hinged top lid with the aircraft accessible from only one face of the box. This configuration requires the aircraft to be lifted out of the storage box followed by the assembly of the aircraft.
- **Reverse Lid Box:** This configuration uses a single hinge at the base, allowing the upper faces of the box to be rotated off of the aircraft. This configuration allows for access to the aircraft from four faces (3 sides plus top face) as it stands upright on the bottom face ready to be rolled off the box. This configuration allows for the timed assembly of the aircraft and reassembly of the box to be maximized.
- **Three Sides Open Box:** Similar to the "hinged door", two added sides of the box fall open on hinges when the top lid is released, allowing access to the aircraft from three faces of the box. This configuration allows for assembly of the aircraft wings within the box, while requiring the aircraft to be picked up or slid out.
- **Fall Open Box:** A configuration where all sides of the box collapse on hinges, allows access to the aircraft from five faces of the box. This configuration allows the entire aircraft to be assembled on the box and rolled off of the box, at the expense of a high reassembly time of the box.
- **Triangle Fall Open Box:** All four sides fall downward when the top hatch is released, allowing complete access to the aircraft. This configuration allows for reduced box weight at the expense of limited space available and increased time to reassemble the box.

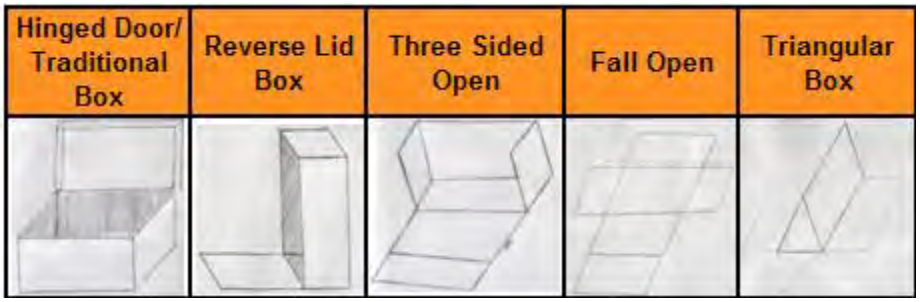

Figure 3: Box Opening Method (left to right):

Materials were evaluated based on physical properties that would produce the least amount of weight while meeting the design requirements for protection of the aircraft. Initial materials considered include balsa reinforced with Kevlar, balsa reinforced with fiberglass, carbon fiber composites with varying weave patterns, corrugated plastic, and plywood.

3.3.2 Release Mechanism Concepts

The rules require that all stores be individually, remotely releasable and that they not be installed while inside the box. These were the primary factors that drove the conceptual design of the payload release mechanisms. The latter restraint made speed of loading a major factor, followed by reliability, and finally weight. The following is a summary of the designs considered:

- **Mint Tin Lid:** A rod attached to the payload is inserted into teeth on the wing or fuselage which close under the insertion load. Pressing down releases the teeth since they are connected to a convex round surface.
- **Bow Release:** A commercially available option used by bow hunters; this provides reliability and light weight.
- **Hook Latch:** A spring-loaded hook latches a rod or slotted rail into place.
- **Spring Loaded Pin:** A spring loaded pin is inside the wing or fuselage and pops into place within an attached fairing on the payload to secure.

3.4 Aircraft Solution Concepts

Wing configurations, wing assembly methods, tail configurations, and tail attachment methods all were considered in order to manage assembly time issues, space allocation within the box, and weight.

3.4.1 Wing Configurations

Several wing configurations were taken into consideration to complete the missions (Figure 4). The list of wing configurations considered includes:

- **Mono-Wing –** This configuration is simple and very predictable in terms of construction and aerodynamic performance. It reduces assembly time while not greatly affecting the weight, simplicity of construction, or space limitations.
- **Bi-Wing –** A bi-wing configuration was considered because it allows for a smaller wing span with similar performance to the mono-wing. Weight, wing assembly, and wing store configurations available are the problems to this design.
- **Flying Wing –** A flying wing configuration was considered for the fact that it would eliminate the fuselage component of the aircraft. Drawbacks include difficulty of manufacturing and takeoff.

Mono-Wing	Bi-Wing	Flying Wing
		

Figure 4: Wing Configuration Chart

In addition, wing assembly methods were analyzed to allow the aircraft to fit into the various boxes discussed above. The list of wing assembly methods include: a single hinged wing, a double hinged wing

a removable wing with a spar insert, and a box assisted removable wing (Figure 5). The following methods were made to increase assembly time at the cost of increased weight, complexity, and reliability.

Wing Insert	Double Hinge	Box Assisted	Single Hinge
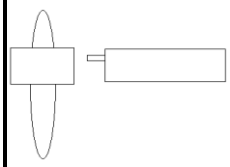	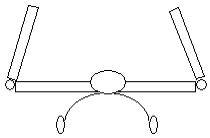	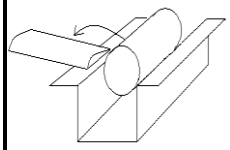	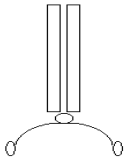

Figure 5: Wing Assembly Methods

3.4.2 Tail Configurations

The tail configurations considered were T-tail, boom-tail, V-tail, and a conventional tail (Figure 6). The simplicity of construction and space allocation in relation to the box configuration were the main factors in selection of the tail.

- **Conventional Tail:** This configuration was the baseline tail design because it is very common. It is simple to make and fits into most box designs.
- **T-Tail:** A T-tail configuration was considered because it would easily work within the rectangular box. **V-Tail :** A V-tail configuration was considered primarily in relation to the triangle box. This configuration maximizes the space allocation for the triangular box but adds some complexity in manufacturing.
- **Twin-Boom Tail:** A boom tail configuration was considered primarily in an attempt to allow for the centerline payload to be move farther aft along the fuselage. This configuration requires more space in the box than the other configurations and adds complexity to the construction of the aircraft.

Conventional Tail	T-Tail	V-Tail	Twin-Boom Tail
			

Figure 6: Tail Configuration Considerations

Several tail attachment methods were explored to allow the aircraft to fit into the various box designs efficiently. The list of tail attachment methods include: a fixed tail, a detachable tail, a hinged tail, and a telescoping tail (Figure 7). Trends for all configurations aside from the fixed tail configuration included an increase in weight, and complexity for added speed.

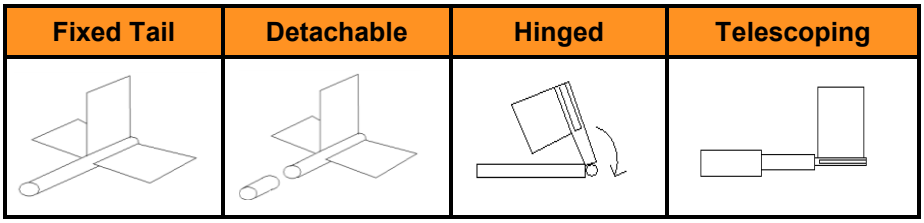

Figure 7: Tail Assembly Methods

3.3.3 Propulsion Concepts

The propulsion team considered various motor placement configurations. Five primary concepts were the tractor, pusher, pusher/puller, twin motors, and twin tractor as seen in (Figure 8).

- **Tractor Configuration:** This configuration is most common in propeller driven aircraft. In this configuration, the motor and propeller are located at the forward most location along the centerline.
- **Pusher Configuration:** This configuration is similar to the tractor configuration, except the propeller is located behind of the wing. Thrust becomes a problem if air is separated prior to reaching the propeller.
- **Pusher/Puller Configuration:** This configuration has a propeller located forward and aft of the wing. Both propellers generate thrust and are located along the centerline. This system consists of two motors and two propellers having the added capability to control torque moments with complex differential rpm motors.
- **Twin Motor Configuration:** The twin configuration is similar to the single tractor configuration; however, it consists of two propellers located port and starboard of the centerline.
- **Boom Mounted Tractor:** This configuration moves the thrust line up via a support rod to reduce the effects of the centerline payload being directly in the propeller wash.

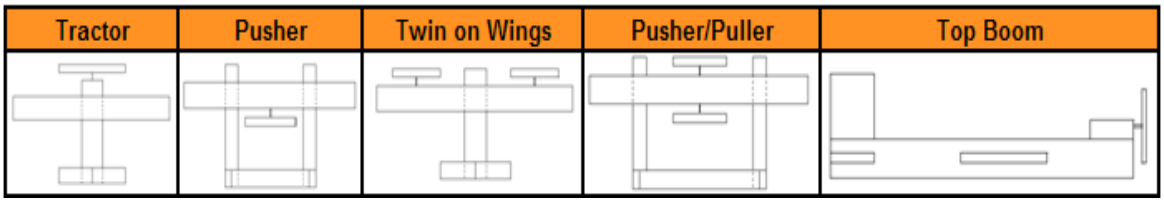

Figure 8: Propulsion Configuration Comparison

3.4.4 Landing Gear Concepts

Multiple landing gear configurations were analyzed to perform the necessary taxiing, takeoff, and landing procedures to fulfill the mission requirements. Handling asymmetric loads and the capability to carry the full centerline payload especially on landing were the determining criteria for selecting a

sufficient landing gear configuration. Therefore, the following solutions for landing gear were analyzed (Figure 9).

- **Tricycle:** This is considered to make taxiing easier and a light weight configuration.
- **Tail Dragger:** This type of landing gear is popular for agricultural aircraft that support large loads, but with small aircraft tend to become difficult to taxi on the runway.
- **Tricycle with Outriggers:** Outriggers added to the tricycle configuration allowed for greater ability to handle asymmetric loads at the cost of increased weight and drag.
- **Bicycle with Outriggers:** A four wheel landing gear concept was analyzed to decrease the number of gear in comparison with the tricycle with outriggers while still being able to taxi with asymmetric loads.

Tricycle	Tail Dragger	Tricycle with Outriggers	Bicycle with Outriggers
	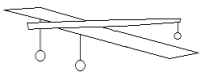		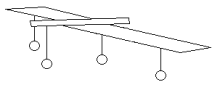

Figure 9: Landing Gear Configurations

3.5 Concept Selection and Results

To find the best solution, a methodical approach was taken in narrowing and selecting from the concepts generated. Each concept category had its own criteria for selection; the following section outlines these methods and the chosen concepts.

3.5.1 Box Design

The five final box designs were compared using a weighted decision matrix, with the simplest design, the Hinged Door, serving as the baseline design for comparison. As seen in Figure 10, the FOMs of speed account for 60% and weight for 20% of the weighted decision matrix. This leaves 10% for both reliability and complexity. This selection determined that the Reverse Lid Box design provided the optimal solution for the aircraft, allowing for a broad range of aircraft; designs with fewer limitations than the triangular box design. Furthermore, the Reverse Lid Box design was determined to maximize the aircraft assembly and box reassembly speeds while maintaining simplicity as compared to other design alternatives.

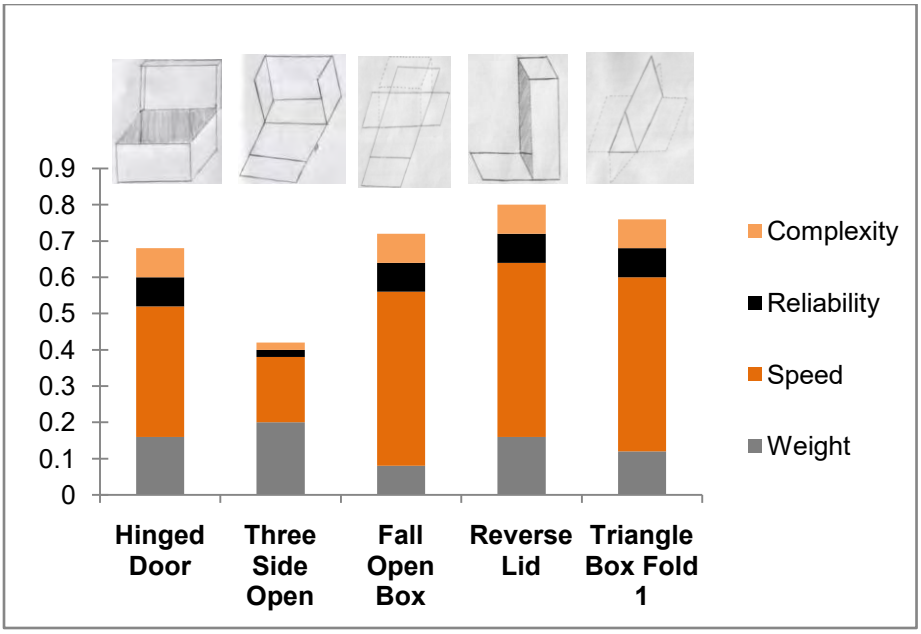

Figure 10: Box Opening Method Weighted Decision Matrix

3.5.2 Aircraft Configuration Selection

To select the best aircraft configuration for the contest requirements, assembly methods for both the wing and tail were analyzed in addition to the traditional tail and wing configurations. Assembly method FOMs includes assembly speed = 40% plus weight, reliability, and strength of the connection at 20% each for a total maximum score of 10 points. Figure 11 reveals the chosen assembly methods were the wing-insert method for the wing and to keep the tail fixed (if possible) within the box.

The aircraft configuration FOMs were assembly speed = 20%, weight = 20%, handling qualities = 30%, and estimated takeoff capability = 30%. This selection prioritized mission completion over optimum score. The best choice was to use a standard monoplane configuration and conventional tail. Although a V-tail was considered extensively during triangle box discussion, the overall decision for the rectangular box also influenced the decision to keep aerodynamic handling qualities simple and predictable (Figure 12).

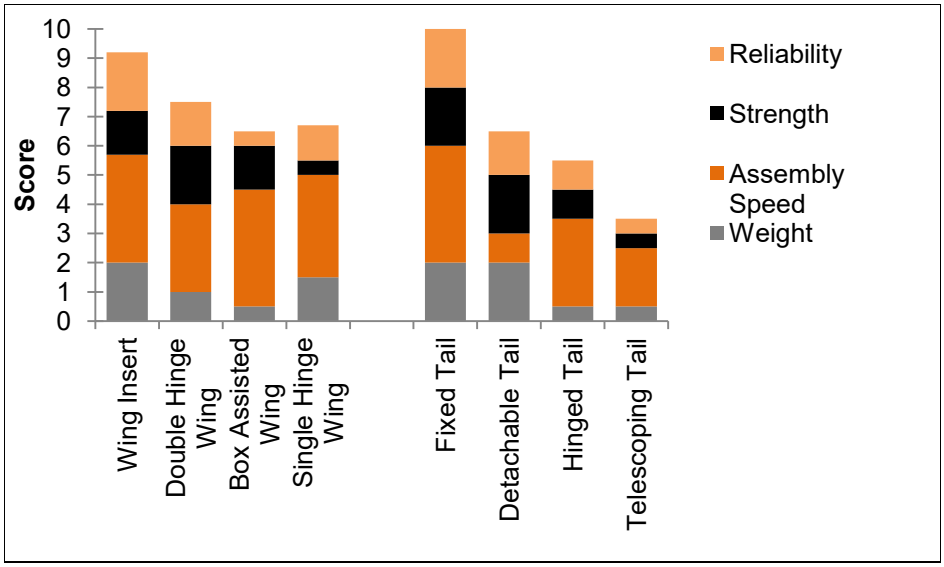

Figure 11: Assembly Method Weighted Decision Matrix

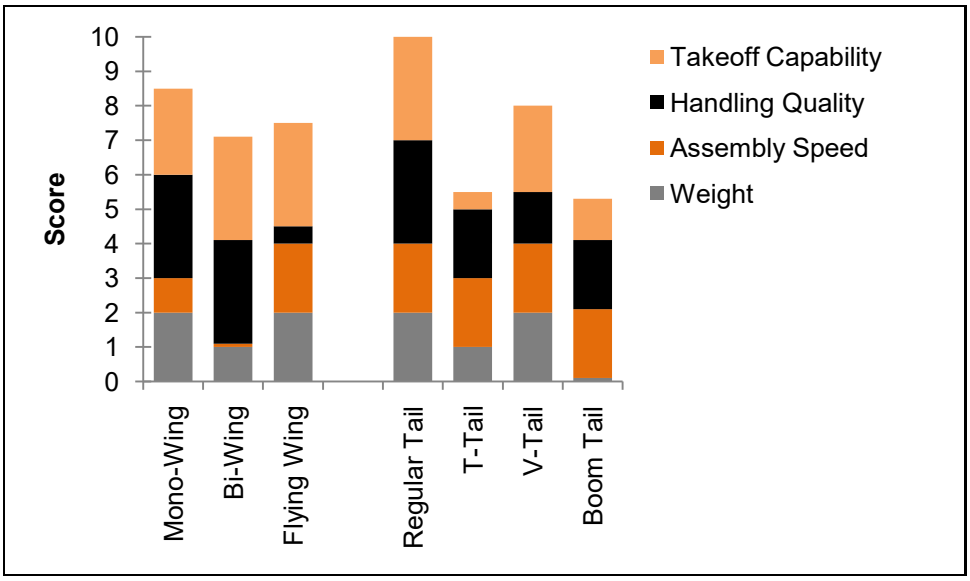

Figure 12: Aircraft Configuration Weighted Decision Matrix

3.5.3 Propulsion Configuration Selection

Selection of the propulsion configuration was based primarily on FOMs of reliability and weight with a simple baseline comparison method. Reliability is simply the ability to setup and operate the given system multiple times with little to no changes or maintenance necessary. Reliability is also an important category simply because failure of the propulsion system would result in failure of the mission requirements. The tractor configuration was determined to be best suited for the mission objectives based upon its weight, takeoff performance, and simplicity.

3.5.4 Landing Gear Configuration

The landing gear selection was based upon the ability of configurations to taxi and takeoff with asymmetric loads. This led the team to consider the lateral shift in the center of gravity. Lateral shift of the total aircraft and payload center of gravity was estimated to be over two feet with a low weight aircraft. The lateral CG shift is must be within the wheels of a given configuration as shown in Figure 13.

Tricycle	Tail Dragger	Tricycle with Outriggers	Bicycle with Outriggers
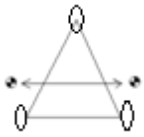	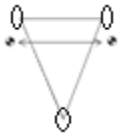	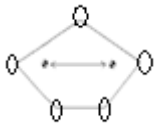	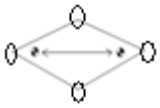

Figure 13: Landing Gear Analysis for Maximum Lateral CG Shift

The results from the initial landing gear analysis showed that some form of outrigger gear was necessary. If the selected landing gear were the bicycle configuration, it was determined that the aircraft would be especially susceptible to premature rolling before rotating to takeoff. In addition, the bow gear selection for the tricycle landing could double as a cradle for the centerline payload when located within the box. Given these considerations, the selected configuration was the tricycle landing gear with outriggers.

3.5.5 Release Mechanism Selection

The FOMs of assembly speed, payload stability, weight, complexity, and number of servos required, were used to compare different options for release mechanisms. By weighting heavily toward speed of assembly, the team decided to use the modified spring loaded hook latch. The design had been proven in previous competitions and was known to be reliable. Therefore, this was the simplest, most reliable latch the team could incorporate into every payload release mechanism and box latch facilitating quick assembly and loading times (Figure 14).

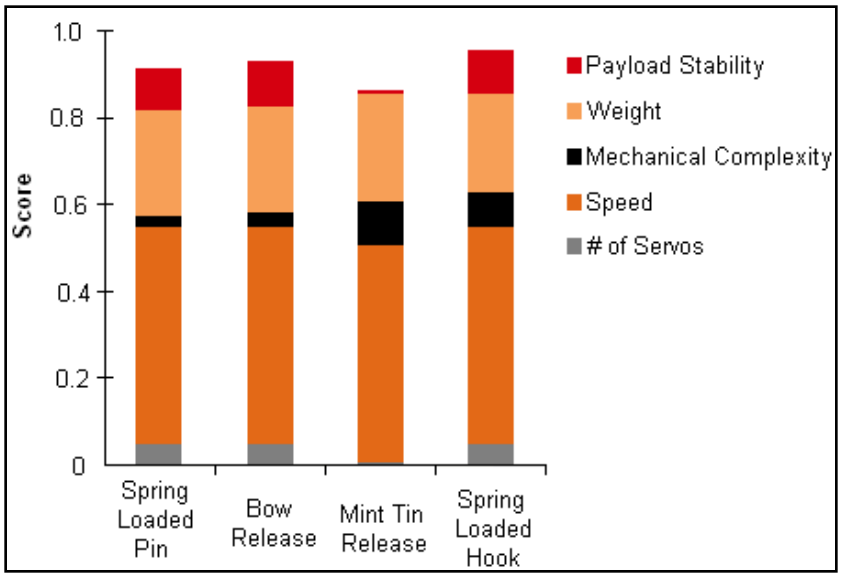

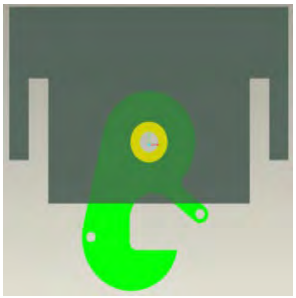

Figure 14: Release Mechanism Weighted Decision Matrix with the Selected Spring Hook Latch

3.6 Overall Configuration

A rectangular box was chosen with a reverse opening lid, which allows for extremely quick assembly times. This is accomplished by the smooth locking mechanisms that snap the wing store payloads onto the wings by moving them upward from a stowed location. Similarly, the centerline payload snaps into place by moving the aircraft forward from the box.

The final aircraft configuration consisted of a simple mid-mount, mono-wing configuration with a conventional tail for predictable handling qualities. It has removable wings with a tapering spar that inserts into a mid-wing connection fixed to a slender fuselage for quick assembly. The figure below shows the general configuration of the aircraft (Figure 15).

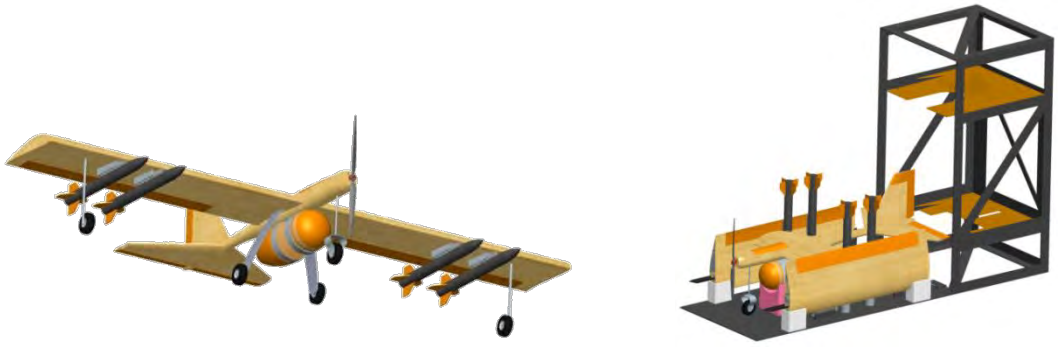

Figure 15: Conceptual Design

4.0 PRELIMINARY DESIGN

This section of the design process involves the analytical mission simulation methods used to optimize the aircraft for maximum score. By using computational and empirical models, the team was able to better estimate flight performance and overcome challenges posed by mission requirements.

4.1 ANALYSIS METHODOLOGY

The following section will describe the methods used by the sub-teams to optimize the design.

4.1.1 Aerodynamic and Propulsion

The overall goal in the preliminary design process was to develop a strategic method to arrive at the best possible aircraft. Above all, Flight Score is the most important parameter to determine an optimum design. Figure 16 illustrates the flow of the preliminary design process and how this was approached. Performance constraints were placed on the optimization program in order to limit unreasonable configurations. The propulsion and aerodynamics groups worked closely together to consider all aspects of the design. Performance and stability calculations are then used to validate the aircraft design.

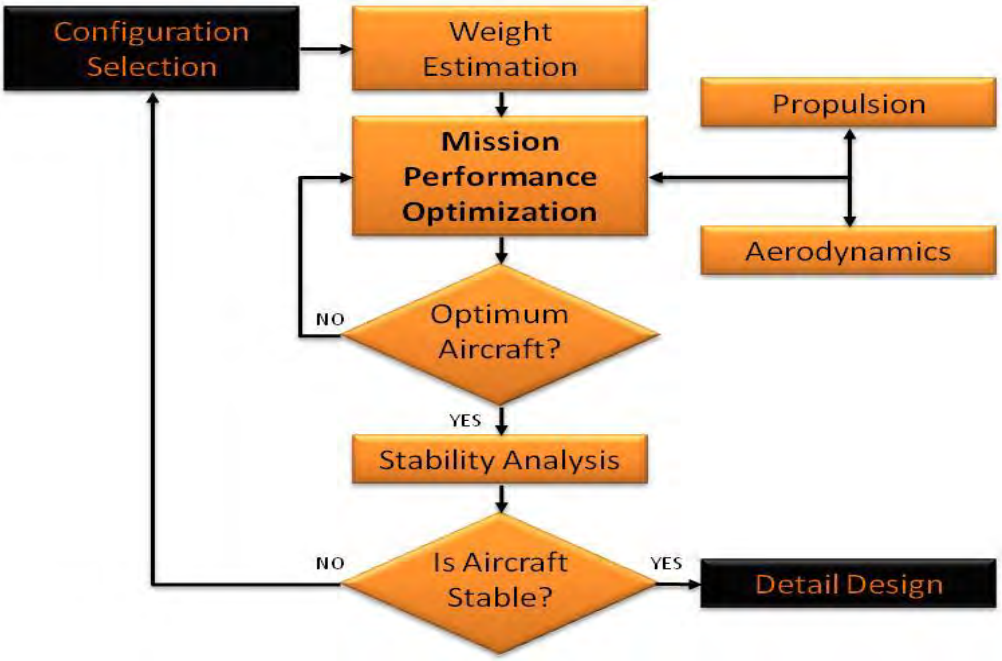

Figure 16: Aircraft Optimization Flowchart

4.1.2 Structures

Having previously selected optimum conceptual designs for box, landing gear, wing insert and release mechanisms, the structures team was given the task of optimizing the material selection for all components. The team considered trades of strength to weight ratio and speed loading.

4.2 Mission Model

Developing a mathematical model to simulate the mission profile is central to the optimization of this aircraft. In order to determine this, proper assumptions must be made for the mission. These assumptions cause limitations in the program as well as a certain degree of inaccuracy.

4.2.1 Mission Assumptions

The figure below shows the limits, assumptions and constraints used in the model in order to predict flight performance (Figure 17).

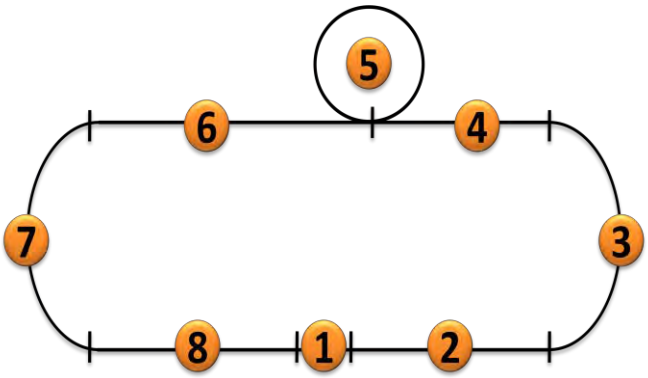

1	Takeoff	Full Throttle
		100 ft T/O Limit
2	Climb	Full Throttle
		50 ft T/O Limit
3	First Turn	Full Throttle
		No Turn Loss
4	Acceleration	Full Throttle
5	360 Turn	Full Throttle
		10 ft Turn Loss
6	Cruise	Cruise Throttle
		$C_{lcruise} < C_{lmax}$
7	Turn	Cruise Throttle
		$C_{lturn} = 0.95\ C_{lmax}$
8	Landing	Throttle Off
		C_{lmax}

Figure 17: Mission Model

Other mission assumptions include:

- **Aircraft Weight Model:** This was assumed based off of previous DBF aircraft and altered for the specific competition. The model calculates the weight based off of aircraft geometry.
- **RAC Best**: In order to predict the RAC for the particular aircraft, a maximum score needed to be assumed. The team chose a top score of 28. This is comparable to the current RAC of 31.5.
- **System Weight:** Since RAC score is contingent upon the aircraft, the storage box, and all internal components, assumptions must be made about these weights. The payload and box weight is estimated to be 20 pounds.

4.2.2 Aerodynamics/Propulsion Uncertainties

Some aspects the can affect aircraft performance were not fully taken into account in the mission model. Limitations include:

- **Stability:** This is an integral part of any aircraft design and especially the case for this competition. With asymmetric wing store payloads, roll stability is critical. Although, stability calculations are not used in optimization, they were later used to validate the design.
- **Wind Predictions**: The mission model accounts for wind velocity but it is limited to a direct headwind or tailwind. Crosswinds and changing wind directions are not considered and can have an effect on flight time.

4.3 Design Trades and Optimization

In order to optimize the aircraft, a balance had to be found between the requirements of the design performance and the need to minimize time and weight. These trades, performed using the methodologies outlined above, are detailed in the following section.

4.3.1 Aerodynamic Optimization and Sensitivity

The mission analysis led the aerodynamics team to develop an optimization code which was based upon mission constraints. Constraint equations include estimated takeoff distance, turn loss, wing span, and power available. The key optimization parameters that the MDO code utilized were cruise velocities for missions 1 and 2, battery weight, wing area, and wing span.

Trends in the optimization results are indicated by the

Figure 18, Figure 20, Figure 19, and Figure 21 below holding battery type and airfoil constant.

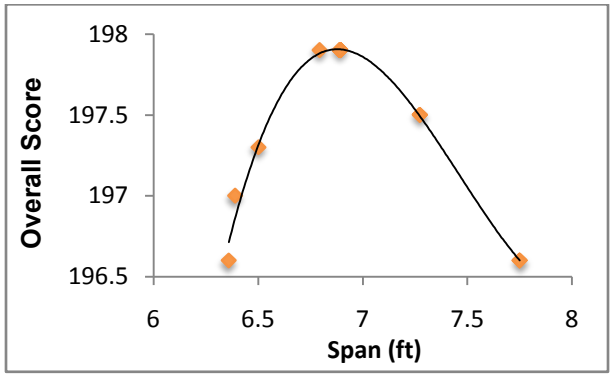

Figure 18: Score vs. Span

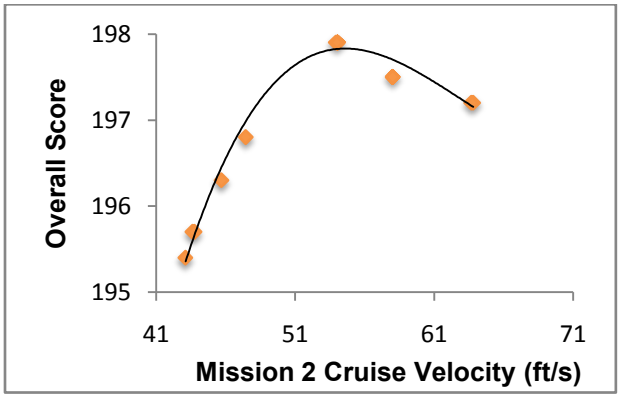

Figure 19: Score vs. Mission 2 V_{cruise}

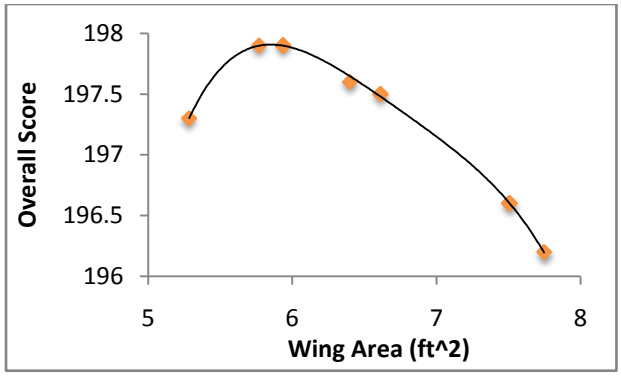

Figure 20: Score vs. Wing Area

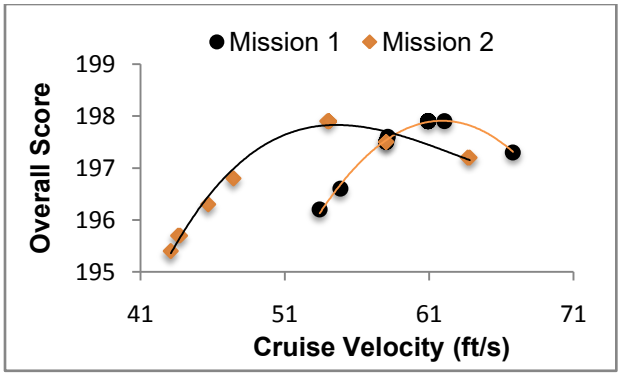

Figure 21: Score vs. V_{cruise}

The values represent the local maxima from the multiple iterations of the mission MDO program seen in

Figure 18, Figure 20, Figure 19, and Figure 21 above. As the score approaches the maximum value, most of the boundary conditions set in the optimization program also reach their limitations, such as take off distance and percentage of battery used. A sensitivity analysis was used to find what parameters could be altered based off of the highest scoring configuration. The goal was to increase performance characteristics while having the lowest possible impact on score.

The trends indicate that an aircraft with an empty weight of 7 pounds will be optimum at (Table 2: Aerodynamic Optimization Results):

$V_{cruise,\ M1}$	$V_{cruise,M2}$	W_{batt}	b_w	S_w	$C_{l,\ cruise}$	# Batteries
55 fps	62.5 fps	1.326 lb	7 ft	6.87 ft^2	0.747	26

Table 2: Aerodynamic Optimization Results

4.3.1.1 Airfoil Optimization and Selection

During the optimization phase, multiple airfoils were used and compared to one another (Figure 22: Airfoil Optimization).

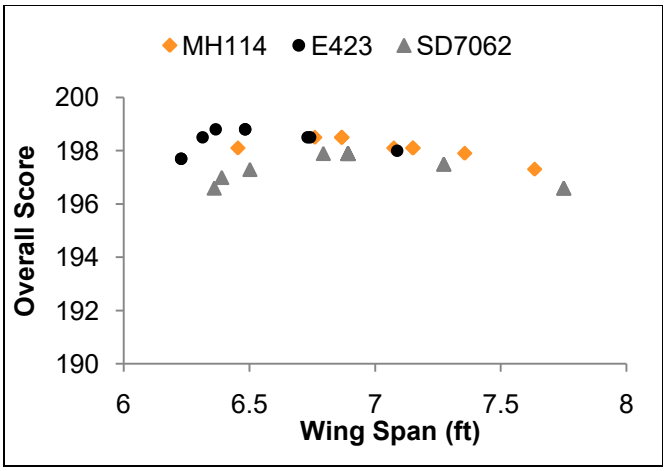

Figure 22: Airfoil Optimization

Top airfoils in the initial analysis were the Eppler 423 and MH114 were separated by less than 1 percent. While running through the iterative optimization process, an experimental airfoil, called the Hatha1, was created from blending the top half of an Eppler 423 and the lower half of an MH114. This airfoil had a 16 percent thickness to chord ratio, which is much higher than all airfoils considered. This is a large benefit to the fabrication of the airfoil. The Hatha1 also had strong aerodynamic performance and was then used as a baseline airfoil in additional optimization runs.

After the aircraft wing geometry and flight performance had been finalized, the cruise lift coefficient was examined and matched with a suitable airfoil. The SILK21 was designed to have a minimum drag point at exactly the fight cruise lift coefficient, while also providing a rather flat bottom to assist in construction. In terms of score, it performed similar to the other top performing airfoils.

The SILK21 high lift airfoil was tested at multiple Reynolds numbers to ensure that it would be able to operate properly at various flight speeds (Figure 23).

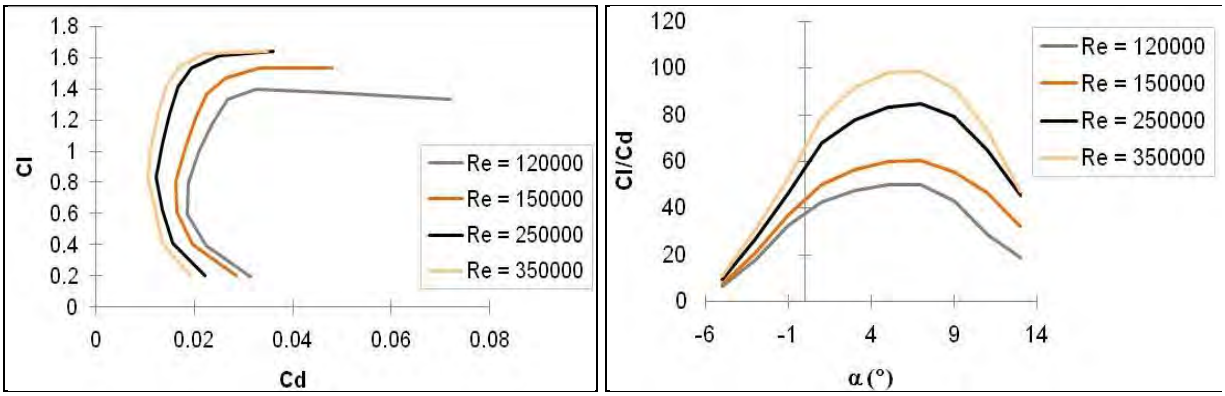

Figure 23: Lift vs. Drag for Various Reynolds Numbers for SILK21

4.3.1.2 Tail Sizing Trades

Finding an empirically reasonable tail to wing area ratio was an early concern for the chosen configuration simply due to physical box limitations. To overcome these challenges with the horizontal tail, a large root chord and small tip chord were used to fit in the box alongside the wing.

For construction, the horizontal and vertical tails have blended airfoils from the root to the tip. The vertical tail uses an NACA 0009 at the root and tapers to a 0012 at the tip, whereas, the horizontal tail starts with a NACA 4409 at the root and ends with a 4412 at the tip. The reason the horizontal tail has an inverted camber is to provide the necessary negative lift for trim at an incidence of zero.

4.3.1.3 Aileron Sizing and Asymmetric Payload Roll Control

The aileron roll capability was calculated from mission 3 requirements. After one lap around the course, the aircraft releases one of its payloads creating a constant asymmetric roll moment. The ailerons create a differential lift that counteract this payload roll moment. The aileron roll equation is unique from

traditional aerodynamic parameters in that it is a function of aileron deflection (δ_a) and velocity. For future analysis, the aileron moment coefficient was presented within the aileron roll moment equation below.

$$L_{ail}(V, \delta_a) = \rho\, V^2\, C_{L\alpha w}\, \tau\, \delta_a\, \frac{c\,(y2 - y1)^2}{2}$$

This aileron moment equation is based upon strip theory and used to analyze roll control methods (Nelson, 1998). Because flight velocities are lowest at takeoff and landing, the goal was to create enough aileron moment to counteract the asymmetric loading before reaching aircraft stall velocity. After the velocity increases, the roll moment from the ailerons is sufficient to control the aircraft in flight.

Noticing that the span of the aileron (y2-y1) is squared in the aileron moment equation, the aileron span was extended to 30 inches with 2.75 inches chord-wise length to allow for enough surface area on the aileron for control.

4.3.1.4 Elevator Sizing

To achieve static and dynamic longitudinal control, the elevator must be properly sized. In order to balance the aircraft for all necessary trim conditions, the elevator to horizontal tail area ratio was determined to be 0.23. The size of the elevator attains a 2 inch chord and 23 inch span. This elevator control allows for trim over a spread of 16 degrees angle of attack and was considered sufficient for all maneuvers required in the three missions.

4.3.1.5 Rudder Sizing

The selected rudder was sized similar to the elevator with a 2 inch chord-wise length and 10 inches in vertical span. A rudder horn extends the vertical tail 2 inches from the fixed end for a total vertical span of 10 inches. This feature allows for increased rudder authority at reduced hinge moment loads.

4.3.2 Propulsion Optimization and Sensitivity

The propulsion team used aerodynamic models and optimization to optimize and select subcomponents.

4.3.2.1 Battery Optimization and Selection

In addition to the mission MDO program and additional computer code was generated to optimize the overall battery configuration. This code used the energy density of each cell and the manufacturers' test data as inputs (ie. 2.0 amp-hours), and then output performance and the number of cells that would be required to complete the mission. From this optimization it was determined that a configuration of 26, 1.5 amp-hour cells would be the highest scoring configuration for the given aircraft configuration.

4.3.2.2 Propeller Sizing

The propulsion team began by using an optimization program that took inputs from the Aerodynamics team (wing size, weight, battery data) and returned important parameters such as thrust, efficiency,

takeoff performance, endurance, and cruise velocity. The team focused on running many iterations with numerous configurations in an effort to choose an optimum overall propulsion system. This was accomplished this by first conducting multiple sensitivity analyses for battery selection, propeller pitch and diameter, gearbox ratios, and various motors.

As you can see in Figure 24 below the overall system efficiency in cruise for this test vehicle seems to peak around a 14 inch propeller diameter; however, the wind speed required to takeoff in 100 feet increases linearly as propeller diameter decreases, limiting the minimum size above 14 inches.

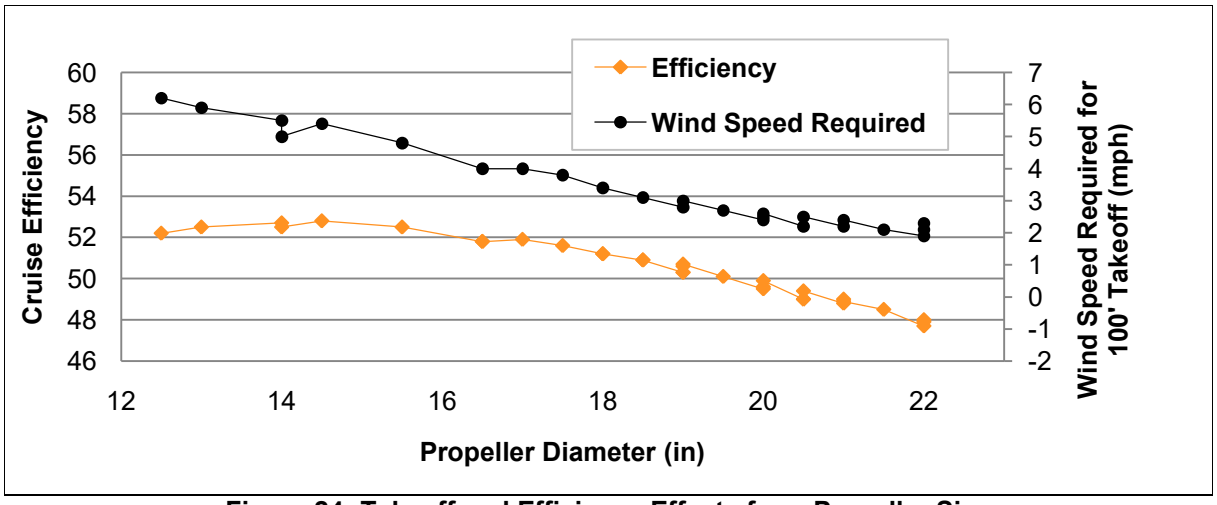

Figure 24: Takeoff and Efficiency Effects from Propeller Size

The team has conducted a thorough weather history analysis of the Tucson area which indicated that the chances of having less than a 2 mph wind were minimal. Therefore, the team chose to create a system that would rely on having at least a 3 mph wind to takeoff in 100 feet. This wind speed requirement meant the propeller diameter must be no less than 18 inches.

4.3.2.3 Motor Selection

Selection was optimized using the previously determined battery configuration of 26 cells. From manufacturer specifications, this size of battery indicated that a maximum of 25 amps could be pulled from each cell. Due to weight, parallel configurations were rejected resulting in a maximum current available of no more than 25 amps. This limited selection to in-runner motors, which are classified by three parameters: Kv (rpm/volts), Io (no load current), and Rm (resistance of motor).

Initial motor selection was performed by conducting a study of motors with different Kv, Io, and Rm values to determine the maximum current drawn and thrust produced at static conditions. In addition to the current limitations of the battery pack, a limitation on the Kv value was implemented due to the availability of commercial gearboxes that would reduce the rpm of the motor to an acceptable propeller velocity. Two graphs were plotted in order to determine an effective range of Kv values for the motor selection in order to maintain a current of less than 25 amps while producing maximum thrust, as seen in Figure 25 and Figure 26. These graphs show that the maximum static thrust, ideal for takeoff conditions,

occurs at a current between 35 and 40 amps; however, due to the current limitation, a motor with a Kv value of less than 1600 RPM/V would be required for an 18 inch diameter propeller and a Kv value of less than 1300 RPM/V for a 20 inch propeller.

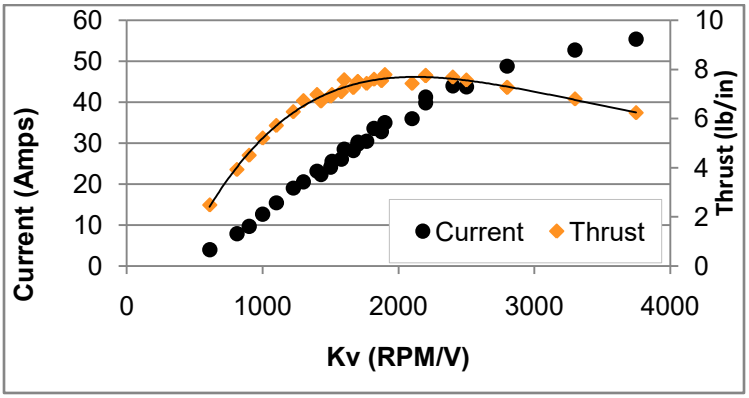

Figure 25: Kv values versus Current and Static Thrust (18 inch diameter propeller, 6:1 gearbox)

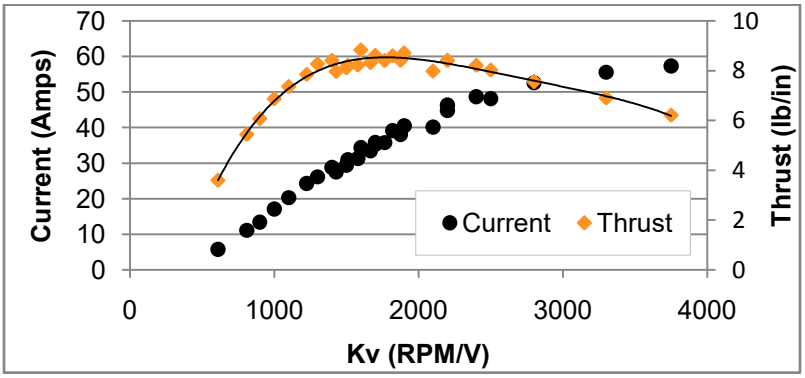

Figure 26: Kv values versus Current and Static Thrust (20 inch diameter propeller, 6:1 gearbox)

The number of possible motors was reduced based on a requirement for a maximum peak power input to the motor of 600 Watts during takeoff with a sustained power input of 300 Watts during cruise velocities. The reduced selection of motors meeting mission criteria for endurance and takeoff distances less than 100 feet can be seen in the Table 3.

Manufacturer	Model	Kv [RPM/V]	Rm [mΩ]	Io [Amps]	Weight [onuces]	Propeller Diameter [in]	Takeoff Distance [ft]	Thrust [lb-in]
Neu	1706/1.5Y	1225	0.022	1.5	5.5	20	125.4	7.85
Medusa	MR-036-050-1300V2-5	1300	0.019	0.65	8.11	20	116.5	8.27
Medusa	MR-028-056-1400V2	1400	0.025	0.9	5.64	19	122.6	7.85
Hacker	B/C40-21L	1429	0.078	0.53	5.54	19	131.9	7.49
Hacker	B/C40-20L	1500	0.0709	0.55	5.54	18.5	131.9	7.43
Mega	ACn22/20/3E	1510	0.047	1.56	7.7	18	135.5	7.22

Table 3: Top Motors with a Takeoff Distance Less Than 100 ft (5 mph Wind Assumed)

4.3.3 Box Sizing

In order to optimize the storage box, materials were analyzed for the construction of the box that would provide protection of the aircraft within the design specifications while providing the minimum weight. Furthermore, additional considerations included: cost of the material and production costs, simplicity of production, and durability of the material with the ability to repair the box in the event of failure. Plywood was chosen as a baseline for subsequent designs that would consider balsa reinforced with Kevlar, balsa reinforced with fiberglass, carbon fiber composites with varying weave patterns, and corrugated plastic.

Test sections of each material were created to conduct both impact and tension testing to determine the failure point of the material. The experimental data was subsequently used to determine the amount of each individual material required to construct the box. From the experimental testing, it was determined that a frame of the selected material could be constructed with a film covering, while still meeting design specifications for the storage box. Weight was heavily emphasized in the selection process. Based upon the FOMs, corrugated plastic was selected for the box, shown in Figure 27.

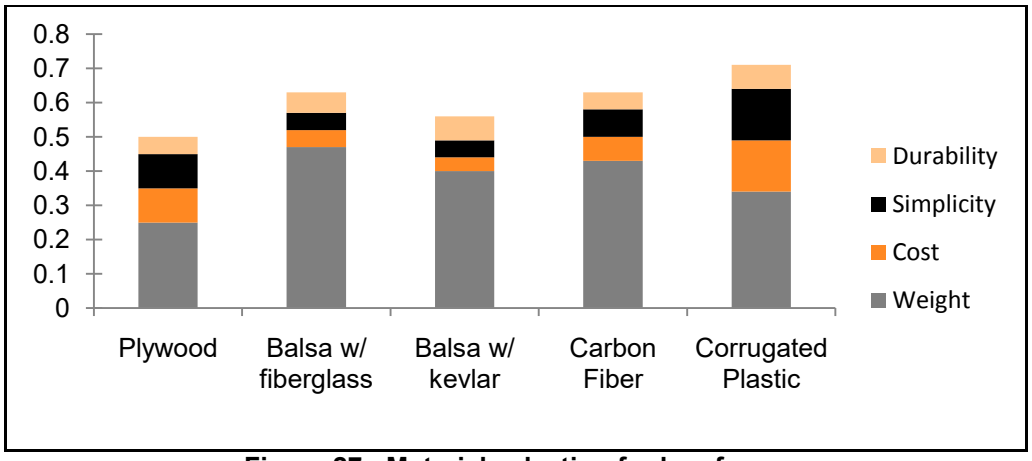

Figure 27: Material selection for box frame

4.3.3.2 Quick Assembly Wing Insert

Many kinds of wing inserts were considered in the initial phase. Weight and assembly time were the deciding factors for the insert design. Previous contest results proved that carbon fiber was the ideal material. Typically, a cylindrical tube has been used for the wing insert, but speed was an issue for the assembly time. A series of iterations lead to a tapered C-Channel as the design. The taper helps guide the wing into the slot, thereby reducing the assembly time as the crew member.

4.3.3.3 Landing Gear

When considering different main landing gear options, OSU's traditional bow gear was considered optimum. Apart from the structural advantages of using a bow gear, it also acted as a cradle to the bottle payload when in-flight. Previous lay-up configurations were considered, but this competition calls for a

more substantial landing gear. Trade studies showed that a 0/45/0/45/Kevlar/balsa/Kevlar/ 45/0/45/0 is the best lay-up configuration. Studies also showed that the main failure was due to the balsa delaminating, and so the balsa was beveled using additional composite layers near the contour.

4.3.3.4 Release Mechanisms

When looking into release mechanisms, the team has decided to design a release hook system. Several materials were considered in the design of the hook and housing that makes up the mechanisms. Because the selected centerline release mechanism also provides structural support to the fuselage as a bulkhead, the material selection considered the integration of the fuselage before weight reduction. Having studied previous mechanism designs, aluminum was selected as an ideal material for the hooks on all release mechanisms because of its durability. A fiber glassed housing around the hook also proved to provide an acceptable strength to weight ratio.

4.4 Estimated Flight Characteristics

The chosen aircraft was studied and optimized to develop a versatile enough design to handle all mission requirements. With carefully selected wing and tail airfoils, a static longitudinal stability analysis was able to balance the aircraft while placing both the wing and empennage incidence angles at zero degrees from the aircraft fuselage. Dynamic stability analyses were conducted to predict the flight characteristics of the aircraft design over a wide range of loading conditions.

4.4.1 Aircraft Lift and Drag

Understanding the parasite drag distribution for the aircraft is important in terms of reducing the flight time for mission 1 and taking off in 100 ft for mission 2. Initially, parasite drag was estimated for the entire aircraft by using drag area (D/q) calculations (Raymer, 1999). As seen in Figure 28 the major components contributing to the parasitic drag are the 5 landing gear and the centerline payload for missions 1 and 2.

Component	D/q (ft^2)
Fuselage	0.01
Horizontal Tail	0.01
Vertical Tail	0.004
Wing	0.079
Gear	0.052
Centerline PL	0.092
Wing Stores	0.019
Interference	0.042
Mission 1,2 total	0.305

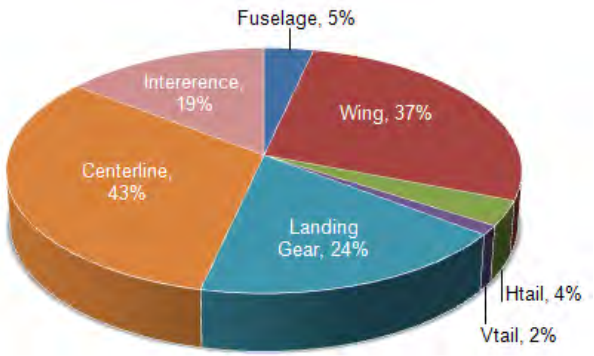

Figure 28: Estimated Drag Contributions for Missions 1 and 2

In Mission 1, the 4 liter payload presents a challenge for parasite drag reduction. The maximum finess ratio possible is 2.5 with a 6” diameter payload and a maximum length of 15”. The actual payload is

11.25” in length and can have fairings rounded at the leading edge and tapered at the trailing edge. Conservative estimates of drag included modeling the payload as a sphere using the Reynolds number in terms of its overall length and the frontal surface area in terms of its maximum diameter. This requires a tradeoff of increasing the Reynolds number due to the length of the payload and the almost unavoidable bluff body at the beginning of the payload. From the tradeoffs of the spherical model, a payload drag of C_{D0}=0.47was estimated (Hoerner, 1965).

The centerline payload overall drag was reduced by using two methods with fairings. To reduce bluff body drag, a shortened spherical dome was placed at the front of the payload. The pressure drag at the rear of the payload was reduced by forming the trailing edge fairing with a concave taper to minimize the diameter, but also not to separate the flow early where additional tapering or rounding becomes ineffective (Arena, 2009). Although the trailing edge does not conform to a point due to the lack of length required, the pressure drag is reduced as much as possible given the payload fairing constraints.

A total C_{Do} of 0.0445 for missions 1 and 2 was found by dividing the drag area by the wing area. This was then used to develop a total aircraft drag polar and L/D ratio vs. Angle of attack shown in the below in Figure 29.

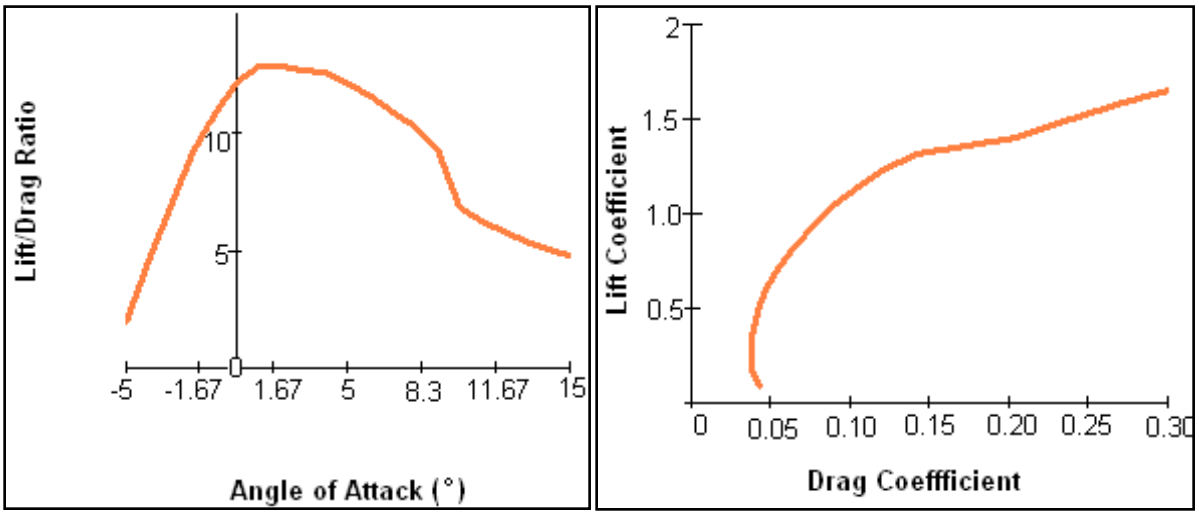

Figure 29: Overall Aircraft L/D vs. AOA and Complete Aircraft Drag Polar

4.4.2 Moment of Inertia Analysis

Initial weight and center of gravity (CG) estimates for the aircraft were used to develop relatively accurate moment of inertia calculations. The CG analysis all three missions determined the direction and amount of estimated CG shift from different payload configurations. For Mission 2, almost ten pounds of weight underneath the aircraft CG produced a 2 inch shift downward in total CG. For Mission 3, CG has the ability to shift more than 10 inches outward from the aircraft centerline. These numbers validated an in-depth study of the moments of inertia for each payload configuration.

Using the initial weight and CG analysis, the dynamic stability analyses utilized different moment of inertias calculated for every mission and payload case described in Figure 30.

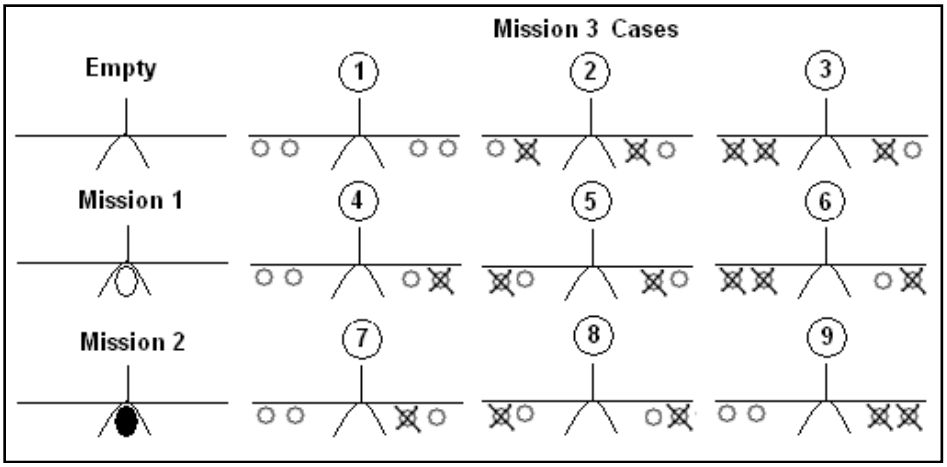

Figure 30: All Possible Payload Configurations within Dynamic Analysis

Using the estimated measurements for weight, location, and size of components on our aircraft, the team was able to determine the static and dynamic stability behaviors for our aircraft.

4.4.3 Stability

The process for achieving static stability for our aircraft configuration required refining a center of gravity model and updating a stability spreadsheet that provided the necessary calculations and graphs for both static and dynamic stability.

4.4.3.1 Longitudinal Stability

The major contributors to pitch stability are the wing, tail, and fuselage. Because our aircraft uses a high lift airfoil, a large negative pitching moment was produced. The incidence required for our wing and tail was set to zero degrees due to a careful selection for an inverted camber airfoil on the tail. This feature allows for greater drag reduction at all angles of attack (AOA's) in comparison with symmetric tails at greater incidence. Aircraft pitch static stability was plotted versus AOA over the expected flight regime for the aircraft and all components in Figure 31.

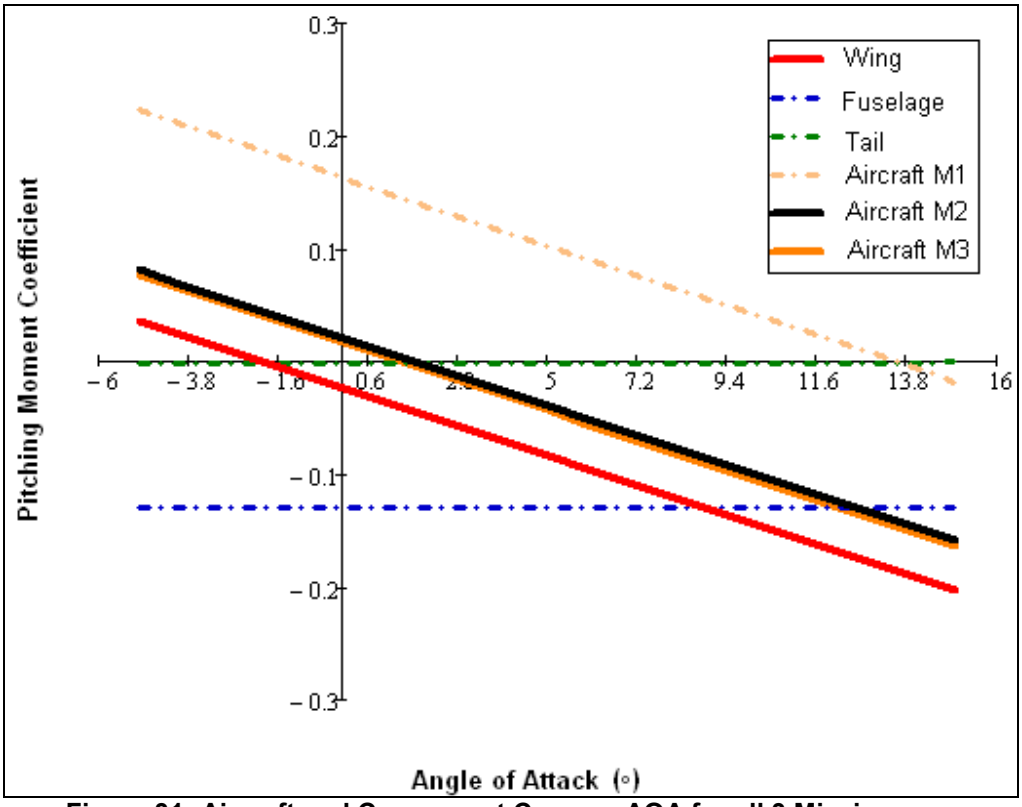

Figure 31: Aircraft and Component $C_{m,cg}$ vs. AOA for all 3 Missions

A constant forward centerline thrust force was assumed above the changing CG of the aircraft and payload configuration. This was the key difference in mission 2 stability as compared to missions 1 and 3.

In the process of updating weight estimations, the wing location was moved aft of its original location based upon the longitudinal static stability analysis. The tradeoff was a small reduction in control due to decreasing tail length in the process of balancing the aircraft pitching moment. For our aircraft, the neutral point for all three missions is $X_{np}/c = 0.4$ with a static margin of 14.7%.

For cruise conditions, the trim angles of attack did vary from mission to mission due to the location of the thrust above the center of gravity location. The vertical CG shift increases the negative pitching moment due to the thrust location above the CG of the aircraft. This is easily corrected by setting the α_{trim} at a positive 2 degrees. To maintain the optimum $C_{l,cruise}$ value of 0.8 for the other missions, the trim angle of attack will be set to -2 degrees.

4.4.3.2 Dynamic Stability

To complete the analysis of the selected configuration, the dynamic stability section calculates the ability of our aircraft to fly straight and level as well as make the necessary maneuvers during the missions. The aerodynamic team's stability program used a spreadsheet tool to output the necessary stability derivatives for the dynamic stability calculations (Nelson, 1998). The stability coefficients for the overall aircraft are found in Table 4: Aircraft Stability Coefficients below.

Lateral Stability Coefficients									
$C_{l\delta r}$	0.005	C_{lp}	-0.841	C_{lr}	0.146	$C_{l\beta}$	0	$C_{l\delta a}$	0.348
$C_{n\delta r}$	-0.077	C_{np}	-0.066	C_{nr}	-0.189	$C_{n\beta}$	0.134	$C_{n\delta a}$	-0.054
$C_{y\delta r}$	0.101	C_{yp}	0	C_{yr}	0.296				

Longitudinal Stability Coefficients									
C_{mu}	0	$C_{m\alpha}$	-0.686	$C_{m\acute{\alpha}}$	-1.811	C_{mq}	-4.343	$C_{m\delta e}$	-0.545
C_{Zu}	-1.305	$C_{Z\alpha}$	-0.096	$C_{Z\acute{\alpha}}$	-0.987	C_{Zq}	-2.368	$C_{Z\delta e}$	-0.297
C_{Xu}	-0.043	$C_{X\alpha}$	0.647						

Table 4: Aircraft Stability Coefficients

By analyzing weights and moment of inertias for all payloads and loading cases, the team was able to estimate the damping and damped natural frequencies for the five longitudinal and lateral modes of motion. The variation in the dynamic stability characteristics from Mission 2 to Mission 3 (fully loaded) presents the greatest range in dynamic modes of motion as seen Figure 32: Missions 2 and 3 (Fully Loaded) Coupled Stability Plots below.

Mode of Motion	Mission 2		Mission 3 Case 1	
	ξ	$i\omega_n$	ξ	$i\omega_n$
Phugoid	-0.016	0.752	-0.041	0.835
	-0.016	-0.752	-0.041	-0.835
Short Period	-4.647	7.437	-8.914	11.417
	-4.647	-7.437	-8.914	-11.417
Roll	-94.357	0	-9.574	0
Dutch Roll	-3.093	7.69	-1.146	4.819
	-3.093	-7.69	-1.146	-4.819
Spiral	0.093	0	0.093	0

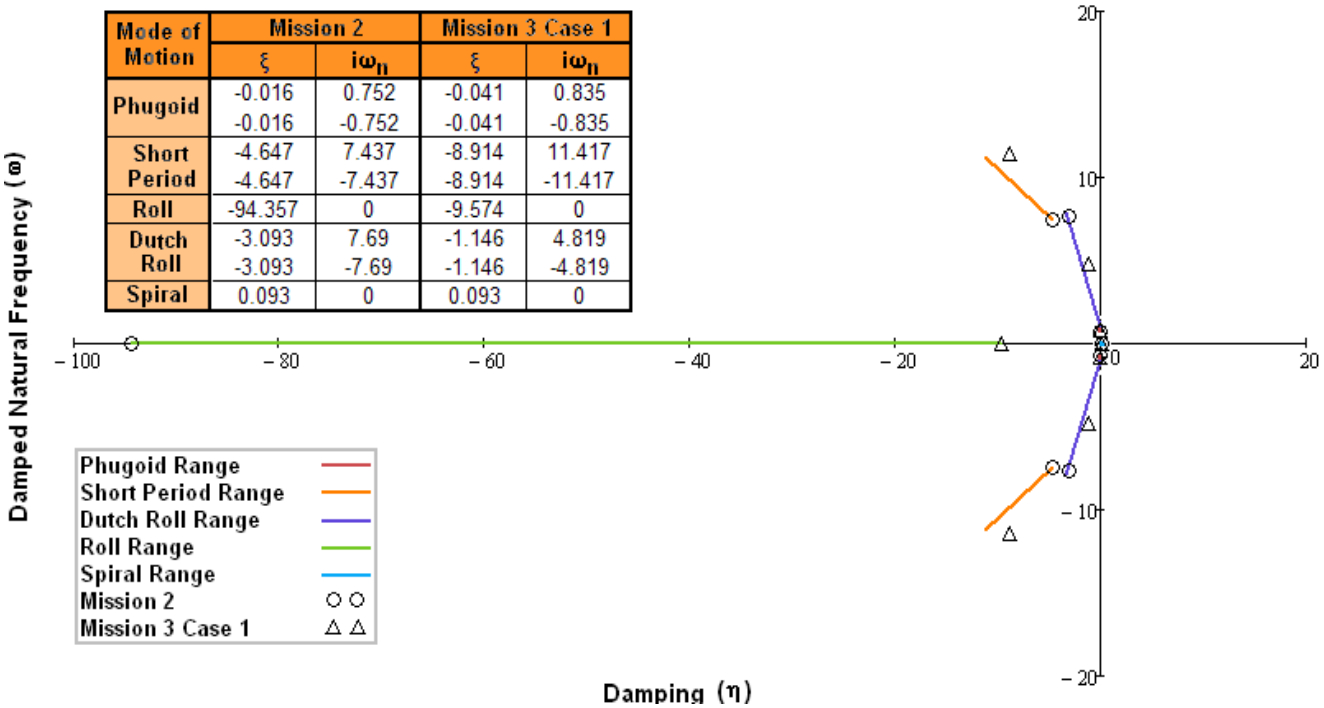

Figure 32: Missions 2 and 3 (Fully Loaded) Coupled Stability Plots

The range of dynamic stability mode analysis presents key information regarding variation in the roll and Dutch roll modes, which vary for every loading case. This data states that aircraft will respond very differently and must be taken into account by the pilot through test flights prior to the competition.

4.5 Estimated Mission Performance

To overcome each mission's various challenges, an analysis for each mission was conducted to estimate aircraft performance.

4.5.1 Mission 1: Flight Time

This mission is the only one that uses the mission flight time in the scoring function. Increasing maximum flight velocity seems to be the best way to reduce flight time, but this is actually not totally the case. Decreasing the cruise time by flying faster will increase the time of the turn because the aircraft will need a larger turning radius. Based off of the mission model, the following table represents the important flight characteristics for this mission (Table 5: Mission 1 Flight Performance Estimates).

Mission 1 Time (s)	80
G-load in Turn	4
G-load from Max Lift	1.15
Bank Angle (degrees)	78
Turn Loss (ft)	19

Table 5: Mission 1 Flight Performance Estimates

4.5.2 Mission 2: Endurance and Structural Capabilities

With a full centerline payload, this mission pushes the limits of aircraft flight performance from a weight standpoint. The heavier weight will cause the takeoff distance to increase leading to an increase in the total number of battery cells needed to takeoff within the 100 foot takeoff limitation. Other limitations such as the structural integrity of the aircraft must be considered in the calculations.

- **Takeoff Distance Estimation:** This distance is intrinsically related to the wind speed and direction. Due to the nonlinearity of this relationship, the exact takeoff distance is difficult to predict. The analytical analysis involved plotting takeoff distance verses head wind and using historical weather data to approximate the wind speed (Figure 33: Takeoff Distance vs. Wind Speed).
- **Battery Endurance:** The battery pack must enable the aircraft to have enough power for takeoff but also have the endurance for all 4 laps of the mission. For score optimization, it was imperative that as much percentage of the battery's energy was used up as possible in order to reduce RAC. Table 6 compares the first two missions and their respective total battery usage.

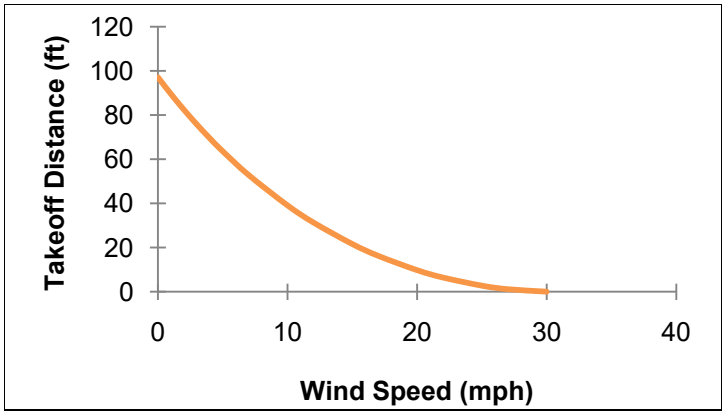

Figure 33: Takeoff Distance vs. Wind Speed

Mission	1	2
% Battery	27.9	89.2

Table 6: Mission Base % of Battery Used

- **Landing Gear Capabilities:** In order to calculate the impact for this mission, the landing speed and descent angle needed to be found; these were approximately 45 feet per second and 9.5 degrees respectively. A simple energy balance conversion enabled the structures team to convert these values to a weight and a height for testing the gear.

4.5.3 Mission 3: Static and Dynamic Roll Asymmetry

The aircraft's static and dynamic stability characteristics during mission 3 change with every lap. While the aircraft is in steady flight, only three cases are needed to analyze the static problems caused by the asymmetric loads (Figure 34).

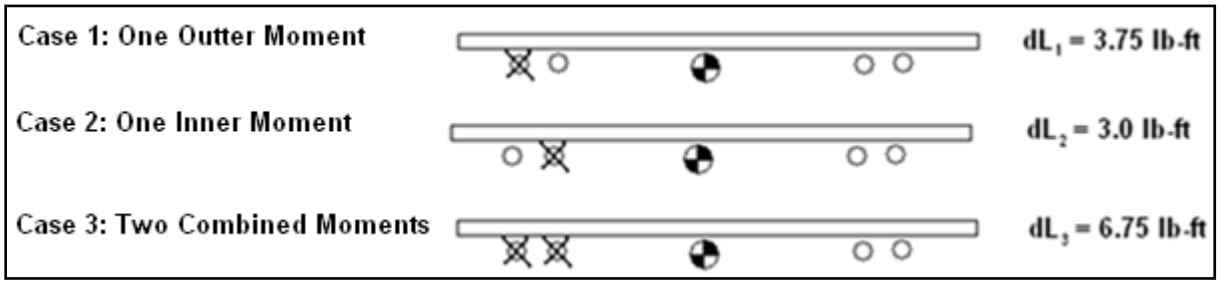

Figure 34: Static Asymmetric Loading Cases

The dL's are the constant differential moments caused by the asymmetric loads for each case. These moments cause problems for the aircraft both before takeoff and landing because the moment control is a function of velocity. In order to have an aircraft capable to complete all three asymmetric cases, the worst case aileron roll moment $L_{ail}(V,\delta_a)$ from the aileron sizing section was plotted versus velocity in Figure 35 for 3 different aileron deflections. Although more graphs were created to represent the different cases, designing around the third static case ensures that the aircraft would be able to fulfill mission requirements.

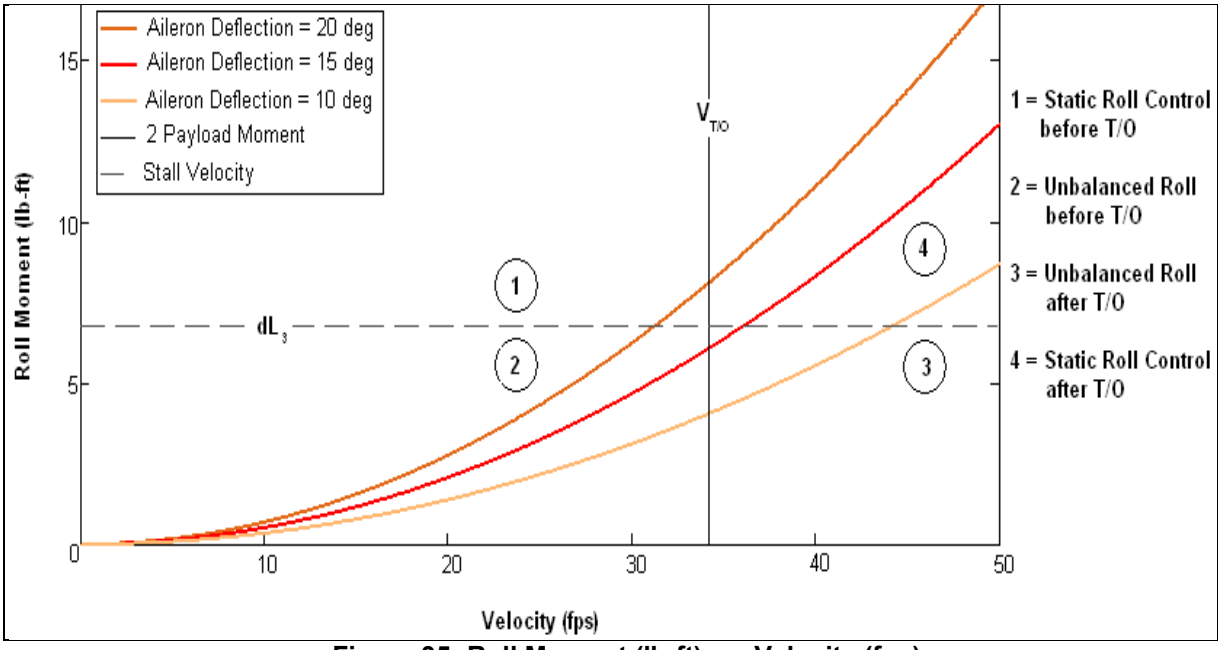

Figure 35: Roll Moment (lb-ft) vs. Velocity (fps)

The takeoff velocity for the aircraft and two asymmetric payloads is represented by the vertical line at 34 fps. The dotted horizontal line represents the constant roll moment produced by the Mission 3, Case 3 asymmetric loading. In order to control the plane before takeoff, the pilot will have ailerons deflected at least 15-20 degrees while rotating the aircraft with a minimum speed of 35 to 40 fps. Typical limitations such as required lift are not a concern because of the significantly lighter payload configurations compared with Mission 2. Also, battery usage over 4 laps should not be a concern on Mission 3 simply because the Mission 2 analyzes a much larger payload at a higher drag coefficient.

Dynamic concerns for asymmetric loading are summarized by the moments of inertia for each case. According to the dynamic calculations for roll stability, case 1 the fully loaded payload configuration causes the slowest response for dynamic roll. In addition, asymmetric loads cause different roll rates depending upon whether the wing stores are either on the port or starboard sides.

5.0 DETAIL DESIGN

During the detailed design phase, every specific sizing and operational parameter was settled so that the aircraft could be manufactured effectively and accurately. During this phase geometrical properties were decided upon and CAD models were rendered in Pro-Engineer Wildfire.

5.1 DIMENSIONAL PARAMETERS FOR FINAL DESIGN

The dimensional parameters for the final design consist of dimensions for the aircraft and the box.

5.1.1 The Aircraft

The final aircraft design parameters detailed below in Table 7 shows the lengths, widths, and diameters of the fuselage, tail, and wing in addition to other important aircraft parameters.

Fuselage			Horizontal Stab			Vertical Stab		
Length	3.63	ft	Airfoil	Inverted NACA 4412 to 4409		Airfoil	NACA 0012 to 0009	
Max Diameter	0.25	ft						
Wing			c_{root}	1.0	ft	c_{root}	1.0	ft
Airfoil	SILK21		c_{tip}	0.33	ft	c_{tip}	0.42	ft
c_w	0.98	ft	b_t	1.92	ft	h_v	0.83	ft
b_w	7.00	ft	S_t	1.28	ft^2	S_v	0.59	ft^2
S_w	6.87	ft^2	AR_V	2.88		AR_V	1.18	
AR_W	7.13		Volume Ratio	0.34		Volume Ratio	0.19	
$c_{aileron}$	2.75	ft	$c_{elevator}$	23.00	ft	c_{rudder}	1.75	in
						$b^1_{rudder\text{-}horn}$	2	in
S_a/S_w	0.17		S_e/S_t	0.23		S_{rud}/S_v	0.24	

Table 7: Aircraft Dimensional Parameters

5.1.2 Storage Box

The final storage box design consists of a corrugated plastic frame with a film covering with outer dimensions of 2'x2'x4'. Foam and corrugated plastic supports are utilized within the box the aircraft, payloads, and equipment.

5.2 Structural Capabilities

The final designed system has the ability to perform the mission requirements and to maximize the score possible through the use of many structural aspects. These aspects form the core of the design and are detailed below.

5.2.1 Storage Box

The final storage box design consists of a corrugated plastic frame with a film covering capable of withstandi withstanding a drop from 6" above the ground. The box consists of a hinge that allows 5 faces of the box to be ra to be raised, leaving the aircraft accessible from 3 sides to the assembly crew. Furthermore, the design of the sto of the storage container allows for the attachment of the payloads and batteries making the aircraft potentially in f potentially in flight-ready within five seconds of opening the container (

Figure 36).

The latch mechanism employed in the box is similar in design to the latch mechanism used for the payloads on the aircraft. The box latch is composed of two sheets of 1/8" plate, a spring loaded latch mechanism pivoting on a delrin rod, and a stud mounted on a piece of 1/8" angle. The plates make up the

[1] The rudder horn is sized from 8 to10 inches above the centerline, along the vertical wing span.

cover plate and back plate of the mechanism, which allow the rest of the components to be secured and protected inside the fiberglass-plywood. The mounting screws are inserted through delrin spacers that will ensure the screws can be tightened appropriately without causing the latch mechanism to bind. The latch is opened by pulling a string or cord upwards, simultaneously releasing the latch and raising the lid of the storage container. The design of the latch also allows for the automatic latching of the box lid by dropping or applying light force to the lid of the box (Figure 37).

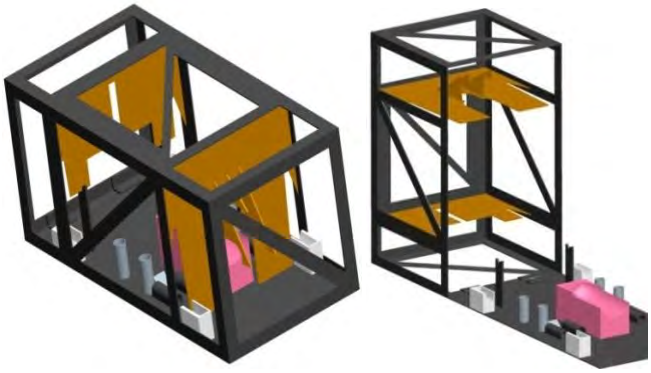

Figure 36: Closed Box and Open Box

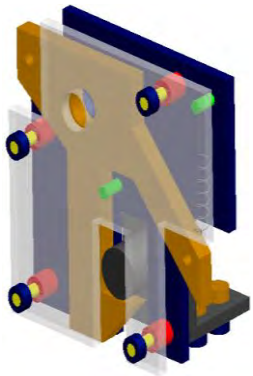

Figure 37: Box Latch

The wing store payloads are designed to be stored in position for quick attachment to the wing itself. The payload attachment rail rests within a slot on the wing. The rail on a payload contains a hole, that when precisely aligned with the latch along the slot on the wing, will secure the payload to the aircraft. The wings are stored in foam cradles which allow the wings to be removed by an upward motion during which the wing store payloads slide up into the wings and lock into place while being simultaneously lifted from their cradles all in a single motion. This single upward motion which attaches the wing store payloads while removing the wing from the box in preparation for the wing attachment to the aircraft. A similar method is employed with the centerline payload of the aircraft, where rolling the aircraft forward will latch the payload to the aircraft.

In order to secure the aircraft, molded support plates are attached to the lid of the storage box that prevent the aircraft from movement in any direction. The support plates will serve as a safeguard in order to mitigate the risk of accidental payload attachment or damage of the aircraft in transport. Furthermore, the supports are designed to protect the aircraft from movement during the storage box drop of 6 inches. The process of lifting the lid of the box removes the supports from the aircraft, allowing unrestrained access to the plane without the need to remove any additional supports or lashings.

The support plates within the box also place the fuselage battery cover in an upward position during storage. Upon removing the lid, the fuselage battery cover can be actuated downwards to secure the batteries. The battery cover incorporates a small wedge that, when secured, pushes the batteries forward to connect power to the aircraft. The battery cover is secured by a small latch, ensuring the cover does not move during flight.

5.2.2 Wing and Wing Attachment Capabilities

The detachable wings are a key aspect of the design. The ability to connect and hold with a carbon fiber spar allows the plane to fly, but this connection must also allow the wings to be attached quickly and reliably during the assembly in the pre-mission. The design accomplishes this through its use of the double tapered carbon fiber insert and the carbon fiber c-channel receiver. These two pieces were molded using CNC precision molds to ensure a perfect fit, giving ease of sliding and confidence in a friction fit once inserted. The third challenge involved in the removable wings is that of power supply and signal path. For this reason, the design incorporates two phono jacks just aft of the spar-insert. These carry the power and signals through to the wing, preventing shorts and allowing for a fast, accurate connection as seen in Figure 38.

Predicted results for the wing tip test were calculated using a 3-point bending test. The minimum designed force the wing should be capable of supporting was calculated at 65 lbs. For a cantilevered beam, calculations indicated the wing needed to support a minimum bending moment of 330 lb-in.

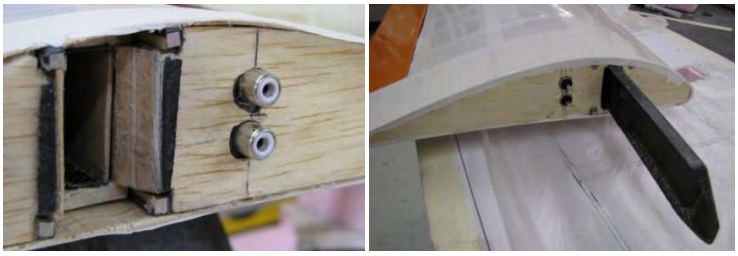

Figure 38: Wing Insert Connection

5.2.3 Landing Gear and Fuselage System

According to this year's rules, no payloads are able to be mounted within the fuselage body. This drove the aircraft design to have a slender 3 inch diameter fuselage sitting 10 inches above the ground. The aircraft fuselage is constructed with a series of 16 bulkheads for structural rigidity across the total fuselage length of 43.6 inches. The nose gears are mounted to a forward bulkhead using Delrin mounting blocks, with a servo horn extending to the side for steering. To support most of the structural load from the large centerline payload, the main gear is mounted to a horizontal plate on two spaced bulkheads. To assemble, the bow-gear is fed through parallel slots in the fuselage and bolted into place. The outriggers are fixed to a reinforced section of the shear web by nylon fasteners beyond the wing stores. In order to save as much of the fuselage structure as possible, nylon bolts have been selected and sized to shear before damaging the structure of the aircraft.

Energy methods predicted the landing gear should at minimum sustain a drop test from a height of 9 inches supporting 15 pounds. In section 8, the structures team performed tests analyzing this capability.

5.2.4 Release Mechanisms

The release mechanisms have huge importance and can affect the performance in every mission. The designed releases, while similar, have subtle and necessary differences between wing tip and centerline. There have also been several feature added to each to optimize their capabilities.

5.2.4.1 Centerline Payload Release Mechanism

The centerline release mechanism, like the wing store release, consists of a spring loaded hook which is retracted by a servo. The hook attaches to a flat rail mounted on the center line simulated fuel tank. The attachment allows the payload to be attached during the removal of the aircraft from the box, which significantly lowers assembly time. This is done by having the payload rail pre-inserted into the slot on the fuselage but ahead of the hook. When the plane is pulled forward, the attach point on the rail will encounter the hook, which then locks into place.

The slot is important as it provides stability for the payload during flight by diminishing the rocking motion in all three planes. The spring also ensures that the hook remains in place, preventing un-commanded releases.

5.2.4.2 Wing Store Payload Release Mechanisms

The wing store release mechanisms have very similar characteristics to the centerline, such as the sliding rail system and basic spring hook configuration. One similarity is the timed-assembly loading; the wing store payloads' rails are latched into the wings as the wings are pulled up from the base of the box, eliminating up to four extra moves. The mechanisms are also activated by one servo to two release mechanisms through the use of positioning and rope connections between the servo and release mechanism, thus, saving weight.

5.2.4.3 Structural Requirements

For both the wing store and centerline release mechanisms, energy methods predicted the minimum required drop test height to ensure structural integrity. The height calculated for drop tests of both payload mechanisms was 9 inches; wing store mechanisms supporting 2 lbs and centerline mechanisms supporting the water-filled 4 liter payload. Structural tests validate this design.

5.3 System Architecture

The need to have a total system capable of releasing five payloads remotely and independently, as well as flying an airplane, called for complex system architecture.

5.3.1 Sub-System Selections

The system architecture of the aircraft primarily consists of the integration between the onboard electrical and mechanical systems. The independent optimization of each component allows for the

selection of sub-systems which will provide a completely integrated system which can then provide an increased level of performance.

5.3.1.1 Battery Pack

The size of the battery pack was optimized to consist of 26, 1.5 amp-hour batteries. The shape and the small size of the fuselage dictated the necessary configuration of the pack. The cells were packaged so that they could easily fit on the designed sled. This sled allows the battery pack to be adjusted forward or aft in order to trim out the aircraft's center of gravity. The cradle was designed such that the battery pack is pushed forward and locked into position when the hatch is closed. The forward motion also pushes the electrical connectors together allowing for *extremely quick connection and securing of the battery pack*. The battery pack subsystem is shown in Figure 39.

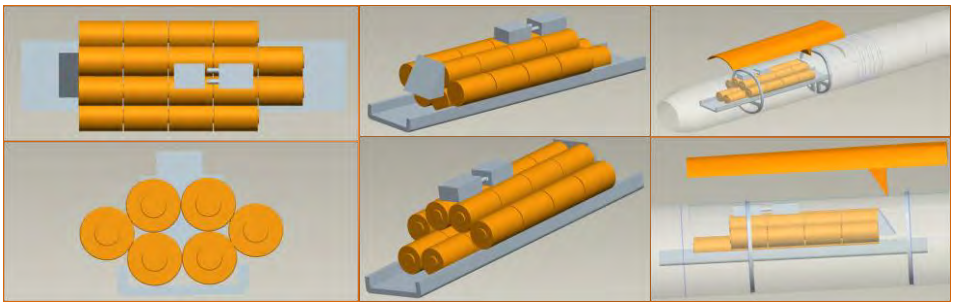

Figure 39: Battery Pack

5.3.1.2 Servo Selection

Based on the aerodynamic force requirements and the payload release mechanism requirements the team selected the Futaba s3102 servo. This servo will be operating on 4.8 volts, and is expected to provide 51.4 oz-in of torque, while weighing only 0.74 ounces. The servo is very rugged and provides a large amount of torque, yet it remains very lightweight in comparison to other servos in its torque class. The excess torque provided by the servo allows for an adequate margin of safety. The excess power also allows to conserve battery power.

5.3.1.3 Centerline and Wing Store Payload Release Mechanisms

The mechanical payload release mechanisms are actuated by the Futaba s3102 servo. Each wing has one servo dedicated to the payloads associated with that wing. An independent servo has been dedicated to the centerline payload due to its large size. A flexible wire is attached to the servo horn and then to the corresponding release actuator. The flexibility of the wire allows for the actuator to only be actuated when the wire is in tension and not compression, thus moving the servo arm to the right only actuates the release to the left of it and vice versa.

5.3.2 Total System Integration

The team's wireless transmitter is capable of transmitting 7 independent signals; however the aircraft requires at least nine signals to perform mission requirements. The team overcame this problem by using a nine channel receiver in conjunction with a signal activated power switch that activates a second receiver, which is programmed to the transmitter. The primary receiver will still be powered on when the secondary receiver is switched on, and both receivers channels will operate simultaneously. The simultaneous signals will not be an issue since the payloads will only be released while the aircraft is stationary on the ground. The release motions will be coupled with control surface deflections until the secondary receiver is switched off. A signal path diagram is included in Figure 40.

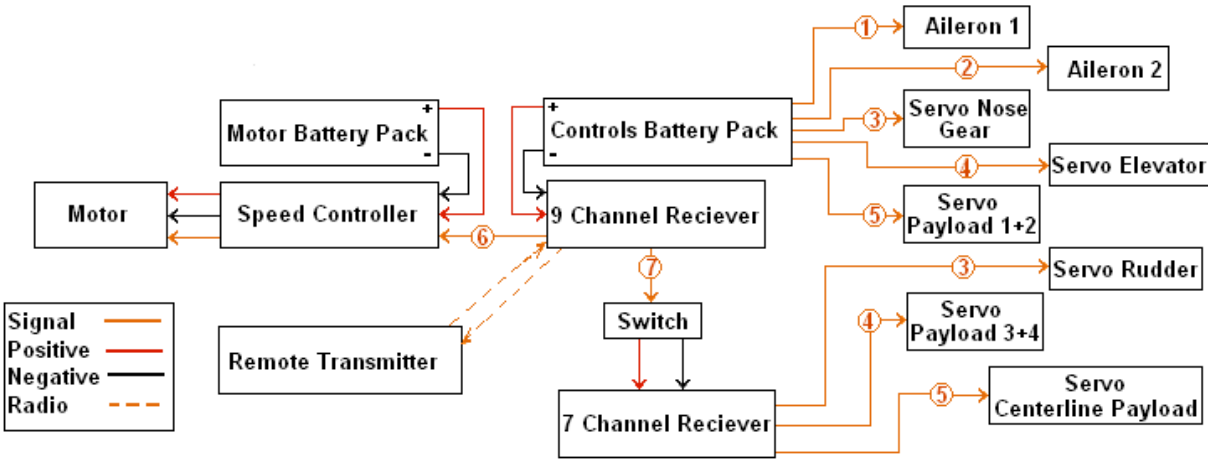

Figure 40: Electronic System Integration

In order to meet the design requirements of a quickly-assembled aircraft system, a way to quickly connect the electrical systems in the removable wings to the main system in the fuselage was needed. Many types of connections were explored in an effort to analyze the speed of connection, the reliability of the connection, and the difficulty of removal. The best solution tested was the standard phono jack available at most electronics stores. This connector allowed for quick and easy assembly, while providing plenty of resistance to prevent unintentional detachment during flight. It also prevented any shorting to occur across the connection and provided a four wire connection with only two connectors per wing. In addition, the phono connectors doubled as an anti-rotation pin for the wing attachment.

5.4 Weight and Balance for Final Design

The weight and balance information for the final aircraft design can be seen below. In Table 8 the individual weights for the major components in the aircraft can be seen along with the various total weights for the aircraft based on all possible payload configurations across all missions. Table 8 also shows the cg shifts in the lateral and vertical directions across the various missions. The aircraft is balanced at 13.5 inches from the leading edge of the fuselage to the quarter chord of the wing in all cases.

Components	X_{cg} [in]	Y_{cg} [in]	Z_{cg} [in]	Weight [lbs]
Motor	3.18	0	0	0.407
Wings	13.50	0	0	0.496
Wiring	0	0	-1	0.091
Gearbox	0.64	0	0.80	0.062
Fuselage	18.13	0	0	0.397
Propeller	-0.64	0	0	0.154
Bow Gear	15.25	0	-5	0.378
Nose Gear	5.25	0	-5.75	0.132
Spar Insert	13.50	1	0	0.277
Outriggers	13.75	±33.25	-7.25	0.106
Vertical Tail	7.19	0	3.75	0.106
Aileron Servo	16.50	±22	0	0.046

Payloads	X_{cg} [in]	Y_{cg} [in]	Z_{cg} [in]	Weight [lbs]
Centerline Empty	13.50	0	-4.5	1.1
Centerline Full	13.50	0	-4.5	9.2
4 WS	13.50	0	-0.151	6.0
1 Inner WS	13.50	-0.411	-0.151	1.5
1 Outer WS	13.50	-0.514	-0.151	1.5
2 Inner or Outer WS	13.50	0	-0.151	3.0
2 Left/or/Right Side WS	13.50	-0.767	-0.151	3.0
1 Outer and 1 Inner WS	13.50	-0.085	-0.151	3.0
2 Outer and an Inner WS	13.50	-0.291	-0.151	4.5
2 Inner and an Outer WS	13.50	-0.364	-0.151	4.5

Components	X_{cg} [in]	Y_{cg} [in]	Z_{cg} [in]	Weight [lbs]
Horizontal Tail	39.29	0	0	0.242
Servo Batteries	15.62	0	0	0.262
Servo Receiver	23.16	0	-1	0.262
Speed Controller	7.95	0	-0.75	0.178
Vertical Tail Servo	38.6	0	5	0.046
Propulsion Batteries	8.66	0	0.5	1.329
Horizontal Tail Servo	38.6	0	0	0.046
Centerline Payload Servo	13.50	0	0	0.046
Release Servos for the Wing Store(WS)	14.25	±27	0	0.046
Inner Wing Store Release Mechanisms	13.50	±24	0	0.015
Centerline Payload Release Mechanism	13.50	0	0	0.040
Outer Wing Store Release Mechanisms	13.50	±30	0	0.015

Total cg and Weight Analysis for the Various Missions	X_{cg} [in]	Y_{cg} [in]	Z_{cg} [in]	Weight [lbs]
Empty No Batteries	15.28	0	-0.442	5.5
Empty with Batteries	13.50	0	-0.245	6.8
Mission 1	13.50	0	-0.663	7.8
Mission 2	13.50	0	-2.772	16.4
Mission 3 - 4 WS	13.50	0	-0.733	12.8
Mission 3 - 1 Inner WS	13.50	-0.411	-0.733	8.3
Mission 3 - 1 Outer WS	13.50	-0.514	-0.733	8.3
Mission 3 - 2 Inner or Outer WS	13.50	0	-0.733	9.8
Mission 3 - 2 Left/or/Right Side WS	13.50	-0.767	-0.733	9.8
Mission 3 - 1 Outer and 1 Inner WS	13.50	-0.085	-0.733	9.8
Mission 3 - 2 Outer and an Inner WS	13.50	-0.291	-0.733	11.3
Mission 3 - 2 Inner and an Outer WS	13.50	-0.364	-0.733	11.3

Table 8: Final Design Weights and Balances

5.5 Expected Flight and Mission Performance

The final aircraft has a maximum coefficient of lift of roughly 1.3 with a maximum lift to drag ratio of about 12.5. The rate of climb for the aircraft is fastest for mission 1 as it has the lightest payload configuration. Mission 2 has the slowest rate of climb since the centerline payload weighing over 9 pounds. Also, the expected stall velocity decreases as the payload weight decreases with the max velocity equal in missions 1 and 2 due to the payload shape while the max velocity in Mission 3 is slightly faster due to the change in payload shape causing reduced parasite drag. Finally, the estimated takeoff distances decrease with the decrease in payload weight. Therefore, it will be shortest for mission 1 in Table 9.

Aerodynamic Factors	
C_{lmax}	1.3
L/D_{max}	12.5

Mission #1 Performance		Mission #2 Performance		Mission #3 Performance	
ROC_{max}	15.4 ft/s	ROC_{max}	5.9 ft/s	ROC_{max}	9.6 ft/s
V_{stall}	28 ft/s	V_{stall}	42.76 ft/s	V_{stall}	36.9 ft/s
V_{max}	70 ft/s	V_{max}	70 ft/s	V_{max}	73 ft/s
TO Distance	15.7 ft	*TO Distance*	97 ft	*TO Distance*	55.1 ft
Flight Time	80 s	*Flight Time*	200 s	*Flight Time*	180 s

Table 9: Expected Mission Performance

5.6 Rated Aircraft Cost (RAC)

Component	Box	Aircraft	Payloads	Transmitter	RAC Estimate
Weight (lb)	8	6.78	15.03	1.67	31.48

Table 10: Rated Aircraft Cost

5.7 Drawing Package

The following sections contain the dimensioned 3-view, the structural arrangement, the system layout/location, and the payload accommodation PRO-E drawings.

5.7.1 3-View Drawing with Dimensions

Figure 41: 3-View Drawing with Dimensions

5.7.2 Structural Arrangement Drawing

Figure 42: Structural Arrangement Drawing

5.7.3 Systems layout/location drawing

Figure 43: Systems Layout/Location Drawing

5.7.4 Payload Accommodation Drawings

Figure 44: Payload Accommodation Drawings

6.0 MANUFACTURING PLAN AND PROCESSES

This phase of the project translated the concepts to constructed components of the aircraft. Due to the time restrictions for this year's competition, a great deal of planning was done in scheduling, construction techniques and materials used. The manufacturing plan was divided into seven major components: Fuselage, Wings, Tail, Landing Gears, Release Mechanisms, Fairing, and Box. The following manufacturing plan defines the alternatives investigated, and the processes selected.

For the manufacturing of all the components included in the system, a set of FOMs were established to help in the manufacturing decision making process. The four chosen FOMs were Weight, Structural Integrity, Ease of Construction, and Maintainability. The construction method must provide enough structural integrity to the system so that it can perform all the required missions. FOMs were based upon the speed of construction and maintenance capabilities for subcomponents.

6.1 MANUFACTURING TECHNIQUES AND PROCESSES INVESTIGATED

The following sections detail both the manufacturing techniques and the various processes investigated for the creation of the final aircraft and box.

6.1.1 Fuselage Structure

Three methods were considered to construct the fuselage.

- **Lost-foam Method:** The Lost-foam method is an extension of the solid foam method. A foam cutout of the fuselage is covered in fiberglass. Once the fuselage has cured, the foam is removed. It reduces weight, but is not easily repairable.
- **Male Mold Method:** The male mold consists of a hardened fuselage half made of foam or MDF board. The balsa is laid up over the mold and allowed to cure under a vacuum. Once the pieces have hardened, the two halves are bonded together. The male mold constrains the inner dimension of the fuselage and leaves the outer portion rough.
- **Female Mold Method:** The female mold is the exact opposite in shape. The balsa is laid inside the fuselage cut out and allowed to cure. The female mold constrains the outer dimension of the fuselage and leaves the inner portion rough. This method produced the best quality.

The female mold method was selected for the fuselage manufacturing process. A foam plug was cut and sanded to the correct dimensions. The foam plugs were coated with hardener and used to form the female molds. The fuselage was constructed by forming two halves laid-up individually, but simultaneously. This process of creating molds to make fuselage is labor intensive, but it makes accurate, strong and light fuselages. The bulkheads internal to the fuselage will be CNC cut to ensure precision. Finally, they will be spot sanded to fit to the composite fuselage and affixed with epoxy.

6.1.2 Wing and Tail Construction Methods

Four Methods of construction were heavily considered to construct the wing.

- **Solid Foam Core Method:** The Solid Foam Core method is the most structurally sound but it is heavier than the other means of construction and leaves no room for the wing store releases.
- **Foam Removal Method:** See methods described in the fuselage section.
- **Mold Method:** See methods described in the fuselage section.
- **Balsa/film Cover Method:** This method involves a buildup which requires making individual components and then assembling them together. After the balsa skeleton is constructed the surface is coated in a film. The film is used instead of fiberglass, which decreases the weight of the wing without removing all structural support. The main disadvantage to using film is that it is very delicate and prone to tearing. This method allows for sufficient space to install the release mechanisms.

The criteria for choosing a construction method is weighted toward the ease of construction and the ability to maintenance the wing (Table 11).

					
Figures of Merit	**Score**	**Balsa/Film Method**	**Foam Core Removal Method**	**Mold Method**	**Solid Foam Core Method**
Weight	0.25	0	1	1	-1
Structure	0.10	1	1	0	1
Ease of Construction	0.35	1	-1	-1	-1
Maintence	0.30	1	-1	-1	-1
Total Score	1.00	0.75	-0.3	-0.4	-0.8

Table 11: Wing Construction Method

The balsa/film method was ultimately chosen for it light weight and space efficient design. The space allows for the release mechanisms to be easily installed and repaired.

To construct the spar, four composite rods made of linear carbon tow pressed onto basswood rods will be made using epoxy and a vacuum. The fiber glassed shear web is bonded to the spars to support the shear loading on the wings using CA glue. The fiberglass process increases amount of strength to the typical shear web to produces a much stronger.

After ribs are added, balsa skin will be laid on. The lightning holes, which will be left, are covered with film to retain the airfoil shape but minimize weight. CNC rib templates and leading edge sanding blocks were used to increase the speed and quality at which the wing was constructed.

Part of the wing construction involves the building of the insert at one end of the wing. The insert was designed to transfer the load between the inboard and outboard sections of the wings. Because the insert was design for speed loading, design decisions were made to help the structural integrity of the insert while still allowing to the wing to go on quickly. The c-channel design was improved by adding a

layer of balsa in the shear web of the insert to help with the torsion problems that c-channels typically have. The insert has two layers of unidirectional carbon fiber on the top and bottom of the insert to support the bending load. The shear web has a layup of [45°/90°/balsa/45°]. Inside the wing, the insert is wrapped to together with the main spars using Kevlar string to tie the spars and insert together and prevents failure to "pry-baring" forces.

6.1.3 Landing Gears

For the landing gear a foam plug was constructed similar to the fuselage. A layer of fiberglass was epoxied to it to ensure that the plug could be reused to lay-up multiple landing gears. Carbon Fiber was cut out in 0/45/90° orientations. Balsa was cut out with the same outline, but 0.25 in smaller on all sides. Kevlar was also placed in between the carbon fiber and balsa for added reinforcement. The final orientation was [0°/0°/balsa/Kevlar/0°/45°/90°/0°/45°]. The materials were laid over a male mold and vacuum bagged over night. When the gear had cured, the holes were drilled at the wheel locations and at the point where the gears mounts inside the fuselage. The advantage of mounting the landing gear inside the fuselage is that they can be tied into the internal bulkheads. The nose gear was laid up using a mushroom gear mold. The mushroom gear was connected to a cylindrical carbon fiber rod. A strip of balsa was put into the carbon layup at the connection point between the carbon fiber and the rod to give a thicker surface to bond to. The two outriggers were constructed in a similar manner as the nose gear. The carbon fiber rod was mounted to directly to a carbon fiber plate and installed in to the shear webs in the wings. Nylon bolts were used to attach the gear to shear webs so that they would shear before any serious damage was done to wing.

6.1.4 Release Mechanisms

Since the all the release mechanisms are similar in operation, the manufacturing complexity is cut dramatically. Due to the materials and dimensions to be used, a Computer Numerical Control (CNC) machine was used to fabricate the outer plates and hooks in the release mechanism. The release mechanisms are assembled by hand and fit into the fuselage. Because of the fast manufacturing time and simple design, several release mechanisms can be made in a relatively short amount of time.

6.1.5 Fairing

The fairings that are attached to the centerline payload are only required to withstand aerodynamic loads. With that in mind, a simple shell can be used to reduce the drag on the payload and it be made with a small amount of material. Two methods were considered to manufacture the fairing.

- **Male Mold Method:** Using a male mold allows the inner dimension of the fairing to be the constrained dimension. This is important for getting a precise fit around the centerline payload.
- **Female Mold Method:** Using the female mold method constrains the outer dimension. This will allow the surface to be smooth and best serve its main purpose of reducing drag.

The female mold was selected for the fairing construction. The outer surface is the most important aspect of the fairing and it would defeat the purpose if the side exposed to the wind was not perfectly smooth.

6.1.6 Box

Because the box is considered in the system weight, the materials and methods of construction used become just as important as the plane. To construct the box, the method selected was the build-up method. This type of method was deemed necessary due to the chances of the boxes changing shape throughout the construction phase. To maintain a quick assembly time, the box must allow for any modifications that may occur in the future. The box design and fabrication is an iterative process. The box is built with lightweight materials and is built around the plane. The prototype box was constructed using corrugated plastic, but other materials under construction are carbon fiber and fiber-glassed balsa.

- **Corrugated Plastic Box:** The first box constructed was made of one layer of corrugated plastic. The hinge on the lid was made using duct tape. An advantage to using the corrugated plastic is that its strength is good and its versatility is unmatched. The material is readily available and can be used to construct quick prototypes. Unfortunately, the plastic was found to be quite flimsy and will need additional reinforcement to perform at the necessary contest level.
- **Carbon Fiber Box:** Carbon fiber was investigated as another option for the box material. The nature of the box design requires a rigid box. Carbon fiber has good strength qualities and, with the right orientations, it can be quite rigid. Carbon fiber must have multiple plys to reach that desired thickness to be rigid. This drastically increased the weight of the box. In addition, the use of composite material requires time to layup the material and then to assemble the box. The manufacturing time was considered in the decision matrix.
- **Fiberglass/Balsa Box:** Using fiberglass coated balsa was another option that was tested. The glassed balsa was light weight and proved easy to work with. However, the balsa lacked the necessary stiffness to keep the box rigid while keeping the weight low. As with the carbon fiber box, the glassed balsa required preparations and curing time to set up before the box could be constructed.

The corrugated plastic box was ultimately chosen as the best material for the box. The plastic can be reinforced in certain areas to provide the necessary rigidity.

6.2 Manufacturing Schedule

A detailed Gantt chart of the construction schedule is shown below Figure 45: Prototype Construction Schedule. The chart shows how the tasks have been divided until the first manufacturing Milestone: The Prototype rollout.

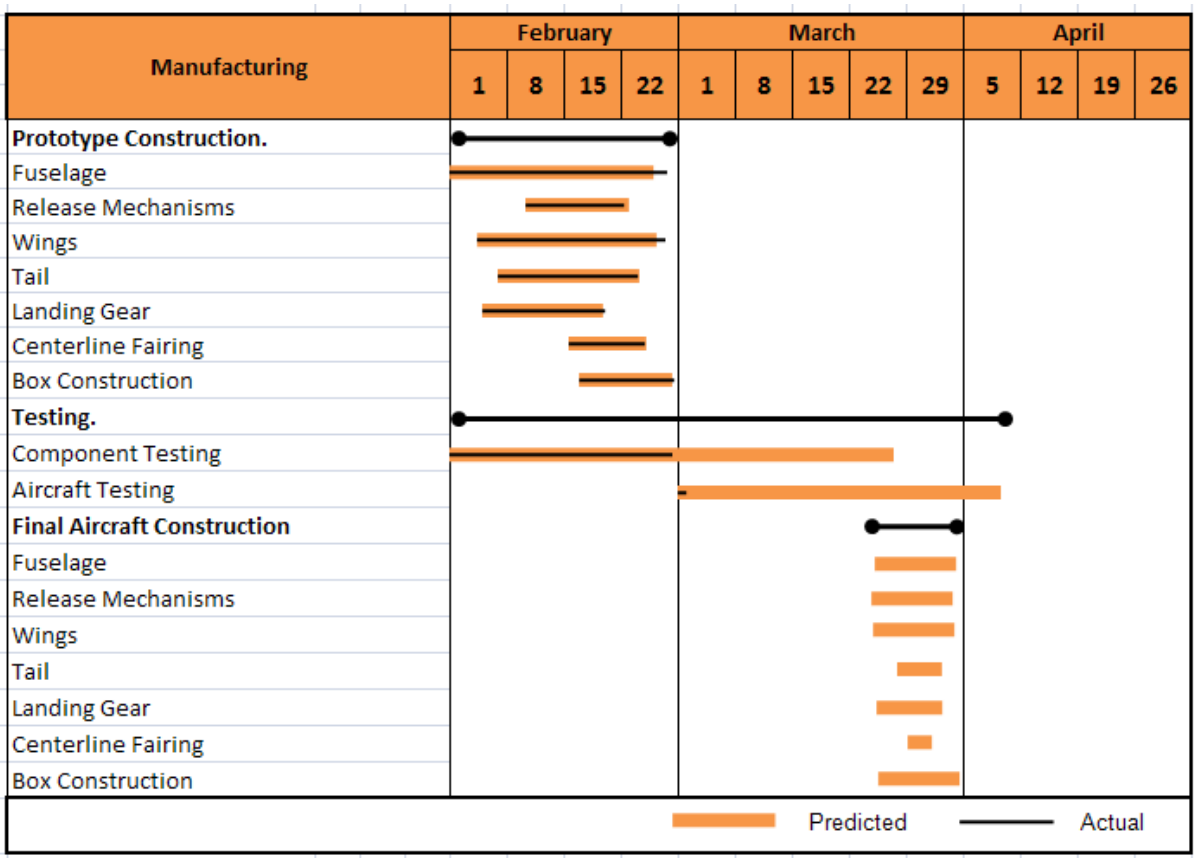

Figure 45: Prototype Construction Schedule

7.0 TESTING PLAN

In the process of designing and building an aircraft, the testing of the various subsystems and total aircraft box system is critical to the success of the team. This includes structural tests of components, propulsion tests for electrical equipment, practice ground loading and assembly times, and flight testing.

7.1 TESTING CHECKLIST/OBJECTIVES

In order to be as effective as possible in the testing phase, the team set test objectives to learn from and improve on. Prototype molds and parts were constructed to develop the necessary skills for the actual plane construction. Other test pieces were built to prove that the design could withstand the actual conditions. This can be seen in Table 13:Pre-Flight Testing Check List below.

Test	Objective	Observation
CLP/WSRS Material Test		
Force required by servo to release	Find servo moment to overcome friction	
CLP/WSRS Impact Test		
Height	Find the height at which the release hook fails	
Main Landing Gear		
Height	Find the height at which gear fails at 15 lbs	
Weight	Find the weight at which gear fails at 9"	
Failure type	Find the failure mode/type	
Timed Assembly for SCF		
Time	Find the time needed to assemble	
Aircraft/Box Damage	Find the which components get damaged the most	
Taxiing/Payload Release Test		
Taxi straight/turns	Check the ease of taxiing straight, turning radius	
Release Independently	Check for interference of release with control surfaces	
Timed Loading Test		
Time	Find time needed to attach the payloads	
Rail/Release Hook Problems	Check for problems in rail/release hook	

Table 12: Testing Checklist and Objectives

Item	Description	Status
Center of Gravity		
C.G. Aircraft	Adjust Battery Back	
C.G. Payloads	Ensure C.G. directly under notch	
Propulsion System		
Batteries	Charged	
Propeller	Secured	
Speed Controller	Programmed	
Electric System		
Motor Secured	Screws tight, firewall secured, motor aligned	
Wires	Connection working, AV jacks undamaged	
Servos	Zeroed and working	
Fuse	Secured	
Miscellaneous		
Wings/Stabilizers	Mounted Securely	
Control Surfaces	Proper deflection, hinges and rods secured	
Release Mechanism	Working independantly, no interference with control surfaces	
Payloads	No lateral movement possible, faired/ballasted	
Battery Hatch	Displaces battery to correct position, secured	
Landing Gear	Secured and Kevlar string attached	
Fail safe	On	

Table 13:Pre-Flight Testing Check List

7.2 Testing Gantt Chart

A Gantt chart was created to document the testing plan and insure that the team was meeting deadlines. The ground and flight testing had proven to be a significant factor in the success of team throughout the years. Therefore, the testing schedule must be followed in order to maximize the amount of testing possible, Figure 46 shows the Gantt chart.

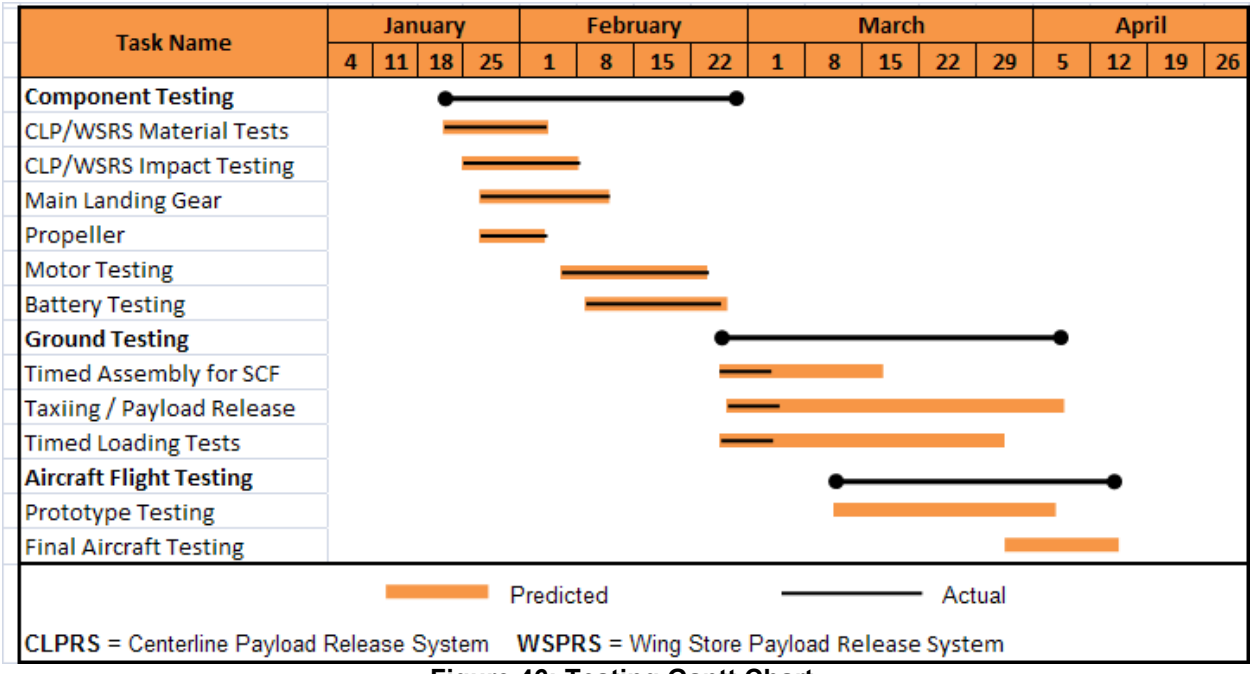

Figure 46: Testing Gantt Chart

8.0 PERFORMANCE RESULTS

The testing objectives outlined in section 7.0 were put into practice and the various components were tested against their theoretical estimations.

8.1 Key Subsystem Performance

The following sections detail the results of the testing of various sub-systems.

8.1.1 Propeller Performance

The team tested propellers in the Oklahoma State University wind tunnel in order to obtain coefficient of power, coefficient of thrust, and efficiency curves. These curves were then input into the team's optimization program in order to obtain more accurate predictions on how well the propulsion system is suited for the mission. Figure 49, Figure 48, and Figure 49 show the C_p, C_t, and efficiency curves for the APC 19x12 propeller while using the MEC 6:1 gearbox and the Medusa MR-028-56-1400V2 electric motor compared with the propeller data taken previously with a test motor.

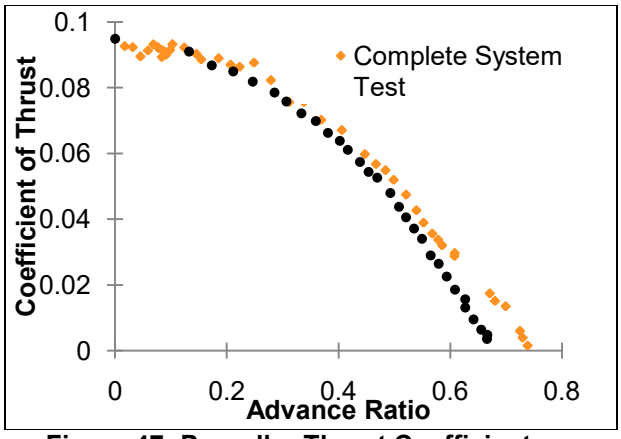

Figure 47: Propeller Thrust Coefficient vs. Advanced Ratio

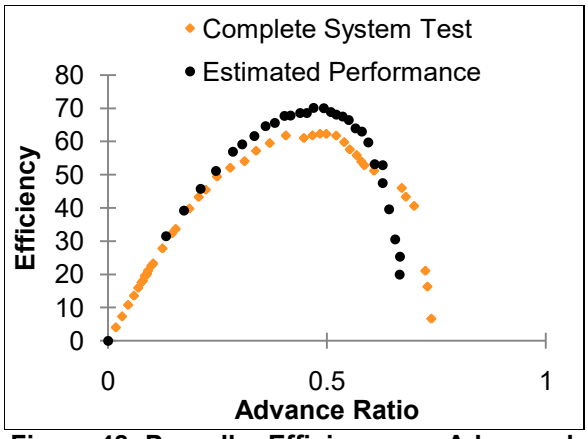

Figure 48: Propeller Efficiency vs. Advanced Ratio

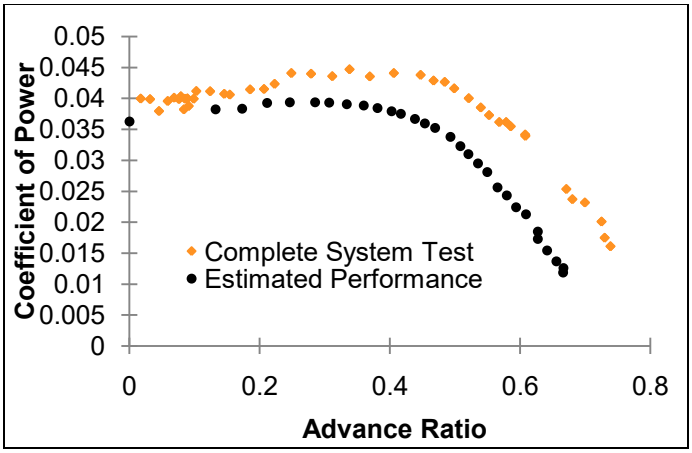

Figure 49: Propeller Coefficient of Thrust vs. Advanced Ratio

8.1.2 Battery Performance

The batteries were tested individually so that the ones with the highest capacity could be used for building the battery packs. After the battery pack was constructed, it was charged then discharged using a computerized battery analyzer. This allowed for a check of inconsistencies between the individual data and the pack data, as well as the manufacturer's data. Figure 50 and Figure 51 show the discharge data from the finished pack and the performance for multiple individual cells.

Figure 50 and Figure 51 above show that although the average Elite 1500 cell only contains approximately 1250 milliamp hour capacity, the pack created from the best cells achieves the manufacturer's expected performance parameter of 1500 milliamp hours. This shows that the estimate of 1000 milliamp hours is conservative and therefore a longer endurance than previously estimated should be observed.

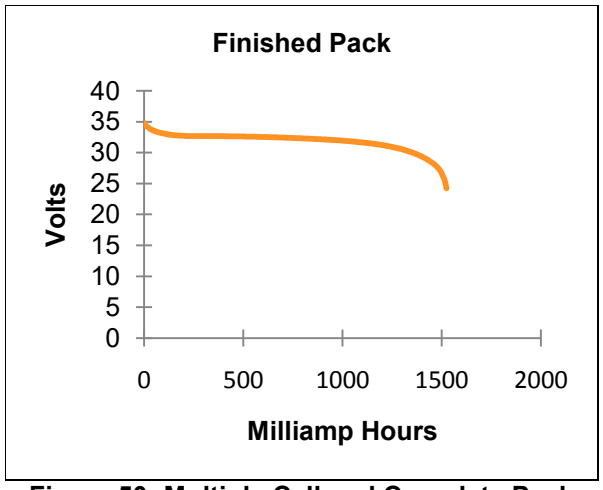

Figure 50: Multiple Cell and Complete Pack Battery Discharge Data

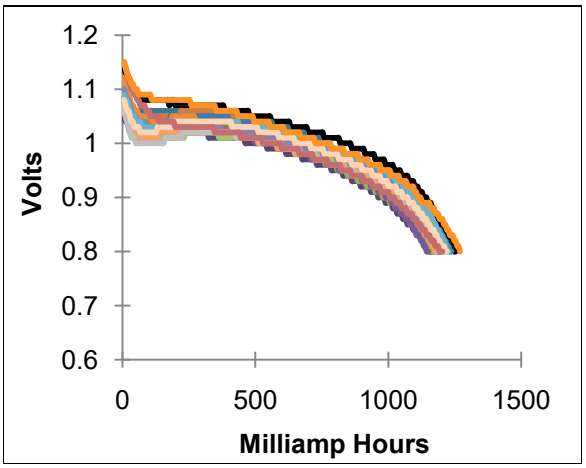

Figure 51: Discharge Data for Multiple Battery Cell

8.1.3 Main Gear Performance

A jig was designed which will place the center of gravity of the weights on the gear at the approximate position expected during takeoff and landing, and was then fixed into place with a guide rod to ensure direct loading and to eliminate bouncing. The jig is in Figure 52 below.

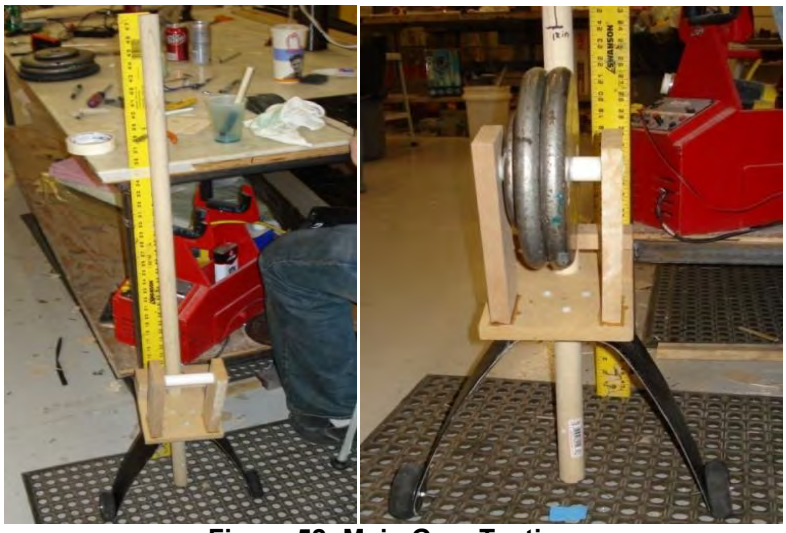

Figure 52: Main Gear Testing

The first test was done with a [45/0/45/0/balsa/Kevlar/balsa/0/45/0/45] layup. Based on the calculations, the main gear must withstand a 16 lb drop from 9" above the ground. The first test was unsuccessful and failed at only 12 lbs from 9" above the ground. After careful analysis, the bow gear was found to have failed to delimitation around the balsa layer. The second test used the same layup, but gave ¼ in more flanges around the edge of the gear. This was done to give the composite more material to bond to. The second test proved successful as it was able to hold 17 lbs from 12" before failing.

8.1.4 Release Mechanism Performance

Fiberglass coated balsa and aluminum were tested for the structure of the centerline release hook. Both hooks were cut out using a CNC mill to reduce manufacturing time. The balsa hook weighed 0.05 ounces while the aluminum hook weighed 0.306 ounces. The fiberglass coated balsa was the first hook prototype tested. The release mechanism was assembled then mounted in the test stand with the four liter centerline payload filled with water and mounted on the hook. The string was pulled until failure occurred with the hook breaking off. The aluminum hook successfully released the centerline payload. The next focus was reducing the necessary pull force needed to minimize the size of servo needed to retract the hook. To minimize the pull force needed, the surface of the hook on which the payload mount rests was filed. The slot on the aluminum release mounting rail was smoothed out with fine-grit sandpaper to reduce friction. Through this process, the needed pull force was reduced to 3.75 pounds. Reducing the force needed allowed for the use of smaller servos in the release mechanisms. Though the aluminum hook weighs more than the balsa hook, its reliability is greater than that of the balsa material.

Fiberglass plywood and aluminum were tested for the wing store hook. The fiberglass hook weighed 0.035 ounces while the aluminum hook weighed 0.105 ounces. The fiberglass hook was mounted in the test stand with a 1.5 pound weight suspended from a mount rail. The string was pulled and the hook retracted with less than two pounds of pull force. The aluminum hook was tested and pulled with a force of 2 pounds. This showed the aluminum rail slid easily into the slot with the aluminum hook (Figure 53: Centerline Payload Release Mechanism Testing).

Figure 53: Centerline Payload Release Mechanism Testing

The next test performed on the prototype simulated a hard landing resulting in increased g-force on the release mechanism. The goal for this test was to determine the maximum height from which the aircraft could drop without the release mechanism malfunctioning. The setup for this test consisted of the aluminum centerline release mechanism being mounted to the test stand. When dropped from a height of nine inches, the stand was rolled to the side on impact. The centerline payload remained secure in the release mechanism. To ensure the release mechanism remained operable, the string was pulled to retract the hook and the centerline payload was successfully released. The payload was reloaded into the

test stand then raised to a height of 15 in. Upon impact, the centerline payload mount failed. The release mechanism remained intact and fully operable. To resolve this problem, the thickness and height of the rail on the centerline mount was increased to allow for more material above the slot in the rail.

For the smaller wing store payload release systems, less rigorous impact tests were performed. To test the materials for hard landing and impact resistance, each hook was mounted in the stand with a 1.5 pound weight suspended below then dropped at various heights. The fiberglass plywood hook failed at a drop height of 8 inches. The aluminum hook withstood a 12 inch drop without failure. From this data, it was easy to conclude that the aluminum hook was the best solution.

8.1.5 Wing Structure Performance

To see that the wing design could with stand the maximum load required by the mission , two tests were set up to check the important parameters: the wing spar strength; and the wing insert joint strength.

To test the wing spar strength, a test section of the wing was built to be loaded directly in a three point bending condition. Analysis was done to determine the maximum load the spar would see at any point in the contest. This was determined to be the 2.5g loading test. After applying a safety factor of 1.15 and converting the load to the prescribed moments for the test section, a required loading of 65lbs was made the goal. The wing was loaded to over 85lbs without failure (Figure 54).

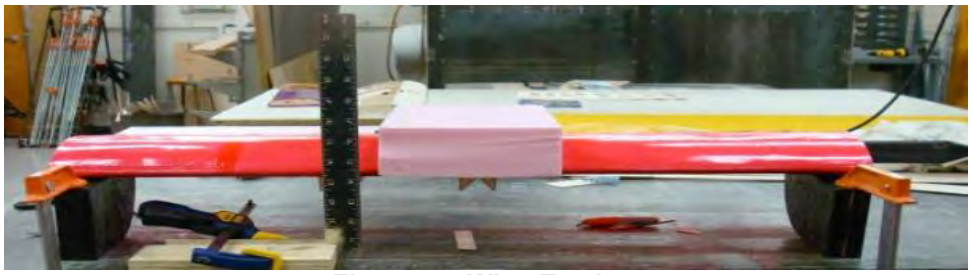

Figure 54: Wing Testing

To test the ability of the wing insert joint, a similar procedure was followed. For this component a cantilevered bending test would be conducted. It was found though a similar method to the spar test that the wing should be able to carry 330lb-in at the tip without failure at the insert joint. The test was conducted and the wing held 450lb-in before failing. This showed the wing strength is sufficient.

8.2 Complete System Performance

The follow section details the complete system performance for assembly and loading testing.

8.2.1 Assembly and Loading Performance

The prototype aircraft has been used to demonstrate, practice and evaluate ground handling performance and handling time. A box prototype has also been made which complements the entire process. Ground crew try-outs were performed to select the fastest set of team members that will perform the assembly task. Ground tests have been done for assembly during the pre-mission stage and mission

3. The preliminary rounds of tests show that assembly time for the pre-mission stage is about 7 seconds and that for mission 3 to be around 5 seconds. Testing techniques are currently being refined in the testing process. Figure 55**Error! Reference source not found.** shows an example run and data of the assembly process.

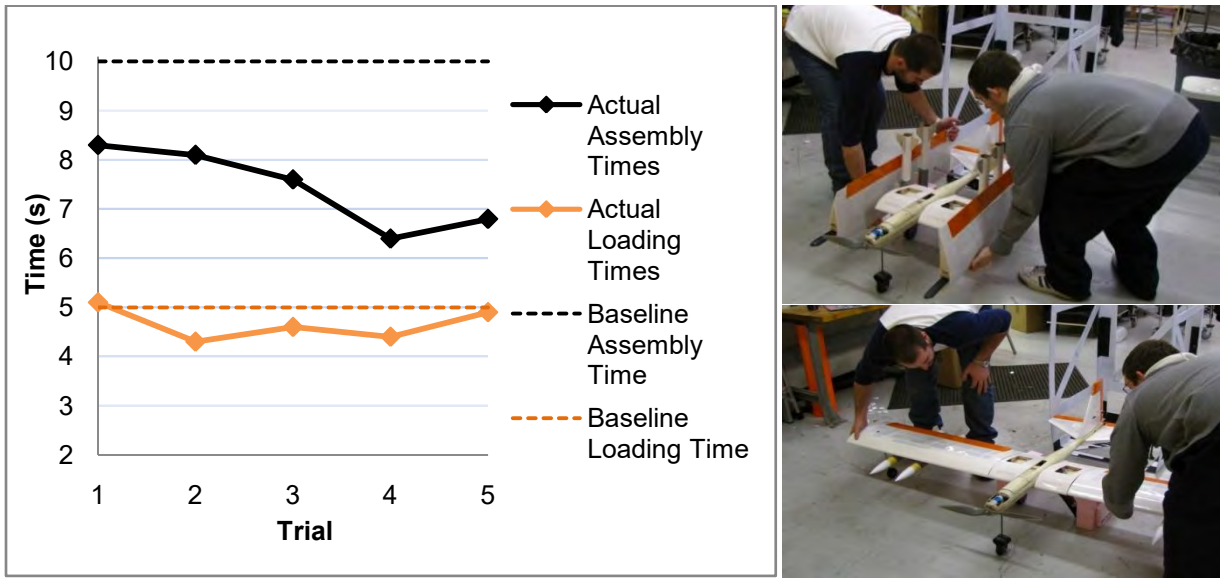

Figure 55: Assembly and Loading Time Tests

8.2.2 Taxiing and Payload Testing

Taxi tests have proven the ability of the aircraft to tote asymmetric loads and release the wing stores.

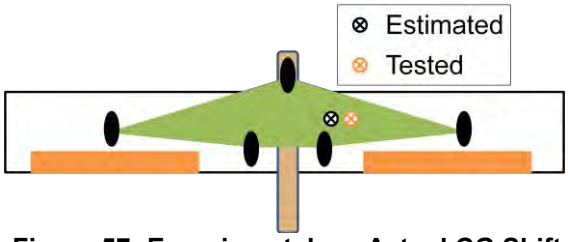

Figure 57: Experimental vs. Actual CG Shift

Figure 56: Taxiing with Asymmetric Loads

8.2.3 Flight Testing Performance

According to the testing schedule, prototype flight testing is scheduled for 3 March pending wind speeds.

9.0 REFERENCES

Arena, A.S. Class notes. Unpublished. 2008.

Hoerner, S. F. *Pressure Drag Fluid-Dynamic Drag.* 1965.

Nelson, R. C. Flight Stability and Automatic Control. 2nd Ed. McGraw-Hill Higher Education. 1998.

Raymer, D.P. Aircraft Design: A Conceptual Approach. 3rd Ed. American Institute of Aeronautics and Astronautics, Inc. Washington, DC. 1999.

SHEET 1

OKLAHOMA STATE UNIVERSITY ORANGE TEAM

2-21-09

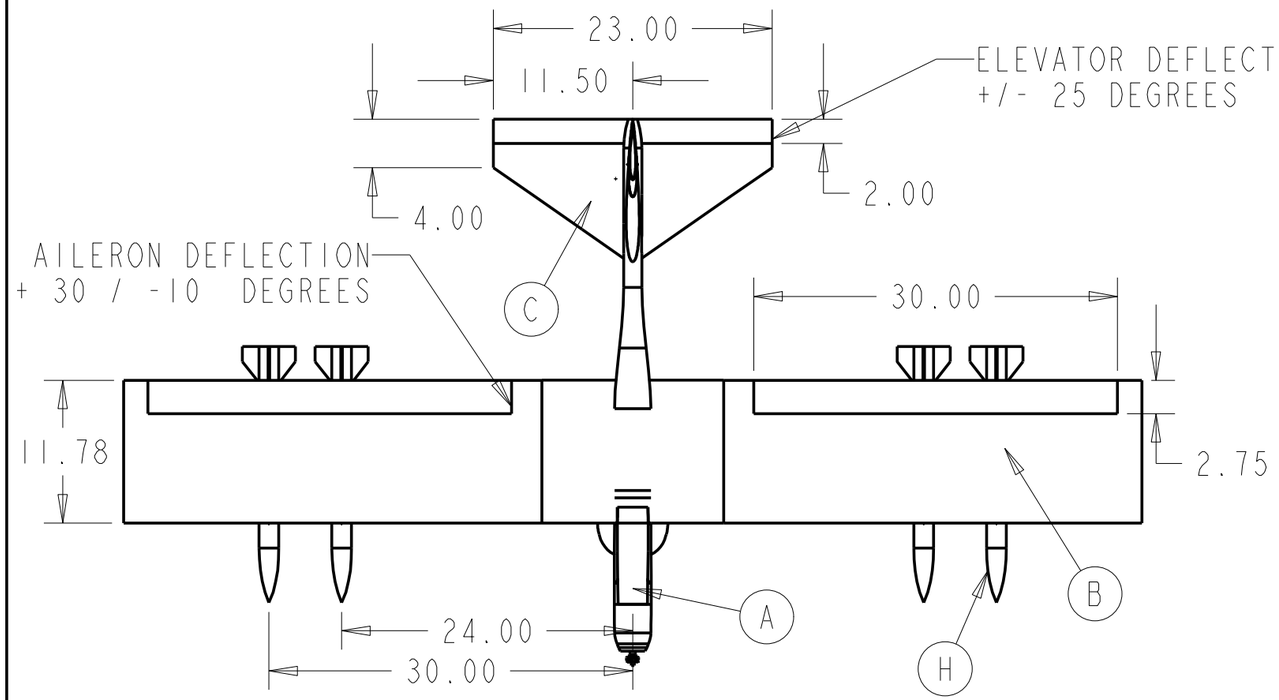

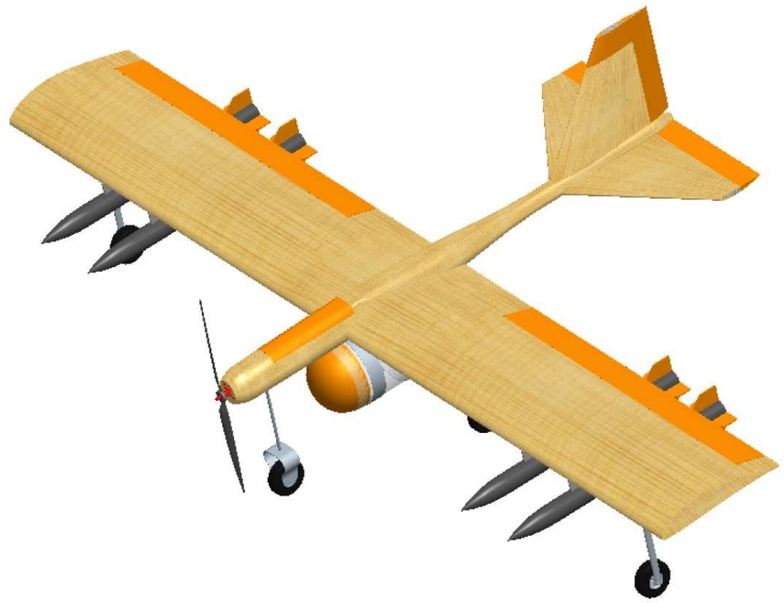

PROP DIAMETER
19 INCHES

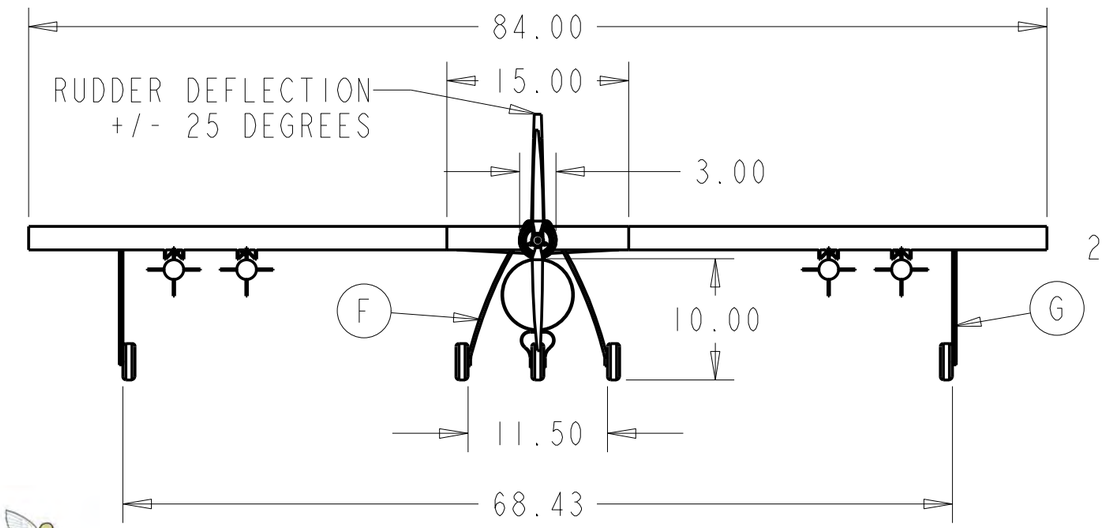

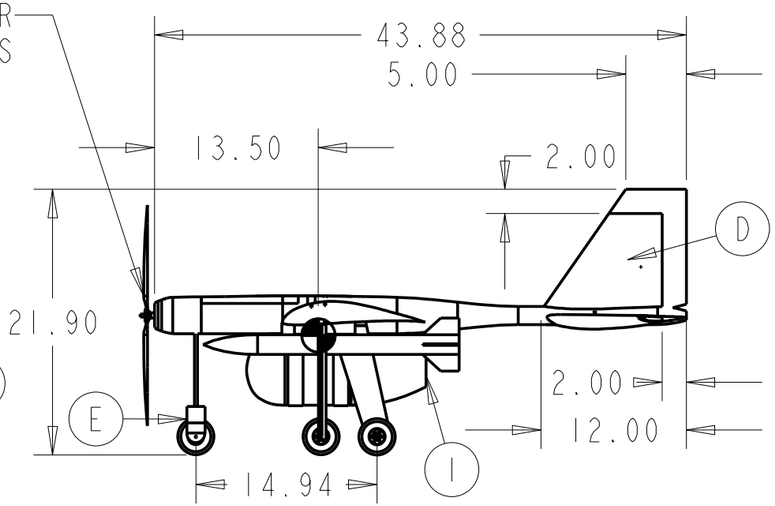

PRIMARY COMPONENT LIST	
A	FUSELAGE
B	WING
C	HORIZONTAL STABILIZER
D	VERTICAL STABILIZER
E	NOSE GEAR
F	MAIN LANDING GEAR
G	OUTRIGGER GEAR
H	WING TIP PAYLOADS
I	CENTER LINE PAYLOAD

PROJECT TITLE
THE SLUGGER

OKLAHOMA STATE UNIVERSITY ORANGE TEAM
CESSNA/RAYTHEON MISSILE SYSTEMS DESIGN/BUILD/FLY 2009

3 - VIEW

CHIEF ENGINEER: J. HILL
STRUCTURES LEAD: C. KAMANI
DRAWN BY: T. HOPKINS
FACULTY ADVISOR: DR. A. ARENA

REVISION 1

NOTE: ALL DIMENSIONS ARE GIVEN IN INCHES

DATE OF APPROVAL: 2-21-09

DRAWING PACKAGE

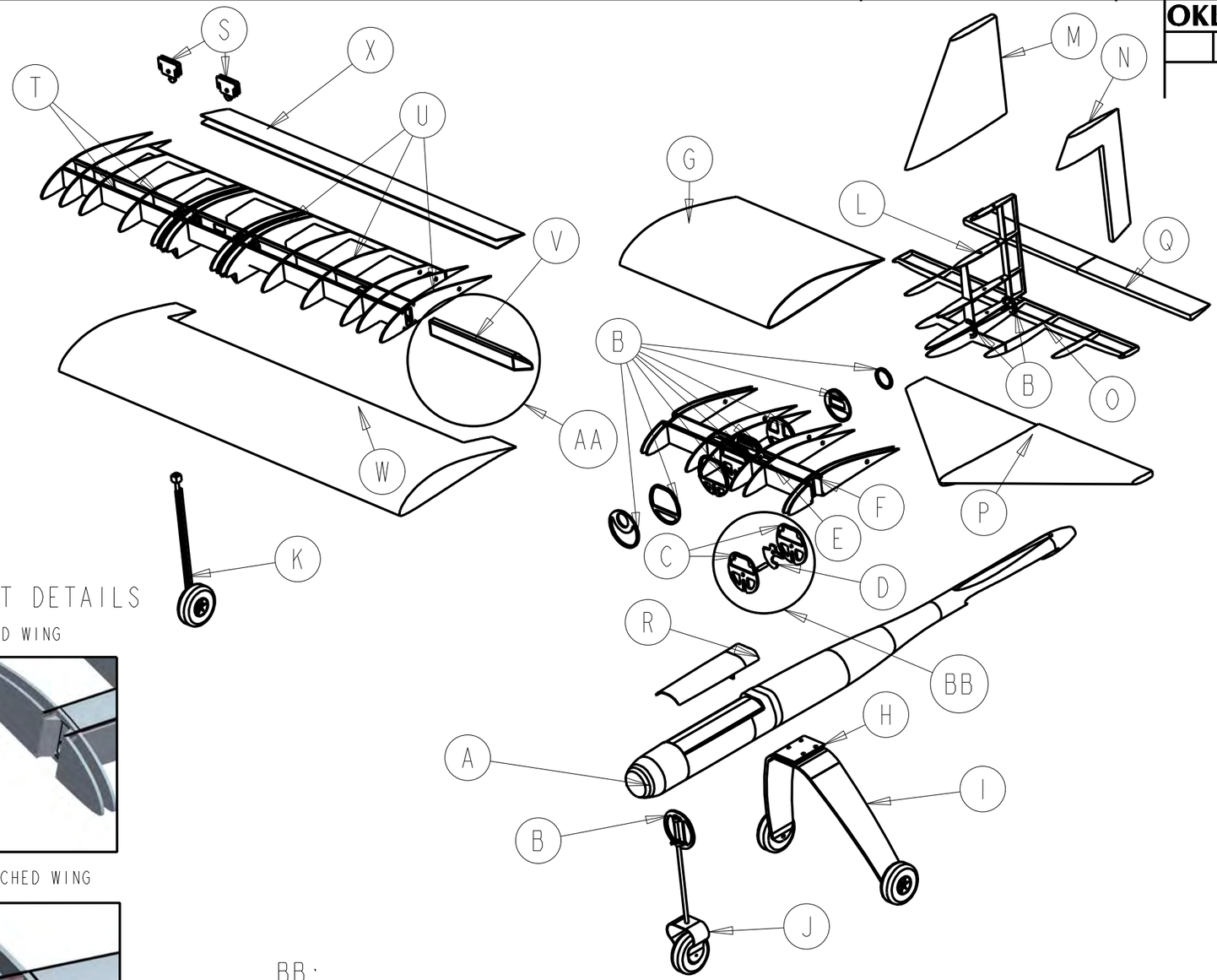

AA:
WING INSERT DETAILS

UN-ATTACHED WING

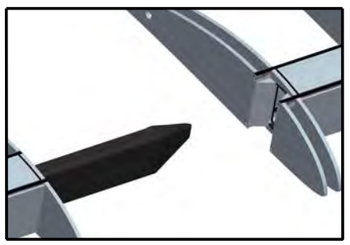

PARTIALLY ATTACHED WING

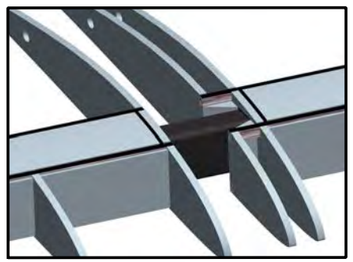

BB:
CENTERLINE RELEASE ASSEMBLY DETAILS

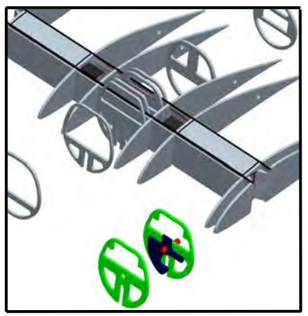

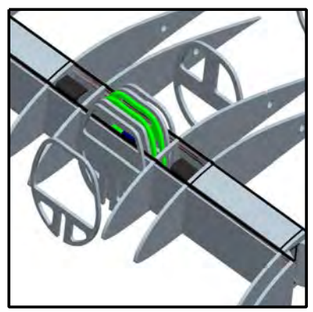

OKLAHOMA STATE UNIVERSITY ORANGE TEAM

2-21-09

	COMPONENT	MATERIAL
B	FUSELAGE BULKHEAD	FIBERGLASS/LIGHT PLYWOOD
C	RELEASE MECH. BULKHEADS	FIBERGLASS/LIGHT PLYWOOD
D	CENTER RELEASE HOOK	ALUMINIUM
E	CENTER WING STRUCTURE	FIBERGLASS/BALSA/CARBON
F	WING INSERT RECIEVER	CARBON FIBER
G	CENTER WING SKIN	BALSA/MONOKOTE
H	MAIN GEAR ATTACH PLATE	FIBERGLASS/LIGHT PLYWOOD
I	MAIN GEAR ASSEMBLY	CARBON/KEVLAR/BALSA LIGHTWEIGHT WHEELS
J	NOSE GEAR ASSEMBLY	CARBON ROD/KEVLAR LIGHTWEIGHT WHEEL
K	OUTRIGGER GEAR	CARBON ROD/AL FARING LIGHTWEIGHT WHEELS
L	VERTICAL TAIL STRUCTURE	BALSA WOOD
M	VERTICAL TAIL SKIN	BALSA/MONOKOTE
N	RUDDER	BALSA/MONOKOTE
O	HORIZONTAL TAIL STRUCTURE	BALSA WOOD
P	HORIZONTAL TAIL SKIN	BALSA/MONOKOTE
Q	ELEVATOR	BALSA/MONOKOTE
R	BATTERY HATCH	FIBERGLASS/BALSA
S	WINGSTORE RELEASE MECH.	ALUMINIUM FIBERGLASS/LIGHT PLYWOOD
T	MAIN WING SPAR	BASSWOOD/CARBON TOW
U	MAIN WING RIBS	BALSA WOOD
V	MAIN WING INSERT	CARBON FIBER
W	MAIN WING SKIN	BALSA/MONOKOTE
X	AILERON	BALSA/MONOKOTE

PROJECT TITLE
THE SLUGGER

OKLAHOMA STATE UNIVERSITY ORANGE TEAM
CESSNA/RAYTHEON MISSILE SYSTEMS DESIGN/BUILD/FLY 2009

CHIEF ENGINEER J. HILL

STRUCTURES LEAD C. KAMANI

DRAWN BY T. HOPKINS

FACULTY ADVISOR DR. A. ARENA

STRUCTURAL ARRANGEMENT

REVISION 1

DATE OF APPROVAL 2-21-09

DRAWING PACKAGE

OKLAHOMA STATE UNIVERSITY ORANGE TEAM

2-21-09

CC:

BATTERY INSTALLATION DETAIL

BATTERY HATCH OPEN

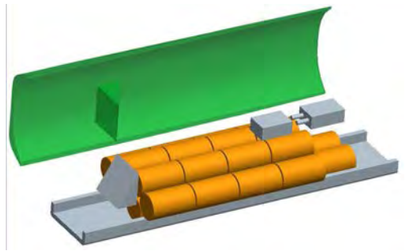

BATTERY HATCH CLOSED

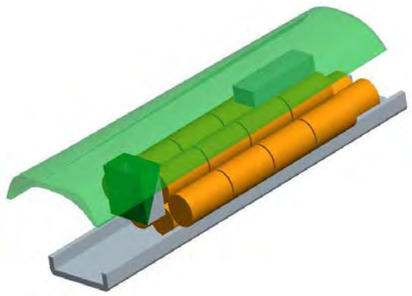

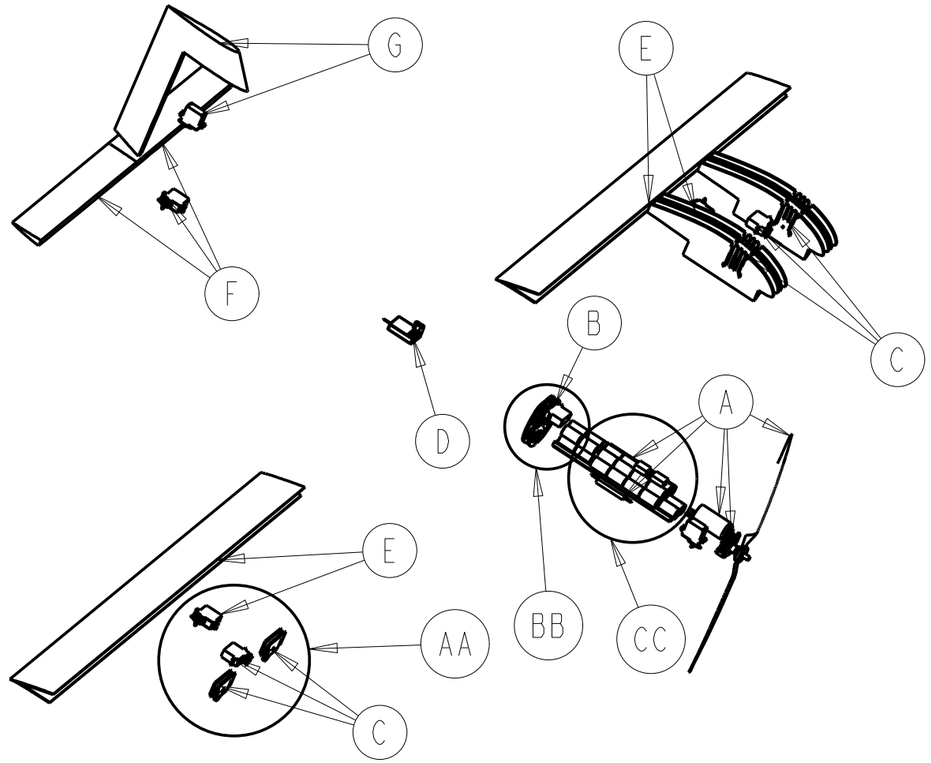

	SUB-SYSTEM	COMPONENTS
A	PROPULSION	MOTOR/BATT/GB/SPEED CONT/PROP
B	CENTERLINE PAYLOAD RELAESE	HOOK/SERVO/MOUNT
C	WING TIP PAYLOAD RELEASE	HOOK/SERVO/MOUNT
D	RECEIVER	RECEIVER
E	ROLL CONTROL	AILERONS/SERVOS
F	PITCH CONTROL	ELEVATORS/SERVO
G	YAW CONTROL	RUDDER/SERVO

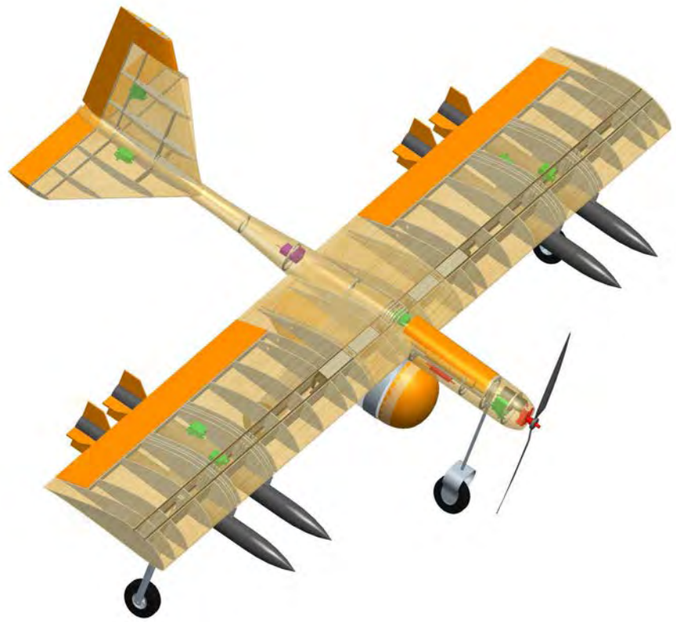

AA:
WINGSTORE RELEASE

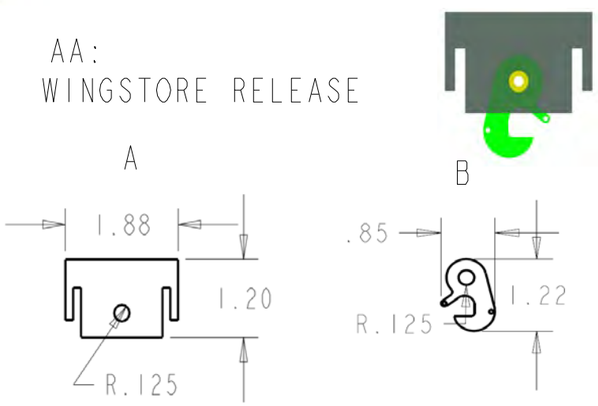

BB:
CENTERLINE RELEASE

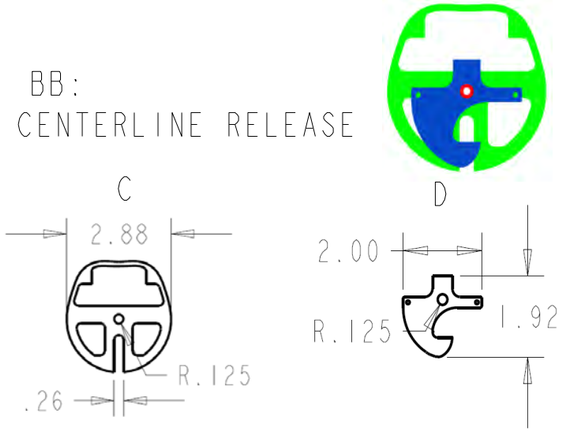

	COMPONENT	MATERIAL	COMMENTS
A	WINGSTORE RELEASE HOOK MOUNTING PLATE	FIBERGLASS/LIGHT PLYWOOD	SLIDES INTO WING RIBS FOR SUPPORT AND EASE OF REMOVAL FOR MAINTENANCE
B	WINGSTORE RELEASE HOOK	ALUMINIUM	CUT PRECIESLY USING COMPUTER NUMERICAL CONTROL MILL
C	BULKHEAD/CENTERLINE RELEASE MOUNT	FIBERGLASS/LIGHT PLYWOOD	EFFICIENTLY TRANSFERS LOAD FROM PAYLOAD INTO FUSELAGE
D	CENTERLINE RELEASE HOOK	ALUMINIUM	CUT PRECIESLY USING COMPUTER NUMERICAL CONTROL MILL

PROJECT TITLE: **THE SLUGGER**

CHIEF ENGINEER: J. HILL
STRUCTURES LEAD: C. KAMANI
DRAWN BY: T. HOPKINS
FACULTY ADVISOR: DR. A. ARENA

OKLAHOMA STATE UNIVERSITY ORANGE TEAM
CESSNA/RAYTHEON MISSILE SYSTEMS DESIGN/BUILD/FLY 2009

SYSTEMS LAYOUT

REVISION 1 | NOTE: ALL DIMENSIONS ARE GIVEN IN INCHES

DATE OF APPROVAL: 2-21-09 | DRAWING PACKAGE |

OKLAHOMA STATE UNIVERSITY ORANGE TEAM

2-21-09

WINGSTORE CONNECTION DETAIL

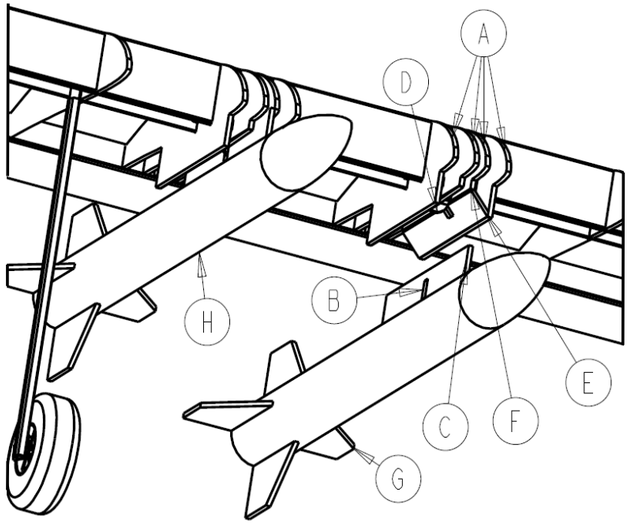

A	RELEASE RIB STRUCTURE
B	ATTACHMENT SLOT
C	GUIDE RAIL
D	HOOK
E	GUIDE BAFFLE
F	RAIL SLOT
G	UNSECURED
H	SECURED

CENTERLINE PAYLOAD FAIRINGS AND DIMENSIONS

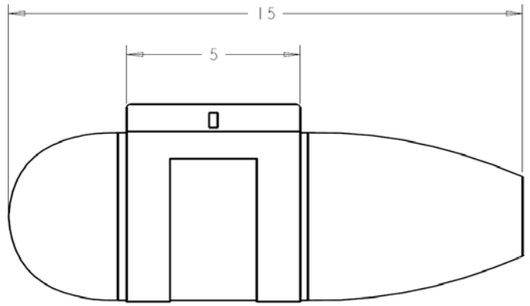

MISSION SPECIFIC PAYLOAD CONFIGURATIONS

MISSION 1 / 2

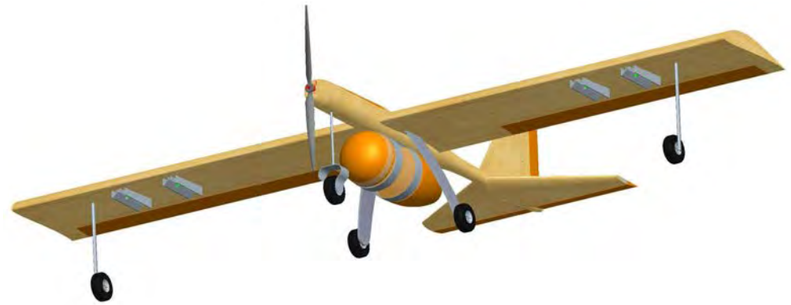

MISSION 3 FULLY LOADED

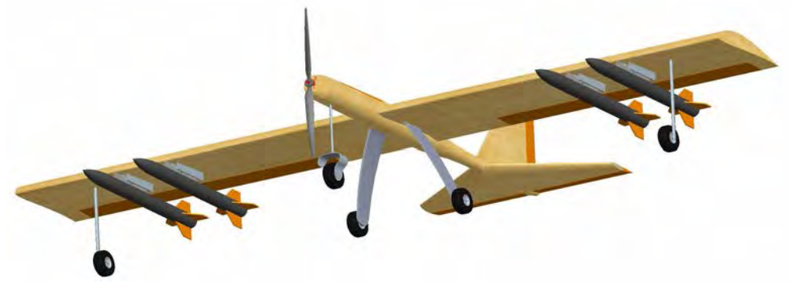

MISSION 3 FULLY ASYMMETRIC

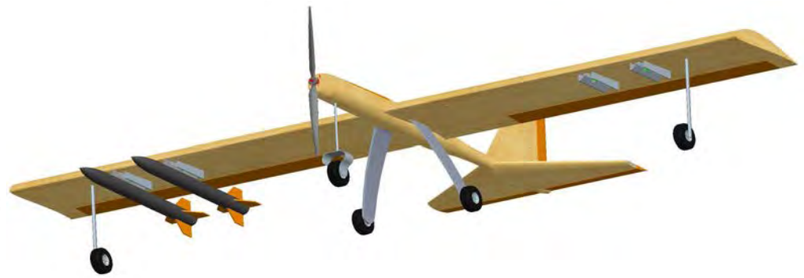

WING TIP AND CENTER LINE PAYLOADS SECURED

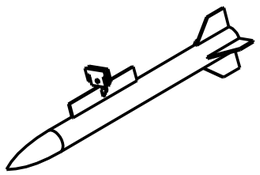

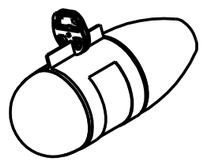

CENTERLINE CONNECTION DETAIL

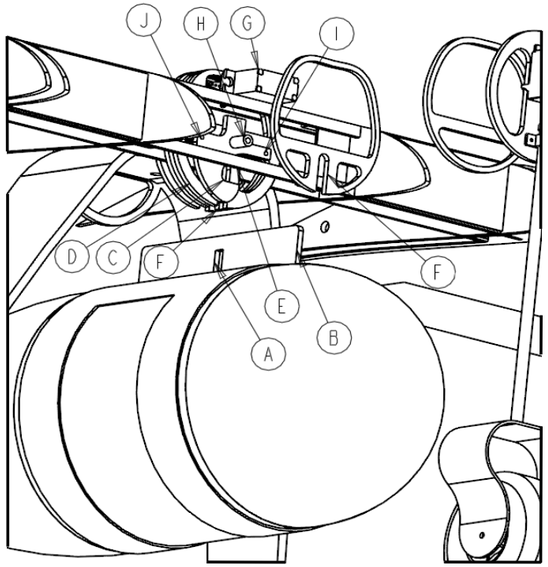

A	ATTACHMENT SLOT
B	GUIDE RAIL
C	HOOK
D	SUPPORT BULKHEAD
E	WING SPAR
F	RECESSED RAIL SLOT
G	SERVO
H	PIVOT BUSHING
I	SPRING ATTACHMENT
J	SERVO ATTACHMENT

PAYLOADS UNSECURED EXPLODED VIEW

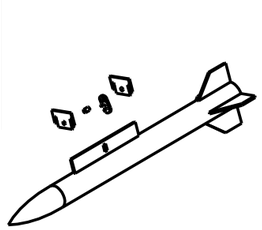

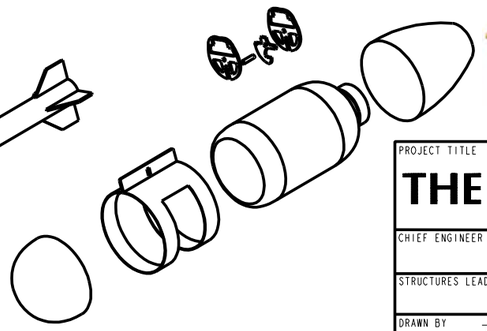

PROJECT TITLE	THE SLUGGER
CHIEF ENGINEER	J. HILL
STRUCTURES LEAD	C. KAMANI
DRAWN BY	T. HOPKINS
FACULTY ADVISOR	DR. A. ARENA

OKLAHOMA STATE UNIVERSITY ORANGE TEAM
CESSNA/RAYTHEON MISSILE SYSTEMS DESIGN/BUILD/FLY 2009

PAYLOAD ACCOMODATION

REVISION 1

NOTE: ALL DIMENSIONS ARE GIVEN IN INCHES

DATE OF APPROVAL 2-21-09

DRAWING PACKAGE

OKLAHOMA STATE UNIVERSITY ORANGE TEAM

2-21-09

STORED SIDE VIEW

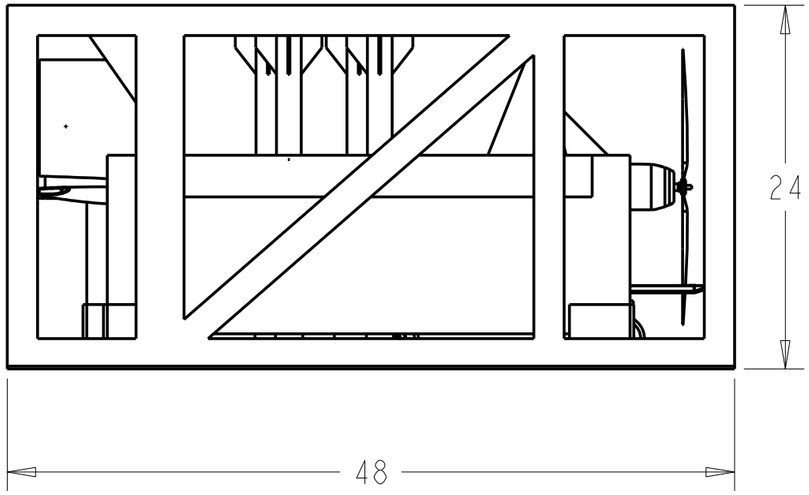

STORED TOP VIEW

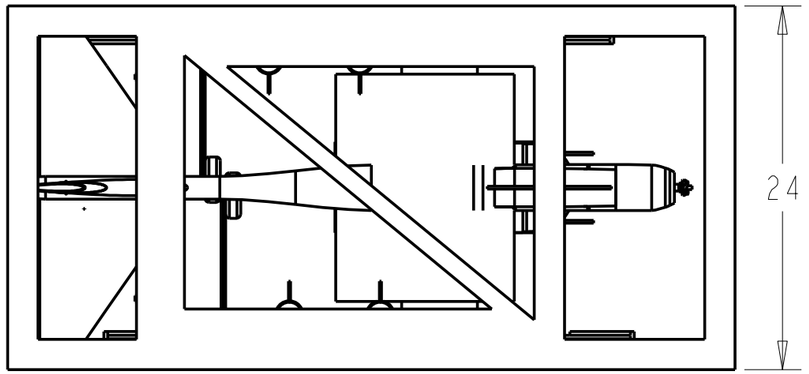

BOX OPEN PRE-ASSEMBLY

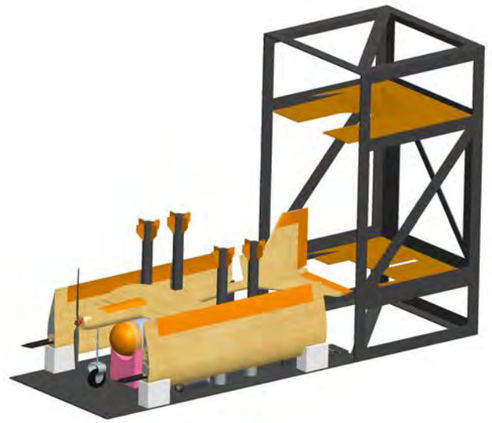

STORED CONFIGURATION

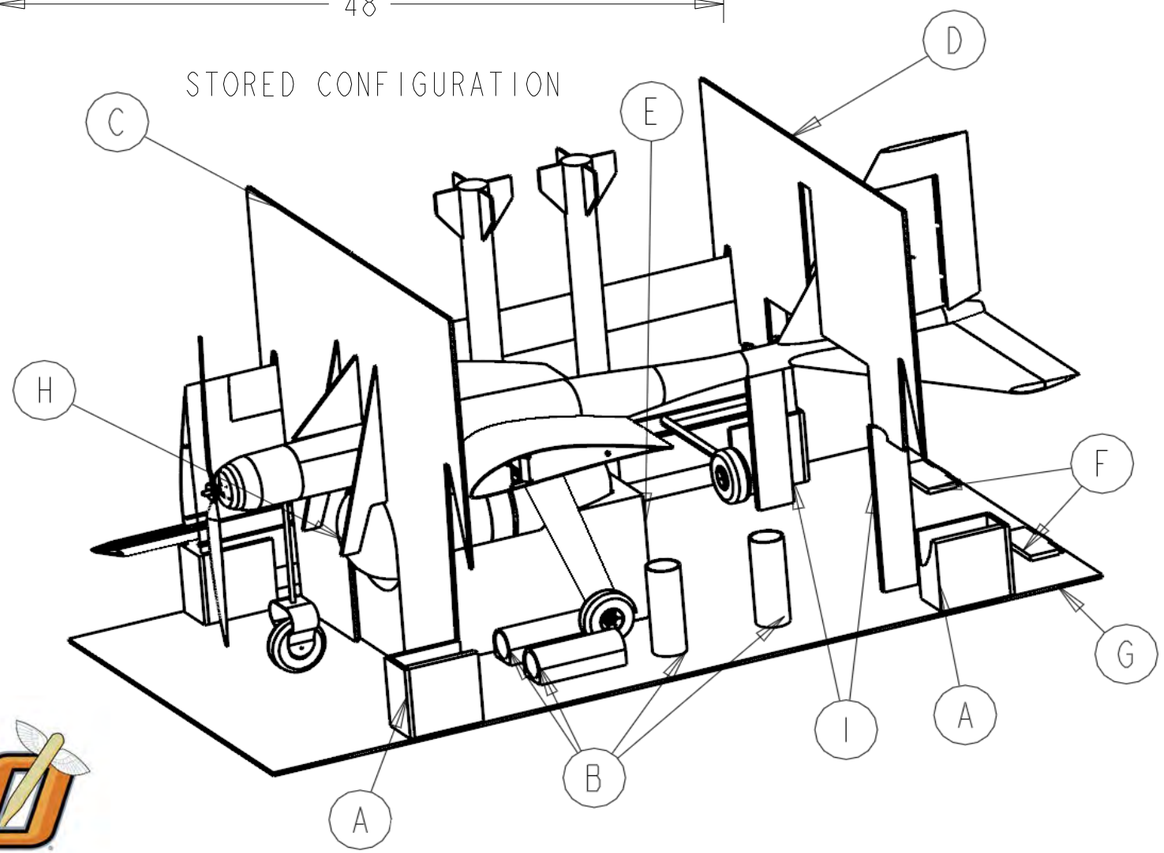

A	WING CRADLE
B	WINGSTORE CRADLE
C	FORWARD RESTRAINT
D	AFT RESTRAINT
E	CENTERLINE PAYLOAD CRADLE
F	BOX HINGES
G	BOX BASEPLATE
H	CENTERLINE PAYLOAD RESTRAINT ARM
I	AFT RESTRAINT SUPPORT ARMS

BOX OPEN POST-ASSEMBLY

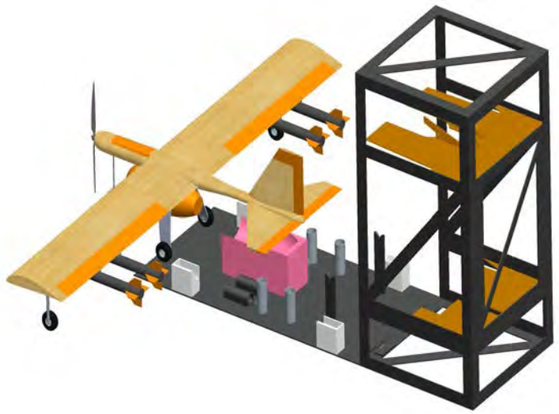

PROJECT TITLE
THE SLUGGER

OKLAHOMA STATE UNIVERSITY ORANGE TEAM
CESSNA/RAYTHEON MISSILE SYSTEMS DESIGN/BUILD/FLY 2009

STORED CONFIGURATION

CHIEF ENGINEER: J. HILL
STRUCTURES LEAD: C. KAMANI
DRAWN BY: T. HOPKINS
FACULTY ADVISOR: DR. A. ARENA

REVISION 1

NOTE: ALL DIMENSIONS ARE GIVEN IN INCHES

DATE OF APPROVAL: 2-21-09

DRAWING PACKAGE

University of Southern California

2009 AIAA/Cessna/Raytheon Design/Build/Fly Competition

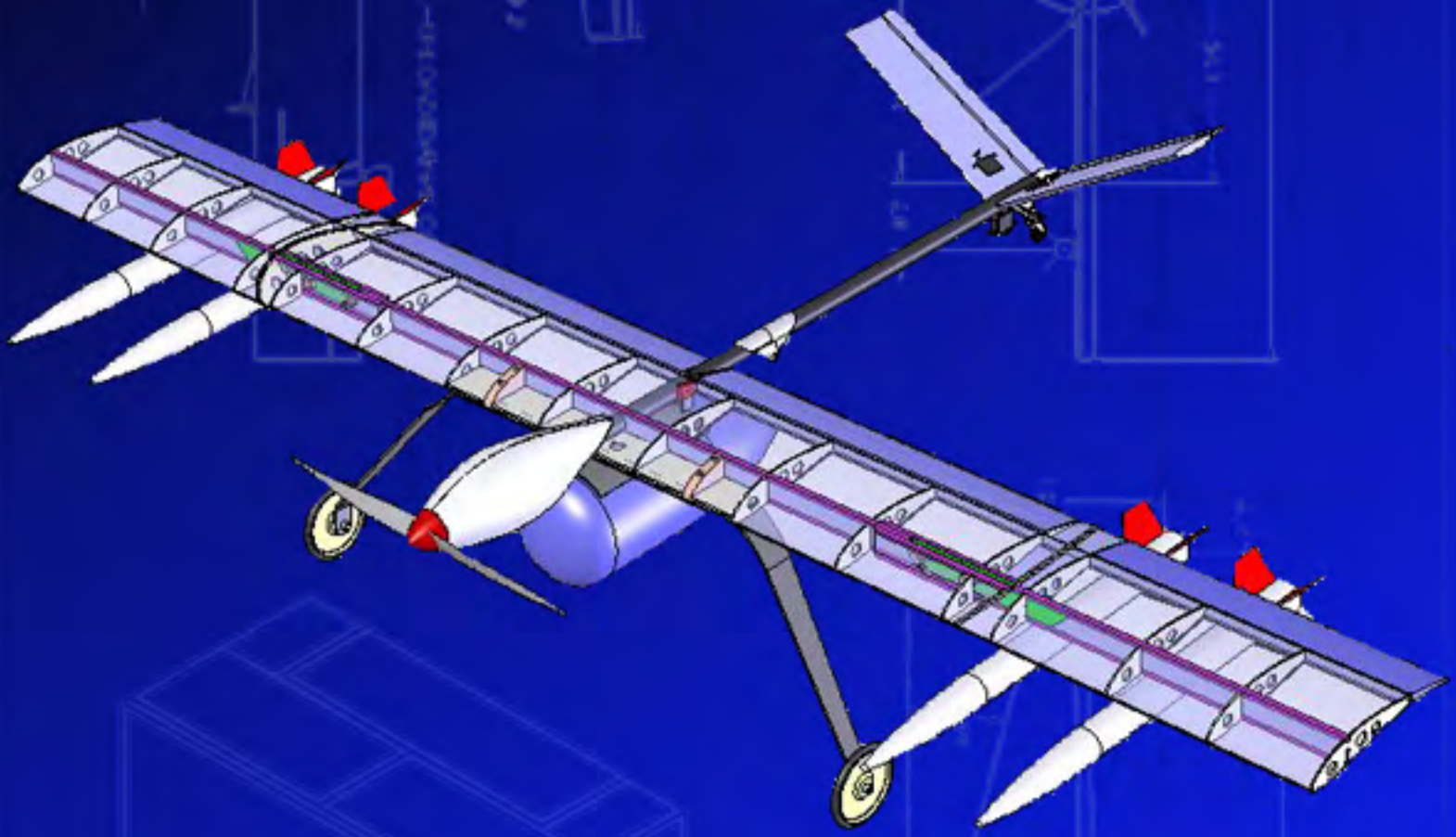

Turbo Encabulator

Aircraft Design Report

Table of Contents

1.0 Executive Summary

This report details the design, construction, testing processes and results of the University of Southern California's submittal for the 2008-2009 AIAA Design/Build/Fly competition. The program's aim was to produce a system that maximized the total score according to the supplied equations. The resulting design was a lightweight, efficient solution capable of completing all ground and flight missions.

The scoring for this year's competition was dependent upon two equally weighted elements: a written report score and a total flight score. The total flight score depended upon three unequally weighted missions: the Ferry Flight (50 points), the Surveillance Flight (75 points), and the Store Release/Asymmetric Loads (100 points). The score of each mission was multiplied by the System Complexity Factor (SCF) – the inverse product of the Rated Aircraft Cost (RAC) and the assembly time of the system. The 2009 requirements defined the RAC as the weight of the storage boxes, air vehicle, and all associated equipment. The ferry flight mission required a fast aircraft capable of a 2-lap dash with the empty tank, while the surveillance flight simply required the completion of 4 aerial laps with a ballasted centerline fuel tank, while. The store release missions required the quick loading of the four wingtip rocket stores before flight and the successive deployment of the rockets.

Through early score analyses and subsequent trade studies, the team determined that the most significant design variable was assembly time followed by the RAC. Analysis showed that the team that assembled and loaded their system the fastest and could complete all missions with a minimal RAC would be the likely winner. Therefore, an aggressive configuration, sizing, and aerodynamic program was pursued to minimize the system's assembly time, loading time, and weight.

The program began with a conceptual design phase to select the primary configuration and the main subcomponents. A list of possible wing-body configurations was first compiled; a figure-of-merit-based downselect process and top-level stability-and-control analyses was used to select the final design. As a result, a simple monoplane configuration was chosen. Concurrently, a clamshell box was selected for the storage container. The ensuing preliminary and detailed design phase was used to develop the monoplane and box concepts in order to maximize score. An aircraft and box pair was constructed after the conclusion of each phase. Trade studies in the team's MDO code and independent subteam examinations varied key system parameters until an optimum solution was converged upon.

The final aircraft used a hybrid balsa-fiberglass build for a lightweight, robust vehicle. The plane's storage box was constructed from a fiberglass-over-foam support frame and covered with a thin nylon. Twelve layers of 3 oz. unidirectional prepreg carbon fiber composed the main bow of the tail-dragger landing gear. With a 6.7 ft wingspan, a total wing planform area of 5 ft^2, and a V-tail, the plane flew with a Neu 1506/2Y/5.2 motor. Fifteen GP 2200 NiMH batteries and a 16x10 propeller were used for the ferry flight, 12 GP 3300s and a 17x10 propeller for the surveillance mission, and 10 GP 4600s with a 17x10 prop were flown for the store release sortie. Assembly time was initially estimated at 9 seconds, while RAC and loading time have been predicted as 28 lb and 5 seconds, respectively.

Flight testing indicated the aircraft was able to satisfy all mission requirements: minimize lap time

for the ferry mission, sufficiently trim the asymmetric load and achieve the necessary endurance for the store release flight, and satisfy TOFL requirements while flying with the ballasted bottle in the surveillance mission. Ground tests confirm minimized assembly and loading times. Together, the *Turbo Encabulator* maximized the flight score as the optimum system solution.

2.0 Management Summary

The 2008-2009 USC AeroDesign Team consisted of 36 undergraduate and graduate students from six different majors. The student-run organization was entirely extracurricular. To maximize efficiency, the team has modeled its organization and methodology after existing industry standards.

2.1 Team Organization

The team used a hierarchical structure to facilitate active collaboration amongst all its members. Figure 1 shows the team architecture. The team leaders were the Program Manager and Chief Engineer. The Program Manager oversaw all aspects of the team and was primarily responsible for facilitating its productivity. She oversaw scheduling, budget, procurement, and weekly team meetings. The Chief Engineer worked actively with the design and manufacturing groups as the iterative nature of the design project required constant communication and cooperation.

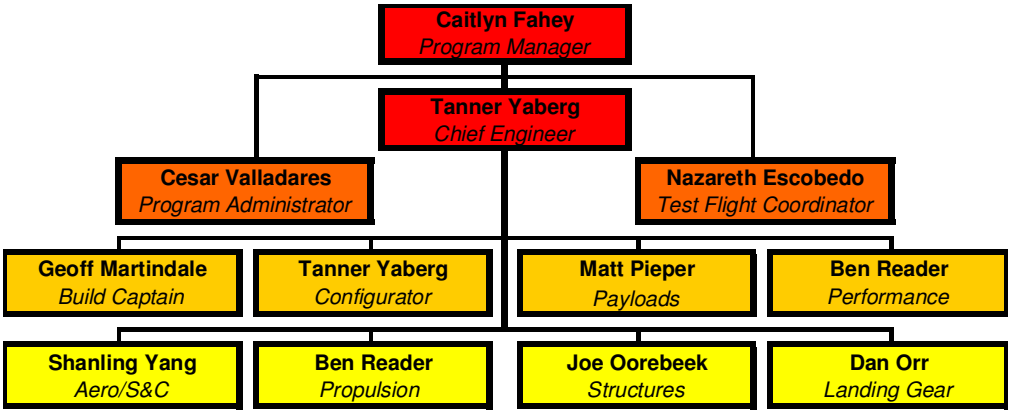

Figure 1: USC AeroDesign Team architecture.

2.2 Subgroups

The individuals shown in Figure 1 led the 10 subgroups into which the team was divided:

- **Program Administrator** was responsible for recording minutes at team meetings. The group aided the Program Manager in procurement and attended school fiscal meetings.
- **Test Flight Coordinator** was responsible for planning and executing all tests that involved the complete aircraft. The test flight coordinator debriefed the pilot after every flight attempt.
- **Build** oversaw the construction of the entire aircraft and individual components. The build captain scheduled lab sessions and maintained the lab facilities and equipment.
- **Configuration** created 3D models of the airplane and subcomponents, as well as the engineering drawings using SolidWorks.
- **Payloads** designed and integrated the loading and deployment systems as well as the restraints for the payloads. This team was also designed and constructed the storage boxes.

- **Performance** was the focal point of the iterative design process. This subgroup led the sizing effort carried out in the team's multidisciplinary optimization tool.
- **Aerodynamics and Stability & Control** used a suite of analytical tools to execute all studies related to the in-flight performance of the airplane.
- **Propulsion** conducted mathematical analysis and testing of the electric motors and batteries.
- **Structures** was responsible for the load-bearing components of the airplane and material testing.
- **Landing Gear** sized and integrated the landing gear into the structural design of the airframe.

2.3 Scheduling

The schedule, shown in Figure 2, was updated weekly by the Program Manager to adapt to unforeseen obstacles and to ensure the team met key milestones such as design reviews and test flights.

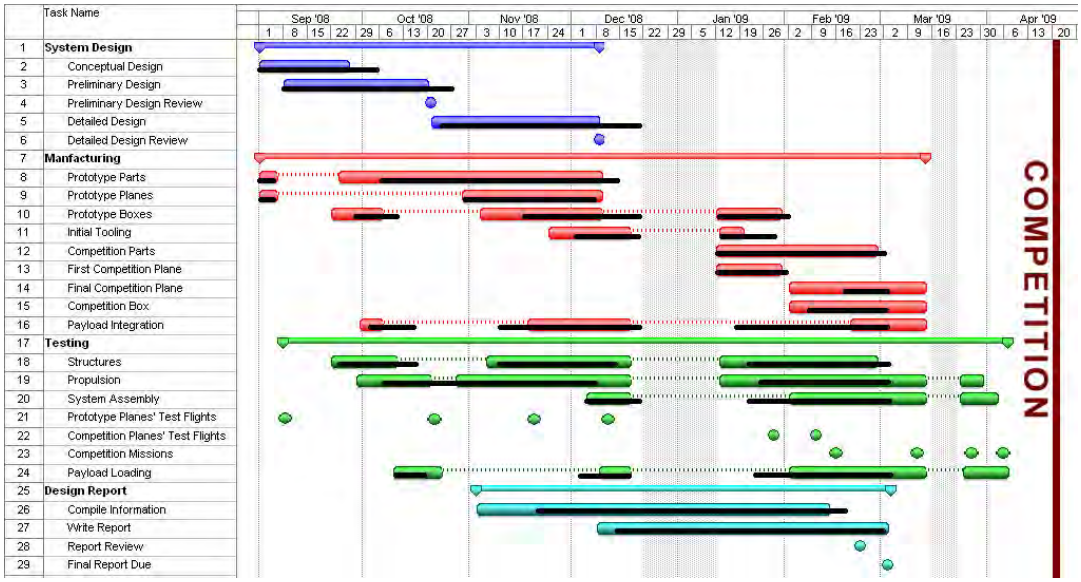

Figure 2: Master schedule with the actual durations shown in black until the date of report submittal.

3.0 Conceptual Design

The 2008-2009 Design/Build/Fly competition consisted of three flight missions and one ground mission. The conceptual design process used to achieve the best solution for each mission began with a detailed examination of the mission requirements, an ensuing score analysis, and a figure of merit analysis for the general configuration. The subsequent selection of secondary systems followed. This process, shown in Figure 3, is discussed in detail below.

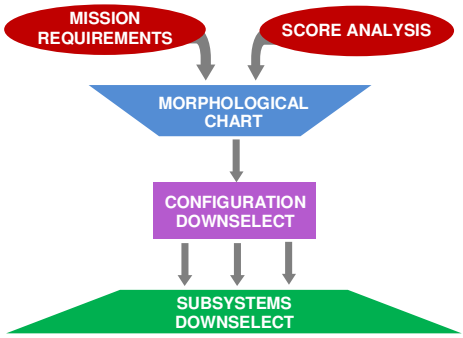

Figure 3: Methodology used to select the airplane and box concepts.

3.1 Mission Requirements

The competition score was determined by SCORE = (Written Report Score) x (Total Flight Score). The total flight score was the sum of the normalized scores of the ground and flight missions, which involved the two types of payloads shown in Figure 4. For the 2009 competition, missions were to be completed in the order presented below.

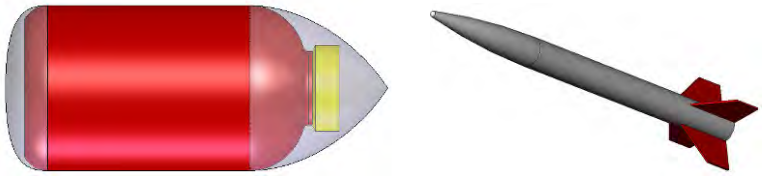

Figure 4: Simulated fuel tank (left) with optional fairings displayed in grey; one Estes Patriot rocket (right).

3.1.1 Assembly Mission

The first task began with the complete system (aircraft, transmitter, flight and receiver battery packs, assembly tools, ballasted payloads, and payload pylons) secured within a maximum of two 2x2x4 ft storage boxes. The loaded boxes' combined weight established the Rated Aircraft Cost (RAC). A 6 in. drop onto any box face tested the durability of each box and its contents.

A pit crew consisting of three team members completed the assembly portion of the ground mission. With the complete system stowed, the pit crew was timed as they removed the airplane from the storage boxes, installed the payloads, and re-secured the boxes and any assembly tools used. The flight-ready airplane demonstrated full functionality once timing concluded. The score for this mission was determined by the System Complexity Factor (SCF), given as SCF = 1 / (Assembly Time x RAC). The SCF was normalized to a maximum of 10 for each team that completed at least one flight mission.

3.1.2 Ferry Flight Mission

The payload for the first flight mission was one empty 4 liter simulated fuel tank carried on the aircraft centerline. It was capable of being remotely released. This plastic bottle measured 11.25 in. long and 6 in. in diameter and weighed approximately 0.6 lb. The addition of fairings was permitted provided that the total length of the payload did not exceed 15 inches.

This timed flight mission required the completion of two laps around the flight course. Timing began once the throttle was advanced and ended once the aircraft crossed the finish line in the air. A successful landing was necessary for completion. The ferry flight's score was recorded as SCORE = SCF / (Flight Time) and was normalized to a maximum of 50 points.

3.1.3 Surveillance Flight Mission

The second flight mission required the vehicle to carry the tank filled entirely with water, for a total weight of approximately 9 lb. Once four aerial laps and a successful landing were completed, the score was recorded as the SCF, with a maximum score of 75 points.

3.1.4 Store Release Flight Mission

Aircraft carried four Estes Patriot rockets, shown in Figure 4, ballasted to 1.5 lb each and measuring 21 in. long. Two rockets were carried on each wingtip. The innermost rocket was placed at a

minimum of 24 in. outboard from the airplane's centerline with at least a 6 in. separation between it and the outboard rocket. Like the simulated fuel tank, each rocket had to be capable of remote deployment.

The timed loading of the wingtip stores was executed before the flight attempt. With the airplane already unpacked and assembled, timing commenced when the rockets were removed from the storage boxes and installed on the vehicle. Once all tools were stowed within the secured boxes, timing stopped. A shake test was performed to ensure no store was loose prior to takeoff.

The aircraft first took off with all four rockets installed, completed one lap, and landed. Upon taxiing to a designated 10 ft square area the pilot deployed one rocket. The plane performed a full stop at the starting line before repeating the procedure until one store remained. The store release sequence was communicated to the pilot immediately before flight and could vary from flight to flight. A maximum of 100 points was achievable for this mission, which was scored by SCORE = SCF / (Loading Time).

3.2 Score Analysis

The first step in the conceptual design process was to perform a comprehensive study of the contest rules and develop a strategy to maximize the team's total score. An initial score analysis was performed to understand the effect that key aspects of the system's design would have on the total score.

3.2.1 Rules Interpretation

In 2009, the project encompassed a broader scope than the team had experienced in past years. The competition favored an airplane capable of completing all the tasks outlined in the rules in order to be competitive, as a larger fraction of the total flight score laid with the latter, more difficult missions. Because the final mission's store release sequence was not disclosed prior to the date of the contest, the team was forced to contend with the possibility of carrying a large asymmetric lateral load.

The first task was to evaluate each variable's effect on the total flight score. The individual mission scores were consolidated into a single equation,

$$FlightScore = \frac{1}{RAC \cdot AT}\left(\frac{50}{FT} + 75 + \frac{100}{LT}\right),$$

where *AT* is the pre-mission assembly time, *RAC* is the Rated Aircraft Cost, *FT* is the ferry mission's flight time, and *LT* is the loading time of the store release task. Table 1 details the percent influence of each component on the total flight score.

Score Variable	Influence on Score (%)
Assembly Time (s)	37.5
RAC (lb)	37.5
Loading Time (s)	16.7
Flight Time (s)	8.33

Table 1. Relative significance of each variable on total score

The results of the study indicated that the two components of the System Complexity Factor, assembly time and RAC, had the greatest impact on the flight score. Contrary to prior years, the RAC now included the weights of the fully packaged storage boxes rather than the weight of the aircraft alone. Together with the value of assembly time, this new RAC requirement highlighted the competition's

emphasis on a system-based solution – a fact further manifested by the SCF's occurrence in each mission's score. Therefore, it was the competition's key measure of performance.

3.2.2 Sensitivity Analysis

An iterative program was developed in Microsoft Excel to identify which components of the SCF most significantly affected the score. These calculations aided in further determining how several physical design parameters drove the flight score. A separate analysis was conducted for each mission. These results were then scaled and added together to form the total flight score.

All system parameters were held constant except RAC, assembly time, and loading time. These variables completely described all four missions' scores except for the ferry task's flight time. Its 8.33% contribution to total score was nominal in comparison to the remaining score constituents. Furthermore, any physical ramifications on the aircraft configuration resulting from flight time studies were fully characterized by the propulsion trade studies presented in the Preliminary and Detailed Design sections.

A flight course was modeled in the Excel program such that the input cruise velocities ranging from 80 to 120 ft/s accurately reflected a flight time. RACs were varied from 21 to 25 lb and assembly times ranged from 11 to 14 seconds. The variables were substituted into each score equation, yielding an array of mission scores. Using data from prior competitions, mission scores were normalized against an assumed best score. Figure 5 shows the overall trends in the total flight scores.

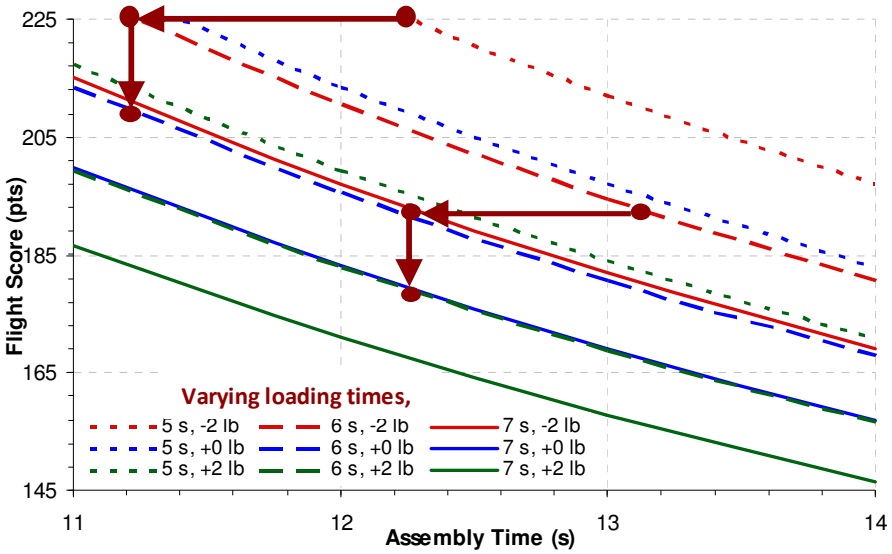

Figure 5: Flight score analysis showing a sampling of cruise velocities and RACs. An 11 second assembly time and a 21 lb RAC was assumed optimum based off of prior competition experience.

3.2.3 Conclusions

Though the results differed slightly at the extremes of the input range, the conclusion was clear. The score was dramatically more sensitive to assembly time than to any other parameter. The same total flight score was achievable for a light plane that was assembled slowly as for a heavy plane that was assembled quickly. Specifically, the results shown in Figure 5 uncovered that 1.5 seconds of assembly time equated to 2 lb of system weight, 1 second of loading time, and a 14 point change in total score. A

subsequent analysis also revealed that 1.3 minutes of flight time per lap could be gained with a 1.5 second quicker assembly time at no detriment to score. It was clear that a fully integrated design—that made some performance sacrifices to favor assembly time—was essential. With the importance of assembly time known, the team moved into the downselect process. The results of the score analysis inspired many of the proposed configurations and motivated many of the decisions during the configuration downselect.

3.3 Configuration Downselect

The downselect process aimed to integrate the major components of the aircraft and its payloads to allow for optimal performance in all missions. Each aspect of the design was analyzed separately.

3.3.1 Morphology Chart

While the storage boxes were the most vital in minimizing assembly time, the aircraft configuration directly affected not only the ground task but the remaining three flight missions as well. Therefore, a comprehensive study was first performed on the plane. Table 2 shows a morphology chart outlining all reasonable selections for the major components of the aircraft. Many unconventional options were considered due to the asymmetric flight loads and in order to minimize assembly time.

System	Solutions			
Body	Conventional	Blended	Lifting	Multiple
Wing	Monoplane	Biplane	Tandem	Joined
	Diamond	Oblique	Blended	
Empennage	Conventional	T-Tail	H-Tail	V-Tail
	Inverted V-Tail	Bronco	Cruciform	
Landing Gear	Tricycle	Bicycle	Retracts	
	Skid Plate	Tip Gear	Tail-Dragger	
Propulsion	Tractor	Pusher	Twin	

Table 2. Morphology Chart

3.3.2 Configurations

The team combined the solutions shown in Table 2 into potential wing-body configurations. Several candidates were eliminated due to complexity and past experience. Subsequent downselects were carried out for the empennage, landing gear, and propulsion. The wing-body configurations and their subsequent reasons for consideration were:

- **Monoplane –** Due to its conventional nature and its past success in the contest, the monoplane was chosen as the baseline configuration against which all other designs were compared.
- **Biplane** – To effectively package the plane in the boxes, a biplane of reduced span but equal wing area was considered.
- **Canard Pusher** – The canard's horizontal stabilizer contributes to the overall lift of the airplane and the motor's location does not disturb the airflow over the wing.
- **Blended Wing Body** – The BWB combines the fuselage with the lifting surfaces. It eliminates the tail and reduces the overall wetted area, resulting in a very high L/D.

- **Joined Wing** – The joined wing sweeps the main wing aft to join it to a forward-swept aft-located wing. Placing the control surfaces on the aft wing eliminates the need for a tail to stabilize and control the plane.

3.3.3 Figures of Merit

The configuration downselect used eight figures of merit (FOM) that were based upon the team's past experience and adjusted to suit the 2009 rules. Each FOM was given a weight based upon its perceived importance to the total score for the competition. The FOM's were:

- **Assembly Time (10)** – As shown in the sensitivity analysis, the system's assembly time was a direct, powerful value in all flight scores.
- **System Weight (8)** – Minimizing system weight decreased the RAC and SCF. It can increase aircraft performance, decrease propulsion system size, and decrease assembly time as well.
- **L/D – Endurance (7)** – The aircraft's endurance was a major concern for the surveillance and store release flights as at least four laps were required.
- **Loading Time (7)** – The loading time was a significant portion of the last—and most heavily weighted—mission.
- **Wetted Area – Speed (5)** – Minimizing the wetted area results in less drag, and therefore a higher top speed when trying to maximize the number of laps flown in the ferry flight mission.
- **Stability & Control (5)** – The airplane must be stable and easily controllable so the pilot can effectively navigate the course, respond to flight disturbances, and land in a controlled manner.
- **Ground Handling (3)** – Precise control is required for successful takeoff and landing. The airplane must also demonstrate the ability to taxi to a designated area and stop at the takeoff position before each lap in the store release mission.
- **Manufacturability (1)** – A consideration of the skills, materials, and time needed to properly construct and repair the design.

3.3.4 Downselect Ratings and Results

Using the weighted FOMs, the proposed wing-body configurations were examined against the baseline monoplane. Each design was assumed to have a sufficient propulsion package and wing area for TOFL. A ternary rating system, described in Table 3, was used to assign a score to each FOM for a particular configuration. The total downselect score for each configuration was the sum of the product of the FOM's weight factor and the rating number.

Score	Configuration's Effect on FOM
-1	Configuration negatively affected FOM
0	Configuration neutral to FOM
+1	Configuration positively influenced FOM

Table 3. Downselect rating system

The downselect, shown in Table 4, revealed that the monoplane received the highest score. However, two additional configurations proved promising. More detailed studies were required to

determine if the vortex drag benefits of an endplated biplane could overcome its disadvantageous system weight. Furthermore, it was unknown if the BWB could be made stable while carrying the store release's asymmetric load. All three configurations were studied through an initial performance sizing examination, a preliminary CAD model, and analyses by the Aerodynamics and Stability & Control team.

Figure of Merit	Weight Factor	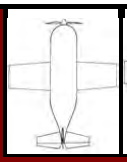 Mono-plane	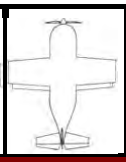 Biplane	 Lifting Body	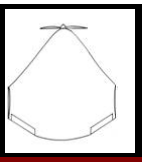 BWB	 Canard Pusher	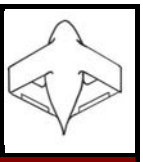 Joined Wing
Assembly Time	10	0	0	0	-1	0	-1
System Weight	8	0	-1	0	1	0	-1
L/D	7	0	1	-1	1	-1	1
Loading Time	7	0	0	-1	-1	0	-1
Wetted Area	5	0	-1	-1	1	-1	-1
S & C	5	0	0	-1	-1	-1	-1
Ground Handling	3	0	0	0	-1	0	0
Manufacturability	1	0	0	0	0	0	-1
TOTAL	**46**	**0**	**-6**	**-24**	**-5**	**-17**	**-29**

Table 4. Configuration downselect

3.3.5 Further Conceptual Analysis

The first task of the Performance team was to create the three configurations sized for a 100 ft TOFL. The output geometries were then given to the Aerodynamics and Stability & Control team for analysis. The construction of foam gliders suggested that the mono- and biplane could both bear the asymmetric lateral load while the tailless BWB, without significant modifications to its geometry, could not.

To quantify these observations, each airplane was modeled and optimized for stability using the team's analytical tool, namely Mark Drela's Athena Vortex Lattice code.[1] A simulated load of two rockets was applied to each model's right wingtip. It was confirmed that the BWB could not be made stable in the lateral axis without excessive wingspan extensions. Packaging would then become more challenging. Moreover, the sweep needed to trim the aircraft in pitch and yaw placed the four wingtip stores significantly aft of the plane's aerodynamic center. Hence the plane was extremely difficult to balance. With an asymmetric load, the already substantial elevon trim drag was further amplified by CG shifts from the rocket deployments.

The monoplane and biplane were stable in all axes given acceptable aileron and rudder deflections. The Configuration team was then responsible for creating a simple outer mold line solid model of these two designs. After sizing the wing takeoff and the tail volume for stability, the geometries were first compared, as shown in Figure 6. The monoplane outperformed the biplane, as its higher aspect ratio yielded a greater cruise efficiency essential to endurance for a given wing area governed by TOFL. More importantly, the weight of the biplane was 9% greater than that of the monoplane, and fears of interference from the additional wing during assembly and store loading arose. As assembly time, system

weight and simplicity were driving factors, the decision was made to pursue the monoplane design.

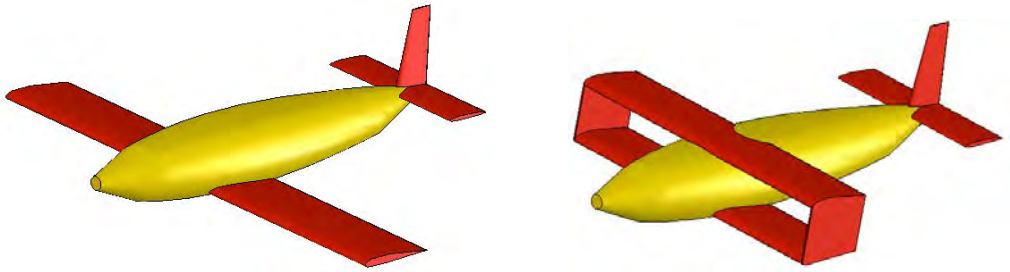

Figure 6: SolidWorks models comparing the OMLs and weights of the mono- and biplanes.

3.4 Systems Downselect

After determining that a monoplane was the best aircraft solution, a downselect was performed for each major subsystem. Decisions regarding these components were made in a logical procession with certain initial decisions affecting those downstream. As with the aircraft configuration, downselects were used to select the optimum configuration for each system. While the ternary rating system of Table 3 still applied, there was no baseline configuration that each option was rated against. Instead, Pugh's method for advanced decision matrices was used, where the sum of the weights is one.[2]

3.4.1 Packaging

Due to the importance of SCF to the total flight score, the initial system downselect evaluated the component that would most greatly affect assembly time and system weight: the storage boxes. It was imperative that they opened quickly and cleanly to facilitate system assembly and payload loading. Furthermore, the boxes had to be designed light enough to benefit RAC.

While a maximum of two boxes was permitted, it was decided that one storage box would save weight. More importantly, by eliminating one box, assembly time would be significantly reduced with the effective use of all three pit crew members. An aircraft that could be adequately packaged into one box would then be sized. The following box configurations were then considered:

- **Clamshell** – A box with unfolding panels provides superior accessibility to the interior contents.
- **Hinged Lid** – The entire top face of a traditional box structure is hinged 225° on one edge. The five remaining faces remain fixed during loading and unloading.
- **Shoebox** – The bottom and side faces are one continuous piece. An upper section with a lip is aligned and fit over the base.

Table 5 shows the optimum box architecture was the clamshell design. Its simple configuration ensured quick opening and closing. Its unfurlable sections offered ample access to the entirety of the enclosed volume, minimizing the possibility for error during the assembly and payload loading tasks. Construction material was assumed the identical for all designs; therefore, weight was not a factor at this stage. Specific packaging details will be discussed in the Preliminary Design section of the report.

Figure of Merit	Weight	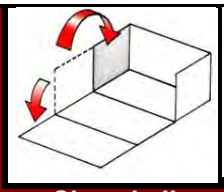 Clamshell	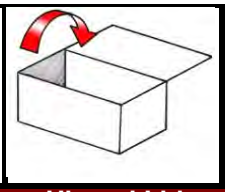 Hinged Lid	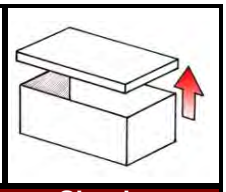 Shoebox
System Assembly Time	*0.55*	1	-1	-1
Payload Loading Time	*0.30*	0	1	0
Component Interference	*0.15*	1	-1	-1
TOTAL	***1.00***	**0.70**	**-0.40**	**-0.70**

Table 5. Storage box downselect

3.4.2 Fuselage

In addition to providing structural support for the empennage and wing, the fuselage has traditionally housed the avionics and payloads in a low drag shell. However, the 2009 contest required all stores to be mounted outside the outer mold line of the aircraft. The types of fuselages considered were:

- **Faired Cylinder –** The traditional design allows for the maximum internal volume.
- **Thin Rod** – A thin rod fuselage would force the centerline payload to be mounted externally in the free stream. A hollow forward fairing could provide housing for the propulsion system.
- **Twin Fuselage** – Two fuselages could better disperse the asymmetric load and allow the simulated fuel tank to be carried in between the individual fuselages.

Based on the criteria presented in Table 6, the decision was made to pursue the thin rod fuselage. By mounting the payloads externally to the rod, precious assembly and loading time was saved. Its slim cross-section allowed for numerous packaging configurations. A more intricate system would have been beyond the scope of current mission requirements and would have hindered RAC.

Figure of Merit	Weight	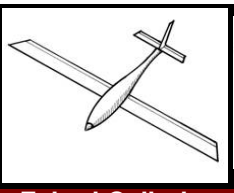 Faired Cylinder	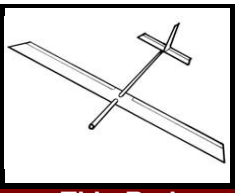 Thin Rod	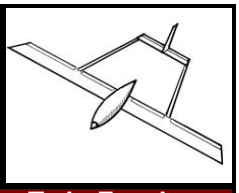 Twin Fuselage
Weight (RAC)	*0.55*	0	1	-1
Drag	*0.30*	0	1	-1
Component Integration	*0.15*	-1	1	0
TOTAL	***1.00***	**-0.15**	**1.00**	**-0.85**

Table 6. Fuselage downselect

3.4.3 Landing Gear

As with past contests, a proper landing gear was needed to maintain control on takeoff and landing. The 2009 contest also demanded precise taxiing to a designated location during the store release mission. Additionally, the landing gear selection also affected the decision on the placement of the water bottle payload. The four gear types included in the downselect were:

- **Conventional Tricycle –** Two wheels compose the main gear with one steerable wheel on the

nose. While stable, prior USC DBF experience has found this option yields heavier main gears.

- **Tip-mounted Tricycle –** The wheels and struts of the main gear are integrated into the wingtips. The wider wheelbase helps prevent tip-over during asymmetric loading.
- **Bicycle –** This light configuration uses two wheels on the centerline and wingtip skegs. Ground handling problems, however, have plagued previous USC bicycle configurations.
- **Tail-dragger –** The main gear is near the front of the plane with a steerable wheel near the empennage. While light, the main gear's length must be long for correct takeoff incidence. Past designs have handled well.

Table 7 shows the optimum landing gear configuration to be a tail-dragger. This configuration provided good handling during crosswind ground roll and provided an advantageous RAC.

		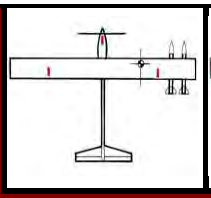	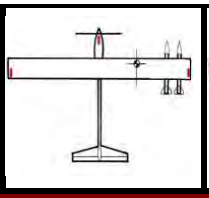	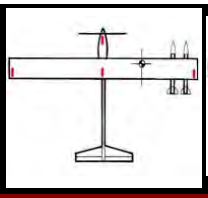	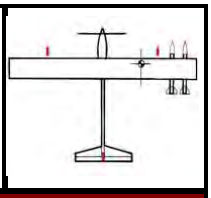
Figure of Merit	**Weight**	**Conv. Tricycle**	**Tip Tricycle**	**Bicycle**	**Tail-dragger**
RAC (Weight)	*0.40*	-1	0	1	1
Ground Handling	*0.30*	1	0	-1	0
Durability	*0.15*	1	0	-1	0
Drag	*0.15*	0	0	1	0
TOTAL	***1.00***	**0.05**	**0.00**	**0.10**	**0.40**

Table 7. Landing gear configuration downselect

3.4.4 Payload Placement

Though the contest rules were specific about the placement of the rockets in the lateral direction, leeway was allowed in their longitudinal positioning. The CG of each rocket was placed at the quarter-chord of the wing in order to eliminate unwarranted pitching moments. All rockets were secured to the underside of the wing to preserve the flow over the top of the airfoil.

An additional consideration was the mechanism needed to compensate for the offset CG during the flight of the asymmetric load. One option was to shift internal weights along the span to counteract this imbalance. However, rather than add additional weight for such a dedicated device, the ailerons were relied upon as a simpler solution. The trim drag induced by a deflected aileron was deemed negligible compared to the detriment to the RAC from an added mechanism.

The simulated fuel tank's CG was also placed at the quarter-chord of the wing. Studies were then needed to determine its vertical placement with respect to the fuselage:

- **Top-mounted** – Mounting the bottle to the top of the fuselage removes any possibility of influence on the landing gear and rotation angle.
- **Bottom-mounted** – By affixing the tank to the plane's underside, the clean upper surface of the wing is preserved. Proximity to the landing gear must be considered.

Table 8 highlights the advantages of a bottle mounted to the underside of the fuselage. There were clear stability advantages during crosswind flight and taxiing. Furthermore, by compactly enveloping

the bottle within the landing gear, tremendous packaging benefits resulted. Specific packaging and loading details will be discussed in depth in forthcoming sections.

Figure of Merit	Weight	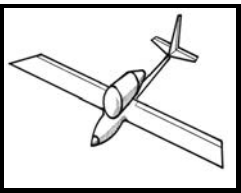 Top-mounted	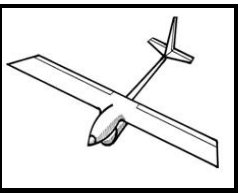 Bottom-mounted
Consolidation	*0.45*	-1	1
Stability	*0.35*	-1	1
Aerodynamics	*0.20*	0	0
TOTAL	***1.00***	**-0.80**	**0.80**

Table 8. Bottle placement downselect

3.4.5 Empennage

The empennage provides stability and control for the airplane during the entire flight regime. Concerns included minimizing assembly time as well as drag and RAC. The designs considered for a single fuselage configuration were:

- **Conventional –** Simple design and simple implementation reduce the RAC associated with a conventional tail while giving all necessary stability and control requirements.
- **T-Tail –** Places the horizontal at the top of the vertical and above the wing wash. Weight concerns arise from the additional structure required and it is ineffective at high angles of attack.
- **V-Tail –** Two surfaces forming a "V" provide both elevator and rudder controls and help decrease wetted area by eliminating one tail surface. Potential RAC increase when coupling rudder controls to a steerable tail dragger wheel.
- **U-Tail –** Two vertical stabilizers are mounted on either end of a horizontal. Gives vertical clearance benefits for comparable stability requirements. The horizontal is more efficiently loaded because the verticals act as winglets.

Table 9 shows the conventional tail as the optimal configuration. Weight and drag are minimized, RAC is increased, and takeoff rotation is unaffected. Though the V-tail and U-tail were also competitive, the conventional design was carried through the reminder of the conceptual design phase.

Figure of Merit	Weight	 Conventional	 T-Tail	 V-Tail	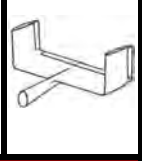 U-Tail
Assembly Time	*0.40*	0	-1	1	1
RAC (Weight)	*0.30*	1	0	0	-1
Stability & Control	*0.20*	1	-1	-1	1
Drag	*0.10*	0	0	1	-1
TOTAL	***1.00***	**0.50**	**-0.60**	**0.30**	**0.20**

Table 9. Empennage configuration downselect

3.4.6 Propulsion

Various motor placements and configurations were studied to identify the most efficient and least obtrusive to system assembly and payload loading. While the competition permits multi-motor configurations, due to practicality and past competition experience only single and twin motor configurations were considered.

- **Tractor –** The propulsion system is located near the front of the airplane where the propeller sees undisturbed air, resulting in higher efficiency.
- **Pusher** – Mounted aft of the main body, the motor and propeller "push" the airplane with less propeller efficiency. Propeller ground clearance becomes a concern for take-off rotation.
- **Twin** – Two motors are used to produce the same thrust as one larger motor. These outboard-mounted motors would be less obstructive during centerline payload loading but may pose a concern while securing the wing-mounted stores.

Based on the study of Table 10, the conceptual decision to pursue a tractor motor was chosen. The higher system efficiency yielded a lower RAC by lowering battery pack weight.

		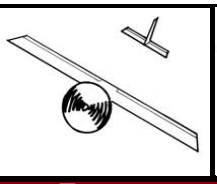	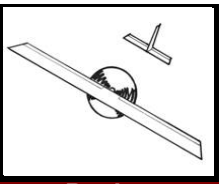	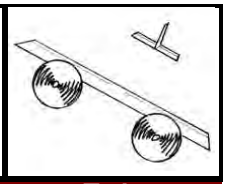
Figure of Merit	**Weight**	**Tractor**	**Pusher**	**Twin**
RAC (Weight)	*0.45*	1	0	0
Efficiency	*0.25*	1	-1	-1
Ground Clearance	*0.20*	0	-1	1
Loading Interference	*0.10*	0	0	1
TOTAL	***1.00***	**0.70**	**-0.45**	**0.05**

Table 10. Propulsion system downselect

3.5 Conclusions

A series of configuration downselects and FOM decision matrices analyzed a combination of overall configurations and subsequent systems. First, a wing-body configuration was chosen from a list generated through a morphological chart and analyzed in a FOM-based downselect that placed a large emphasis on decreasing assembly time and weight. A monoplane was determined as the optimum wing-body over several other non-conventional contenders. Payloads, which must be secured quickly, will be mounted externally to the bottom of the fuselage and wing. They will be restrained with a pin fastened within the aircraft's interior. A tractor motor will propel the aircraft and a conventional tail will be used to meet the stability and control requirements. A tail-dragger landing gear configuration will control the aircraft on the ground during takeoff, landing, and taxiing. The air vehicle and ground system will be stored in a single clamshell box. The final conceptual configurations can be seen in Figure 7.

Figure 7: Conceptual design aircraft and model of the storage box (shown open and closed).

4.0 Preliminary Design

The preliminary design phase was used to optimize components down-selected in the conceptual design phase. The team knew from its score analysis that an aggressive sizing program was essential to be competitive. For the 2008 competition, the team designed, built, and flew a prototype aircraft in October. This was based upon the results of the preliminary design. Since this year's design was more challenging, a prototype was again needed to validate the results of the analytical tools used to meet the competition requirements and ensure the best solution of the complete system

4.1 Analytical Tools

The team used a collection of internally-developed optimization programs and commercially-available software. These modeled the competition missions, sized the optimum aircraft and box, and analyzed the predicted performance of the major components. Design work began with analysis of the entire system and subsequently proceeded to each subgroup.

4.1.1 Multidisciplinary Optimization

The key subgroup on the team during preliminary design was the Performance team. This team created and maintained the multidisciplinary optimization (MDO) code called PlaneSizer, shown in Figure 8. This is a legacy element of USC's DBF team. It has been continually rewritten and enhanced every year. PlaneSizer was used to perform the key sizing trade studies used during the design process.

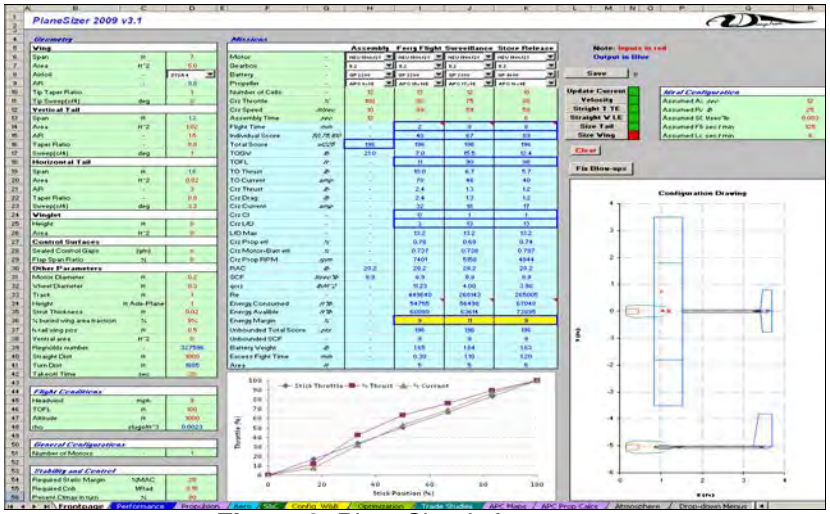

Figure 8: PlaneSizer's frontpage.

PlaneSizer was structured around a network of interlinked Excel worksheets corresponding to each discipline that model nearly every aspect of the airplane. The global flowchart shown in Figure 9 illustrates how the operator first made educated guesses on plane geometry. Concurrently, an estimate of the propulsion module (shown in gold) was formulated to size the remaining aircraft parameters (shown in cardinal). Multiple iterations were made within the propulsion system model, which are then transferred to the aircraft solution. After system convergence, the operator determined the plane had been optimized.

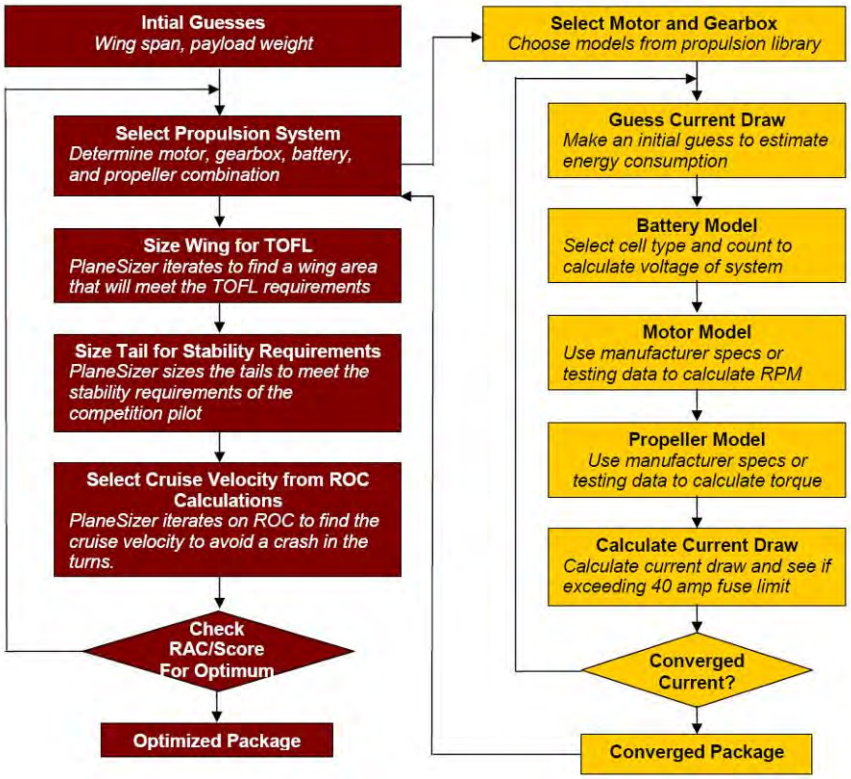

Figure 9: Global flowchart for MDO and propulsion models.

4.1.2 Mission Model

The mission model is the key element of PlaneSizer that is updated every year. It provides the basis for preliminary design given the specific competition parameters. The 100 ft TOFL and 4 lb battery limit were initial constraints. Secondly, the fastest assumed assembly and loading times and lowest RAC were entered. The number of takeoffs, laps, and landings for each mission were then input. A site analysis, discussed later, was used to select an appropriate assumption for wind direction and speed.

From input specifications and initial calculations, the mission model sized the majority of the plane geometry. The calculated values returned from PlaneSizer included the wing area necessary for TOFL, the energy consumption throughout the various segments of each mission, velocity at equilibrium cruise, and the takeoff gross weight. With a converged solution, the mission model calculated the performance of the plane throughout each mission's flight regime and assigned it a total score normalized to the assumed best score. Deficits in performance and score indicated a need for further optimization.

4.1.3 Additional Analytical Tools

The subgroups of the team used a collection of analytical tools to support PlaneSizer's vast libraries of data on propulsion components, airfoils, stability, and mass properties. These tools provided independent tests of PlaneSizer's configuration and verified that the most optimized plane was selected.

The Aerodynamics and S&C group used two programs written by Mark Drela of MIT: XFOIL[3] and Athena Vortex Lattice (AVL) Code[1]. XFOIL, a 2D airfoil analysis program, allowed for the addition of flaps, airfoil camber, and modifications to thickness to improve performance. This program created drag polars for the airfoil selection process. A program called XFLR5[4] allowed for further 2D modification through the hybridization of multiple airfoils. A vortex lattice process calculated the 3D aerodynamic performance of individual surfaces or of entire aircraft. AVL determined angles of incidence of lifting surfaces, optimized the performance of the empennage, and stabilized the aircraft in flight.

The Landing Gear team used "Landing Gear Design[5] (© 2005)," a program developed by industry advisor Blaine Rawdon. After choosing the gear's frontal profile, maximum g-force, sink rate and the desired material properties, the program found the gear dimensions for the desired maximum deflection and dampening. The Structures team developed a tool that followed a similar iteration process.

Finally, the Configuration group used SolidWorks to create 3D models of individual components and the entire system assembly, from which 2D drawings were prepared for the manufacturing team.

4.2 Performance Trade Studies

The sensitivity analysis in the conceptual design phase verified that the assembly time had the greatest influence on the total score, followed by system weight, loading time, and cruise velocity. To learn how to improve in these areas, a comparison between prior winning teams' performances was made followed by an investigation into the score's response to variable permutations.

4.2.1 Competitor Analysis

Traditionally, USC has been too conservative in weight sizing. This has resulted in propulsion systems that have produced large amounts of thrust and swift cruise velocities when needed. However, these systems have proved too heavy to contend with top-tier competitors. The team recreated the past years' winning planes in PlaneSizer based off given data. Teams were chosen for their superiority in variables pertinent to the 2009 missions, i.e. assembly and loading times, cruise velocities, and minimized RACs. Table 11 shows dramatic differences between USC's plane and those of the winners in the 2007 and 2008 competitions. Though USC has done well in assembly time, loading time, and cruise velocity for speed missions, its large RAC has proven fatal in several cases. The goal of this reverse-engineering procedure was to isolate key assumptions that led to overly cautious designs; structural safety factors and weight estimations were then modified and the competition site in Arizona was analyzed.

	OSU	MIT	USC
Assembly Time (s)	8.19	7.20	6.78
RAC (lb)	3.17	3.15	4.69
Loading Time (s)	8.65	9.30	7.13
Cruise Velocity (ft/s)	58.8	43.1	88.6

Table 11. Comparison of USC's core sizing criteria with those of its main competition

4.2.2 Site Analysis

To help moderate the heavy propulsion package and excessive empty weight, an assumed headwind on takeoff was incorporated into the mission model. In the past, this assumption allowed for considerably lighter propulsion systems and thus dramatically smaller airplanes. While an inherent risk is associated with predicting the weather, the team believed it was a necessary step in order to gain a competitive advantage. The recorded wind speed during the competition weekend over the last five years was collected from *wunderground.com*[6]. These values were averaged and plotted for each hour of the competition, as shown in Figure 10. A 9 mph headwind was a prudent estimate for takeoff conditions.

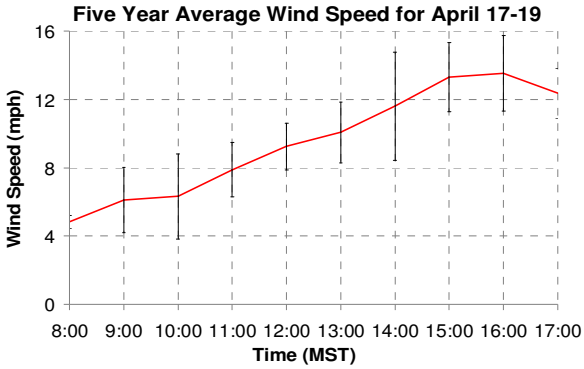

Figure 10: Compiled average wind speed data for the competition site over the past five years with standard deviation. Direction is predominately from NW to SE, the same direction as the runway.

4.2.3 Trade Studies

After the mission model had been updated, the Performance group used PlaneSizer to perform trade studies on the individualized components of the airplane. Due to the packaging constraints, the interfering wing was examined to determine how span affected the score. The span was varied from the 5 ft minimum defined by the placement of the rocket stores to an 8 ft maximum determined by the 4 ft length of one box. Wings that could fold or telescope were considered. Cell count was varied until TOFL was met. As Figure 11 shows, there was a negligible 2% benefit to the total score with an increase in wingspan as 78% of the total flight score was obtained by simply completing the course (along with a ground task multiplier). Therefore, the dimensions of the wing were selected based off packaging and stability and control requirements while the score was left optimized by other parameters.

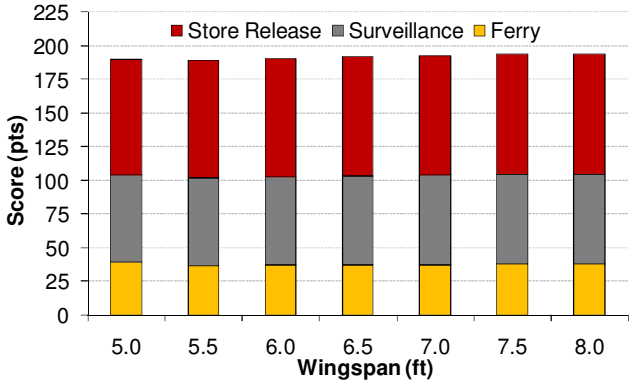

Figure 11: Trade study showing the overall trend of the wingspan's effect on each mission's score.

4.3 Packaging

After a single box in a clamshell configuration was chosen in the conceptual design phase, work proceeded on configuring the aircraft for storage and selecting the payload storage and installation methods. Given the strong influence of assembly time, the initial decisions regarding the box were allowed to drive the aircraft design rather than the scoring characteristics of the airplane. The decisions made in this phase thus preceded those regarding subsequent subsystems.

4.3.1 Aircraft System Storage

The severity of the 2x2x4 ft maximum box size was further amplified by the decision to use only one box. To fully realize the assembly and loading time benefits of this design, the system needed to be packaged efficiently within the allotted volume. Removable wings were dismissed, as the act of attaching two wing halves would have undoubtedly prolonged assembly time. Likewise, the joints necessary to support telescoping wings were deemed too complex and too detrimental to RAC. Finally, the two-face fold was abandoned in favor of a three-section fold design that increased accessibility to the internal volume and minimized the possibility of human error. The three hinged sections were spring loaded to automate the action of opening the box.

The aircraft was placed on its landing gear within the box. This orientation allowed for efficient assembly and loading once the box was opened. A 5.6 ft wingspan was the maximum allowable for the given storage configuration. Though the aspect ratio of the aircraft suffered as a result, winglets could be added to recover the lost efficiency while abiding by the span constraint. Hinged wingtips were selected as the best method for folding the wing within the allotted dimensions. Similarly, a tail boom joint was added in order to preserve its moment arm and package it within the box frame. The avionics and transmitter were placed within their own dedicated compartment within the box. The compartment was encased with foam to absorb energy transferred from the drop.

4.3.2 Payload Storage and Installation

With the orientation of the plane selected, the payloads were mounted within the box in such a way that the effort required to install each store was minimal. Each store's mount was aligned with its corresponding cavity on the plane prior to assembly. The rockets were stacked vertically on each side wall and automatically clipped into the bottom of the wing with the opening of the box. The simulated fuel tank was mounted to the bottom frame, directly underneath the fuselage and between the landing gear. As a pit crew member reached for the aircraft after the box was unfurled, he or she simply depressed the fuselage to clip the bottle into place.

4.4 Structures

Because of RAC's direct correlation to the total score, the main objective of the structural design group was to develop the most weight-efficient structure for the system. Also, the structure of the airplane needed to be as unobtrusive as possible to facilitate faster assembly and loading times. With these two requirements, it was necessary to decide on manufacturing techniques during the preliminary design phase of the program. As justified in the Manufacturing Section, a hybrid building technique was selected.

High strength-to-weight composite materials were used to transfer loads while light materials such as foam and balsa were used in non-structural areas.

4.4.1 Box Structure

To satisfy contest requirements and maximize strength-to-weight, an open frame design with a thin plastic covering was chosen as shown in Figure 12. A prototype was first constructed out of 1 in. diameter PVC pipe. Though the PVC was heavy, it provided an excellent means of validating the analytical tools used to size the box and a preliminary estimation of assembly time and methods. With the plane and ground system secured within, the prototype was successfully dropped from 6 in. and rotated about all faces.

To lighten the box's weight, carbon tubes were investigated as a suitable alternative to the PVC pipe. Using CosmosWorks[7], the exact outer diameter, wall thickness and length of each member was sized for a 5g fully loaded drop test. Test coupons indicated a 50% weight savings over the PVC pipe.

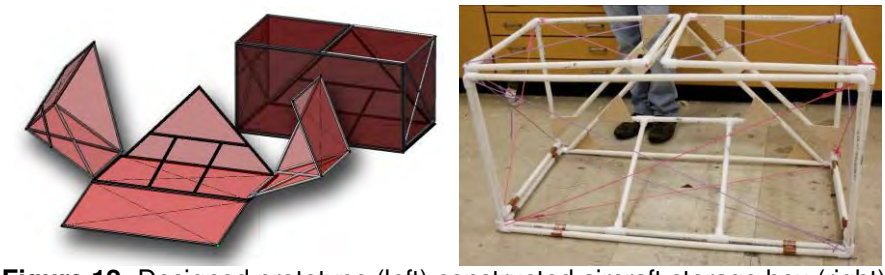

Figure 12: Designed prototype (left) constructed aircraft storage box (right).

4.4.1 Aircraft Components

An analytical study was conducted to determine the worst-case in-flight and landing loads the aircraft's components would experience. 5g aerial maneuvers loaded with the four wingtip stores and the full tank attached were initially studied. An elliptical span loading was assumed for in-flight loads. Shear loads and bending moments were then determined at incremental spanwise stations, as seen in Figure 13. An acceptable factor of safety was then incorporated into the design.

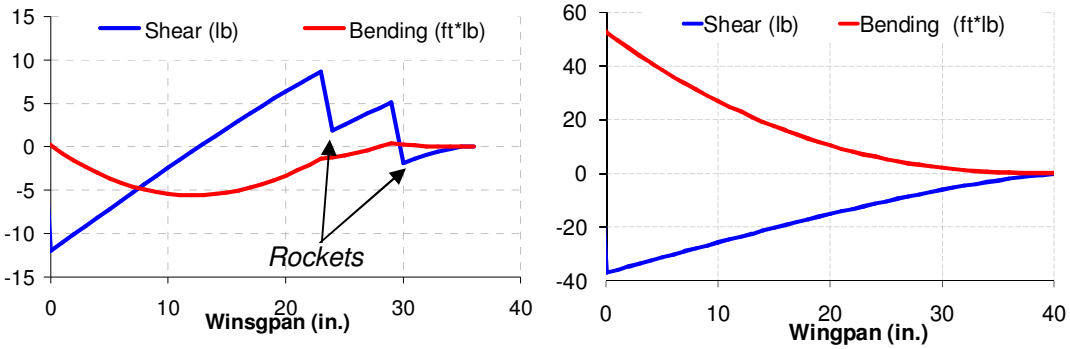

Figure 13: Shear force and bending moment for a 5g aerial turn for rockets (left) and bottle (right).

4.4.2 Wing Structure

The main structure of the wing, the spar, was one of two central structural elements of the aircraft. It supported the rocket payloads and transferred the landing loads into the main gear. With an unswept,

untapered wing, the spar ran along the quarter-chord and was constructed using a balsa built-up technique. Square cross section spruce caps were fastened to the end grain balsa shear web. Two lightweight aluminum hinges were embedded along the spar to accommodate the folding outboard wing sections, shown in Figure 14. Each hinge was sized for a 5g landing with two rockets on each wingtip.

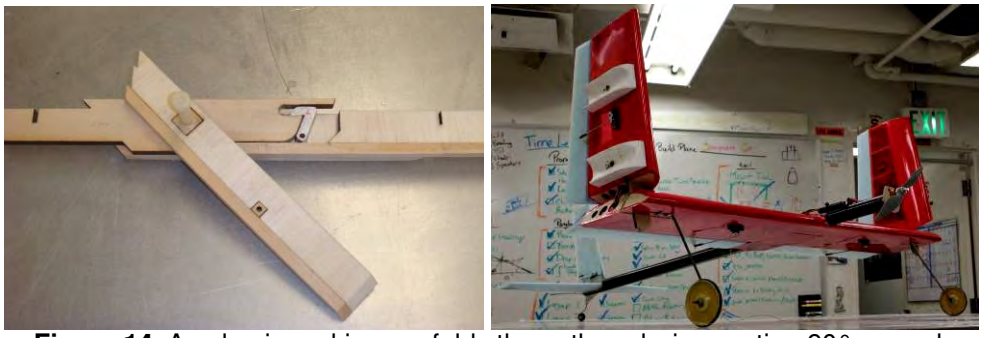

Figure 14: An aluminum hinge unfolds the outboard wing section 90° upward.

While MonoKote was the lightest covering material analyzed, initial tests showed that the airfoil shape was ultimately distorted by the use of the plastic. Tension in the material between the balsa ribs produced scalloping which disrupted the airflow over the wing's top surface. To rectify this error, balsa sheeting was applied to the top surface, while the lower surface remained covered with MonoKote.

4.4.3 Fuselage Structure

The second main structural component, the fuselage, transferred the loads of the bottle, motor, and empennage during flight. Design evolved from a rod to a hollow carbon fiber tube to bolster strength and reduce weight. Like the wing, the tail boom required a joint in order to fit the fuselage into the box. However, the tail boom joint was less limited in its axes of motion. The joints considered were:

- **J-notch** – A pin on one end of a tube is inserted into a groove of another. The crew member then twists and pulls to lock the tubes in place.
- **Pin** – Two tubes are connected by a pin that expands into an alignment hole.
- **Hinge** – The only design that physically unites the tubes at all times, an axle hinges the two tubes, limiting motion to one axial rotation.
- **Telescope** – A series of carbon tubes of varying diameter telescope into multiple sections.

Table 12 shows that the hinged tail boom was the configuration of choice. Because the two tubes began in a linked state, its assembly time far exceeded that of any other design.

		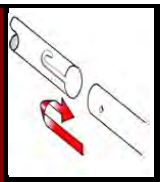	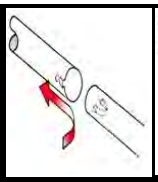	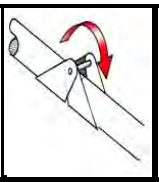	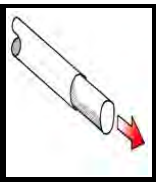
Figure of Merit	**Weight**	**J-notch**	**Pin**	**Hinge**	**Telescope**
Assembly Time	*0.50*	-1	-1	1	0
RAC (Weight)	*0.30*	0	0	0	-1
Durability	*0.20*	1	1	1	-1
TOTAL	***1.00***	**-0.30**	**-0.30**	**0.70**	**-0.50**

Table 12. Tail boom hinge downselect

Figure 15 visualizes the load paths of the fuselage from the empennage, landing gear, wings, and propulsion system. Elliptical span loading was assumed for in-flight loads. While the carbon fuselage transferred much of the loads, a motor mount was needed to disperse the loads over a larger area.

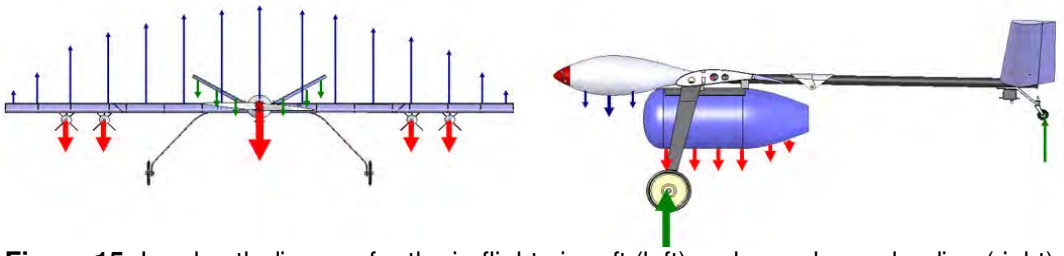

Figure 15: Load path diagram for the in-flight aircraft (left) and upon heavy landing (right).

4.5 Payloads

The Payloads team's primary purpose was to configure payload arrangements and design fast and efficient payload restraints. Factors taken into account were payload CGs and relative loading times for the centerline and wingtip stores.

4.5.1 Payload Restraints

With the location of all payloads determined, the mounts attaching the payloads to the aircraft were decided upon. Though the two deployable stores were mounted at different locations, the same method of attachment was used for both. The release mechanism was assumed identical until selected in the preliminary design phase. The four store mounts analyzed were:

- **Blade** – A thin rectangular blade is fixed to each payload. The blade's sides align with slots in the plane's interior. Locking clips hold the store into place.
- **Pin** – A single dowel protruding at the payload's CG fits into a circular recess in the aircraft's skin. The pin is secured via a locking clip inserted into a slot in the pin's surface.
- **Dual Pin** – Similar to a single pin, two dowels protruding from the stores provide added stability.

Table 13 indicates that the blade's improved durability and potential for reducing loading time made it the correct choice for securing the payload to the aircraft. Methods were implemented to ensure that the payloads would survive the shake test and could be inserted quickly into the alignment hole.

		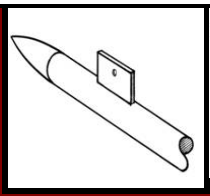	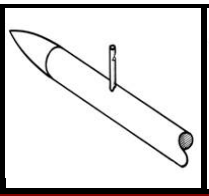	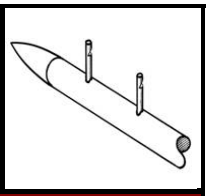
Figure of Merit	**Weight**	**Blade**	**Pin**	**Dual Pin**
Loading Time	*0.40*	1	0	-1
Weight	*0.25*	0	1	0
Durability	*0.20*	1	0	0
Drag	*0.15*	0	0	-1
TOTAL	***1.00***	**0.60**	**0.25**	**-0.55**

Table 13. Store restraint downselect

4.5.2 Release System

The condition that all aircraft stores must be remotely deployable drove the design toward a payload release system that was both lightweight and reliable. Once again, a single system was shared by both types of stores. Two methods for actuation were considered:

- **Servo** – The servo arm is connected to the store's locking pin via a small pushrod. An input from the transmitter signals the servo arm to actuate, pulling the locking pin and releasing the store. One servo is assigned to each store; thus five channels are devoted to the release system alone.
- **Muscle Wire –** A current is run through a thin wire that contracts from the induced temperature change. The contraction force pulls the locking pin attached to the wire's end, releasing the store.

Table 14 indicates that the muscle wire release system was the chosen means of deploying the rockets and water bottle payloads. Its measured 8 lb of linear force was more than enough to deploy the heaviest of the payloads. Its 0.3 oz. weight was a 40% savings over the 0.5 oz. servo.

		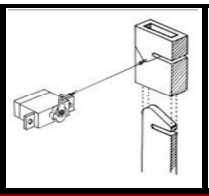	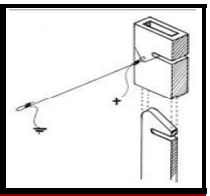
Figure of Merit	**Weight**	**Servo**	**Muscle Wire**
Weight	*0.50*	-1	1
Durability	*0.30*	1	0
Reliability	*0.20*	1	0
TOTAL	***1.00***	**0.00**	**0.50**

Table 14. Store release downselect

4.6 Aerodynamics

The Aerodynamics team researched several different concepts to update PlaneSizer's model of a monoplane's aerodynamic performance. This led to many valuable resources that influenced the design of the monoplane configuration selected in the conceptual design phase.

4.6.1 Airfoil Optimization

The airfoil library was updated to contain airfoils that performed well at the low Reynolds numbers determined by PlaneSizer. Because of the imposed 100 ft TOFL, high lift was initially valued over low drag at cruise. The airfoil coordinates were obtained[8] and analyzed in XFOIL. Drag polars were then created for over 100 airfoils using XFOIL. These candidate airfoils were narrowed down to the five with the best C_{lmax} for further analysis and modification. The S1223 was promising due to its high C_{lmax}. However, its high drag at low C_ls aroused suspicion as an efficient airfoil was needed at the low C_l of the high-speed delivery task. A flow visualization by XFOIL confirmed that the flow separation.

To remedy this poor characteristic, XFLR5 was used to blend the S1223 with a lower drag airfoil, the LA203KB, in a 50-50 ratio. The trailing edge was thickened to enhance C_{lmax} and facilitate manufacturing. The resulting geometry, the SYa4, displayed a drag bucket at two of the three flight missions' C_Ls while the drag was also acceptable for the remaining mission. Much of the C_{lmax} of its parent was retained. The drag polars are shown in Figure 16.

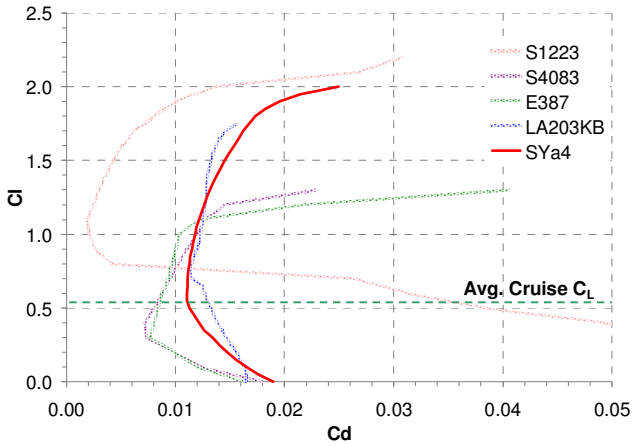

Figure 16: Drag polars of the candidate airfoils.

A final boundary layer visualization study in XFOIL confirmed that flow over the SYa4 remained attached at the takeoff and cruise C_Ls seen during flight. Figure 17 shows a comparison between the S1223 and the hybridized SYa4 at the surveillance mission's cruise C_L and at takeoff.

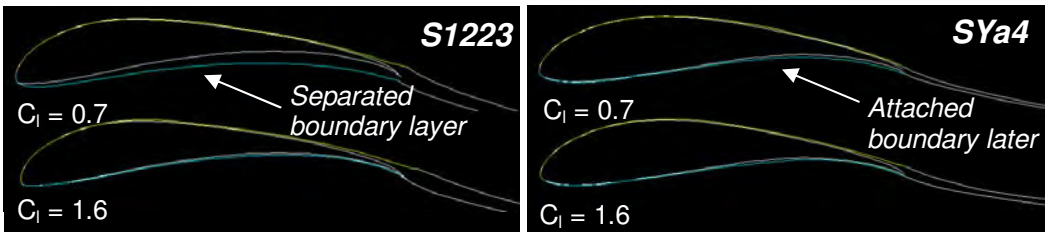

Figure 17: XFOIL 2D boundary layer visualization.

4.6.2 Payload Optimization

The 2009 competition rules allowed for the addition of fairings to the centerline store provided that the total length of the bottle did not exceed 15 inches. The Aerodynamics team experimented with several fairing designs that would lessen the drag on the blunt bottle. Sighard Hoerner's *Fluid Dynamic Drag*[9] was first consulted for guidance on shaping each design. The information shown in Figure 18 indicated that by simply adding a rounded protrusion to the forebody, a 72% reduction in C_{D0} was obtained. However, further analysis was required to comprehend the effects of an afterbody fairing on the drag.

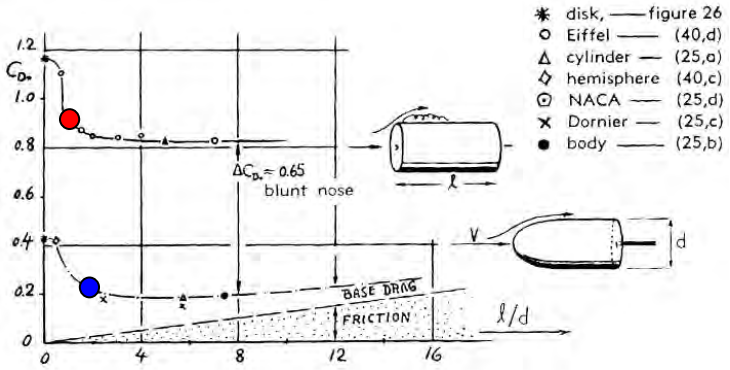

Figure 18: Effect of a forward fairing on a cylinder (Hoerner). The estimated C_{D0} of a standard 11.25 in. bottle (red dot) was compared to that of a 15 in. faired cylinder (blue dot).

The original bottle was first examined in the CFD program COSMOSFloWorks at the cruise velocity predicted for the bottle's ferry flight, shown in Figure 19. The team then modeled several fairing designs in SolidWorks and performed similar analyses in COSMOSFloWorks. The candidates were then narrowed to three based on the preliminary computational results. Three-quarter scale models of these three were prototyped and tested in a wind tunnel. The Reynolds number of the scaled models was matched to that of the full scale payload to ensure similar flow behavior.

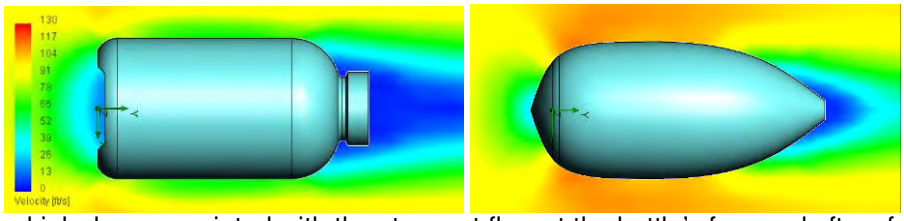

Figure 19: The high drag associated with the stagnant flow at the bottle's fore and aft surfaces (left) was mitigated by the addition of an aerofairing (right).

Figure 20 shows the flow visualization of the three scaled models and the original centerline store. Luminescent oil dots were placed under an ultraviolet light to capture the flow field around each profile. The blunt faces of the bare bottle (upper left) produced the largest drag of four designs, while the rapid aft contraction shown in the upper right forced premature separation and negated the benefits of its small cross section. The thickened cross section of the largest fairing, however, eased the flow around the forward curve while its moderate upsweep angle retained flow attachment as shown in the lower left corner. The final design that retained the small cross section and reasonable afterbody contraction of its predecessors also exhibited low drag and optimal flow characteristics. Its C_D was a meager 0.7% greater than the optimum. This trait, together with its ease of construction, advocated its implementation.

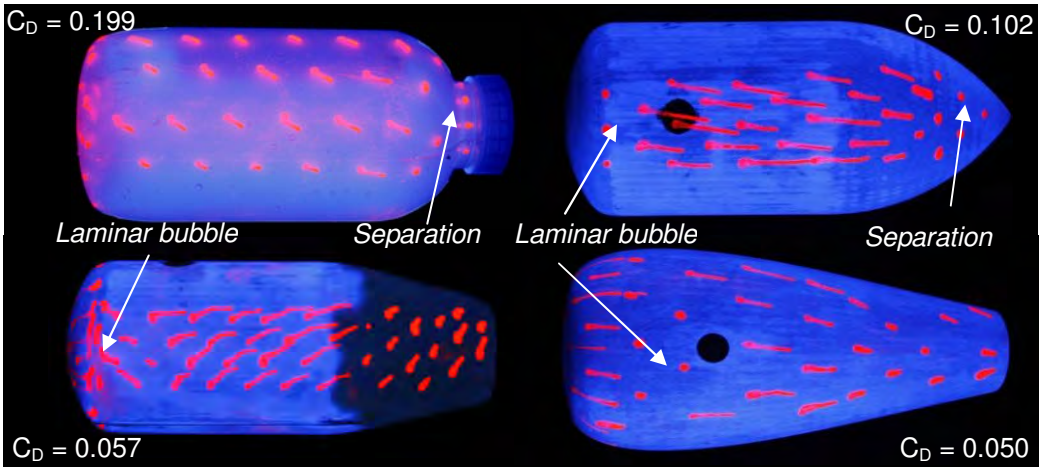

Figure 20: Flow visualization around the original centerline store and three fairing designs. The bottom left geometry, with its low C_D and favorable flow characteristics, was later applied to the full scale payload. Angled streamlines resulted from the effect of gravity on the oil before maximum speed was reached.

Though the placement of the wingtip stores was primarily influenced by packaging and stability and control requirements, the Aerodynamics team once again consulted Hoerner to determine if the lateral separation of the rockets needed to be increased from the defined minimum to reduce interference

drag. It was discovered that the rockets, with a separation-to-diameter ratio of 3:1, was already benefiting from the minimum drag achievable for the defined geometry.

4.7 Stability and Control

Stability and control analysis was carried out in AVL. The preliminary goal was to determine whether or not the asymmetric load could be made stable and controllable. Once this was complete, the empennage was optimized under the constraints imposed by other subsystems.

4.7.1 Stability Requirements

The team has established its stability requirements through a combination of industry rules of thumb and pilot input on the handling of prototype aircraft. The additional challenge of the asymmetric loading and the crosswinds previously experienced at the contest site forced modifications to the standard lateral-directional criteria. The stability targets are shown in Table 15.

SM = 20% *Derived from Flight Testing of USC's variable stability platform 2002-2004*	$C_{n\beta}$ = .0756 1/rad. *Derived from Flight Testing of USC's variable stability platform 2002-2004*
$C_{l\beta} \leq \frac{C_{n\beta}}{2}$ *Limitation on Spiral Stability to reduce gust and crosswind response*	$C_{n\beta} \cdot \beta_{SideSlip} = C_{n\theta r} \cdot \delta_r$ *Crosswind Landing Equilibrium; Require V_{xw} > 5 mph for no fin stall @ β_{xw}*

Table 15. Essential stability requirements

4.7.2 Empennage Sizing

The Stability & Control team modeled the aircraft in AVL based on PlaneSizer's initial geometry. The required C_L predicted by PlaneSizer was input into AVL, which adjusted the airplane's angle of attack accordingly. Various C_Ls were defined depending upon the mission and stage of the flight.

It was first confirmed that the tail was working effectively in the presence of the wing's downwash. Next, it was verified that the plane was not stalling during the takeoff-critical surveillance mission. The empennage control surfaces were then sized to meet the stability requirements dictated by PlaneSizer. The program was then instructed to deflect the control surfaces to create a zero pitching, roll, and yaw moment, ensuring that each surface was not deflected more than 15° to prevent the onset of stall. AVL was used to set the angles of incidence for the wing and tails for zero control surface deflection and zero alpha at the energy-critical store release cruise C_L.

Constraints set forth by the wingtip stores' placement limited the downward aileron deflection required to trim the asymmetric load. The aircraft was then fitted with full-span ailerons, separated only by the hinge needed to fold each outboard wing section, to reduce the resultant deflection. The chord of the aileron was also increased by 20%. Multiple iterations on the aileron and rudder surface areas and mixing converged on an adequately sized control surfaces that satisfied all stability and control requirements.

4.8 Propulsion

The propulsion system of the airplane was tasked with providing sufficient thrust to make the 100 ft TOFL, speed for the ferry flight, and endurance for the surveillance and store release missions. Though the motor remained fixed and the heaviest battery pack was used in the measurement of RAC, it was critical to optimize the propulsion system for each mission in order maximize flight performance.

4.8.1 Iterative Techniques

The propulsion configuration was optimized in PlaneSizer using the iterative technique shown in Section 4.1.1. First, the propeller was varied in diameter and pitch to achieve optimum prop efficiency in cruise and high static thrust at takeoff while respecting a current limit. Battery count and wing area were then adjusted to achieve the needed TOFL without exceeding the system's current draw. Theoretical gearboxes were assessed to achieve a compromise between propeller and motor efficiencies in takeoff and cruise conditions. The theoretical Kv_{Motor}/(Gear Ratio) ratio was used to identify commercially available motor/gearbox/battery combinations. Repetition produced an optimum kit.

The 2009 rules allowed teams to customize a separate battery pack and propeller for each mission. The iterative technique was repeated for each mission until a common motor and gearbox pair was converged upon for both missions. Battery pack and propeller combinations were then chosen for their ability to maximize the individual mission scores.

In recent years, USC has failed to accurately predict the demonstrated performance of propulsion systems. This inaccuracy has often translated into excessive takeoff field length and diminished endurance. While both propeller and battery packs had been mapped extensively, the motor had remained largely unstudied. An electric motor dynamometer/thrust stand combination, shown in Figure 21, was fabricated specifically to rectify these deficiencies and pinpoint errors in sizing. The mechanism allowed for investigation of takeoff static thrust, maximum current draw, and endurance.

Figure 21: Motor dyno (left) shown with measurement equipment.

4.8.2 Motors

In the initial downselect process, a single tractor motor was decided upon. Due to the limitations imposed upon TOFL and the aircraft's wingspan, a large static thrust was desired. The optimum motor/propeller package needed a high thrust-to-weight ratio for the takeoff-critical surveillance mission's 9 lb payload. The following motor types were considered for a motor type downselect:

- **Brushed –** While inexpensive, they are inefficient and heavier than newer brushless motors.
- **Brushless –** These motors are capable of high RPM at a lower weight than brushed motors. A

gearbox is usually required to lower the propeller's RPM, allowing for a larger, more efficient prop.

- **Out-Runner –** A type of brushless motor without a gearbox that generates higher torque.

The following FOM were considered in the downselect:

- **Torque** – Higher torque allows use of larger, more efficient propellers.
- **RPM** – A proper pairing of RPM and a propeller yield maximum efficiency. Higher RPM are beneficial for higher static thrust.
- **Efficiency** – Higher efficiency, measured in internal resistance at zero power r_o and inductance l_o, yields a lower propulsion system weight.

Table 16 shows that a brushless motor configuration was superior. Since a large static thrust was needed, propeller diameter and RPM were major concerns. The high RPM available coupled with the ability to use a larger diameter propeller and gearbox made the light brushless motor desirable.

Figure of Merit	Weight	Brushed	Brushless	Out-Runner
RAC (Weight)	*0.30*	-1	1	0
Torque	*0.25*	0	0	1
RPM	*0.30*	0	1	0
Efficiency	*0.15*	-1	1	0
TOTAL	***1.00***	**-0.45**	**0.75**	**0.25**

Table 16. Motor type downselect

While iterating to find the optimum configuration, the propulsion team compared new brushless motors to those already contained in the library, as well as several new out-runners to help validate the decision to fly with a brushless motor.

To match the desired RPM and to lower the motor's current draw, a gearbox type was required for the motor. A planetary gearbox was used due to its light weight and high efficiency, which reduced battery weight by lowering the required capacity.

4.8.3 Batteries

An initial decision was made between the two types of batteries allowed in the competition: nickel-cadmiums (NiCad) and nickel-metal hydrides (NiMH). While NiCads offered a lower internal resistance, beneficial for limiting the voltage drop with higher current draws, NiMHs were chosen for their superior energy density. Since a 40 Amp fuse limited the current draw from the battery pack, thereby negating the advantage of NiCads, the lower pack weight of a comparable NiMH clinched its selection.

Due to the strong influence of system weight on flight score, the propulsion database was updated with smaller capacity batteries. With the flexibility to vary the flight pack and propeller size for each mission, the opportunity to use smaller capacity cells when appropriate became even more attractive. It was apparent that the speed-critical ferry flight did not require as high of a capacity as the surveillance and store release flights, for which endurance was the primary sizing factor. Several airplanes were sized in the MDO using a fixed motor and gearbox pair for the battery types shown in Figure 22. Cells were added until TOFL was met and the cell capacity was checked to ensure the plane would complete each mission with the maximum score.

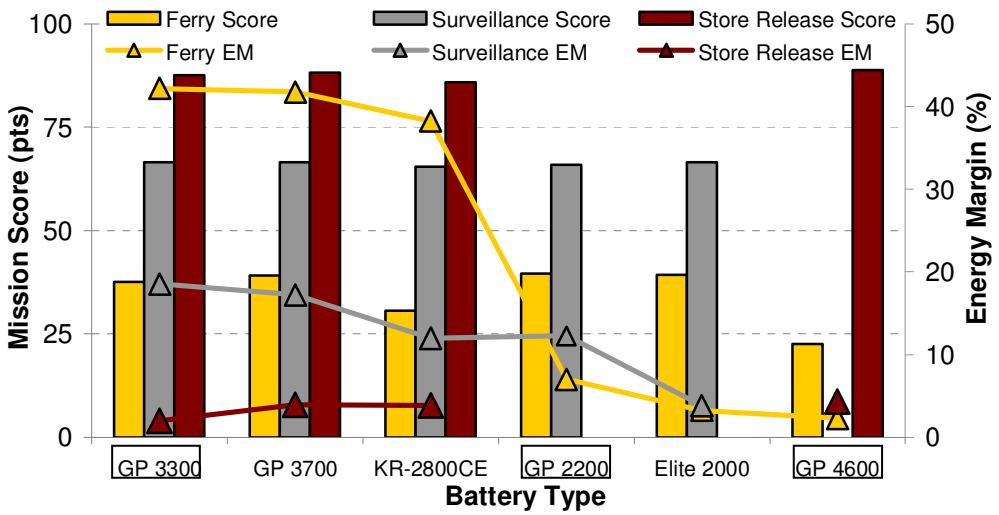

Figure 22: For a given battery type, cell count was varied while the motor, propeller, and wing area remained fixed. Absent mission scores indicate an inability to complete individual mission objectives.

The highest scores for the ferry flight were achieved with the GP 3300s, 3700s, and the 2200s. However, the sizeable battery pack weight required by the former two cell types lowered the total flight score dramatically. The Elite 2000s, while performing well, exhibited double the advertised internal resistance and proved unreliable during battery discharge testing. The dependable GP 2200s were thus selected. Energy margin was not a consideration for this speed-driven mission. The GP 3300s achieved the greatest score and energy margin for the surveillance flight, while the GP 4600s yielded the greatest score and energy margin for the store release mission.

4.8.4 Propulsion Package Study

To validate the choice of a brushless in-runner motor and battery type selection, flight scores calculated from each completed package were pitted against one another. Based on the motor model chosen, the battery type, cell count, gear ratio, and propeller size were adjusted to give a propulsion package capable of making TOFL and completing the aerial missions. The six best performers are shown in Figure 23. The propulsion configuration that yielded the highest total score was a 1506/2Y Neu brushless motor with a 5.2:1 gear ratio. The ferry flight required a 16x10 electric APC propeller and 16 GP 2200 cells, while the surveillance and store release flights required a 17x9 APC propeller with 12 GP 3300s and 10 GP 4600s, respectively.

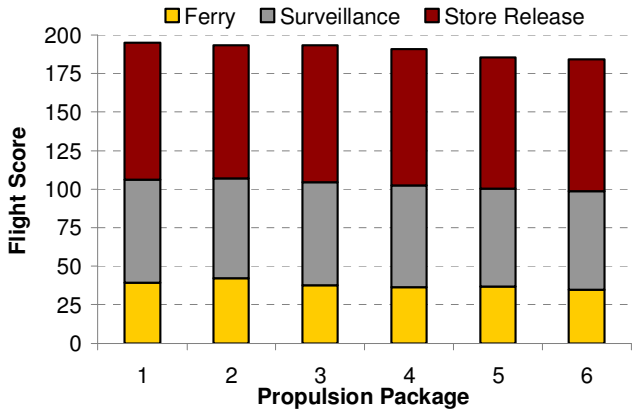

Propulsion Package	Motor Type	Gearbox Ratio	Cell Type	Cell Count	Propeller
1	Neu 1506/2Y	5.2	GP 2200, GP 3300, 4600	15, 12, 10	16x10, 17x8, 17x10
2	KIRA 600-17	5.1	HR-4, RC 2400, GP 3700	23, 16, 12	19x10, 19x10, 20x10
3	Neu 1105/3.5Y	3.36	GP 2200, 3700, 4600	14, 13, 11	12x9, 17x8, 14x10
4	Neu 1509/2.5D	3.1	GP 2200, 3700, 4600	12, 12, 10	12x9, 13x8, 13x7
5	Neu 2215/2Y	None	RC-2000, GP 2200, 4600	15, 20, 12	15x9, 11x6, 13x8
6	AstroFlight 25	3.69	GP 2000, RC-2400, GP 4600	14, 19, 11	16x9, 19x8, 18x10

Figure 23: Propulsion package trade study. Battery cell count, capacity, and propeller size were varied to make TOFL and complete each mission.

4.8.5 Propellers

Propeller size and wing area can each be altered to decrease the aircraft's TOFL. Since the contest allowed for a separate propeller per mission, the wing area was sized solely for the more strenuous TOFL requirements of the highly loaded surveillance mission. Each mission's score was tracked as propeller diameter and pitch was varied in the MDO code, as seen in Figure 24. Because the ferry mission's TOFL was barely affected by propeller selection, the 16x10 was chosen for its ability to maximize the mission's score. While several larger diameter props increased the energy margin, this parameter was not essential to the speed mission. Additionally, the larger props increased the takeoff current well beyond the limit of the fuse. The 17x9 was chosen for the surveillance and asymmetric loading tasks. These propellers satisfied both thrust and endurance requirements, as each met the 100 ft required TOFL while exhibiting the best energy margin in cruise.

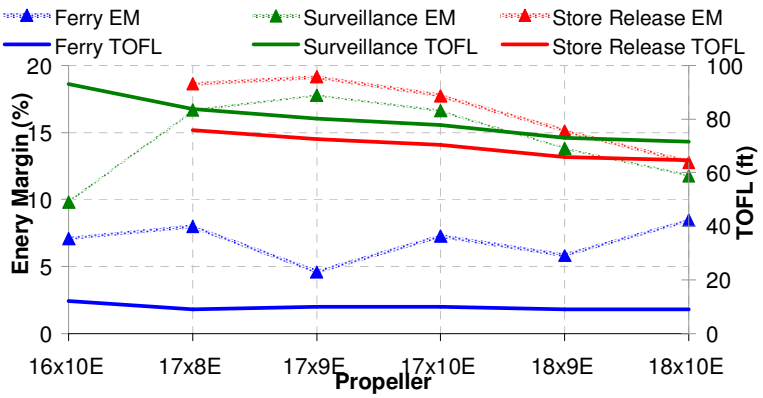

Figure 24: Six APC propellers were varied to meet TOFL and energy margin requirements. Propeller diameters greater than 20 in. exceeded the 40 Amp current limit and hindered takeoff rotation.

4.9 Landing Gear

A tail-dragger landing gear configuration was selected in the conceptual portion of the design. The main bow gear was integrated directly to the wing spar to distribute its upward and aft forces on landing. It was mounted flush to the bottom spar cap to prevent flow separation. Figure 25 shows the shape of the main gear designed to provide the needed dampening and deflection for an assumed worst-case 5g landing at maximum flying weight with an 8 ft/s sink rate.

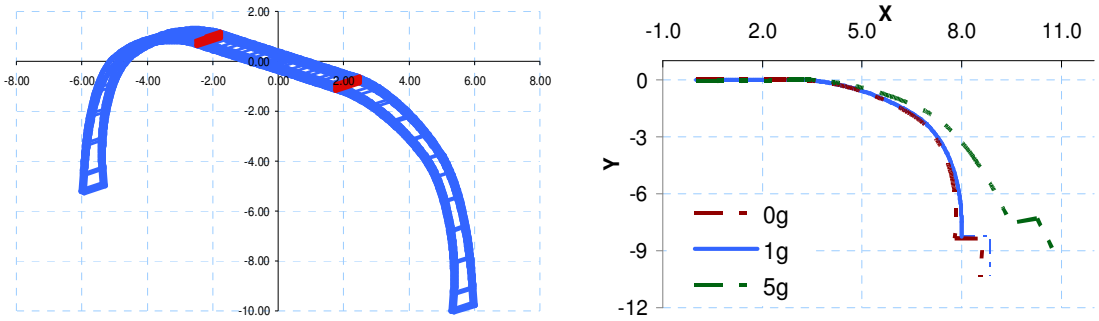

Figure 25: Landing gear analysis program's depiction of main landing gear under varying loads.

For proper rotation, the main gear was placed 15° forward of the center of gravity, as shown in Figure 26. To contend with the asymmetric load, the bow's stance was widened such that the CG was offset 45° laterally from the main gear. The angle between the contact points of the two main gear wheels and the CG necessary to prevent a rollover under a 1g side force was determined to be 54º. The tail gear was placed at 10º, or 2º below stall, to provide empennage ground clearance during takeoff rotation. Furthermore, the addition of brakes was necessary to ensure the proper ground handling during the taxiing and stopping portion of the store release mission. A pushrod was affixed to the tail wheel which provided sufficient steering when mixed with the rudder.

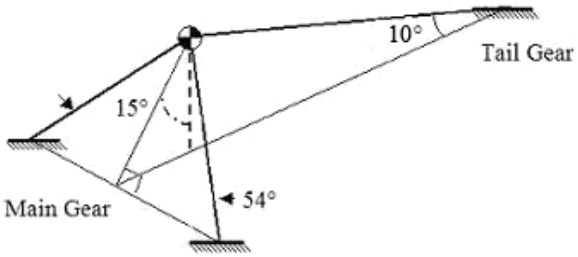

Figure 26: Angles required for stable landing gear ground handling.

4.10 Weight

A weight buildup of the entire system was made. A spreadsheet was created that contained the actual measured weights of the components and the densities of the construction materials, allowing for a RAC prediction of each proposed configuration. The weight build-up, compiled in the structural sizing program, was used to validate the weight estimates used in the team's MDO code. Since structural sizing depended on the weight of every component, this tool allowed more efficient communication between groups. An accurate weight estimate was crucial for performance characteristics like TOFL and energy margin. Figure 27 shows the system's weight buildup with ballasted payloads.

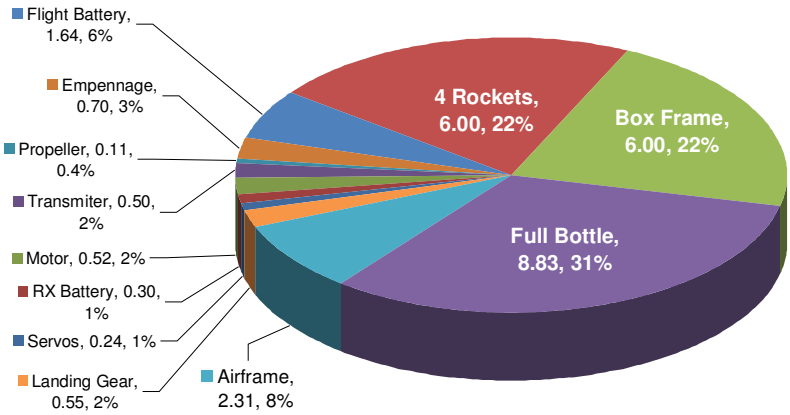

Figure 27: Weight buildup of each component. Weights are shown in lb and percentage of the total RAC.

4.11 Preliminary Design Summary

Through an iterative process led by the team's MDO code and supported by a suite of analytical tools, the team converged on an optimum configuration, as presented in Table 17. It was constructed and test flown in December, as shown in Figure 28. This design was presented in a formal preliminary design review delivered to a panel of industry experts. The reviewers provided feedback and advice which was incorporated into the detailed design phase.

Design Parameters			
l *[in.]*	47.0	**RAC** *[lb]*	27.64
b *[ft]*	5.6	**SM** *[%]*	20
S_{trap} *[ft^2]*	5.00	$C_{n\beta}$ *[1/rad]*	0.114
AR	6.3	$C_{l\beta}$ *[1/rad]*	-0.060
$(L/D)_{max}$	15.3	$\delta_{elevator\ max}$ *[deg]*	14.2
C_{D0}	0.008	$\delta_{aileron\ max}$ *[deg]*	15.5
C_{Lmax}	1.6	$\delta_{rudder\ max}$ *[deg]*	5.6
α_{TO} *[deg]*	10	**Motor**	Neu 1506/2Y

Performance	$C_{Lcruise}$	$C_{Dcruise}$	L/D_{cruise}	e	v_{cruise} *[ft/s]*	TOFL *[ft]*	Energy Margin *[%]*
Ferry	0.10	0.020	5.00	0.85	102	14	23
Surveillance	0.40	0.028	12.4	0.96	79	92	6
Store Release	0.30	0.026	12.4	0.36	80	81	8

Table 17. Solution design and performance through the preliminary design phase

Figure 28: One of two preliminary performance demonstrators is shown in flight and stowed.

5.0 Detailed Design

The knowledge gained from the testing of the preliminary design system provided an excellent starting point for the detailed design phase. The issues encountered were resolved in time for a series of steady, level flights and successful box tests. Most importantly, there was a clear understanding of the issues that needed to be addressed in the final design phase.

5.1 System Architecture

5.1.1 Packaging

Preliminary testing of two performance demonstrators revealed that the 5.6 ft span was inadequate to trim the asymmetric load which resulted in the low efficiency factor shown in Table 17. It was discovered that by inverting the flight vehicle within the storage box, over one additional foot of wingspan was achievable. While the new 6.7 ft span had no affect on the total score, the vortex drag benefit increased the energy margin of the critical store release mission by 75% as shown in Figure 29. Additional roll trim drag benefits resulted from the increased span. The team was unwilling to sacrifice the automated rocket loading for fear of losing a significant time advantage. Therefore, the wingtips were hinged downward to retain the gravity-assisted loading method.

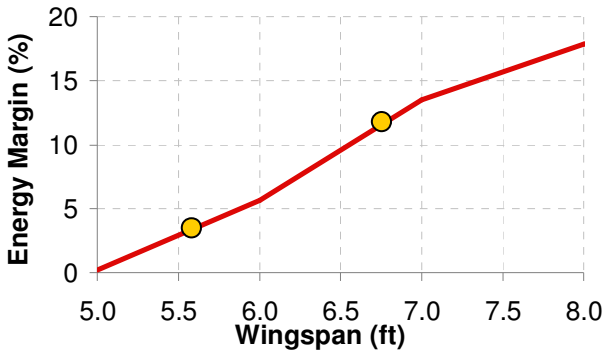

Figure 29: Prior and current values of energy margin are indicated by yellow dots.

The inverted storage placed the bottle above the body of the aircraft. This forced an empennage redesign as the tail boom now needed to fold under the aircraft. The protruding vertical stabilizer collided with the fuselage. It was found that a V-tail, the runner-up to the conventional tail in the conceptual downselect, folded underneath the wing-body and neatly enveloped the components without sacrificing tail boom length. The V-tail design was further optimized by the Stability and Control team.

However, the new packaging method posed problems for the centerline store, which was to be bottom-loaded onto the fuselage. Rather than supporting the 9 lb simulated fuel tank for all possible drop test orientations, which forced a heavier support structure, it was decided that a separate container would be created for the bottle. This container was designed to be as small and as lightweight as possible. The estimated 2 lb of structural weight savings gained from the new box configuration meant that the action of mounting the bottle to the fuselage could occur 1.5 seconds slower with no score penalty, as discussed in the Conceptual Design section. In addition, while the removal of the bottle from the main box diminished

the configurator's grounds for selecting the V-tail, the aerodynamic and S&C benefits (detailed in ensuing sections) justified its continued use. For a further span increase, the tail boom was free to hinge over the aircraft's belly. These modifications are summarized in Figure 30.

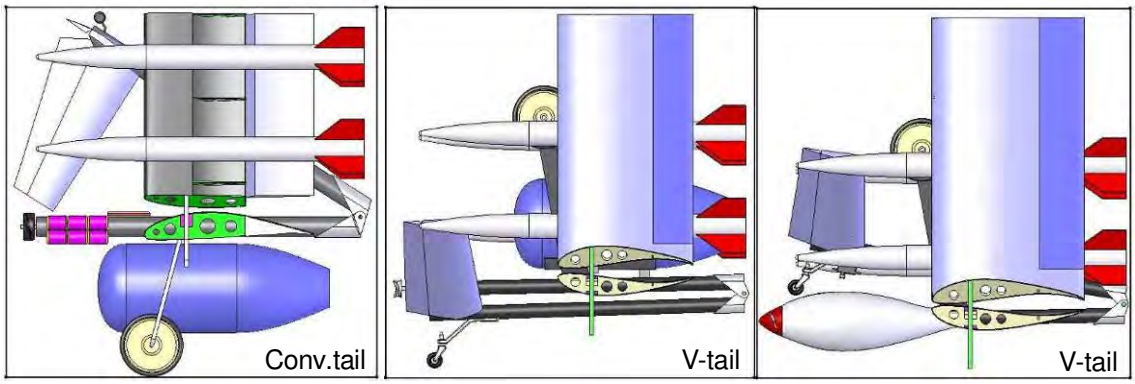

Figure 30: From left to right, the evolution of the vehicle storage configuration is shown. Center section wingspan was kept constant while the outboard folding section grew with each iteration.

5.1.2 Aerodynamics

With the increase in wingspan, initial concerns regarding the efficiency of a low aspect ratio aircraft were mitigated. The 38% increase in aspect ratio provided equivalent vortex drag benefits as 12 in. winglets, a design originally valued for its ability to increase the effective aspect ratio with an imposed span constraint. The simplicity and weight saving of the straightforward span extension prompted the dismissal of the unreasonably tall winglets. Flight testing verified the 6.7 ft span demonstrated a 32% increase in efficiency over the 5.6 ft span for the asymmetric load.

The flight tests also provided a great deal of information that was incorporated into the final design. The highly-cambered, highly-loaded airfoils worked well and did not stall on the bottom surface of the wings at low C_Ls. The SYa4 behaved as XFOIL predicted. However, it was shown that the aircraft was not making the 100 ft TOFL with the heavy payload. It was established that a 20% chord split flap deflected 45° offered a 25% increase in C_{Lmax}. By preserving the airfoil's top surface, flow remained attached across the highly-cambered surface, allowing an additional increase in lift for the already high-lift airfoil. Flaps were incorporated inboard of the wing hinge to avoid collisions with the wingtip stores. Figure 31 shows the drag polar and lift curve slope for the aircraft with the implementation of a split flap.

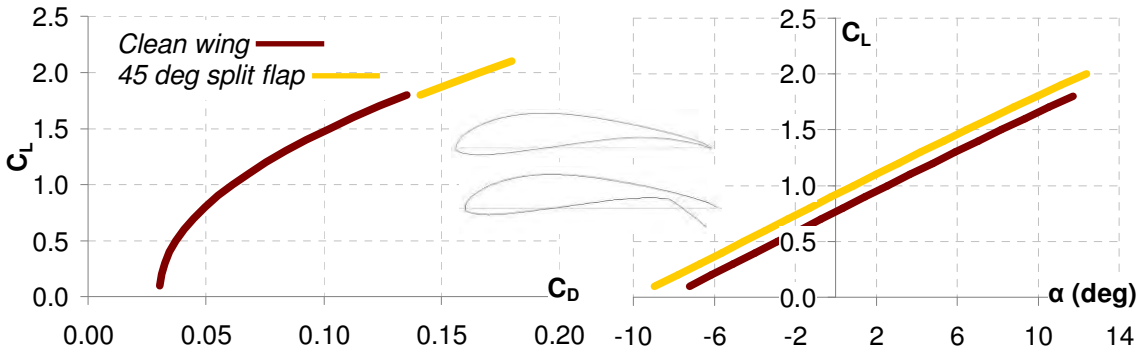

Figure 31: Aircraft drag polar for the surveillance mission inclusive of split flaps.

The remaining area of concern for the detailed design was drag reduction. A preliminary drag buildup, shown in Figure 32, indicated that the unfaired centerline store produced 38% of the total system's drag. This penalty was easily mitigated by the inclusion of the fairing presented in the Preliminary Design section. Aerodynamic fillets were added to junctions between the tail and fuselage as well as at the wing's trailing edge and fuselage joint. An additional fairing was added at the aircraft's nose to encase the motor and batteries. This shell was designed as thin as possible to reduce effects on RAC.

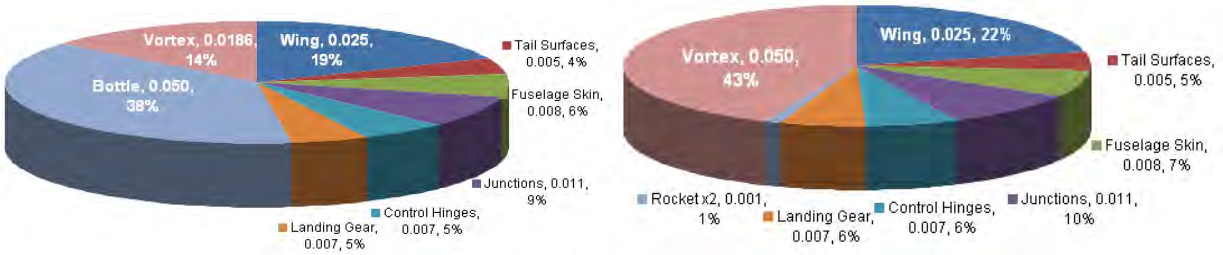

Figure 32: Surveillance (left) and store release (right) drag buildup.

5.1.3 Stability and Control

While pitch and yaw requirements were met, initial flight tests indicated a large discrepancy in roll rate between the centerline store and asymmetric flights. Trailing edge extensions were subsequently added to the ailerons and the deflections were allocated to high and low gains to augment control output. The related stability derivatives were back calculated and used as new targets in the AVL model.

The V-tail satisfied yaw stability requirements for crosswind, asymmetric flight and provided a 10% wetted area benefit. Flight testing verified its superior effectiveness over the conventional tail in pitch and yaw and its ability to arrest the large sink rate exhibited on landing for the ballasted water bottle.

Trefftz-plane plots of the system, shown in Figure 33, were used to verify optimum performance. Wingtip stall tendencies were prevented by ensuring that the location of the 2D C_{Lmax} was inboard of the 50% semispan and that the 0.85*C_{Lmax2D} position did not exceed the 90% semispan station in. Local span C_Ls for the wing and tail, given by the purple lines, did not exceed the section C_{Lmax} at any point, indicating the surfaces were not stalled. Elliptical wing loading in cruise was validated for symmetrically loaded cases. The angle of attack of the aircraft was zeroed for the cruise-critical store release mission while the wing setting angle was governed by the takeoff-critical surveillance mission. The corresponding stability derivatives are shown in Table 18.

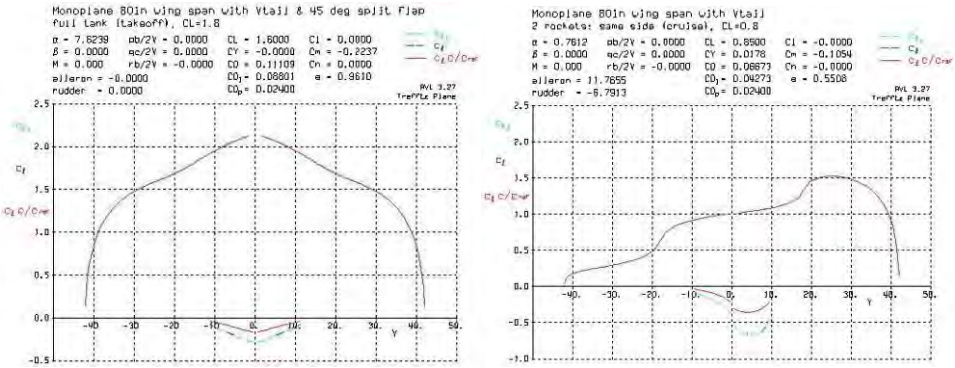

Figure 33: Trefftz plots of the surveillance mission's takeoff (left) and asymmetric cruise (right).

	Surveillance	Asymmetric		Surveillance	Asymmetric
$C_{L\alpha}$	5.961	5.911	$C_{l\beta}$	-0.051	-0.060
$C_{m\alpha}$	-1.304	-1.363	$C_{m\beta}$	0.000	0.000
SM	21.88	23.06	C_{lq}	0.000	1.244
C_{lp}	-0.576	-0.737	C_{mq}	-18.072	0.422
C_{np}	-0.049	-0.056	C_{nq}	0.000	0.009
C_{lr}	0.228	0.263	C_{nr}	-0.048	-0.048

Table 18. Key stability derivatives for the two critical missions. Units are [*1/rad*]

5.1.4 Structures

The primary focus of the Structures team involved adjusting for unexpected results observed during preliminary design testing. It was revealed that the wing skin and D-box suffered irreparable buckling damage upon hard landing, further verified by an independent laboratory test. The data collected was used to reconstruct shear and bending moment diagrams for a 5g landing with the ballasted bottle, shown in Figure 34. The results were used to refine the construction materials and methods.

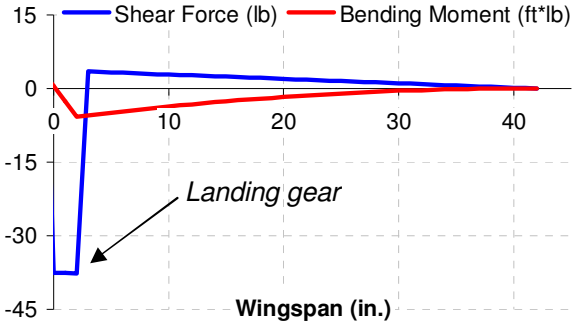

Figure 34: The shear force and bending moment for a 5g landing with the ballasted bottle.

While the balsa-sheeted wing was effective at preserving the airfoil profile between ribs, it did little to combat the 37 lb shear force of landing and 46 ft*lb bending moment of a 5g turn with the bottle (Figure 13). One layer of 1 oz. fiberglass was applied to the top and bottom of the wing skin after the creation of a wing mold. This sandwich structure provided a lightweight solution that neutralized buckling and offered precision and repeatability during manufacturing. The D-box was outfitted with partial ribs that extended from the leading edge to the main spar. These balsa pierces were placed in between the existing ribs. The bottom of the D-box was reinforced with a balsa sub-floor layered with several plies of fiberglass that prevented unwanted torsion from the main landing gear. Figure 35 shows the improved design.

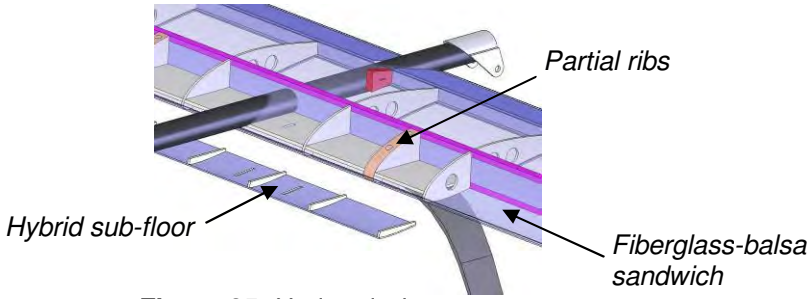

Figure 35: Updated wing structure.

Through both COSMOSWorks simulations and a preliminary examination of test sections, the carbon tube box structure yielded promising results. However, the 32 members summing to over 13 ft in length were simply too time and resource consuming to construct, test to failure, and reconstruct. Alternative construction methods were then sought out. Foam triangular cross sectional members covered with 1 layer of 1 oz. fiberglass were selected as appropriate for box construction. This manufacturing method saved time without sacrificing strength or weight.

5.1.5 Landing Gear

Initial prototype test flights showed excellent ground handling characteristics from the tail-dragger configuration once brakes and tail wheel steering were added. A wire was fed down the bow gear and wrapped around a drum mounted to the inside surface of each wheel. A servo pulled the wire in tension which tightened the coil and applied sufficient friction for braking.

New methods developed in the lab allowed for simple construction of main gear molds that could be altered as the design progressed throughout the semester. The final main gear was made from 12 layers of unidirectional carbon fiber. Table 19 lists several key characteristics designed into the main gear. A cantilever tail wheel with pull-pull steering was mounted to the aft portion of the fuselage.

Design Parameters		
Sink Rate = ROS	8.00	*ft/s*
Energy Absorbed = E_{strut}	21.0	*in.-lb*
Strut Spring Rate = K_{strut}	90.4	*lb/in.*
Maximum Deflection = ΔZ_{strut}	0.83	*in.*
Static Deflection = 1g ΔZ_{strut}	0.08	*in.*

Table 19. Main landing gear characteristics and deflection

Analysis of past carbon bow gears showed that only half the weight was attributed to the carbon. The other half was due to the two tires, hubs, and axles. In an effort to save system weight, custom wheels and axles were designed. A 3 in. outer wheel diameter was chosen to bridge large gaps in the uneven pavement encountered during testing. A rubber O-ring was placed around the Kevlar wheel and hub to provide traction. Axles were directly integrated into the wheel hub and main gear from brass pipe. This design reduced the wheel weight 50% from the original 0.20 lb weight used on past airplanes. Though the lifespan of one wheel was only about ten flights, it was adequate for the contest missions.

5.1.6 Payloads

Both the wingtip and centerline store release and storage systems performed admirably during testing. However, it was found the addition of fiberglass to the rocket fin-body junction was necessary for each store to survive remote deployment. Further fiberglass reinforcements were added to the locking pin mechanism within the wing as repeated deployments wore down the wooden components.

An extra mounting pin was added to the bottle to contend with the torsional instability of the heavy store. The 9 lb weight initially concentrated on the single muscle wire pin was better dispersed through two mounting points. These attachment points were placed such that the CG of the bottle was just aft of the forward support. A single release system freed the pin in the aft support, causing the payload's

tapered end to pivot downward and the main support to slide from its grooves. This improved system was more reliable and less demanding on the fragile muscle wire system.

The final step in the payload release design was to develop a remote deployment system, shown in Figure 36. A circuit was constructed that first read the pulse width modulation signal from receiver. A comparator converted this signal to a binary digital logic code that was next translated by microcontroller. MOSFET transistors accepted this low-voltage, low-current signal and actuated the muscle wire corresponding to the store selected for release.

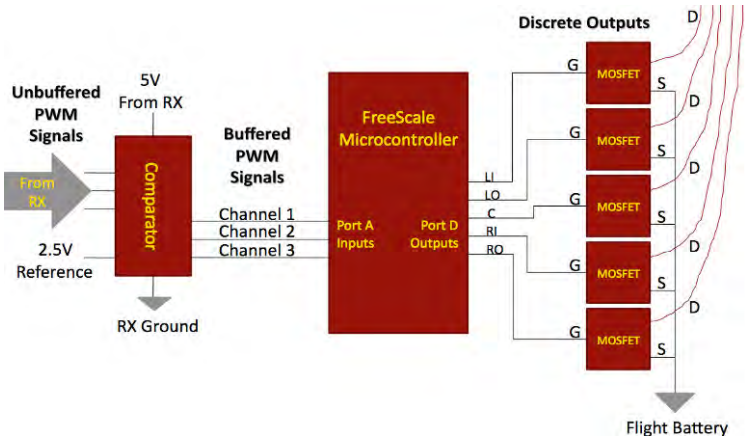

Figure 36: Block diagram of remote release circuit. *G*, *S,* and *D* are the gate, source, and drain terminals. Payload locations are represented by left (*L*), center (*C*), right (*R*), inboard (*I*), and outboard (*O*).

A 3-position switch on the transmitter allowed the pilot to select the left, centerline, or right wing stores. The user then positioned a double-throw switch to select an inboard or outboard wingtip store (both switch positions were valid for the simulated fuel tank). A final spring-and-return switch input the deployment command. As a failsafe, this switch needed to be held in position for 3 seconds in order to prevent inadvertent deployments. The five receiver channels otherwise needed for independent payload release were thus reduced to three, freeing up two channels needed for brakes and flaps.

The comparator and microcontroller each drew power from the receiver battery pack, while the MOSFETS were powered by the flight pack. The 1 Amp, 6 V draw from flight batteries was a negligible loss for the weight and channel-saving benefits generated. Figure 37 shows the prototype board.

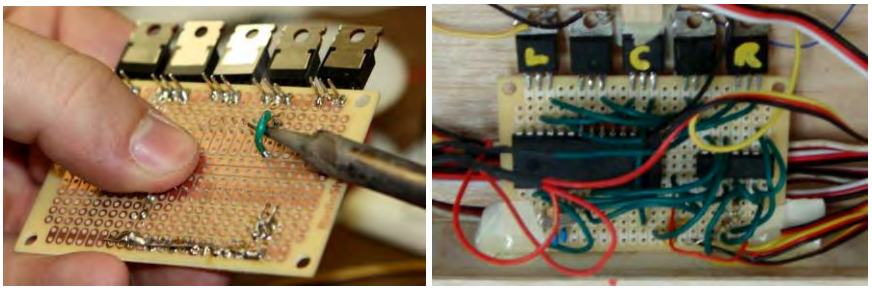

Figure 37: MOSFETS were installed in the payload release circuit (left) before aircraft integration (right).

5.1.7 Propulsion

The motor, the heart of the propulsion system, selected in the preliminary design phase

performed largely as expected. Slightly more propeller pitch was added to increase thrust without sacrificing endurance for the surveillance and store release missions. One cell was subtracted from the ferry mission's flight pack to improve efficiency. The remainder of the detailed design phase focused on improving the unbalanced energy margins displayed in Table 17. To optimize the performance of the propulsion system, its cruise efficiency was calculated as a function of current using the MDO code. The efficiency of the entire system was calculated as the ratio of power output to input power. The power consumption was simply voltage from the battery pack multiplied by the current draw.

Figure 38 shows the cruise efficiency and the power consumption of the propulsion system plotted against the current draw from the battery pack for each mission. The store release flight was the most efficient mission at both takeoff and cruise. Since this task was driven by endurance, the high efficiency at the cruise throttle setting was desirable. The lightweight ferry flight mission, flown at 85% throttle, was optimized to fly at only 2.5% less efficiency than the system's maximum efficiency of the system, while the surveillance mission demonstrated a mere 6% loss in efficiency. Table 20 lists characteristics of the propulsion system for the three flying missions.

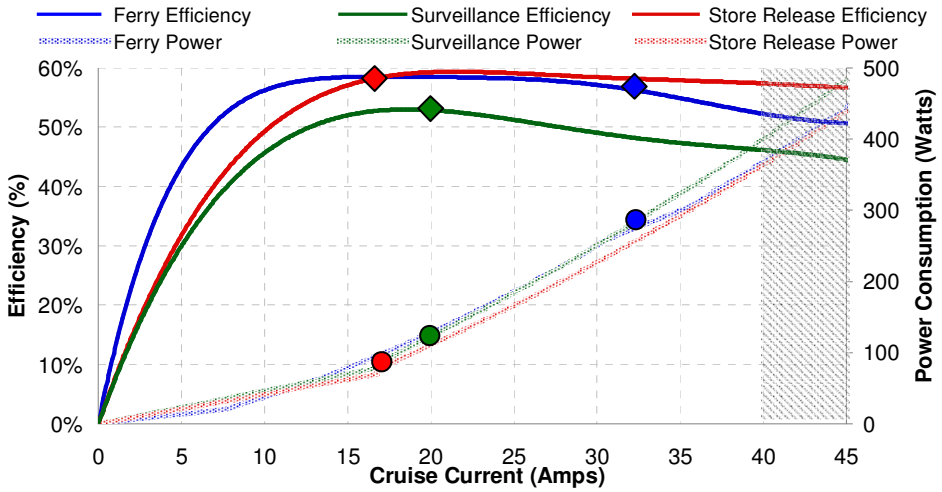

Figure 38: Propulsion system efficiency (diamonds) and power consumption (circles) were studied for all cruise conditions. The 40 Amp current limit was imposed by the mandatory slow-blow fuse.

	Ferry	Surveillance	Store Release
Propeller	16x10 APC	17x10 APC	17x10 APC
Battery Pack	15 GP 2200s	12 GP 3300s	10 GP 4600s
V_{crz} *(ft/s)*	85	70	70
I_{TO} *(Amps)*	68	54	52
I_{crz} *(Amps)*	32	20	17
Energy Margin *(%)*	3	13	4
Throttle (%)	85	70	70

Table 20. Propulsion performance summary for the flight missions

5.2 Mission Performance and System Geometry

Before the design was frozen and manufacturing began, the team hosted a critical design review where industry experts critiqued every aspect of the design. The tables below document the geometry, flight performance, and mission performance of the final design shown in Figure 39.

GEOMETRY		RAC *[lb]*	
Fuselage		*Air Vehicle*	4.1
Length [in.]	45.5	*Flight Battery*	1.6
Width [in.]	0.8	*Receiver Battery*	0.3
Height [in.]	0.8	*Transmitter*	0.5
Wing		*Assembly Tools*	0.0
Airfoil	SYa 4	*Ballasted Tank*	8.8
Span [ft]	6.7	*Ballasted Rockets*	6.0
Wing Area [ft^2]	5.0	*Air Vehicle Box*	6.0
Aspect Ratio [n.d.]	8.9	*Bottle Box*	0.6
Taper Ratio	1.0	***TOTAL***	**27.97**
Incidence [deg.]	-1.0	**CHANNEL DISTRIBUTION**	
Chord [in]	8.6	*Channel 1*	Inboard aileron
V-Tail		*Channel 2*	Ruddervator
Airfoil	Inverted Clark-y	*Channel 3*	Throttle
Span [in.]	24.0	*Channel 4*	Ruddervator
Root Chord [in.]	5.0	*Channel 5*	Outboard Aileron
Taper Ratio	0.8	*Channel 6*	Brakes
Ruddervator Chord [%]	30	*Channel 7*	Store Release L/R/C
Incidence [deg.]	0.0	*Channel 8*	Store Release I/O
Moment Arm [in.]	46.8	*Channel 9*	Store Release Deploy
SYSTEMS			
Motor	Neu 1506/2Y	*Speed Controller*	Castle Creations Phoenix 60
Battery Types	GP2200, 3300, 4600	*Servos*	82 Metal Gear
Gear Ratio	5.2	*Radio*	Futaba T9CAP Super
Propellers	16x10E, 17x9E, 17x10E	*Receiver, Pack*	Futaba 9319, Futaba NR-4J

Table 21. Aircraft geometry, systems, and system RAC

FLIGHT AND MISSION PERFORMANCE			
Design Parameters		**Surveillance Mission**	
C_{Lmax}	2.13	*ROC [fpm]*	845
C_{LTO}	1.81	*Cruise Speed [fps]*	63.0
$(L/D)_{max}$	13.4	*Stall Speed [fps]*	34.4
C_{D0}	0.027	*TOFL [ft]*	90
OEW [lb]	6.2	$C_{L\ Cruise}$	0.80
Avg. Re$_c$	335,921	$C_{D\ Cruise}$	0.078
$T_{A\ max}$ *[lb]*	9.5	*e*	0.94
$(W/S)_{max}$ *[lb/ft^2]*	3.10	*Propeller*	17x10
		Battery Cell Count	12
		Takeoff Current [Amps]	54
		Max δ_r, δ_a [deg]	12.4, 0
Ferry Mission		**Store Release Mission**	
ROC [fpm]	2621	*ROC [fpm]*	841
Cruise Speed [fps]	96.0	*Cruise Speed [fps]*	59.0
Stall Speed [fps]	22.3	*Stall Speed [fps]*	30.8
TOFL [ft]	11	*TOFL [ft]*	91
$C_{L\ Cruise}$	0.10	$C_{L\ Cruise}$	0.60
$C_{D\ Cruise}$	0.059	$C_{D\ Cruise}$	0.053
e	0.90	*e*	0.70
Propeller	16x10	*Propeller*	17x10
Battery Cell Count	15	*Battery Cell Count*	10
Takeoff Current [Amps]	68	*Takeoff Current [Amps]*	52
Max δ_r, δ_a [deg]	8.5, 0	*Max δ_r, δ_a [deg]*	11.8, 6.9

Table 22. Aircraft design and performance specifications

WEIGHT & BALANCE OF AIR VEHICLE						
Design Parameters						
$W_{airframe}$ [lb]	5.90	W_{boxes} [lb]	6.60	$W_{ground\ system}$ [lb]	2.44	
Mission Parameters						
		Ferry	***Surveillance***	***Store Release***		
$W_{batteries}$ [lb]		1.46	1.64	1.63		
$W_{propeller}$ [lb]		0.11	0.17	0.17		
W_{motor} [lb]		0.52	0.52	0.52		
OEW [lb]		6.53	6.59	6.59		
$W_{max\ payload}$ [lb]		0.40	8.85	6.00		
MTOGW [lb]		8.39	17.08	14.22		
Store Arrangements						
	W_{store} [lb]	$X_{from\ nose}$ [in.]	$Y_{from\ center}$ [in.]	$X\ CG_{plane}$ [in.]	$Y\ CG_{plane}$ [in.]	
Unloaded	--	--	--	10.52	0.00	
Empty Tank	0.40	10.52	0	10.52	0.00	
Ballasted Tank	8.85	10.52	0	10.52	0.00	
4 Rockets	6.00	10.52	-30, -24, 24, 30	10.52	0.00	
3 Rockets (2I, 1O)	4.50	10.52	-24, 24, 30	10.52	4.90	
3 Rockets (2O, 1I)	4.50	10.52	-30, -24, 24	10.52	-3.92	
2 Rockets (2I)	3.00	10.52	-24, 24	10.52	0.00	
2 Rockets (2O)	3.00	10.52	-30, 30	10.52	0.00	
2 Rockets (1I, 1O)	3.00	10.52	-24, 30	10.52	1.17	
2 Rockets (1 Side)	3.00	10.52	24, 30	10.52	10.56	
1 Rocket (I)	1.50	10.52	24	10.52	5.83	
1 Rocket (O)	1.50	10.52	30	10.52	7.28	

Table 23. Weight and balance documentation of air vehicle, systems, and stores

Figure 39: Final aircraft (left) and vehicle storage box (right) configurations.

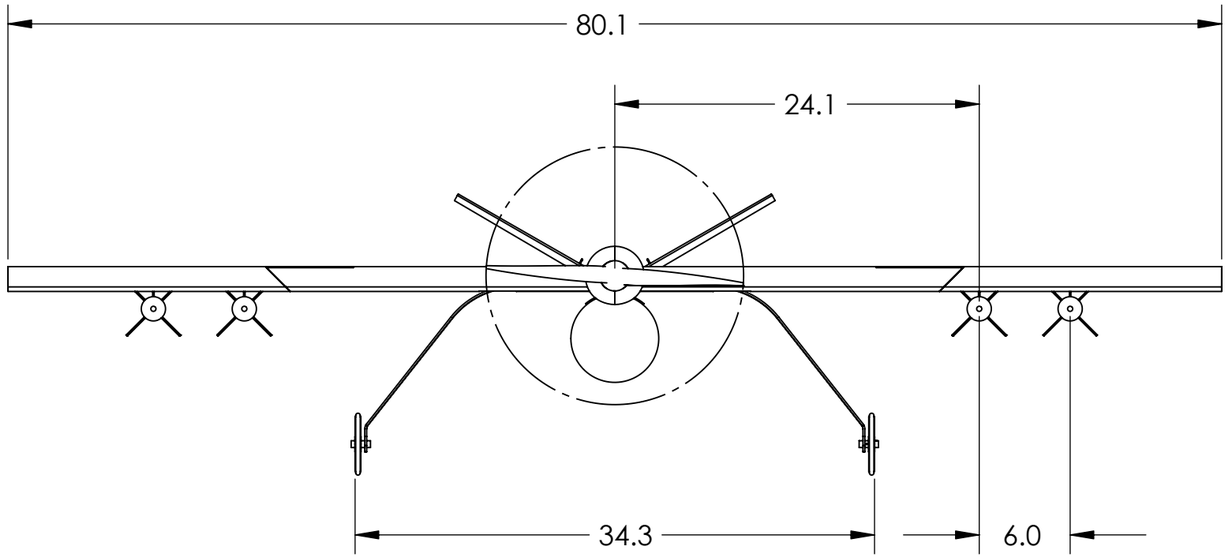

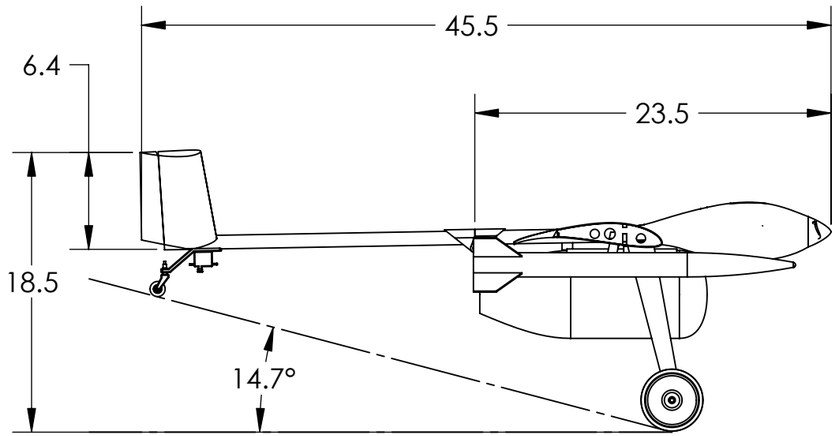

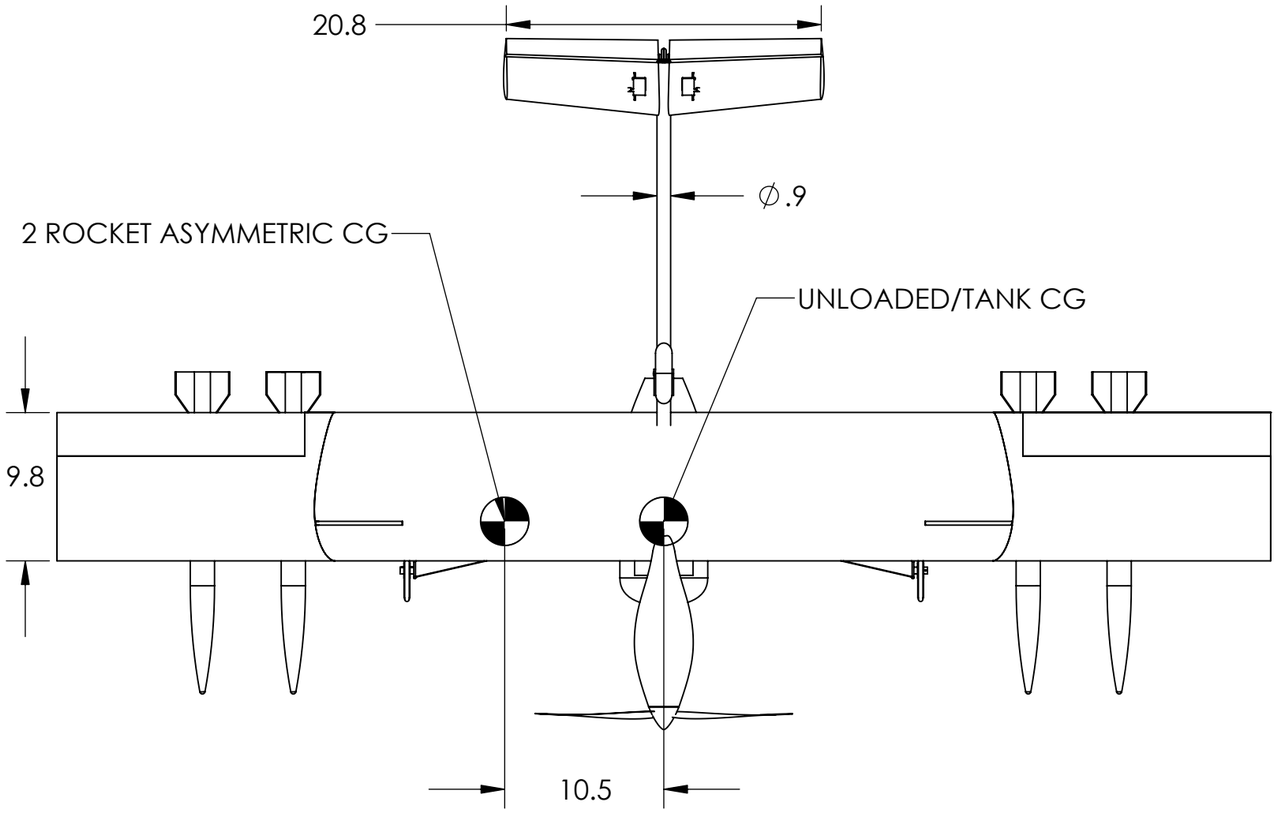

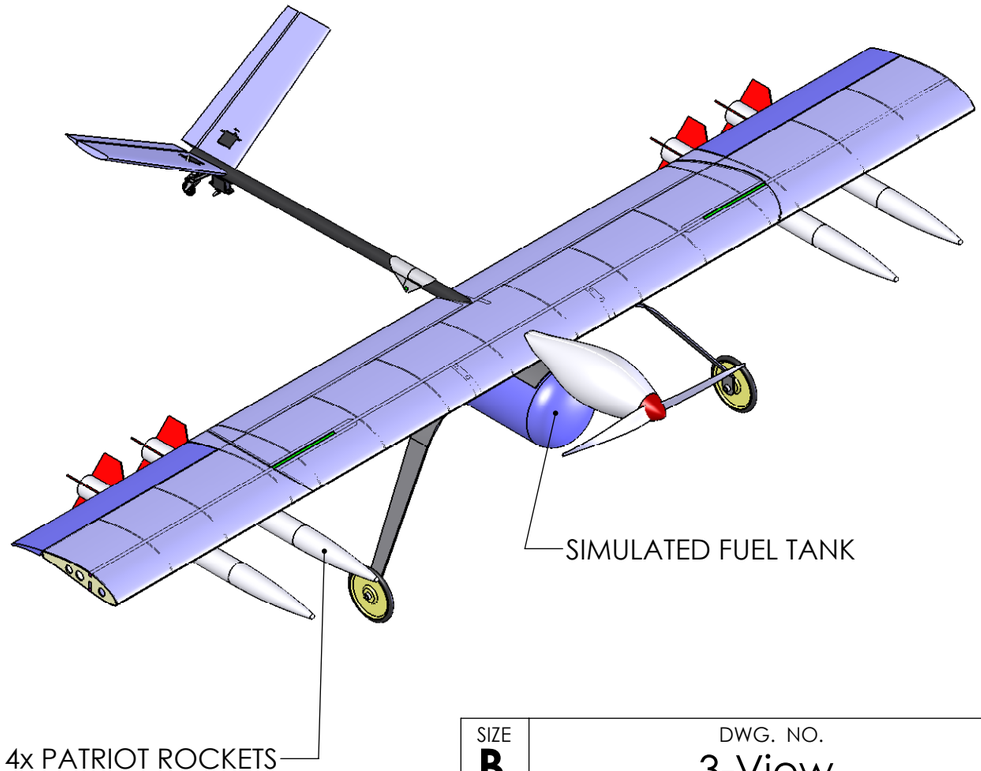

SIZE	DWG. NO.	REV
B	3-View	3
SCALE: 1:10	UNITS: IN	SHEET 1 OF 4

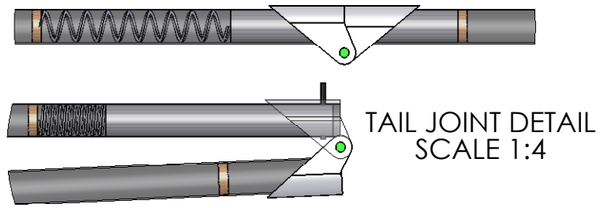

TAIL JOINT DETAIL
SCALE 1:4

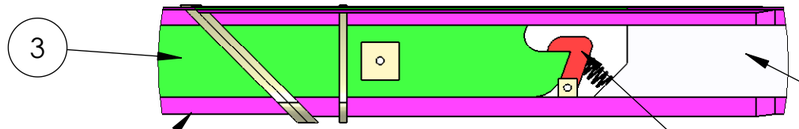

WING JOINT DETAIL
SCALE 1:2

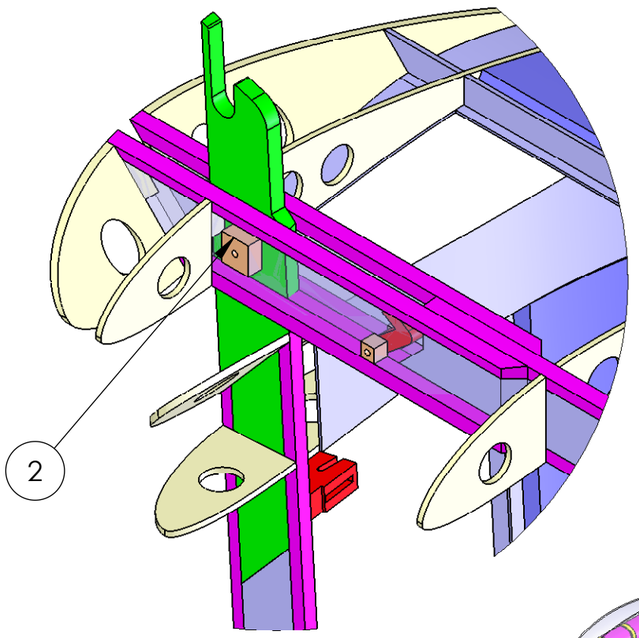

DETAIL A
SCALE 1 : 2

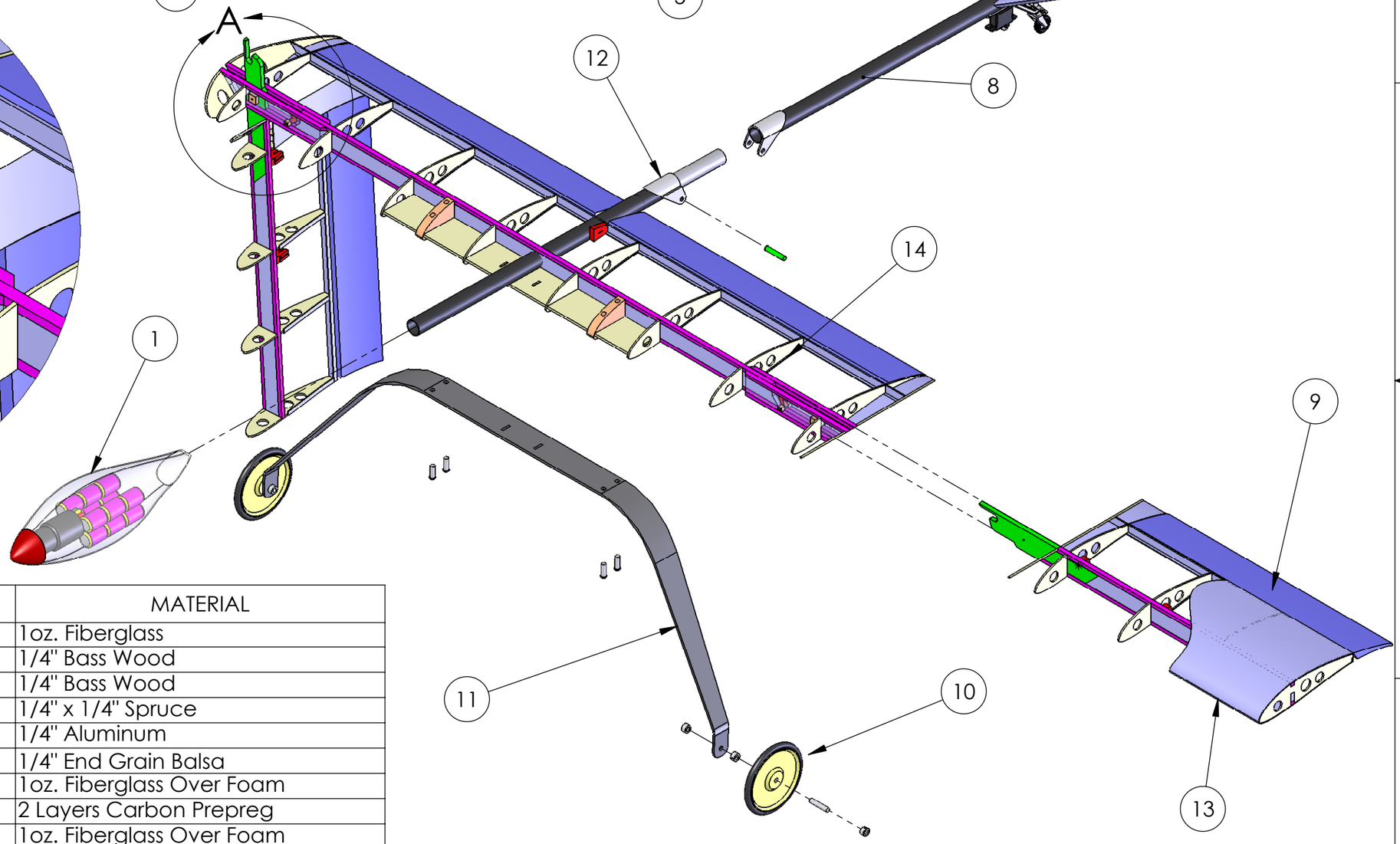

PART NUMBER	DESCRIPTION	MATERIAL
1	Fuselage Fairing	1oz. Fiberglass
2	Hinge Bearing Blocks	1/4" Bass Wood
3	Wing Joiner	1/4" Bass Wood
4	Spar Caps	1/4" x 1/4" Spruce
5	Clip	1/4" Aluminum
6	Shear Web	1/4" End Grain Balsa
7	Tail Surfaces	1oz. Fiberglass Over Foam
8	Tail Boom	2 Layers Carbon Prepreg
9	Flaps/Ailerons	1oz. Fiberglass Over Foam
10	Wheels	Kevlar with 3" O-Rings
11	Main Landing Gear	12 Layers Carbon Prepreg
12	Tail Joint	Carbon/ Aluminum Joiner
13	Wing Sheeting	3/32" Balsa with 3/4 oz. Fiberlass
14	Wing Rib	1/8" Lasercut Balsa

SIZE	DWG. NO.	REV
B	Structural Arrangement	3
SCALE: 1:6	UNITS: IN	SHEET 2 OF 4

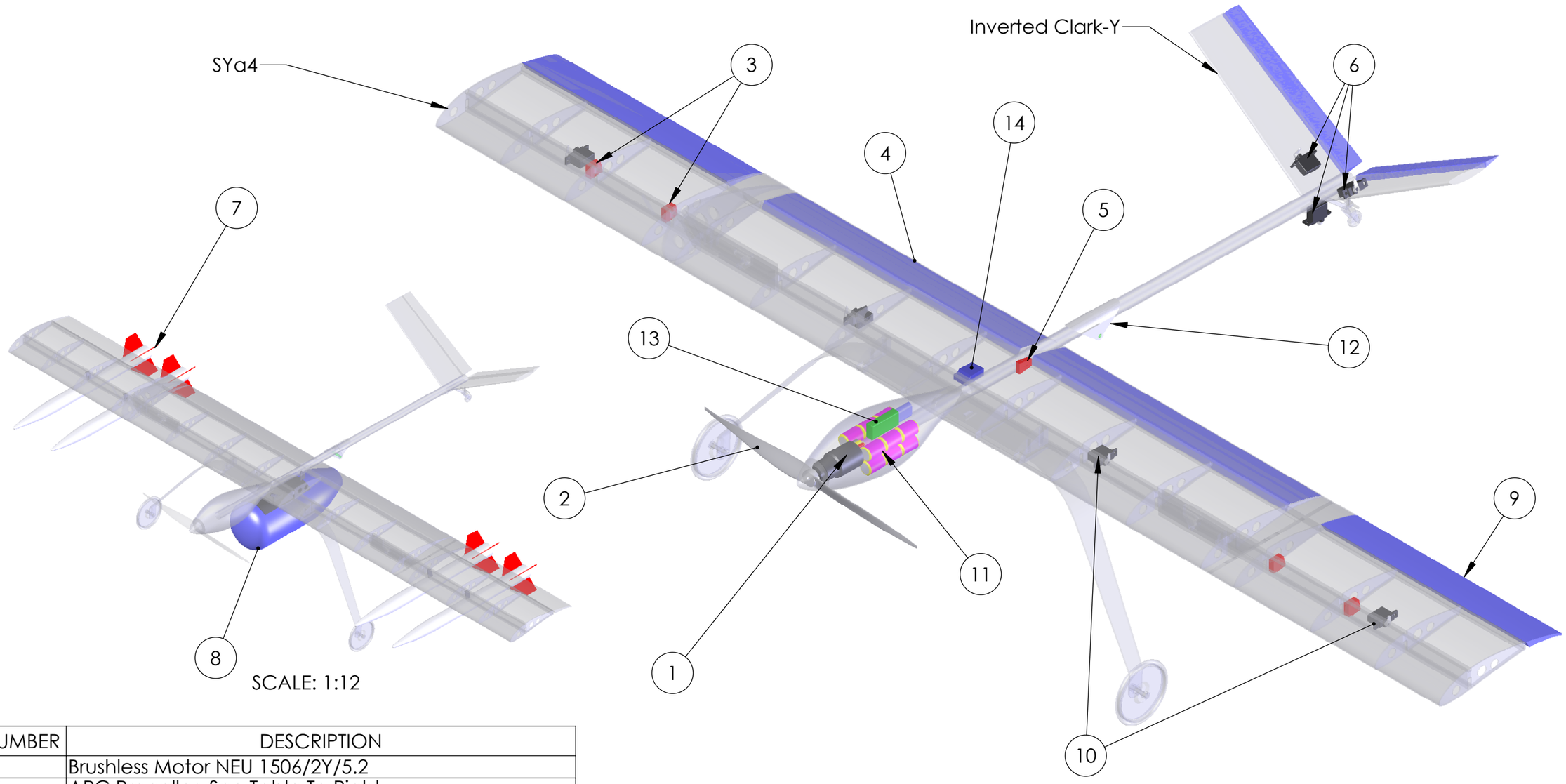

SCALE: 1:12

PART NUMBER	DESCRIPTION
1	Brushless Motor NEU 1506/2Y/5.2
2	APC Propeller, See Table To Right
3	4x Rocket Release Blocks
4	2x Flaperons
5	Bottle Release Block
6	3x HS-82MG Tail Servos
7	4x Patriot Rockets
8	Simulated Fuel Tank
9	2x Aileron
10	4x HS-82MG Wing Servos
11	NiMH Batteries, See Table To Right
12	Tail Boom Hinge
13	Castle Creations Phoenix 60 ESC
14	Futaba 9 Channel Reciever

	FERRY	SURVEILLANCE	STORE RELEASE
PROPELLER	16x10E	17x10E	17x10E
BATTERIES	15x GP2200's	12x GP3300's	10x GP4600's

SIZE	DWG. NO.	REV
B	Systems Layout	3
SCALE: 1:6	UNITS: IN	SHEET 3 OF 4

TIMELINE	2 SECONDS	4 SECONDS	9 SECONDS
Payload Crew #1	Runs to Open Right Panel	Lifts and Flips Plane Tip	Straightens Tail, Gets TX Runs Back
Payload Crew #2	Runs to Open Left/Front Panel	Lifts and Flips Plane Tip	Clips Tail, Close Box, Runs Back
Payload Crew #3	Runs to Extract Bottle	Installs Bottle, Takes Flipped Plane	Places Plane, Runs Back

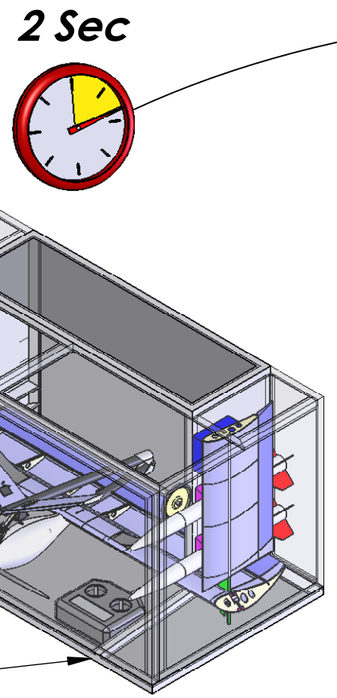

START

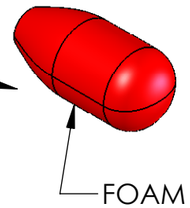

FOAM
BOTTLE BOX

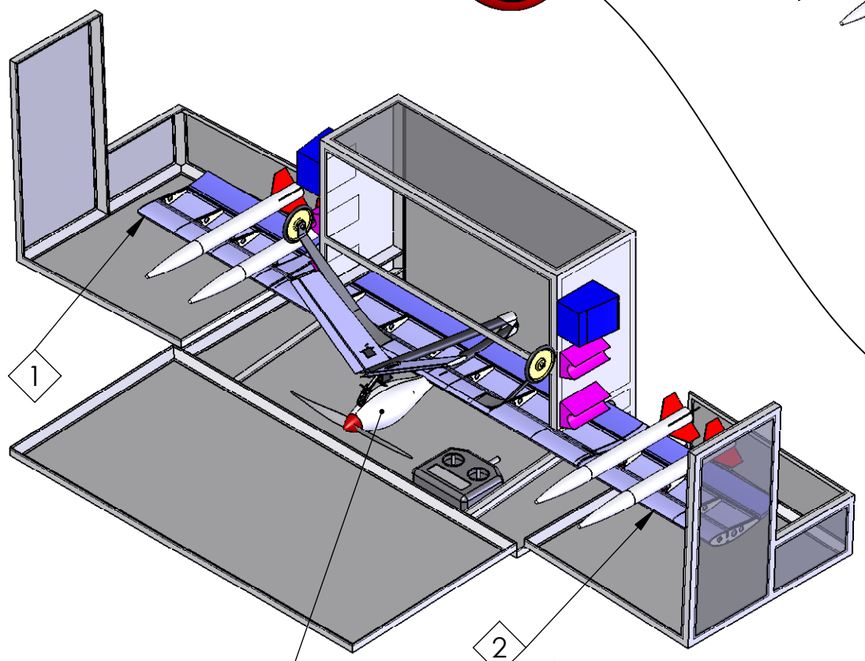

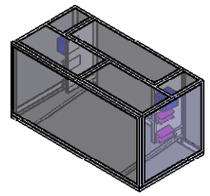

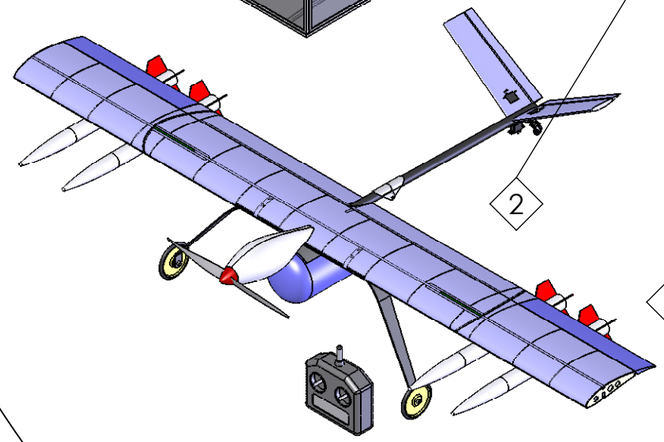

FINISH

9 Sec

WING STORES IN GROUND AND FLIGHT ATTITUDE

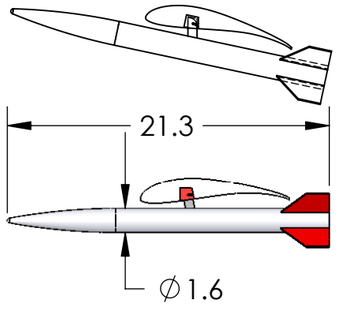

SCALE: 1:10

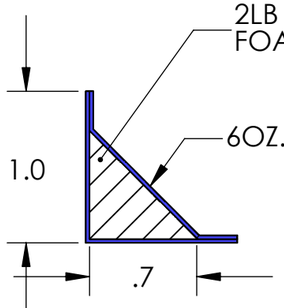

BOX FRAME MEMBER CROSS SECTION
SCALE: 1:1

BOTTLE AND MOUNT HARDWARE

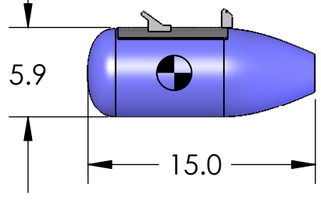

SCALE: 1:10

FOAM BLOCK PREVENTS ROCKETS FROM LOADING

ROCKET RESTRAINT PIN PULL TO OPEN BOX AND LOAD ROCKETS

0.2" CLEARANCE BEFORE INTALLED

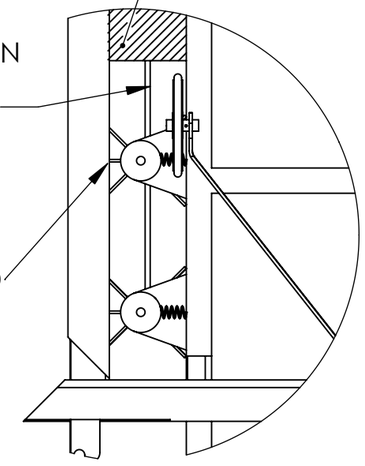

UNINSTALLED STORES DETAIL
SCALE: 1:6

SIZE	DWG. NO.	REV
B	Payload Accommodations	3
SCALE: 1:15	UNITS: IN	SHEET 4 OF 4

6.0 Manufacturing Plan and Processes

The manufacturing process of the program followed a detailed plan to ensure each component was constructed accurately and delivered on time. The preferred construction method of each component was determined through a FOM analysis of each manufacturing technique.

6.1 Schedule

Timely construction was vital to the coordination of the subgroups. Ample time was allotted to assemble each system component and to provide adequate time for testing. The waterfall schedule, shown in Figure 40, was kept in the lab to keep team members informed of the current tasks.

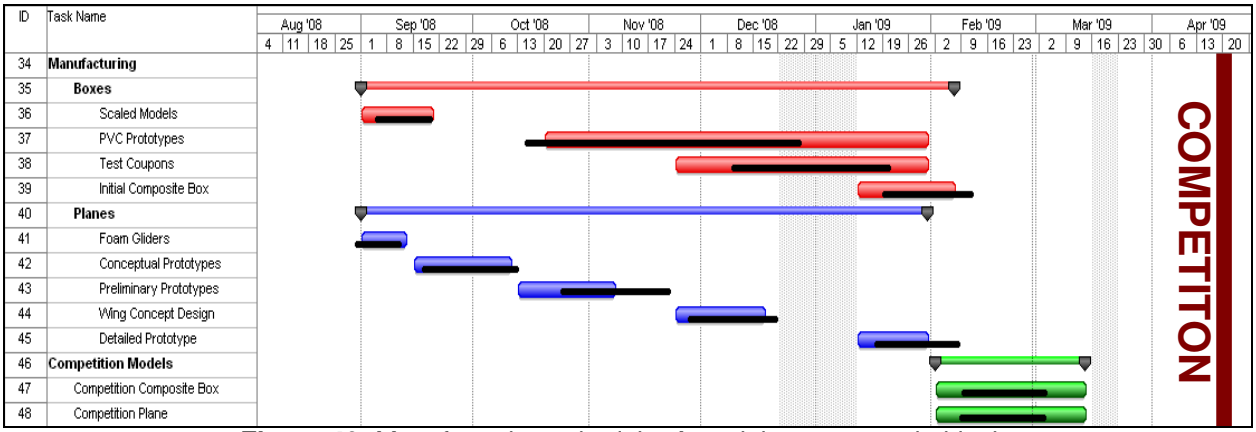

Figure 40: Manufacturing schedule. Actual times appear in black.

6.2 Manufacturing Techniques

Each component of the system had to satisfy a multitude of design requirements. The following construction methods were considered with the desire for quality, high strength-to-weight ratio parts:

- **Balsa Wood Buildup** – Lightweight balsa is used to define the shape. Areas of high stress are reinforced by spruce, plywood, or composites. A reusable jig is often constructed for alignment.
- **Molded Composite** – A polished plug serves as the exact solid model of the desired part. A female mold is made over the plug. Prepreg or wet lay-up composites are processed in this mold. While creating the initial molds can be time consuming, many parts can be made in a short time.
- **Fiberglass-Over-Foam** – A foam core is cut by a hot-wire cutter or sanded to the desired shape and then covered with fiberglass and resin in a wet lay-up. The fiberglass skin carries the main loads of the structure while the foam remains as part of the structure and helps maintain rigidity.
- **Hybrid** – Composites are used in areas of high stress concentration while balsa built-up sections retain the shape of the part in non-structural areas.

6.3 Figures of Merit

Qualitative analysis of each manufacturing technique was completed with a FOM analysis:

- **Skill Level –** The students' experience and construction abilities affected quality and time. A score of -1 was given if the number of experienced students was less than three, 0 if three to seven students, and +1 if more than seven students.

- **Building Time –** Building time accounts for a part's total manufacturing hours determined through previous experience. Building techniques that required more than 18 man-hours were given a score of –1, between 10 to 18 hours a 0, and less than 10 hours a +1.

The skill and time criteria were compared for each manufacturing technique in Table 24.

Technique	Balsa Build-Up	Molded Composite	Fiberglass over Foam	Hybrid
Skilled Members	3	9	8	6
Skill Score	**0**	**1**	**1**	**0**
Man Hours	10	16	6	18
Time Score	**0**	**0**	**1**	**0**

Table 24. Skill matrix

Several other factors were considered in the subsystem construction technique downselects:

- **Weight –** Weight was the most vital build parameter as it directly affected the competition score.
- **Ultimate Strength –** Each component must be strong enough to support the design loads.
- **Reparability –** This defines the ability to make damage repairs between flight attempts.
- **Cost –** With a fixed budget, the cost of materials and repairs was considered during design.

6.4 Manufacturing Downselects

6.4.1 Fuselage

The fuselage was designed as a thin, hollow tube as determined in the Preliminary Design sections. The required length-to-diameter of the fuselage boom was too high to warrant balsa or hybrid construction. Table 25 shows molded composite as the optimum construction method.

Figure of Merit	Weight	Molded Composite	Fiberglass over Foam
RAC (Weight)	*0.35*	0	-1
Ultimate Strength	*0.23*	1	0
Skill Score	*0.17*	1	1
Time Score	*0.12*	0	1
Reparability	*0.08*	0	1
Cost	*0.05*	-1	0
TOTAL	***1.00***	**0.35**	**0.02**

Table 25. Fuselage manufacturing technique downselect

Two layers of 3 oz. unidirectional prepreg were laid up at +/- 45° over a mandrill of the required length. After curing at the manufacturer's specifications, the tube was cut to accommodate the boom's hinge. Two layers of 1 oz. fiberglass provided a thin aerofairing around the propulsion system. Figure 41 shows the constructed fuselage tube and hinge.

Figure 41: Carbon fiber fuselage tube and tail boom hinge.

6.4.2 Wing

The aircraft was designed with hinged wings, providing a quick means for assembly at the expense of joint weight. Therefore, weight reduction drove the construction process. Compared to molded composites and balsa buildups, the hybrid approach allowed weight savings in the non-structural section of the wing while concentrating strength into precise load paths as summarized in Table 26.

Figure of Merit	Weight	Balsa Buildup	Molded Composite	Fiberglass over Foam	Hybrid
RAC (Weight)	*0.35*	1	0	-1	1
Ultimate Strength	*0.25*	0	1	0	1
Skill Score	*0.20*	0	1	1	0
Time Score	*0.08*	0	0	1	-1
Reparability	*0.07*	-1	0	1	0
Cost	*0.05*	1	-1	0	0
TOTAL	***1.00***	**0.33**	**0.40**	**0.00**	**0.52**

Table 26. Wings manufacturing downselect

In each hybrid wing section, shown in Figure 42, 1/4 in. square spruce caps sandwiched the 1/4 in. end grain balsa shear web of the I-beam spar. One-eighth inch balsa ribs were laser cut from the 3D CAD model. Ribs were spaced every 6 in. spanwise and held in proper orientation using a jig. The wing was covered in 3/32 in. balsa sheeting sandwiched between two layers of 3/4 oz. fiberglass. The top layer of fiberglass was laid into a wing mold, covered next by the balsa core and the interior layer of glass before the structure was vacuum bagged. Fiberglass-over-foam control surfaces were used.

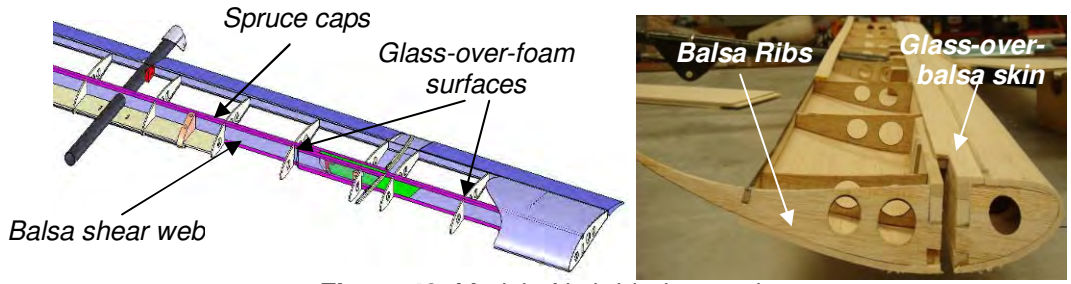

Figure 42: Model of hybrid wing section.

6.4.3 Empennage

The balsa buildup method proved to be the lightest solution for the empennage requirements. However, to preserve the airfoil, the fiberglass-over-foam method was preferable. In Table 27, the empennage construction technique downselect is shown.

Figure of Merit	Weight	Balsa Buildup	Molded Composite	Fiberglass over Foam	Hybrid
RAC (Weight)	*0.35*	1	0	0	0
Reparability	*0.20*	-1	-1	1	-1
Skill Score	*0.15*	0	1	1	0
Time Score	*0.15*	0	0	1	-1
Ultimate Strength	*0.10*	-1	1	0	1
Cost	*0.05*	1	-1	1	0
TOTAL	***1.00***	**0.10**	**0.00**	**0.55**	**-0.25**

Table 27. Empennage manufacturing technique downselect

The V-tail was CNC hot wired before one layer of 1 oz. glass was laid up over the foam. The hybrid structure was rigid enough to support itself without the need for carbon fiber spars. Control surfaces were cut from the tails and attached with tape hinges.

6.4.4 Landing Gear

The material and construction methods were optimized for a tail-dragger landing gear configuration with a bow main gear. Table 28 shows the best main gear was a composite lay-up.

Figure of Merit	Weight	Composite Lay-Up	Metal Wire	Oleo Metal Struts
RAC (Weight)	*0.25*	1	0	-1
Ultimate Strength	*0.20*	1	-1	-1
Skill Level	*0.17*	0	1	0
Building Time	*0.08*	0	1	1
Reparability	*0.20*	0	1	-1
Cost	*0.10*	0	1	-1
TOTAL	***1.00***	**0.45**	**0.35**	**-0.67**

Table 28. Landing gear manufacturing technique downselect

Twelve layers of 3 oz. unidirectional prepreg carbon fiber were laid over a custom aluminum form, shown in Figure 43, and oven-cured in a vacuum bag. Carbon was chosen for its superior strength-to-weight ratio. The commercially available tail gear was attached to the rudder for steering. To save weight, the wheels were manufactured in-house. The lightest and most durable method for constructing wheels was a composite lay-up because of its high strength-to-weight ratio. Kevlar was chosen because of carbon's inherently brittle nature. The downselect can be seen in Table 29.

Figure of Merit	Weight	Composite Lay-Up	Aluminum	Wood
RAC (Weight)	*0.25*	1	-1	1
Ultimate Strength	*0.20*	0	1	-1
Skill Level	*0.17*	1	-1	1
Building Time	*0.08*	0	-1	0
Durability	*0.20*	0	1	-1
Cost	*0.10*	0	1	0
TOTAL	***1.00***	**0.42**	**0.00**	**0.02**

Table 29. Wheels manufacturing downselect

The wheels, shown in Figure 43, were made of two Kevlar halves that were bonded together. Each half comprised of 3 layers of 6 oz. Kevlar and shaped on an aluminum mold. A 3 in. O-ring around the center of the wheel provided the necessary traction. The axles were constructed from brass tubes.

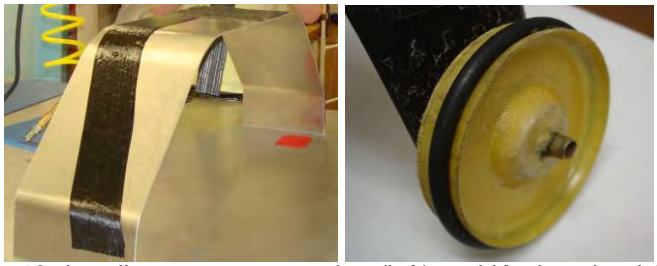

Figure 43: Landing gear construction (left) and Kevlar wheel (right).

6.4.5 Storage Boxes

Based on the geometry presented in the Detailed Design section, the material for the storage boxes' construction was selected as shown in Table 30. While the high strength-to-weight ratio of carbon fiber was initially enticing, the construction process was too time-consuming to allow for adequate testing and modification of the design. The same structure could be built with a fiberglass-over-foam technique for the strength-to-weight ratio and in far less time.

Figure of Merit	Weight	Balsa Buildup	Molded Composite	Fiberglass over Foam	Hybrid
RAC (Weight)	*0.35*	-1	0	0	-1
Ultimate Strength	*0.25*	-1	1	1	0
Skill Score	*0.20*	0	1	1	0
Time Score	*0.08*	0	0	1	-1
Reparability	*0.07*	1	-1	-1	-1
Cost	*0.05*	1	-1	0	0
TOTAL	***1.00***	**-0.48**	**0.33**	**0.46**	**-0.50**

Table 30. Storage box manufacturing downselect

Equal length test coupons were constructed and tested before determining a 1.5 in. triangular cross section beam was needed to sufficiently survive the drop test. A sample box joint was constructed out of 2 lb foam and one layer of 1 oz. fiberglass.

7.0 Testing Plan

A comprehensive test program was implemented that extended from the beginning of the program to the competition. The main objective of all the testing was to verify the predictions of the MDO and other analytical tools. Additionally, the test program was used in the development and improvement of the airplane and its components. Finally, the test program was the absolute determinate in the integration of the air vehicle, ground station, and boxes. This section summarizes the main testing objectives, plans, and methodology that drove the final design presented in the previous sections.

7.1 Schedule

A schedule was developed and maintained that synchronized with the design and building phases of the project. This schedule is shown in Figure 44.

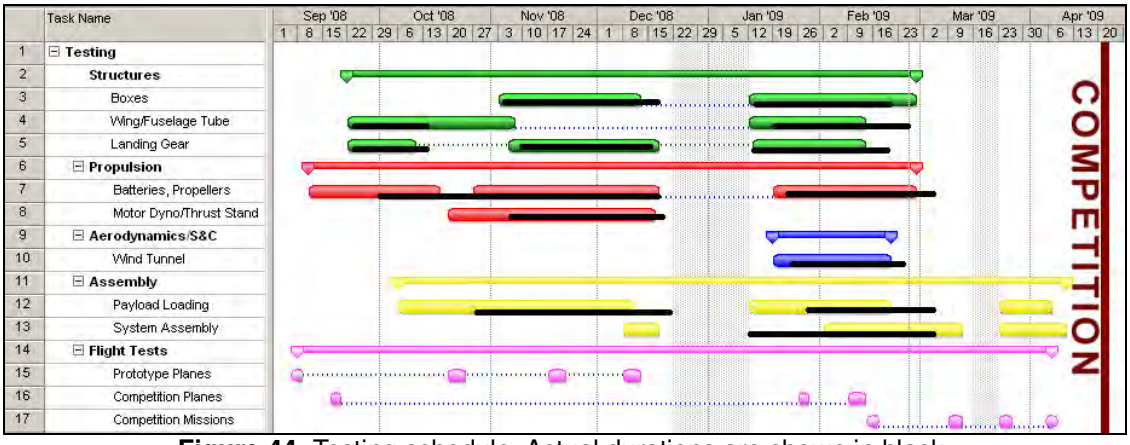

Figure 44: Testing schedule. Actual durations are shown in black.

7.2 Subsystem Testing

The designs of individual subsystems were assessed both before and after the completion of manufacturing to select and refine the system architecture.

7.2.1 Propulsion

The Propulsion team verified the selected propulsion package through testing of individual and collective components. Testing began with the purchase of an array of batteries with various capacities. Through charging and discharging individual cells and assembled packs, the actual capacity, discharge rate, and internal resistance of each tested battery type was determined. These tests were used to prove the validity of the manufacturer's specifications as well as the accuracy of the sizing models used. Many cell types that showed promise in the MDO were discarded for poor performance. A propeller mapping program was designed to measure the C_T and C_P of various propellers mounted on a thrust stand in a wind tunnel. The recorded values correlated well with PlaneSizer's archives.

The final propulsion component tested was the motor. Initially, a selected motor was run at 10 V without a propeller to determine the no-load current. A dynamometer/thrust stand tested each motor across a wide RPM range as various braking loads were applied by different propellers. Important parameters such as Kv, motor efficiency, torque were determined. The calculated internal resistances provided an estimate of efficiency losses which rectified initial endurance overestimations.

7.2.2 Landing Gear

Initial testing to validate the results of the main gear sizing program showed the ultimate strength of the designed gear to be too conservative. High speed footage was taken of several bow gears dropped from a fixed height under varying loads. The resultant deflection at impact indicated that the ultimate strength of the gear could be safely reduced with a 30% decrease in width.

7.2.3 Storage Boxes

The first step in confirming the configuration and structural design of the two storage containers involved the construction of miniature models of the entire system based off configuration drawings. Once the scaled components fit effectively into the box, a full scale PVC model was created to which the next aircraft was tailored. By the conclusion of the preliminary design phase, all systems were stored properly.

Testing of the construction material then commenced. Three tube coupons of equal length were formed from PVC, carbon fiber, and various cross sections of fiberglass over foam. After the relative weights were recorded, each sample was loaded to simulate the drop test loads. A physical drop test was performed with the PVC mockup loaded with the air vehicle and all support equipment. Loading and assembly trial runs were practiced once the automated rocket loading system was installed.

7.2.4 Structures

To validate the sizing of the wing shear web and spar caps, destructive test methods were used. Weights were applied to the test wing to simulate in-flight loads. Additional weight was applied until the test section broke. This allowed the Structures team to calculate the ultimate strength of the wing and compare it to the predicted strength. With this knowledge, wing behavior was more accurately predicted

and excess weight was minimized. The carbon tube fuselage was also loaded at its hinge to simulate a hard landing with the ballasted bottle.

7.2.5 Payloads

Payload loading and assembly time were major factors of flight score. This motivated the construction and testing of several mock-up payload mount and release ideas. The winning restraint design was further optimized to be as light and fast-to-load as possible through full-scale ground crew testing. The continuous remote deployment of all stores assessed the lifespan of the muscle wire and blade mount systems. The Payloads team was also responsible for manufacturing each bottle fairing to be tested in the wind tunnel.

7.3 Flight Testing

While the assessment of individual components of the subsystems provided valuable information, it was the tests of the collective system that were reflective of competition performance. Once every subsystem had been optimized, each completed aircraft was flight tested.

7.3.1 Flight Vehicles

This year the team developed and flew a balsa prototype at the onset of the conceptual design phase knowing an early start was critical. In addition to encouraging involvement of new members, this aircraft was intended to simulate the manufacturing techniques and flight characteristics of the competition aircraft. While the platform was by no mean optimized, its flights were valuable for observing the flying qualities of the various payloads.

Several iterations followed the initial design. Each one was an invaluable platform for testing, aerodynamics, stability and control, payloads and propulsion systems. The first competition-grade *Turbo Encabulator* airframe was flown immediately after the detailed design phase. The test program proceeded from trim flights to competition missions.

7.3.2 Aircraft Testing Implementation

For test flights, a preflight checklist was used to ensure the safe operation of all airplane components prior to flight. This checklist is shown in Table 31.

Action	Description	
Remove Fuse	□ Ensure that the aircraft is not armed	
Check CG	□ Use scales to verify that the aircraft is properly balanced	
	□ Record the total weight of the aircraft	
Check Rx Connections	□ Ch. 1- Inboard aileron	□ Ch. 2- Ruddervator
	□ Ch. 3- Throttle (ESC)	□ Ch. 4- Ruddervator
	□ Ch. 5- Outboard aileron	□ Ch. 6- Brakes
	□ Ch. 7- Store release (L/R/C)	□ Ch. 8- Store Release (I/O)
	□ Ch. 9- Store release (deploy)	
Range Check	□ Retract Transmitter antenna	□ Record fail-safe distance
	□ Check for signal at 100 ft.	□ Vary aircraft orientation
Check data recorder	□ Secure to airframe	□ Check electrical connections
Check control surfaces	□ Secure mechanical/electrical connections	□ Proper deflection/direction
Check ESC	□ Secure to airframe	□ Plug into motors
Check batteries	□ Verify packs are peaked	□ Plug into ESC
	□ Secure to airframe	
Check hatch	□ Secure mechanical connections	
Arm	□ Clear prop	□ Insert Fuse

Table 31. Pre-flight checklist

The checklist in Table 32 was created to collect pertinent data during and after the test flight.

Data	Description
Current Draw	□ Hold plane stationary and record current draw at TO & cruise throttle
TOFL	□ Reference runway markings to measure distance
Velocity	□ Record take-off velocity with radar gun and wind velocity
	□ Record cruise velocity with radar gun and wind velocity
Throttle Settings	□ Record throttle setting at take-off
	□ Record throttle setting at cruise
Pilot Comments	□ Record stability/handling problems
Time in Air	□ Use stopwatch to calculate time from lift-off to touch-down
Trim Angles	□ Measure control surface angles after trim flight

Table 32. Checklist of data to be collected during and after test flight

8.0 Performance Results

Though the detailed design phase provided an estimate of aircraft and subsystem performance, it was discovered through testing that the demonstrated performance varied slightly from the model.

8.1 Subsystem Performance

8.1.1 Aerodynamics

Test flights verified XFOIL and AVL as accurate estimators of angle of attack, trim settings and tail efficiency. A tip-stall tendency was corrected by removing irregular wing twist inadvertently incorporated during construction. More significantly, PlaneSizer's 5 ft^2 wing area was not sufficient to lift the ballasted bottle within the 100 ft TOFL requirement. Instead of sacrificing cruise drag for a larger surface area, split flaps were explored instead. The high-lift devices were deployed during takeoff and climb-out and were

retracted in cruise to minimize excess drag – an essential aspect for preserving the ferry flight's speed and the surveillance mission's endurance. Ground rolls were repeated at varying flap settings until a deflection of 45° yielded a 25% increase in C_{Lmax} and a TOFL of 90 ft. This value agreed with prior XFOIL predictions. Larger deflections provided no aerodynamic benefit.

At the close of the design phase, it was found that the MDO was under-predicting the parasite drag of the simulated fuel tank. As a result, attempts at the surveillance flight fell short of endurance requirements. Wind tunnel tests were performed on different bottle fairing configurations. Tests at cruise Reynolds numbers provided a more accurate representation of the payload drag, and the results were subsequently reincorporated into PlaneSizer.

8.1.2 Stability and Control

AVL provided an adequate evaluation of flight conditions and resultant stability characteristics. Flight testing revealed pitch authority was undervalued by 10-15% with the ballasted bottle's high sink rate. Control surface area and deflection were then increased for more effectiveness. The initial aileron geometry proved inadequate for lateral-directional asymmetric trim and was thus modified with a greater moment arm (through the addition of wingspan), surface area, and higher gains. Test flights were also used to prove the ample crosswind capabilities of the aircraft under all loading conditions.

8.1.3 Propulsion

Early test flights showed a need for more propeller pitch to bolster takeoff performance. A new propeller was selected, analyzed and tested. A motor dynamometer measured the power, torque and efficiency of multiple motors using various propellers to apply aerodynamic braking loads. The power curve is shown in Figure 45 Predicted values varied by 6-8% from the recorded data.

A final test mapped the transmitter's stick throttle to the produced thrust and current as dead zones were observed at the extremes of stick's range. Using the competition propulsion package, the stick position was varied in discreet increments while the current and voltage were recorded. Figure 45 shows the geometric throttle position was under-predicting the produced thrust by 16% at half throttle and 6% at cruise throttle. This discrepancy was factored out in PlaneSizer, while the pilot was notified of the trend so that informed decisions could be made in flight.

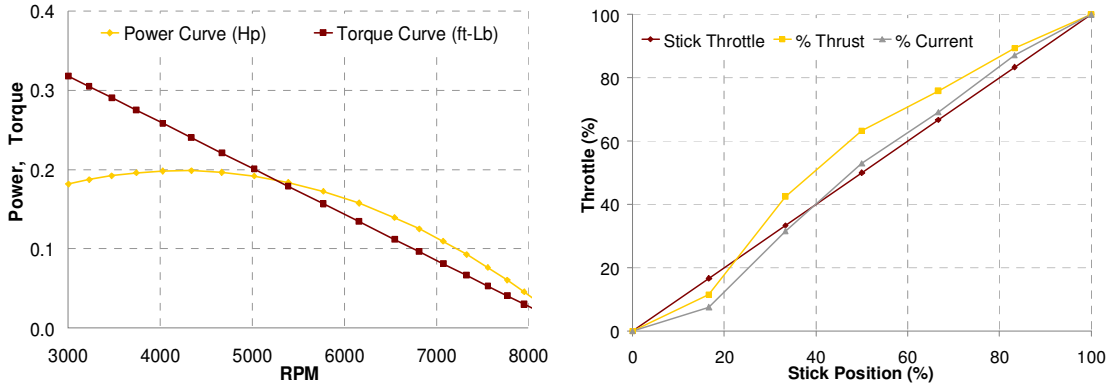

Figure 45: Power and torque data obtained by the dynamometer (left) and throttle mapping (left).

8.1.4 Structures

Figure 46 shows a 1.9 ft cantilevered wing section consisting of a balsa shear web, spruce spar caps, and a balsa skin laminated with one layer of 1 oz. fiberglass. Under 14 ft*lb of torque, the balsa sheeting began to scallop while 22 ft*lb of torque deformed the airfoil significantly. Shear web failure witnessed at 32 ft*lb ultimately ruptured the D-box sheeting. The observed ultimate load was 12% less than that predicted. This deficiency was reconciled by laying a single layer of fiberglass on the underside of the skin. Subsequent tests validated the modification; the new design gained back 20% in ultimate load. The data verified the structures sizing program which then sized the wing with a 1.5 FOS.

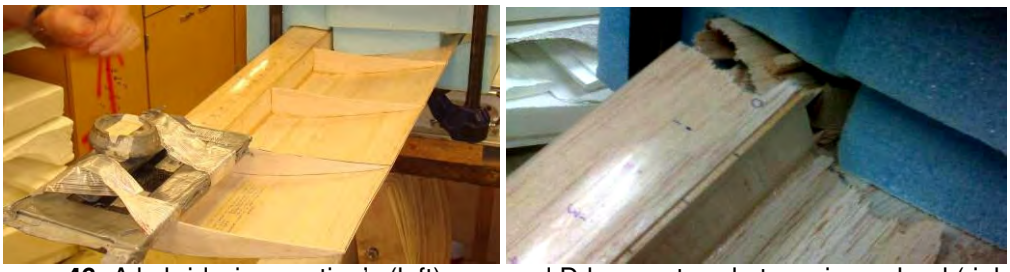

Figure 46: A hybrid wing section's (left) spar and D-box ruptured at maximum load (right).

8.1.5 Landing Gear

Static testing provided a means of comparing the predictions from the gear sizing program to physical data, as shown in Table 33. The energy absorption falls within the predicted range, while the vertical deflection is 29% greater than the predicted. Flight tests substantiated the strength and placement of the main gear and tail wheel for all payload arrangements. The gear was sized adequately to endure the hard landing loads applied during test flights. The primary modes of failure for torsional and linear loads were tested to confirm the ultimate strength of the part as shown in Figure 47.

	Energy Absorption (in.*lb)	Vertical Deflection (in.)
Predicted	22.32	1.24
Measured	21 ± 1	1.6 ± .1

Table 33. Test data verifying the model's validity

Additionally, minor toe-in of the wheels produced considerable ground handling problems that were easily rectified in the construction phase. The preliminary spring-actuated tail wheel steering failed to provide enough control at low speed and was therefore replaced by a pushrod system.

Figure 47: A half bow main gear (left) was loaded past its predicted maximum before delaminating (right).

8.1.6 Payloads

Overall, the muscle wire release system, shown in Figure 48, functioned well over an extensive useable lifespan. Material fatigue occurred not with the muscle wire itself but with the balsa retaining clip. Unintentional misalignment produced friction between it and the interior wing structure. Repeated payload deployments and loading wore down each clip until it was no longer able to lock the store's blade into place. A single layer of fiberglass was applied to the surface of each clip to prevent further abrasion.

The simulated fuel tank's CG was misaligned in the longitudinal axis during the first deployment test. By moving its CG further forward such that only 20% of its weight rested on the locking pin, the forward end of the centerline store was guaranteed to unhook once the aft pin was disengaged.

Figure 48: A wingtip store is released by a contraction of the muscle wire that pulls a locking pin.

8.1.7 Storage Boxes

After constructing a full scale PVC prototype, minute construction and integration discrepancies resulted in component misalignment that was not predicted by the CAD model. The precision of the 3D assembly was much greater than that attainable by the team's manufacturing techniques. Corrections were made in the form of spacers or additional material.

8.1.8 Subsystem Summary

A summary of problems encountered during subsystem performance testing is shown in Table 34.

ISSUE	SOLUTION
Aerodynamics	
Tip-stall tendency	Removed unintentional wing twist
Excessive TOFL	Added split flaps
Excessive parasite drag	Aerofairings added to bottle
Stability & Control	
Ineffective pitch control	Increase %-chord of ruddervator
Insufficient lateral trim	Increase aileron area, moment arm
Propulsion	
High battery internal resistance	Test temperature at discharge; remove defective cells
ESC cutoff	Lower minimum cutoff voltage
Structures	
Premature spar/skin failure	Add fiberglass-balsa sandwich structure
Landing Gear	
Unstable ground handling	Remove toed in wheels; add pushrod steering
Payloads	
Failure to secure wingtip stores	Reinforce fatigued clips with fiberglass
Failure to deploy centerline store	Move bottle's CG forward
Storage Boxes	
Component misalignment	Refine construction methods
Excessively robust structure	Remove excess non-structural weight

Table 34. Issues encountered during testing and their corresponding solutions

8.2 System Performance

8.2.1 System Packaging

Once the aircraft and box prototypes were completed, the ground crew rehearsed the timed assembly and loading of the system. Task delegation issues were resolved by formulating an itinerary for each pit crew member over the course of the assembly and loading processes. At the time of report submittal, practice assembly times were nearing that of the assumed best.

8.2.2 Aircraft Solution

The 2008-2009 program has completed seven test flights throughout the course of the year: one during the conceptual design phase and three during each the Preliminary and Detailed Design phases. Flight testing expanded in scope from proof of airworthiness to the ability to lift all payload combinations to trimmed competition laps. At the time of report submittal, the first competition-worthy version of the *Turbo Encabulator* aircraft was performing proficiently, as predicted in the detailed design phase. The RAC had been minimized, integrated solutions for all payload arrangements had been selected, the 100 ft TOFL requirement was satisfied, and two-lap and four-lap missions were commencing.

9.0 References

[1] Drela, Mark and H. Youngren. "Athena© Vortex Lattice Program." 22 Aug 2008. <http://web.mit.edu/drela/Public/web/avl/>.

[2] Ullman, David G. The Mechanical Design Process. 1992. Ed. Jonathan Plant and Amy Hill. 3rd ed. New York: McGraw-Hill Higher Education, 2003.

[3] Drela, Mark. "XFOIL Subsonic Airfoil Development System." 3 Sept 2008. <http://raphael.mit.edu/xfoil/>.

[4] "XFLR5." 29 Oct, 2008. <http://xflr5.sourceforge.net/xflr5.htm>.

[5] Rawdon, Blaine. "Landing Gear Design." 2005.

[6] "Tucson, Arizona." Weather Underground. Sept 2008 <http://www.wunderground.com/cgi-bin/findweather/getForecast?query=tucson#History>.

[7] SolidWorks. "COSMOSWorks." 2007.

[8] *"UIUC Airfoil Coordinate Database."* 29 Oct, 2008. <http://www.ae.uiuc.edu/m-selig/ads/coord_database.html>

[9] Hoerner, Sighard. *Fluid Dynamic Drag.* Boston, 1965.